
Electronic Thesis and Dissertation Repository

6-20-2018 11:00 AM

Constant Envelope DCT- and FFT- based Multicarrier Systems

Rayan Alsisi

The University of Western Ontario

Supervisor

Dr. Raveendra Rao

The University of Western Ontario

Graduate Program in Electrical and Computer Engineering

A thesis submitted in partial fulfillment of the requirements for the degree in Doctor of Philosophy

© Rayan Alsisi 2018

Follow this and additional works at: <https://ir.lib.uwo.ca/etd>



Part of the [Systems and Communications Commons](#)

Recommended Citation

Alsis, Rayan, "Constant Envelope DCT- and FFT- based Multicarrier Systems" (2018). *Electronic Thesis and Dissertation Repository*. 5473.

<https://ir.lib.uwo.ca/etd/5473>

This Dissertation/Thesis is brought to you for free and open access by Scholarship@Western. It has been accepted for inclusion in Electronic Thesis and Dissertation Repository by an authorized administrator of Scholarship@Western. For more information, please contact wlsadmin@uwo.ca.

Abstract

Discrete Cosine Transform (DCT)- and Fast Fourier Transform (FFT)- based Orthogonal Frequency Division Multiplexing (OFDM) systems with a variety of angle modulations are considered for data transmission. These modulations are used with the purpose of achieving Constant Envelope (CE) transmitted signals, for superior power efficiency with nonlinear High Power Amplifier (HPA), typically used at the transmitter in OFDM systems. Specifically, four angle modulations are considered: i) Phase Modulation (PM); ii) Frequency Modulation (FM); iii) Continuous Phase Modulation (CPM); and iv) Continuous Phase Chirp Modulation (CPCM). Descriptions of DCT- and FFT- based OFDM systems with M-ary Pulse Amplitude Modulation (MPAM) mapper, with these modulations, are given and expressions for transmitted signals are developed. The detection of these signals in Additive White Gaussian Noise (AWGN) and multipath fading channels is addressed. The receiver structure consists of arctangent demodulator followed by the optimum OFDM receiver for memoryless PM and FM modulations. However, for CPM and CPCM modulations that have inherent memory, arctangent demodulator followed by correction with oversampling technique is used prior to the optimum OFDM receiver. Closed-form expressions for Bit Error Rate (BER) have been derived and are function of: i) Signal-to-Noise Ratio, (E_b/N_0) ; ii) Modulation parameters; iii) Number of amplitude levels of M-PAM mapper; and iv) parameters of multipath fading environment.

It is shown that, in general, BER performance of CE-DCT-OFDM system is superior compared to that of conventional DCT-OFDM system, when the effect of HPA in the system is taken into account. Also, it is observed that CE-DCT-OFDM system outperforms CE-FFT-OFDM system by nearly 3 dB. The DCT- and FFT-OFDM systems with CPM and CPCM modulations are superior in BER performance compared to

PM and FM modulations in these systems. The use of CPCM in OFDM systems can provide attractive trade off between bandwidth and BER performance. The performance of CE-DCT-OFDM and CE-FFT-OFDM systems over Rayleigh and Rician frequency non-selective slowly-varying fading channels are illustrated as a function of channel parameters and the penalty in SNR that must be paid as consequence of the fading is determined.

Acknowledgements

All praise and thanks to Allah, the most gracious most merciful, for bestowing upon me His countless bounties, and strength and patience to complete my doctoral study. Without His guidance and blessings, nothing is possible.

I owe much gratitude and deep appreciation to my supervisor Prof. Raveendra K. Rao for giving me this unique opportunity to work in his group and learn from his vast knowledge and experience. His time is always available for discussion, encouragement, insightful guidance, consistent support, invaluable advice, and constructive criticism. Undoubtedly without his dedication my Ph.D thesis would not have taken this shape.

Acknowledgements are due to Islamic University of Madinah for granting and providing scholarship and financial support through Saudi Cultural Bureau in Canada to completing my PhD program at the University of Western Ontario

I would like to express my deepest gratitude to my parents, brothers, and sister for their encouragement and support over the years. The role of parents in my upbringing and their prayers have played a major part in what I am today. I wish that I can compensate them for their love and support all the past years. I would also like to show my sincere gratitude to my wife and my children for being beside me during the PhD journey.

Rayan Alsisi

Dedication

To: *my parents, my siblings, my wife, and my children*

Table of Contents

Abstract	i
Acknowledgements	iii
Dedication	iv
List of Tables	viii
List of Figures	x
List of Abbreviations	xvi
1 Introduction to Thesis	1
1.1 Introduction	1
1.2 Basics of OFDM	5
1.3 Peak-to-Average Power Ratio (PAPR) in an OFDM System	9
1.4 Constant Envelope Signals and Systems	15
1.5 Literature Survey and Motivation	16
1.6 Thesis Objectives	22
1.7 Thesis Organization	23
1.8 Conclusions	24
2 Generic FFT- and DCT-OFDM System	25
2.1 Introduction	25
2.2 Baseband OFDM System	25
2.2.1 FFT-OFDM Signal	28
2.2.2 DCT-OFDM Signal	29
2.3 Guard Interval/Cyclic Prefix	30
2.3.1 FFT-OFDM System	30
2.3.2 DCT-OFDM System	34
2.4 PAPR of OFDM Signals	37
2.4.1 PAPR Statistics	37
2.4.2 Models of HPA and their effects	40
2.5 Conclusions	45

3	Constant Envelope DCT- and FFT-OFDM Systems with PM	46
3.1	Introduction	46
3.2	Signals in DCT- and FFT-OFDM Systems with PM	47
3.3	CE-OFDM Transmitter	47
3.4	CE-OFDM Receiver: Signal Detection and Performance	50
3.4.1	Phase Demodulator	51
3.4.2	OFDM Demodulator	53
3.4.3	BER Probability of CE-OFDM system	55
3.5	Performance of CE-OFDM system over Fading Channels	57
3.5.1	Frequency Non-Selective Fading Channel	57
3.5.2	BER performance of CE-OFDM system	58
3.5.3	Rayleigh Fading Channel	59
3.5.4	Rician Fading Channel	61
3.6	Numerical Results and Discussion	62
3.6.1	Performance in AWGN Channel	62
3.6.2	Performance over Fading Channels	66
3.7	CE-DCT- and DCT-OFDM Systems with TWTA Amplifier	73
3.8	Conclusions	76
4	Constant Envelope DCT- and FFT-OFDM Systems with FM^{4,5} . . .	77
4.1	Introduction	77
4.2	DCT- and FFT-OFDM Signals with FM	78
4.3	CE-OFDM Transmitter	78
4.4	CE-OFDM Receiver: Signal Detection and Performance	79
4.4.1	FM Demodulation	80
4.4.2	OFDM Demodulator	82
4.5	Performance of CE-OFDM System over Fading Channels	84
4.6	Numerical Results and Discussion	86
4.6.1	Performance in AWGN Channel	86
4.6.2	Performance in Fading Channels	93
4.6.3	Effect of TWTA Amplifier on System Performance	97
4.6.4	Comparison of PM and FM with DCT- and FFT-OFDM	99
4.7	Conclusions	101

5	Constant Envelope DCT- and FFT-OFDM Systems with CPM⁶	102
5.1	Introduction	102
5.2	Signals in DCT- and FFT-OFDM Systems with CPM	103
5.3	OFDM System with CPM: Transmitter	105
5.4	OFDM System with CPM: Receiver	107
5.4.1	Phase Demodulation and OFDM Demodulator	108
5.4.2	BER Probability of OFDM system with CPM	109
5.5	Performance over Fading Channels	111
5.6	Numerical Results and Discussion	112
5.6.1	Performance in AWGN Channel	112
5.6.2	Performance over Fading Channels	115
5.7	CE-DCT- and DCT-OFDM Systems with TWTA Amplifier	123
5.7.1	Comparison of BER of OFDM System with FM, PM and CPM	125
5.8	Conclusion	127
6	Constant Envelope DCT- and FFT-OFDM Systems with CPCPM⁷	128
6.1	Introduction	128
6.2	Signals in DCT- and FFT-OFDM Systems with CPCPM	129
6.3	OFDM System with CPCPM: Transmitter	130
6.4	OFDM Sytem with CPCPM: Receiver	132
6.4.1	Analysis over AWGN Channel	132
6.5	Performance over Fading Channels	135
6.6	Numerical Results and Discussion	136
6.6.1	Performance over AWGN Channel	136
6.6.2	Performance over Fading Channels	140
6.6.3	Effect of TWTA Amplifier on System Performance	147
6.6.4	Comparison of DCT- and FFT-OFDM system with FM, CPM, and CPCPM	148
6.7	Conclusion	150
7	Conclusions	151
7.1	Introduction	151
7.2	Summary of Contributions	151
7.3	Suggestion for Further Research	154
	Curriculum Vitae	170

List of Tables

Section		Page
3.1	Comparison of CE-DCT- and CE-FFT-OFDM systems (2-PAM mapper) at $P_b = 10^{-5}$ as a function of h_p	62
3.2	Comparison of CE-DCT- and CE-FFT-OFDM systems (4-PAM mapper) at $P_b = 10^{-5}$ as a function of h_p	63
3.3	Comparison of CE-DCT- and CE-FFT-OFDM systems (8-PAM mapper) at $P_b = 10^{-5}$ as a function of h_p	65
3.4	Comparison of probability of bit error performances of CE-DCT-OFDM system over AWGN, Rician and Rayleigh channels.	72
3.5	Comparison of probability of bit error performances of CE-FFT-OFDM system over AWGN, Rician and Rayleigh channels.	72
4.1	Comparison of CE-DCT- and CE-FFT-OFDM systems (2-PAM mapper) at $P_b = 10^{-5}$ as a function of h_f	87
4.2	Comparison of CE-DCT- and CE-FFT-OFDM systems (4-PAM mapper) at $P_b = 10^{-5}$ as a function of h_f	88
4.3	Comparison of CE-DCT- and CE-FFT-OFDM systems (8-PAM mapper) at $P_b = 10^{-5}$ as a function of h_f	89
4.4	Comparison of probability of bit error performances of CE-DCT-OFDM system ($M = 2, h_f = 0.7$) over AWGN, Rician ($K = 6$ dB) and Rayleigh channels	96
4.5	Comparison of probability of bit error performances of CE-FFT-OFDM system ($M = 2, h_f = 0.7$) over AWGN, Rician ($K = 6$ dB) and Rayleigh channels	96
5.1	Comparison of CE-DCT- and CE-FFT-OFDM systems (2-PAM mapper) at $P_b = 10^{-5}$ as a function of h	113
5.2	Comparison of CE-DCT- and CE-FFT-OFDM systems (4-PAM mapper) at $P_b = 10^{-5}$ as a function of h	114
5.3	Comparison of CE-DCT- and CE-FFT-OFDM systems (8-PAM mapper) at $P_b = 10^{-5}$ as a function of h	115
5.4	Comparison of probability of bit error performances of CE-DCT-OFDM system over AWGN, Rician and Rayleigh channels.	121
5.5	Comparison of probability of bit error performances of CE-FFT-OFDM system over AWGN, Rician and Rayleigh channels.	121
6.1	Comparison of CE-DCT- and CE-FFT-OFDM systems (2-PAM mapper) at $P_b = 10^{-5}$ as a function of $(h, 0.15)$	137

List of Tables

6.2	Comparison of CE-DCT- and CE-FFT-OFDM systems (4-PAM mapper) at $P_b = 10^{-5}$ as a function of $(h, 0.15)$	138
6.3	Comparison of CE-DCT- and CE-FFT-OFDM systems (8-PAM mapper) at $P_b = 10^{-5}$ as a function of $(h, 0.15)$	139
6.4	Comparison of CE-DCT- and CE-FFT-OFDM systems (2-PAM mapper) at $P_b = 10^{-5}$ as a function of $(1, w)$	140
6.5	Comparison of CE-DCT- and CE-FFT-OFDM systems (4-PAM mapper) at $P_b = 10^{-5}$ as a function of $(1, w)$	141
6.6	Comparison of CE-DCT- and CE-FFT-OFDM systems (8-PAM mapper) at $P_b = 10^{-5}$ as a function of $(1, w)$	142
6.7	Comparison of CE-DCT-OFDM system ($M = 2, (0.9, 0.15)$) over AWGN, Rician ($K = 6$ dB) and Rayleigh channels	142
6.8	Comparison of CE-FFT-OFDM system ($M = 2, (0.9, 0.15)$) over AWGN, Rician ($K = 6$ dB) and Rayleigh channels	147
7.1	E_b/N_0 required at $P_b = 10^{-5}$ for various modulations in an OFDM system (2-PAM mapper).	152
7.2	Power penalty required for various modulations in an OFDM system (2-PAM mapper) over fading channels at $P_b = 10^{-5}$	153
7.3	Expressions for bandwidth of transmitted signal in CE-OFDM system for various modulation.	154

List of Figures

Section		Page
1.1	Representation of a three-path wireless channel.	2
1.2	Power vs. delay profile for a three-path wireless channel.	2
1.3	Transfer function of a three-path wireless channel.	3
1.4	Spectrum of FFT-based OFDM signal with $N = 8$ and $X(n) = +1$ for all n	7
1.5	Spectrum of DCT-based OFDM signal with $N = 8$ and $X(n) = +1$ for all n	8
1.6	Block diagram for generation of OFDM signal.	8
1.7	DCT-OFDM signal as a function of time.	11
1.8	Real and imaginary parts of FFT-OFDM as a function of time	12
1.9	Instantaneous power of DCT-OFDM signal.	13
1.10	Instantaneous power of FFT-OFDM signal.	13
1.11	Transfer characteristics of typical HPA.	14
1.12	Block diagram of CE-OFDM system.	17
1.13	Instantaneous powers of signals in DCT-OFDM and CE-DCT-OFDM systems.	17
2.1	The generic block diagram of DCT- and FFT-OFDM baseband transceiver system.	26
2.2	Signal space diagrams for (a) 2-PAM and (b) 4-PAM mappers.	27
2.3	Discrete time signal at the output for MPAM mapper.	27
2.4	OFDM symbol with CP	31
2.5	Structure of OFDM demodulator using a bank of N correlators	32
2.6	OFDM symbol with symmetric extension.	34
2.7	Symmetries for (a) $x(k)$ and (b) $h(k)$ to convert linear convolution into a symmetric convolution.	36
2.8	CCDF of PAPR of an OFDM signal for $N = 32, 64, 128, 256, 512$, and 1024	39
2.9	CCDFs of PAPR of DCT- and FFT-OFDM signals for $N = 32$	39
2.10	AM/AM functions for SSPA (for $p = 3, 10$) and TWTA for $A_{sat} = 2$	42
2.11	AM/PM function for TWTA for $\alpha_\phi = \pi/12$ and $\beta_\phi = 0.25$	42
2.12	BER performance of DCT-OFDM (8-PSK, $N = 64$) system with SSPA for various values of IBO.	43
2.13	BER performance of DCT-OFDM (8-PSK, $N = 64$) system with TWTA for various values of IBO.	44
2.14	Efficiency (η_A) of Class A HPA as a function of IBO.	44
3.1	Transmitter and receiver structures for CE-OFDM system with PM	48
3.2	Ideal bandpass filter characteristic	50
3.3	Phasor diagram of $y(t)$	51

3.4	Structure of OFDM demodulator	54
3.5	Signal constellation of MPAM demapper	55
3.6	Probability density function of Rayleigh random variable as a function of σ	59
3.7	Probability density function for Rice random variable for $\sigma = 1$ and various values of a	60
3.8	Probability of bit error performances of CE-DCT- and CE-FFT-OFDM systems for (2-PAM mapper) over AWGN channel.	63
3.9	Probability of bit error performances of CE-DCT- and CE-FFT-OFDM systems for (4-PAM mapper) over AWGN channel.	64
3.10	Probability of bit error performances of CE-DCT- and CE-FFT-OFDM systems for (8-PAM mapper) over AWGN channel.	64
3.11	Probability of bit error performance of CE-DCT-OFDM system as a function of M for $h_p = 0.6$ over AWGN channel.	65
3.12	Probability of bit error performance of CE-FFT-OFDM system as a function of M for $h = 0.6$ over AWGN channel.	66
3.13	Probability of bit error performance of CE-DCT-OFDM system as a function of h_p and M over AWGN channel.	67
3.14	Probability of bit error performance of CE-FFT-OFDM system as a function of h_p and M over AWGN channel.	67
3.15	Comparison of analytical and simulation results for CE-DCT-OFDM system (4-PAM mapper) over AWGN channel.	68
3.16	Comparison of analytical and simulation results for CE-DCT-OFDM system (8-PAM mapper) over AWGN channel.	68
3.17	Probability of bit error performances of CE-DCT- and CE-FFT-OFDM systems (2-PAM mapper) over Rayleigh fading channel.	69
3.18	Probability of bit error performances of CE-DCT- and CE-FFT-OFDM systems (4-PAM mapper) over Rayleigh fading channel.	69
3.19	Probability of bit error performances of CE-DCT- and CE-FFT-OFDM systems (8-PAM mapper) over Rayleigh fading channel.	70
3.20	Probability of bit error performances of CE-DCT- and CE-FFT-OFDM systems (2-PAM mapper) over Rician fading channel ($K = 6$ dB).	71
3.21	Probability of bit error performances of CE-DCT- and CE-FFT-OFDM systems (4-PAM mapper) over Rician fading channel ($K = 6$ dB).	71
3.22	Probability of bit error performances of CE-DCT- and CE-FFT-OFDM systems (8-PAM mapper) over Rician fading channel ($K = 6$ dB).	72
3.23	Comparison of probability of bit error performances of CE-DCT-OFDM system (2-PAM mapper, $h_p = 1$) over AWGN, Rician ($K = 6$ dB) and Rayleigh channels.	73
3.24	Comparison of probability of bit error performances of CE-FFT-OFDM system (2-PAM mapper, $h_p = 1$) over AWGN, Rician ($K = 6$ dB) and Rayleigh channels as a function of SNR.	74
3.25	Probability of bit error performances of CE-DCT- and CE-FFT-OFDM systems (4-PAM mapper, $h_p = 0.5$) as function of Rice factor for Rician Channel.	74

3.26	Probability of bit error performances of CE-DCT-OFDM and performance of DCT-OFDM systems as a function of IBO for TWTA.	75
4.1	Transmitter and receiver structures for DCT- and FFT-OFDM systems with FM	80
4.2	Probability of bit error performances of CE-DCT- and CE-FFT-OFDM systems (2-PAM mapper) over AWGN channel.	87
4.3	Probability of bit error performances of CE-DCT- and CE-FFT-OFDM systems (4-PAM mapper) over AWGN channel.	88
4.4	Probability of bit error performances of CE-DCT- and CE-FFT-OFDM systems (8-PAM mapper) over AWGN channel.	89
4.5	Probability of bit error performance of CE-DCT-OFDM system as a function of M for $h_f = 0.6$ over AWGN channel.	90
4.6	Probability of bit error performance of CE-FFT-OFDM system as a function of M for $h_f = 0.6$ over AWGN channel.	91
4.7	Probability of bit error performance of CE-DCT-OFDM system as a function of h_f and M over AWGN channel.	91
4.8	Probability of bit error performance of CE-FFT-OFDM system as a function of h_f and M over AWGN channel.	92
4.9	Comparison of analytical and simulation results of BER for EC-DCT-OFDM system (4-PAM mapper) over AWGN channel.	92
4.10	Probability of bit error performances of CE-DCT- and CE-FFT-OFDM systems (2-PAM mapper) over Rayleigh fading channel.	93
4.11	Probability of bit error performances of CE-DCT- and CE-FFT-OFDM systems (4-PAM mapper) over Rayleigh fading channel.	94
4.12	Probability of bit error performances of CE-DCT- and CE-FFT-OFDM systems (8-PAM mapper) over Rayleigh fading channel.	94
4.13	Probability of bit error performances of CE-DCT- and CE-FFT-OFDM systems (2-PAM mapper) over Rician fading channel ($K = 6$ dB).	95
4.14	Probability of bit error performances of CE-DCT- and CE-FFT-OFDM systems (4-PAM mapper) over Rician fading channel ($K = 6$ dB).	95
4.15	Probability of bit error performances of CE-DCT- and CE-FFT-OFDM systems (8-PAM mapper) over Rician fading channel ($K = 6$ dB).	96
4.16	Comparison of probability of bit error performances of CE-DCT-OFDM system (2-PAM mapper, $h_f = 0.7$) over AWGN, Rician ($K = 6$ dB) and Rayleigh channels.	97
4.17	Comparison of probability of bit error performances of CE-FFT-OFDM system (2-PAM mapper, $h_f = 0.7$) over AWGN, Rician ($K = 6$ dB) and Rayleigh channels.	98
4.18	Probability of bit error performances of CE-DCT- and CE-FFT-OFDM systems (4-PAM mapper, $h_f = 0.5$) as a function of Rice factor for Rician Channel.	98
4.19	Probability of bit error performances of CE-DCT-OFDM and DCT-OFDM systems as a function of IBO for TWTA.	99

4.20	Probability of bit error performances of DCT-OFDM system (4-PAM mapper) with PM ($h_p = 0.6$) and FM ($h_f = 0.6$) over AWGN, Rician ($K = 6$ dB) and Rayleigh channels.	100
4.21	Probability of bit error performances of FFT-OFDM systems (4-PAM mapper) with PM ($h_p = 0.6$) and FM ($h_f = 0.6$) over AWGN, Rician ($K = 6$ dB) and Rayleigh channels.	100
5.1	Rectangular frequency pulse shaping function $f(t)$	104
5.2	Phase function $g(t)$ for rectangular frequency pulse function	104
5.3	Phase $\phi(t)$ in a CE-DCT-OFDM system (2-PAM mapper) with 8 subcarriers.	105
5.4	Transmitter and receiver structures of OFDM system with CPM	106
5.5	Probability of bit error performances of CE-DCT- and CE-FFT-OFDM systems (2-PAM mapper) over AWGN channel.	113
5.6	Probability of bit error performances of CE-DCT- and CE-FFT-OFDM systems (4-PAM mapper) over AWGN channel.	114
5.7	Probability of bit error performances of CE-DCT- and CE-FFT-OFDM systems (8-PAM mapper) over AWGN channel.	115
5.8	Probability of bit error performance of CE-DCT-OFDM system as a function of M for $h = 0.6$ over AWGN channel.	116
5.9	Probability of bit error performance of CE-FFT-OFDM system as a function of M for $h = 0.6$ over AWGN channel.	116
5.10	Probability of bit error performance of CE-DCT-OFDM system as a function of h and M over AWGN channel.	117
5.11	Probability of bit error performance of and CE-FFT-OFDM system as a function of h and M over AWGN channel.	117
5.12	Comparison of analytical and simulation results for CE-DCT-OFDM system (2-PAM mapper) over AWGN channel.	118
5.13	Comparison of analytical and simulation results for CE-DCT-OFDM system (4-PAM mapper) over AWGN channel.	118
5.14	Probability of bit error performances of CE-DCT- and CE-FFT-OFDM systems (2-PAM mapper) over Rayleigh fading channel.	119
5.15	Probability of bit error performances of CE-DCT- and CE-FFT-OFDM systems (4-PAM mapper) over Rayleigh fading channel.	120
5.16	Probability of bit error performances of CE-DCT- and CE-FFT-OFDM systems (8-PAM mapper) over Rayleigh fading channel.	120
5.17	Probability of bit error performances of CE-DCT- and CE-FFT-OFDM systems (2-PAM mapper) over Rician fading channel ($K = 6$ dB).	121
5.18	Probability of bit error performances of CE-DCT- and CE-FFT-OFDM systems (4-PAM mapper) over Rician fading channel ($K = 6$ dB).	122
5.19	Probability of bit error performances of CE-DCT- and CE-FFT-OFDM systems (8-PAM mapper) over Rician fading channel ($K = 6$ dB).	122
5.20	Comparison of probability of bit error performances of CE-DCT-OFDM system (2-PAM mapper, $h = 0.7$) over AWGN, Rician ($K = 6$ dB) and Rayleigh channels.	123

5.21	Comparison of probability of bit error performances of CE-FFT-OFDM system (2-PAM mapper, $h = 0.7$) over AWGN, Rician ($K = 6$ dB) and Rayleigh channels.	124
5.22	Probability of bit error performances of CE-DCT- and CE-FFT-OFDM systems as function of Rice factor.	124
5.23	Probability of bit error performances of CE-DCT- and of DCT-OFDM systems as a function of IBO for TWTA model.	125
5.24	Comparison of probability of bit error performances of DCT-OFDM system (4-PAM) with PM ($h_p = 0.6$), FM ($h_f = 0.6$) and CPM ($h = 0.6$) over AWGN, Rician ($K = 6$ dB) and Rayleigh channels.	126
5.25	Comparison of probability of bit error performances of FFT-OFDM system (4-PAM) with PM ($h_p = 0.6$), FM ($h_f = 0.6$) and CPM ($h = 0.6$) over AWGN, Rician ($K = 6$ dB) and Rayleigh channels.	126
6.1	Phase and frequency as a function of time for $x(k) = \pm 1$	130
6.2	Block diagram of CE-OFDM system with CPCPM	131
6.3	Probability of bit error performances of CE-DCT- and CE-FFT-OFDM systems (2-PAM mapper) as a function of $(h, 0.15)$ over AWGN channel.	136
6.4	Probability of bit error performances of CE-DCT- and CE-FFT-OFDM systems (4-PAM mapper) as a function of $(h, 0.15)$ over AWGN channel.	137
6.5	Probability of bit error performances of CE-DCT- and CE-FFT-OFDM systems (8-PAM mapper) as a function of $(h, 0.15)$ over AWGN channel.	138
6.6	Probability of bit error performances of CE-DCT- and CE-FFT-OFDM systems (2-PAM mapper) as a function of $(1, w)$ over AWGN channel.	139
6.7	Probability of bit error performances of CE-DCT- and CE-FFT-OFDM systems (4-PAM mapper) as a function of $(1, w)$ over AWGN channel.	140
6.8	Probability of bit error performances of CE-DCT- and CE-FFT-OFDM systems (8-PAM mapper) as a function of $(1, w)$ over AWGN channel.	141
6.9	Comparison of analytical and simulation results of BER for CE-DCT-OFDM system (4-PAM mapper) over AWGN channel.	142
6.10	Probability of bit error performances of CE-DCT- and CE-FFT-OFDM systems (2-PAM mapper) over Rayleigh fading channel.	143
6.11	Probability of bit error performances of CE-DCT- and CE-FFT-OFDM systems (4-PAM mapper) over Rayleigh fading channel.	143
6.12	Probability of bit error performances of CE-DCT- and CE-FFT-OFDM systems (8-PAM mapper) over Rayleigh fading channel.	144
6.13	Probability of bit error performances of CE-DCT- and CE-FFT-OFDM systems (2-PAM mapper) over Rician fading channel ($K = 6$ dB).	144
6.14	Probability of bit error performances of CE-DCT- and CE-FFT-OFDM systems (4-PAM mapper) over Rician fading channel ($K = 6$ dB).	145
6.15	Probability of bit error performances of CE-DCT- and CE-FFT-OFDM systems (8-PAM mapper) over Rician fading channel ($K = 6$ dB).	145
6.16	Comparison of probability of bit error performances of CE-DCT-OFDM system ($M = 2, (0.9, 0.15)$) over AWGN, Rician ($K = 6$ dB) and Rayleigh channels.	146

6.17	Comparison of probability of bit error performances of CE-FFT-OFDM system ($M = 2, (0.9, 0.15)$) over AWGN, Rician ($K = 6$ dB) and Rayleigh channels.	146
6.18	Probability of bit error performances of CE-DCT- and CE-FFT-OFDM systems (4-PAM mapper, $(0.9, 0.2)$) as a function of Rice factor.	147
6.19	Probability of bit error performances of CE-DCT-OFDM and DCT-OFDM systems as a function of IBO for TWTA.	148
6.20	Probability of bit error performances of DCT-OFDM system (4-PAM mapper) with CPCM ($h = 0.8, w = 0.1$), CPM ($h = 0.6$) and FM ($h_f = 0.6$) over AWGN, Rician ($K = 6$ dB) and Rayleigh channels.	149
6.21	Probability of bit error performances of FFT-OFDM systems (4-PAM mapper) with CPCM ($h = 0.8, w = 0.1$), CPM ($h = 0.6$) and FM ($h_f = 0.6$) over AWGN, Rician ($K = 6$ dB) and Rayleigh channels.	150
7.1	Bandwidth as a function of modulation parameters ($N = 64, T = 1$) for various angle modulation in an OFDM system.	155
7.2	Spectral efficiency as a function of modulation parameters (8PAM mapper, $T = 1$, and $N = 64$) for various angle modulation in an OFDM system.	155

List of Abbreviations

WLAN	Wireless Local Area Network
MCM	Multicarrier Modulation
OFDM	Orthogonal Frequency Division Multiplexing
ISI	Inter-Symbol Interference
ICI	Inter-Carrier Interference
FFT	Fast Fourier Transform
IFFT	Inverse Fast Fourier Transform
DCT	Discrete Cosine Transform
IDCT	Inverse Discrete Cosine Transform
PAPR	Peak-to-Average-Power Ratio
PM	Phase Modulation
FM	Frequency Modulation
CPM	Continuous Phase Modulation
CPCM	Continuous Phase Chirp Modulation
CE	Constant Envelope
PAM	Pulse Amplitude Modulation
MPAM	M-ary Pulse Amplitude Modulation
CFO	Carrier Frequency Offset
PSK	Phase Shift Keying
MPSK	M-ary Phase Shift Keying
SSPA	Solid State Power Amplifier
TWTA	Traveling-Wave Tube Amplifier
PLC	Power Line Communication

QAM	Quadrature Amplitude Modulation
MQAM	M-ary Quadrature Amplitude Modulation
JPEG	Joint Photographic Experts Group
MPEG	Moving Picture Experts Group
BPSK	Binary Phase Shift Keying
HPA	High Power Amplifier
ASK	Amplitude Shift Keying
PTS	Partial Transmit Sequence
LS	Least Square
MMSE	Minimum Mean Square Error
SNR	Signal-to-Noise Ratio
BER	Bit Error Rate
AM	Amplitude Modulation
RMS	Root Mean Square
BPF	Band Pass Filter
LPF	Low Pass Filter
PSD	Power Spectral Density
LOS	Line of Sight
pdf	Probability Density Function
PDF	Probability Distribution Function
S/P	Serial-to-Parallel Converter
P/S	Parallel-to-Serial Converter
CFO	Carrier Frequency Offset

CSI	Channel State Information
AWGN	Additive white Gaussian Noise
ML	Maximum Likelihood
D/A	Digital-to-Analog Converter
A/D	Analog -to- Digital Converter
CCDF	Complementary Cumulative Distribution Function
ICT	Information and Communication Technologies
IEEE	Institute of Electrical and Electronics Engineers
i.i.d	independent and identically distributed
SPS	Symmetric Periodic Sequence
QPSK	Quadrature Phase Shift Keying
IBO	Input Power Backoff

Chapter 1

Introduction to Thesis

1.1 Introduction

The search for better ways of living has been instrumental in advancing human civilization. Over the last few decades, wireless communication has experienced rapid development and has become indispensable to modern civilization. For instance, the latest generations of cellular systems, data networks, Wireless Local Area Networks (WLANs), home and personal networks are few examples. Between 2009 and 2014, global mobile traffic increased nearly 66 times with an annual growth rate of 131 percent [1]. The communication system design in these systems and networks has been always dominated by the behavior of channel [2, 3]. Over a typical wireless channel, multipath propagation occurs due to reflections of the transmitted signal by objects and obstacles in the channel environment. Figure 1.1 illustrates a link with three reflecting paths between two devices located at points A and B. Due to the relative mobility of the devices these points and the possibility that the reflecting objects in the environment are also mobile, the wireless channel environment will be continuously changing over time. The channel is analytically described by its impulse response in time-domain or, alternatively, in the frequency-domain, by its transfer function. In Figures 1.2 and 1.3 are shown characteristics of a three-path wireless channel between points A and B. The profile of the channel shows that each path has its own associated delay and power. Over the first path the transmitted signal arrives at the receiver $1 \mu s$ after it is transmitted and over the third path the signal arrives with a $11 \mu s$ delay.

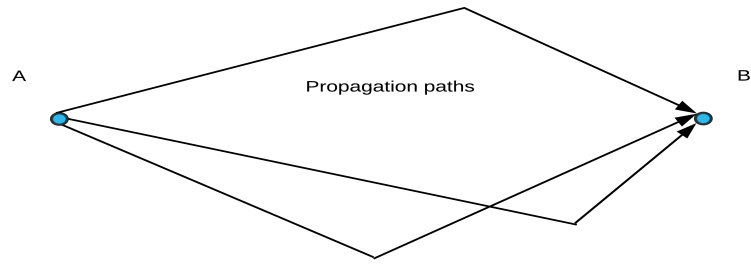


Figure 1.1: Representation of a three-path wireless channel.

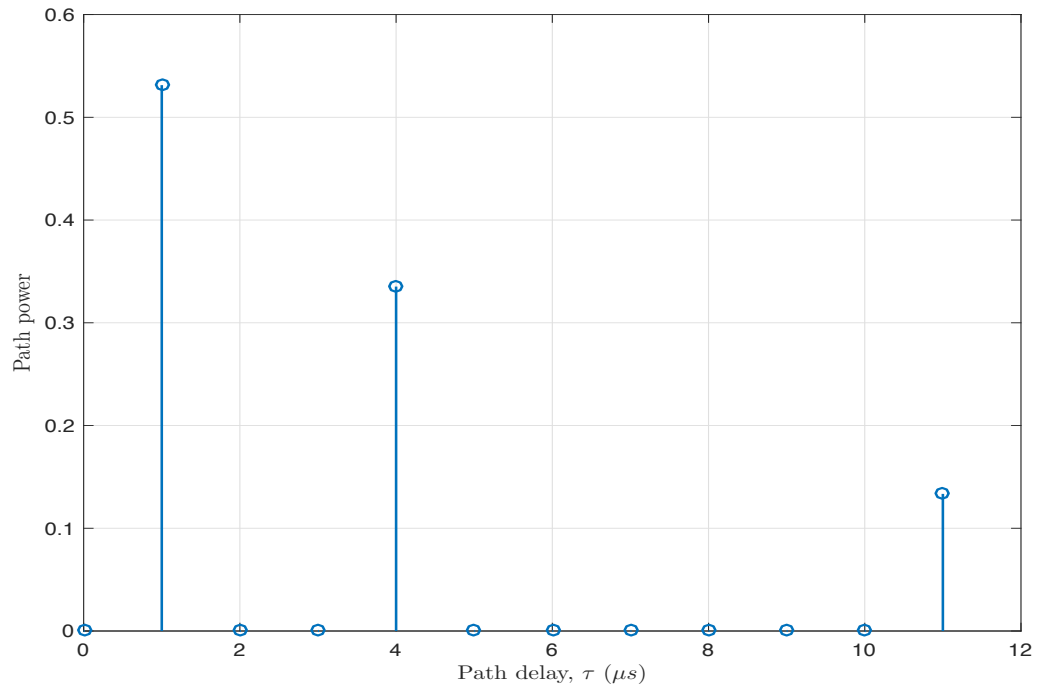


Figure 1.2: Power vs. delay profile for a three-path wireless channel.

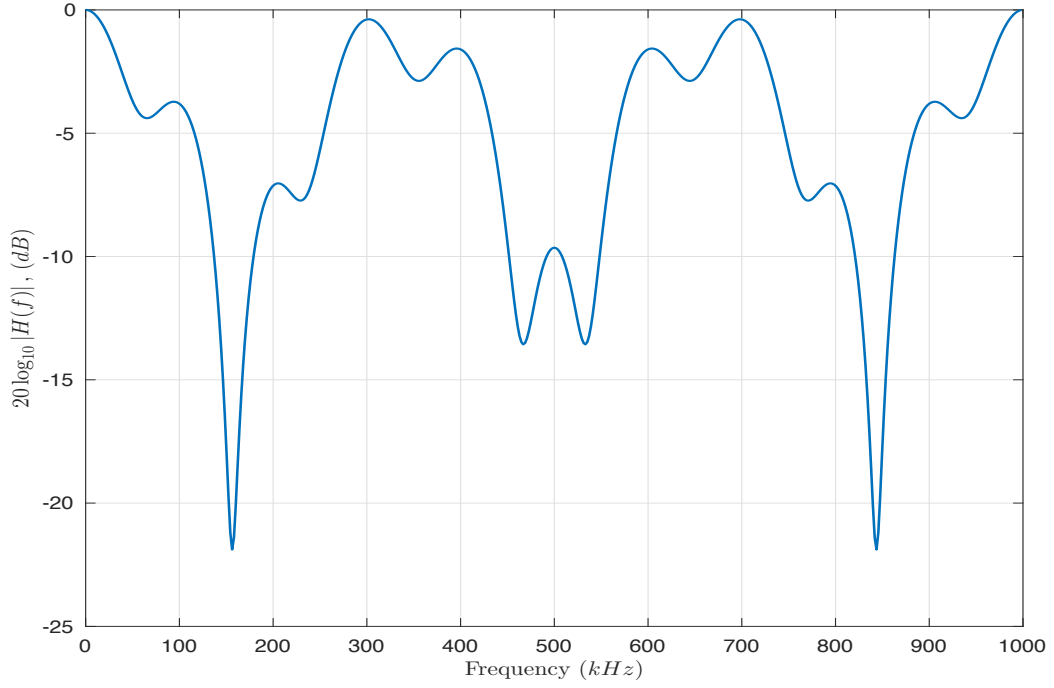


Figure 1.3: Transfer function of a three-path wireless channel.

In a single carrier system, the symbols are transmitted serially and the transmitted signal can be written as [4]:

$$x(t) = \sum_j X_j q(t - (j - 1)T_s) \quad (1.1)$$

where X_j are data symbols obtained from an arbitrary modulation constellation, $q(t)$ is the transmit pulse shape and T_s is the data symbol duration. The received signal can be written as [4]:

$$y(t) = x(t) * h(\tau; t) + n(t) = \int_{-\infty}^{\infty} h(\tau; t) s(t - \tau) d\tau + n(t) \quad (1.2)$$

where $h(\tau; t)$ is the response of the channel at time t due to an impulse applied at time $(t - \tau)$ and $n(t)$ is the additive noise.

For a 3-path channel shown in Figure 1.1, the time dispersion causes spreading of the modulation symbols in time domain, also known as the delay spread, and thus inter-

symbol interference (ISI) is introduced. This is reflected in frequency domain, by the inverse relationship between bandwidth and delay spread. Since the delay spread are distinct, the frequency response of the channel, $H(f)$, will exhibit power fluctuation as shown in Figure 1.3. Such fluctuation in the frequency domain will distort the received signal. Therefore, dispersion in the time domain leads to frequency-selectivity in the frequency domain. The coherence bandwidth of the channel, B_c , can be determined by the reciprocal of maximum delay spread, τ_{max} . That is, $B_c = 1/\tau_{max}$. If bandwidth of the transmitted signal is greater than coherence bandwidth of the channel, the channel is said to be frequency-selective and the signal is severely distorted by the channel. However, if bandwidth of the transmitted signal is smaller than the coherence bandwidth of the channel, the channel is said to be frequency-nonselective [4]. For a single carrier system the coherence bandwidth of the channel is smaller than the modulation bandwidth and, therefore, the frequency selectivity effect of the channel cannot be ignored. For example consider a transmitted signal $s(t)$ given by (1.1) over a 1 MHz channel shown in Figure 1.2. The signal bandwidth is nearly equal $1/T_s$ Hz. Therefore, if $s(t)$ with a bandwidth of 1 MHz, $T_s = 1/(1 \times 10^6) = 1\mu s$, is transmitted over a channel with $\tau_{max} = 11\mu s$, ISI spans over, 11 symbols (τ_{max}/T_s). Such severe ISI must be corrected at the receiver to provide reliable communication. Thus, in a single-carrier system, equalization is essential to compensate for this ISI. There exists a number of techniques [5, 6, 7] for equalization and they require estimation of channel by transmitting training sequence known to the receiver. These estimation techniques vary in complexity, and accuracy [8, 9] and require long training times with added problems of convergence due to time-varying nature of the channel.

Multicarrier Modulation (MCM) is a wideband technique that is designed to overcome the problems of transmitting information using a single carrier system over multipath propagation environment. It has been demonstrated that such an MCM technique is asymptotically optimum for high data rate transmission [10, 11]. Furthermore, MCM is more robust than a single carrier system to severe multipath fading over the channel, which is typical over a mobile wireless channel [12, 13]. In an MCM system the input bit stream is converted into many parallel low data rate substreams that are transmitted using different orthogonal subcarriers. Since symbol duration on each substream is increased it makes the system less sensitive to channel delay spread. Also, MCM still

maintains the original transmission rate and the bandwidth of each subchannel is much less than the total bandwidth occupied by the signal and consequently has less coherence bandwidth of the channel which mitigates the ill effects of multipath fading to a large extent. In an MCM system, since several streams of data are transmitted simultaneously, a fade occurring over the channel is spread out over many parallel symbols and each subcarrier experiences flat fading instead of frequency selective fading, thereby making equalization simple and of reasonable complexity [14, 15, 16]. Moreover, when a heavy fade occurs over a certain subcarrier, only part of the symbol under the affected subcarrier will be destroyed while others will not be affected.

Orthogonal Frequency Division Multiplexing (OFDM) is a subclass of Multicarrier Modulation in which subcarriers in the system are chosen to be overlapping and orthogonal to each other. Such a system is highly bandwidth efficient due to overlapping spectra of adjacent subcarriers. The extraction of data over each individual subcarrier is still possible as long as the orthogonality condition is maintained. However, orthogonality among the subcarriers is destroyed due to ISI introduced over the multipath channel. To eliminate the ISI almost completely, a guard time is introduced for each transmitted OFDM block. The guard time is chosen larger than the expected maximum delay spread of the channel, τ_{max} , to overcome the effects of ISI. Consider an OFDM system with N number of subcarriers, then the symbol period is given by $T = NT_s$. If $N = 250$ is chosen in the system, the symbol period is $T = NT_s = 250\mu s$, which is nearly 23 times that of $\tau_{max}=11 \mu s$. Therefore, ISI can be eliminated by using a guard time greater than $\tau_{max}=11 \mu s$ in this example.

1.2 Basics of OFDM

The OFDM system was first proposed by Chang in 1966 [17] to mitigate the effects of multipath channel without losing data rate, for a bandlimited channel. Subsequently, Saltzberg analysed the performance of such a system [18], and concluded that "the strategy of designing an efficient parallel system should concentrate more on reducing crosstalk between adjacent channels than on perfecting the individual channels themselves, since the distortions due to crosstalk tend to dominate". A major contribution to OFDM was presented by Weinstein and Ebert [19], who showed that the system can be implemented

using Fast Fourier Transform (FFT) technique for modulation of data symbols. However, such a system with FFT suffered from ISI problems. Another important contribution was due to Peled and Ruiz [20], who introduced the concept of cyclic prefix (CP) to overcome the problem of the ISI in an OFDM systems. OFDM has been adopted in several communications standards such as IEEE 802.11a/g/n [21, 22, 23], HIPERLAN/2 [24], IEEE 802.16a/d/e [25, 26] and IEEE 802.20 [27]. In all these standards FFT-based OFDM system is used [28, 29, 30, 31]. More recently, there has been growing interest in DCT-based OFDM system due to its attractive properties [32]-[49].

OFDM signaling consists of a set of orthogonal subcarriers that are independently modulated by data. The OFDM signal is the sum of these modulated subcarriers and it can be expressed as:

$$x(t) = \sum_j \sum_{n=0}^{N-1} X_j(n) \varphi_n(t - (j-1)T), \quad (j-1)T \leq t \leq (j)T \quad (1.3)$$

In (1.3), N is the number of OFDM subcarriers that are transmitted during the j^{th} block. The data symbols obtained from an arbitrary modulation constellation, $(X_j(0), \dots, X_j(N-1))$, modulate the N OFDM subcarrier, $(\varphi_0(t), \dots, \varphi_{N-1}(t))$, over the j^{th} signaling interval. T is the OFDM symbol period and the subcarriers meet the orthogonality condition. That is,

$$\int_0^T \varphi_n(t) \varphi_k^*(t) dt = \begin{cases} 1 & n = k \\ 0 & otherwise \end{cases} \quad (1.4)$$

In an FFT-based OFDM system, complex exponential functions are used as orthogonal subcarriers and are given by:

$$\varphi_n(t) = \sqrt{\frac{1}{T}} e^{j2\pi f_n t}, \quad 0 \leq t < T, \quad n = 0, 1, \dots, N-1 \quad (1.5)$$

where the frequency of the n^{th} subcarrier is $f_n = n/T$ Hz and the subcarrier spacing required to achieve orthogonality is given by $1/T$ Hz.

In a DCT-based OFDM system, cosinusoidal functions are used as orthogonal subcarriers

and are given by:

$$\varphi_n(t) = \sqrt{\frac{2}{T}} \cos(2\pi f_n t), 0 \leq t < T, n = 0, 1, \dots, N-1 \quad (1.6)$$

where the frequency of the n^{th} subcarrier is $f_n = n/2T$ Hz and the subcarrier spacing required to achieve orthogonality is given by $1/2T$ Hz.

The spectra of FFT- and DCT-based OFDM signals are shown in Figure 1.4 and 1.5, respectively. It is noted that at the n^{th} subcarrier frequency contributions due to all subcarriers except the n^{th} subcarrier are zero. Also it is noted that subcarriers overlap and therefore the system is spectrally efficient.

A block diagram for generation of OFDM signal is shown in Figure 1.6. A high rate serial data stream is converted into many low-rate parallel data streams. These parallel data streams are then mapped to modulation symbols, for example using an MPAM mapper, which are then modulated onto the orthogonal subcarriers. The sum of the modulated subcarriers represents the transmitted OFDM signal.

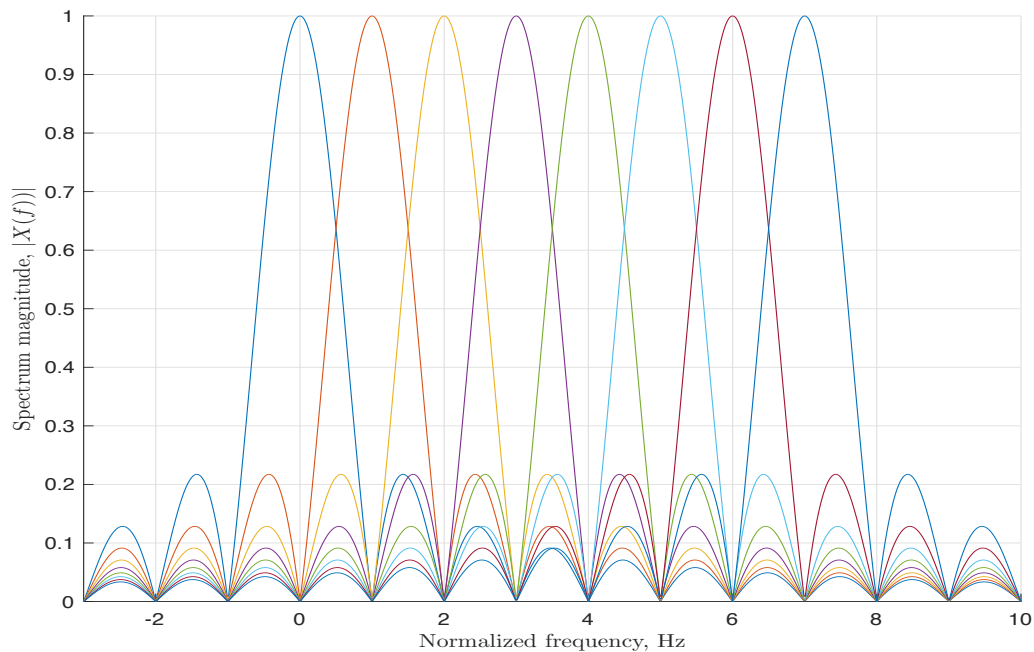


Figure 1.4: Spectrum of FFT-based OFDM signal with $N = 8$ and $X(n) = +1$ for all n .

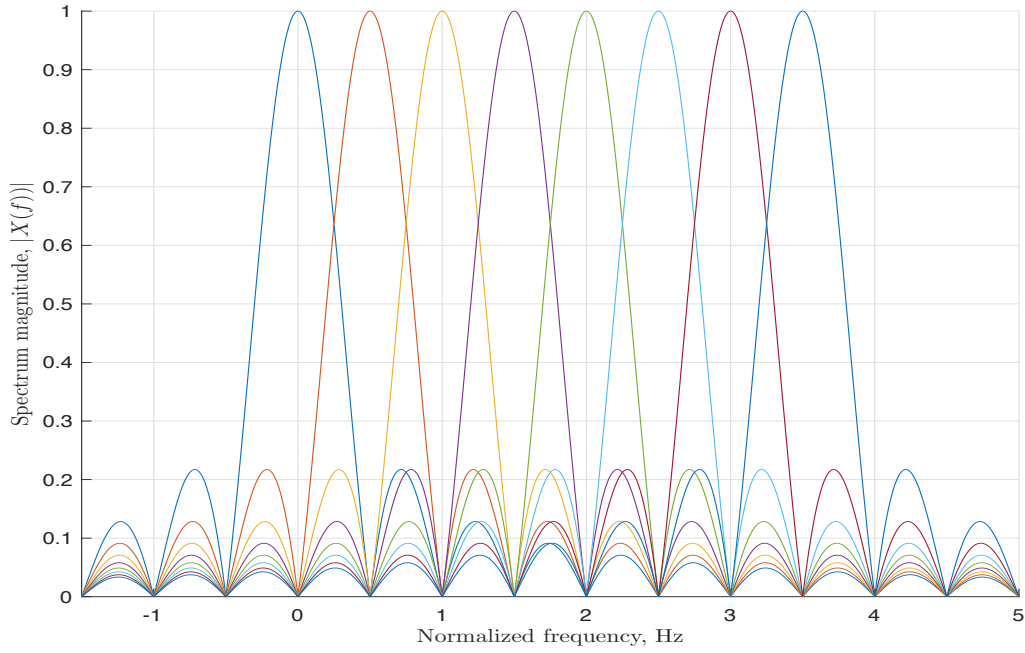


Figure 1.5: Spectrum of DCT-based OFDM signal with $N = 8$ and $X(n) = +1$ for all n .

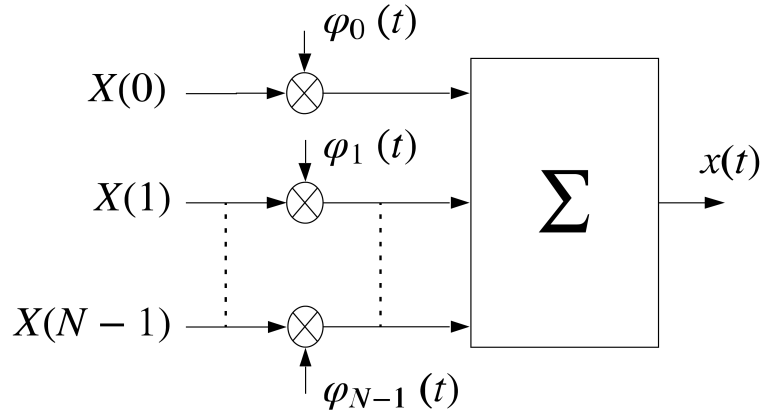


Figure 1.6: Block diagram for generation of OFDM signal.

The advantages of DCT-based OFDM system over FFT-based OFDM system are:

1. In DCT-based OFDM system, the set of basis functions is well-known to have excellent spectral compaction and energy concentration properties. Moreover, the

system has better frequency-selective filter bank compared to that in an FFT-based system. As a result, the channel estimation and also the system performance can be improved in noisy environments [33, 37].

2. Using IDCT for modulation and DCT for demodulation in a DCT-based OFDM system results in better integrated system with reduced overall implementation cost [33, 37]. The DCT is widely adopted in image/video coding standards (e.g. JPEG, MPEG, H.261 [50, 51]).
3. The DCT uses real arithmetic compared to the complex arithmetic in FFT. This reduces the signal processing complexity and power consumption in the system, especially when an MPAM mapper is used [33, 37].
4. In the presence of frequency offset in an OFDM system, due to the energy-compaction property of DCT, the ICI coefficients in DCT-based OFDM system are concentrated around the main coefficient. As a result, the system is robust to Carrier Frequency Offset (CFO) [33, 44].
5. When modulation symbols are real-valued, the bandwidth of a DCT-based OFDM system is half the bandwidth of a corresponding FFT-based OFDM system [38].

The disadvantage of DCT-based OFDM system compared to an FFT-based OFDM system is the additional prefilter needed at the receiver to satisfy the symmetric channel impulse response constraint for short channels. For long channels, an FFT-OFDM system also requires a prefilter to shorten the channel [33, 37]. From now onwards DCT- and FFT-based OFDM systems would be referred to as DCT-OFDM and FFT-OFDM systems, respectively.

1.3 Peak-to-Average Power Ratio (PAPR) in an OFDM System

The transmitted OFDM waveform has high amplitude fluctuations caused by the summation of several modulated sinusoids, resulting in high values of PAPR. Using (1.5), in

(1.3), the FFT-OFDM signal can be written as:

$$x_{FFT}(t) = \sum_{n=0}^{N-1} X_{FFT}(n) e^{j2\pi nt/T}, 0 \leq t < T, \quad (1.7)$$

where the scaled data symbols $X_{FFT}(n)$ are chosen from an M -point signal constellation such as MPSK, MQAM, or MPAM, N is the number of subcarriers and T is the duration of the OFDM symbol. It is noted that the suffix j in (1.3) has been dropped for convenience. The signal can be written as:

$$x_{FFT}(t) = \sum_{n=0}^{N-1} \{\Re[X_{FFT}(n)] + j\Im[X_{FFT}(n)]\} * \{\cos(2\pi nt/T) + j\sin(2\pi nt/T)\} \quad (1.8)$$

The real and imaginary parts of $x_{FFT}(t)$ are:

$$\Re[x_{FFT}(t)] = \sum_{n=0}^{N-1} \Re[X_{FFT}(n)]\cos(2\pi nt/T) - \Im[X_{FFT}(n)]\sin(2\pi nt/T) \quad (1.9)$$

and

$$\Im[x_{FFT}(t)] = \sum_{n=0}^{N-1} \Im[X_{FFT}(n)]\cos(2\pi nt/T) + \Re[X_{FFT}(n)]\sin(2\pi nt/T) \quad (1.10)$$

Similarly using the basis functions in (1.6), the DCT-OFDM signal can be written as:

$$x_{DCT}(t) = \sum_{n=0}^{N-1} X_{DCT}(n) \cos(\pi nt/T), 0 \leq t \leq T \quad (1.11)$$

The signal can be written as:

$$x_{DCT}(t) = \sum_{n=0}^{N-1} \{\Re[X_{DCT}(n)] + j\Im[X_{DCT}(n)]\} * \{\cos(\pi nt/T)\} \quad (1.12)$$

The real and imaginary parts of the signal are:

$$\Re[x_{DCT}(t)] = \sum_{n=0}^{N-1} \Re[X_{DCT}(n)] \cos(\pi n t / T) \quad (1.13)$$

and

$$\Im[x_{DCT}(t)] = \sum_{n=0}^{N-1} \Im[X_{DCT}(n)] \cos(\pi n t / T) \quad (1.14)$$

Figures 1.7 and 1.8 show plots of DCT-OFDM and FFT-OFDM signals, for $N = 16$ and $X(n) \in \{\pm 1\}$ (BPSK signal constellation), respectively. It is observed that the amplitude of OFDM signals fluctuates over an expansive range of values.

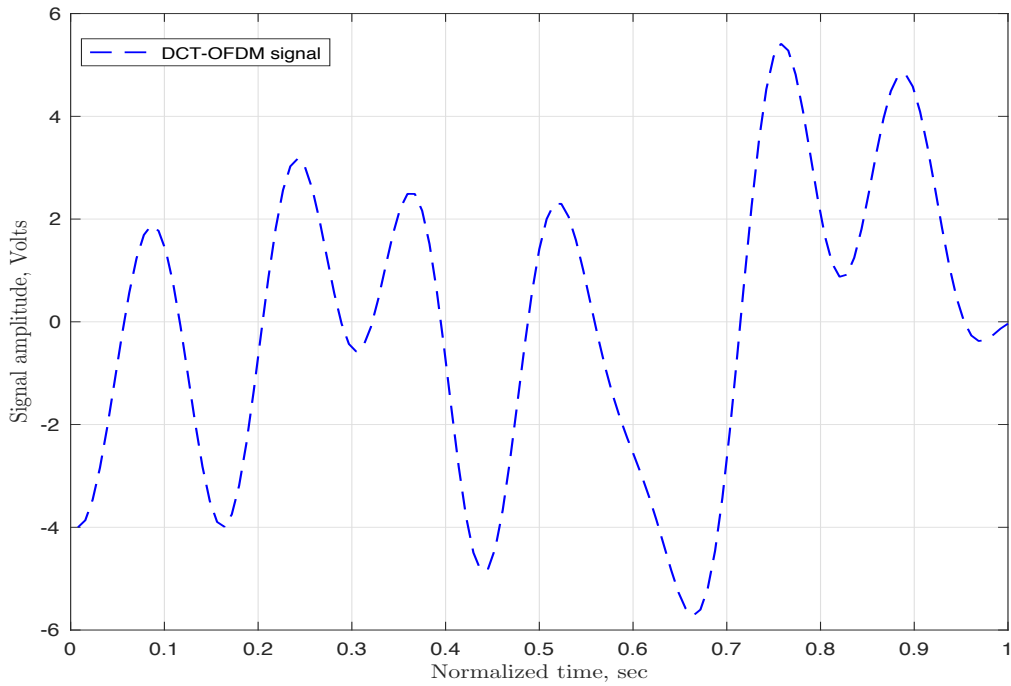


Figure 1.7: DCT-OFDM signal as a function of time.

The instantaneous signal powers of DCT-OFDM and FFT-OFDM signals are plotted in Figures 1.9 and 1.10, respectively. The ratio of the peak power and the average power of the signals in these figures are $10\log_{10}(4.058) = 6.1 \text{ dB}$ and $10\log_{10}(4.279) = 6.3 \text{ dB}$, respectively. It is noted that in these OFDM signals the peak power is nearly 4 times that of the average power. In general, the transmitted OFDM signals have high PAPR and, therefore a HPA with a large linear range is required in the system at the front end of the

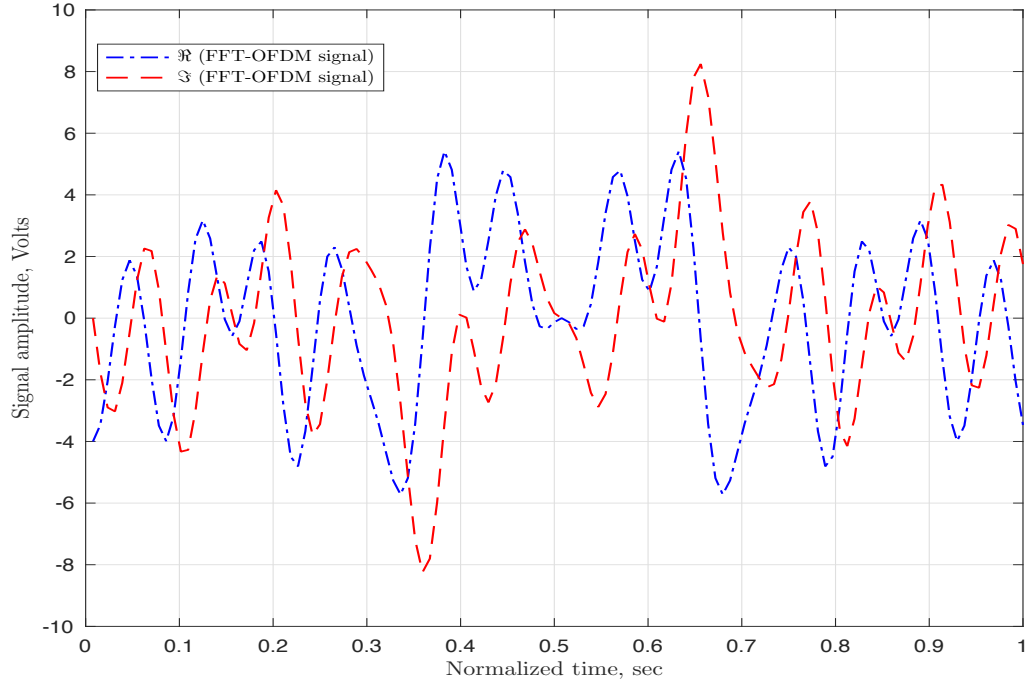


Figure 1.8: Real and imaginary parts of FFT-OFDM as a function of time .

transmitter; otherwise the transmitted OFDM signal will be nonlinearly distorted which results in a loss of subcarrier orthogonality and hence turn degrades the performance of the system. The typical transfer characteristics of a HPA is shown in Figure 1.11 and consists of a linear region followed by a nonlinear region leading to the maximum output level. It is noted that the HPA has limited linear region, beyond which it saturates to the maximum output level. In the linear range the output power is equal to the input power multiplied by a gain factor, but as the input power increases beyond the linear range, the output power saturates.

The most efficient operating point is at the saturation point. However, for signals, with large PAPR the operating point must be moved to the left for linear amplification. Therefore, the average input power level must be decreased. This method of decreasing the input power level is referred to as the input power backoff (IBO). In order to maintain the peak input power level of the signal less they as equal to at the saturation level, the IBO must be equal to the value of PAPR of the signal. It is noted that the HPA efficiency is reduced significantly with an increase in the value of IBO. For example, the required IBO for the DCT-OFDM signal shown in Figure 1.9 is 6.1 dB . At this value of backoff,

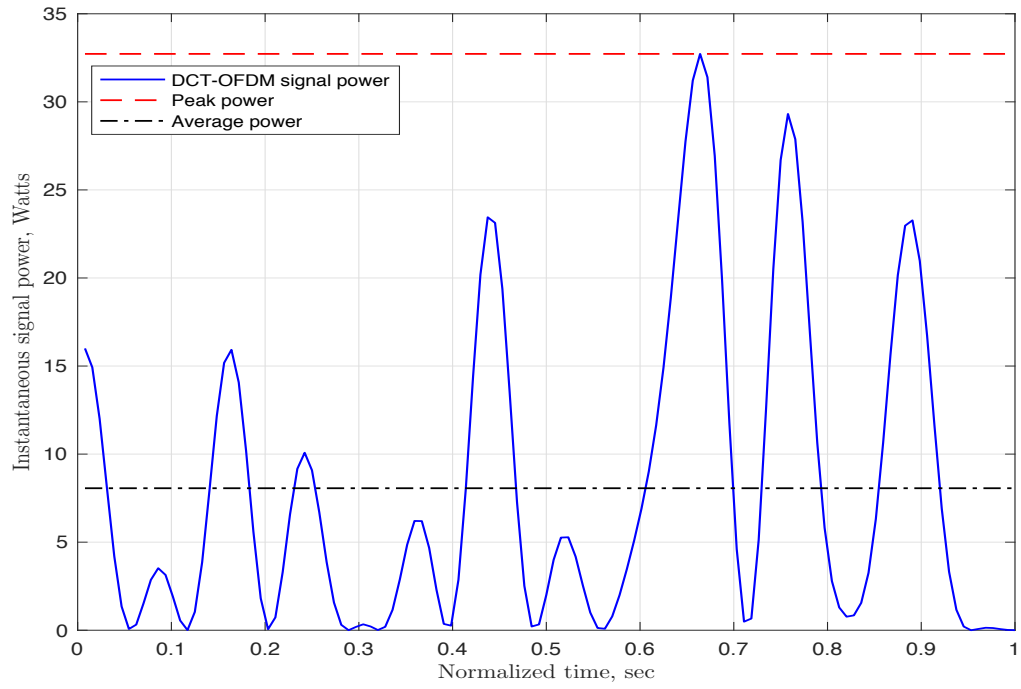


Figure 1.9: Instantaneous power of DCT-OFDM signal.

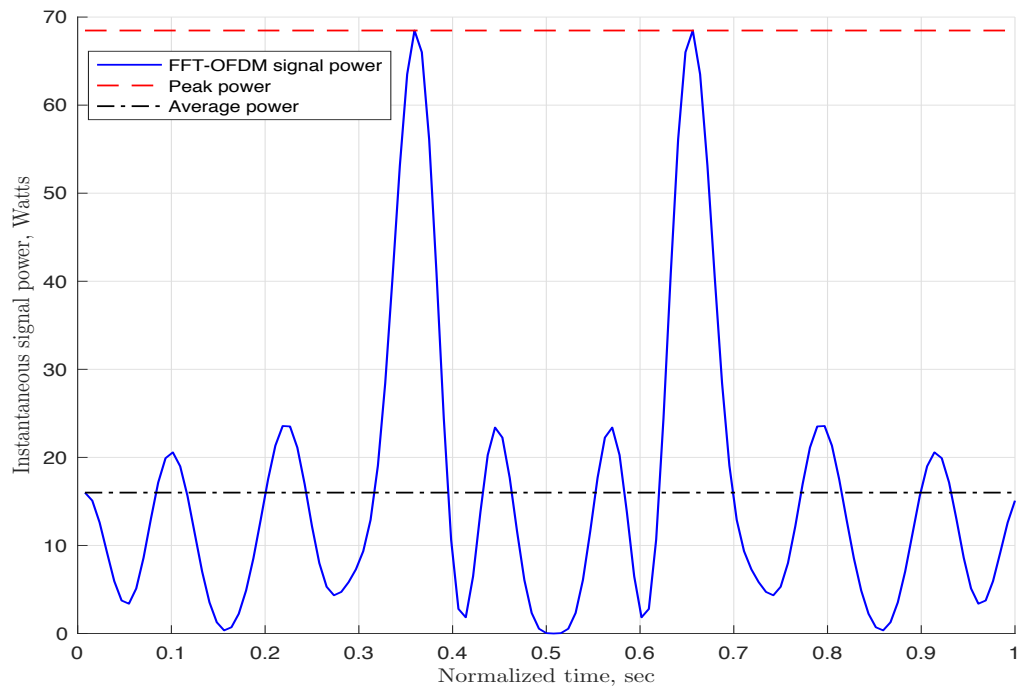


Figure 1.10: Instantaneous power of FFT-OFDM signal.

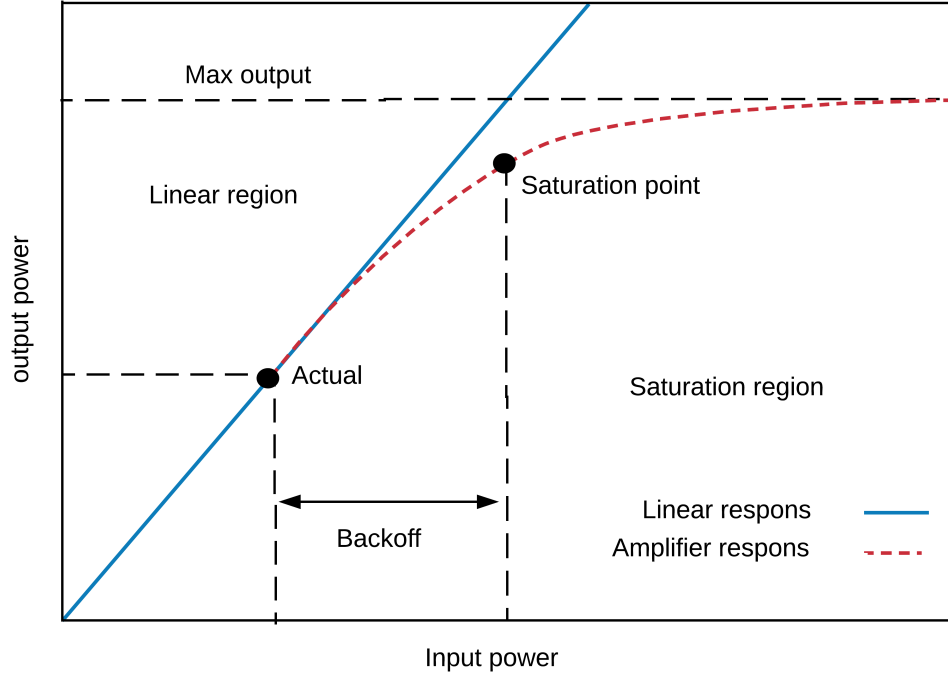


Figure 1.11: Transfer characteristics of typical HPA.

the efficiency of a Class A high power amplifier is $\frac{0.5}{10^{6/10}} \times 100 = 12.3 \%$ compared to 50 % with zero IBO [52, 53]. In general, the high PAPR of OFDM signals requires careful consideration particularly in the context of reducing energy costs in the overall system design, as HPA is typically an integral part of the system. A major source for reducing energy costs is to increase the efficiency of the HPA. However, this efficiency is directly related to PAPR of the input OFDM signal. The problem becomes serious in OFDM transmission as it is applied in many wireless standards. The PAPR problem thus prevents OFDM from being adopted in the uplink communication standards, and, besides power efficiency, it can also place severe constraints on the output power and hence the coverage area in the downlink.

1.4 Constant Envelope Signals and Systems

The general expression for Constant Envelope (CE) baseband signal can be written as:

$$s(t) = A_c e^{j\phi(t)} \quad (1.15)$$

where A_c is the signal amplitude and $\phi(t)$ is the information carrying phase. The instantaneous and the average power of the signal in (1.15) are the same. Therefore, the PAPR of the signal is 0 dB. The benefit of such a signal is that it does not require backoff. The HPA in the system can therefore be operated at the optimal saturation point thereby maximizing the average transmit power. This will in turn maximize the power efficiency of HPA. Constant envelope signals are highly attractive in systems where HPA is used. Therefore, it is important to embed digital information into the phase $\phi(t)$ in (1.15). In the literature, constant envelope Continuous Phase Modulation (CPM) [54, 55] has been extensively examined for digital transmission using single carrier system. When multi-carrier OFDM signal is embedded in the phase $\phi(t)$, it is possible to obtain CE-OFDM signal. Such a signaling technique involves integration of multicarrier and constant envelope techniques in a single system as shown in Figure 1.12. The high PAPR OFDM signal in the system is converted into a 0 dB PAPR CE-OFDM signal. This permits HPA to operate near saturation level thus achieving maximum power efficiency. Figure 1.13 shows a comparison of instantaneous power of the DCT-OFDM and CE-DCT-OFDM signals.

In order to generate constant envelope signal given by (1.15), the modulating signal $\phi(t)$ must be real-valued. In general, the modulating signal in an OFDM system is complex-valued. A real-valued modulating signal, however, can be obtained by taking IFFT of a conjugate symmetric vector. For example, if the input data vector $[X_{FFT}(0), \dots, X_{FFT}(N-1)]$ of size $1 \times N$ is given, a conjugate symmetric vector $[X_{FFT}(0), \dots, X_{FFT}(2N-1)]$ of size $1 \times 2N$ can be obtained that satisfies the following conditions:

$$X_{FFT}((N+n)) = X_{FFT}^*(N-n), \quad n = 1, 2, \dots \quad (1.16)$$

and

$$X_{FFT}(0) = X_{FFT}(N) = 0 \quad (1.17)$$

The IFFT of this vector is given by:

$$x_{FFT}(k) = \sum_{n=0}^{2N-1} X_{FFT}(n) e^{j2\pi kn/2N}, \quad (1.18)$$

Using (1.16) and (1.17), (1.18) can be written as

$$x_{FFT}(k) = \sum_{n=1}^{N-1} X_{FFT}(N-n) e^{j2\pi k(N-n)/2N} + X_{FFT}^*(X(N-n)) e^{-j2\pi k(N-n)/2N}, \quad k = 0, \dots, 2N-1 \quad (1.19)$$

Using $B + B^* = 2\Re[B]$, (1.19) can be written as:

$$= 2\Re \left\{ \sum_{n=1}^{N-1} X_{FFT}(n) e^{j2\pi kn/2N} \right\} \quad (1.20)$$

Using the formula $\Re[BC] = \Re[B]\Re[C] - \Im[B]\Im[C]$, (1.20) becomes

$$x_{FFT}(k) = 2 \sum_{n=1}^{N-1} \Re[X_{FFT}(n)] \cos(2\pi kn/2N) - \Im[X_{FFT}(n)] \sin(2\pi kn/2N) \quad (1.21)$$

Thus, $x_{FFT}(k)$, $k = 0, \dots, 2N-1$, is a real discrete-time signal. The equivalent continuous-time real-valued OFDM signal is given by:

$$x_{FFT}(t) = 2 \sum_{n=1}^{N-1} \Re[X_{FFT}(n)] \cos(2\pi nt/T) - \Im[X_{FFT}(n)] \sin(2\pi nt/T) \quad (1.22)$$

In the case of DCT-OFDM system, the modulating signal generated by the system is always real for real input data vector.

1.5 Literature Survey and Motivation

The FFT-based OFDM system has been extensively examined in the literature [56, 57, 58, 59, 60]. In recent years, several researchers have been investigating the use of alternative discrete transform technique such as DCT in place of FFT in OFDM systems

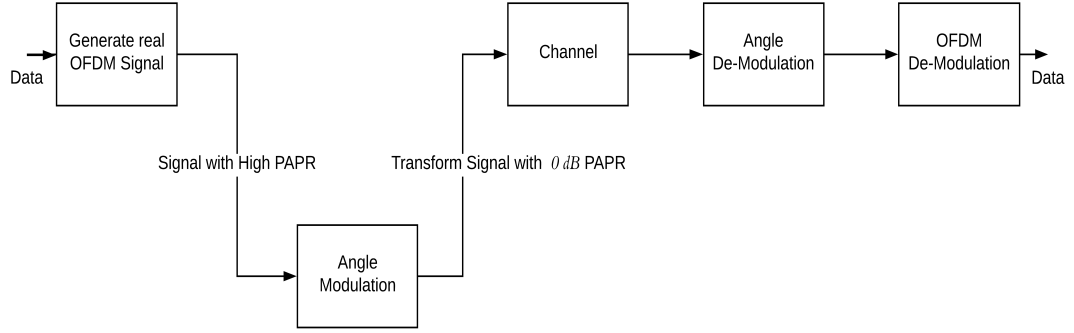


Figure 1.12: Block diagram of CE-OFDM system.

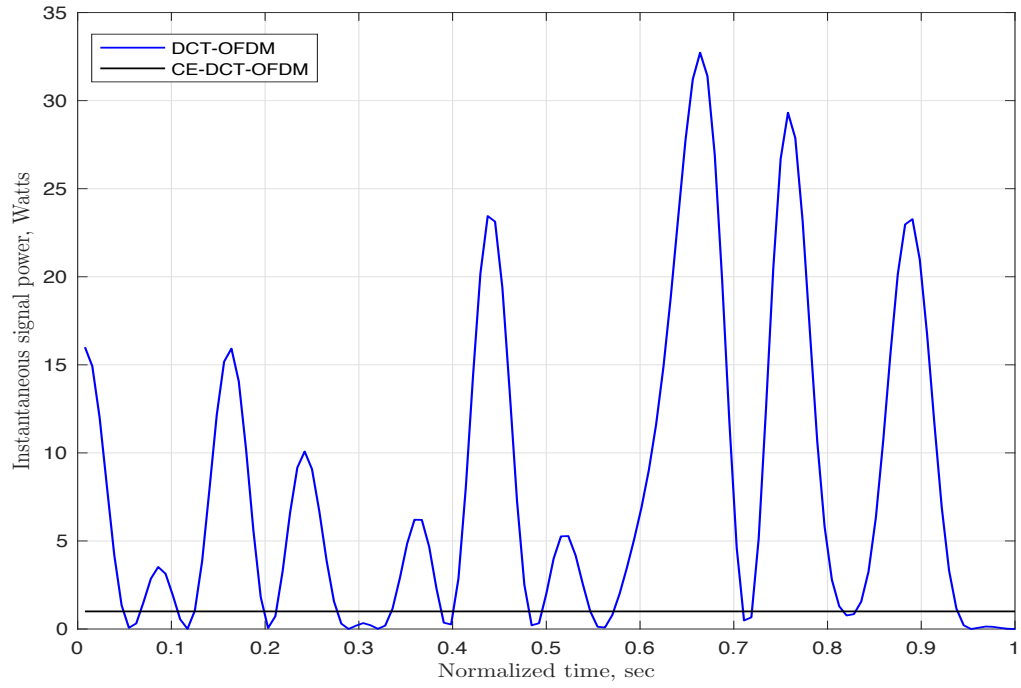


Figure 1.13: Instantaneous powers of signals in DCT-OFDM and CE-DCT-OFDM systems.

[39, 40, 41]. These studies show that the major advantage of using DCT in an OFDM system is that it can achieve better noise-immunity and hence can provide better BER performance than the conventional FFT-based OFDM system. Also, DCT-OFDM system can reduce the overall implementation cost.

In [42], it is noted that, particularly, for one-dimensional (1-D) mappers (real-valued formats), such as BPSK and MPAM, DCT-OFDM system can completely avoid the in-phase/quadrature-phase (IQ) imbalance problem, which is typically present in conventional FFT-OFDM system. In addition, it is possible to use fast DCT algorithm to achieve fewer computational steps in the system than using corresponding FFT algorithm. In [38], DCT is used to implement multicarrier modulation because of the bandwidth advantage it offers. A DCT-OFDM system is proposed in [43] using \sqrt{M} -ary Amplitude Shift Keying (ASK) mapper. A DCT-based implementation can also be employed in an OFDM system with 2-D modulations (complex-valued formats) [44].

The performance analysis of DCT-OFDM system over a variety of multipath fading channels is considered in several recent works. By using a symmetrically extended data sequence, a DCT-OFDM system is examined in [45]. For the case of static and exponentially decaying channel profiles, with intersymbol interference (ISI), it is shown that the lower bound on throughput of DCT-OFDM system is greater than that of the DFT-OFDM system. The conditions on the impulse response of a frequency-selective channel for diagonalization using DCT into parallel, decoupled, and memoryless subchannels are derived in [36]. In [44], the performance of the DCT-OFDM system with a zero-padding guard interval scheme and an MMSE receiver over time-varying multipath Rayleigh fading channel is investigated. The results show that employing a DCT-OFDM system rather than the conventional DFT-OFDM system can provide better bit error probability performance.

Several algorithms to correct Carrier Frequency Offset (CFO) by using DCT in an OFDM system, over an AWGN channel are examined in [46]. Due to the energy-compaction property of DCT, there is less ICI leakage to adjacent subcarriers in DCT-OFDM system than in an FFT-OFDM system, and thus is robust to frequency offset [44, 33]. In [33], it is shown that DCT Type-II multicarrier system can perfectly diagonalize frequency-selective channels without requiring channel knowledge. It is also observed that DCT-OFDM transceiver with and without the Partial Transmit Sequence (PTS) can achieve

average power reduction compared to the conventional FFT-OFDM system [47]. In [48], several channel estimation methods for DCT-OFDM system are proposed such as Least Square (LS), Minimum Mean Square Error (MMSE), and Compressed Sensing estimators.

A major drawback of OFDM system is that the transmitted signal suffers from high values of PAPR which results in spectral broadening and intermodulation distortion particularly when the signal is passed through a nonlinear HPA before transmission over the channel [61, 62]. Thus, a large amount of input power backoff is required which leads to reduced efficiency of HPA [54, 63]. There are several techniques to deal with the PAPR problem in an OFDM system such as coding, partial transmission sequences, clipping and filtering, selected mapping, tone reservation and interleaving etc [64, 65, 66, 67, 68, 69]. These techniques offer a variety of trade-offs in terms of complexity, performance and spectral efficiency. It is noted that these techniques do not completely eliminate the PAPR problem and may or may not require side information to be communicated to the receiver. Constant Envelope OFDM (CE-OFDM) designs can completely eliminate the problem of PAPR in an OFDM system. In such a system, angle modulation is used in place of I-Q modulation to create constant envelope transmitted signal with 0 dB PAPR. This permits HPA to operate near saturation level and thus achieving maximum power efficiency [70]. Due to this major advantage, CE-FFT-OFDM is being researched for applications in wireless [70]-[91], optical [92, 93, 94], powerline [95, 96] and satellite [97, 98] communications as well as in radar systems [99, 100].

OFDM system with angle modulation is proposed in [71]. In such a system, orthogonal time functions are employed to transmit data by using “amplitude or frequency modulation, or any other type of modulation suitable for the transmission of continuously varying time functions.”

In [72], a constant envelope signaling approach is proposed in which the complex OFDM signal is split into signals and then phase modulation is used. Since the standard complex OFDM signal is split into two constant envelope signals, bandwidth efficiency is traded off by this approach for power efficiency. It is shown using simulations that the bit error performance of such a system is poorer compared to that of the corresponding conventional OFDM system by a few decibels. In [73], the performance of phase-modulated OFDM in AWGN channels is studied. The analysis shows poorer bit error rate performance

for low frequency subcarriers than for high frequency subcarriers. In [74], the suitability of constant envelope multi-carrier modulation technique for the implementation of 1Gbps wireless link at 60 GHz is investigated. This technique combines OFDM and phase modulation to achieve: (i) constant envelope signal which allows HPA to operate near saturation level and thus maximizing power efficiency, and (ii) robust performance over multipath fading channel. When OFDM with PM is compared with OFDM with CPM, it is observed that the latter suffers from a 3 dB performance loss, when differential demodulation is used. In [75], a constant envelope binary OFDM system with PM is presented and analyzed in AWGN channel. Approximate bandwidth requirements are predicted using the Carson's rule and the root-mean square bandwidth for Gaussian angle modulated process. In the study of BER performance, a high carrier-to-noise ratio assumption ($CNR > 10dB$) is made in the analysis and ideal filters are used in the receiver frontend. Estimates are made on the transmitted data symbols by using IFFT demodulation at receiver. It is shown that the modulation index controls the spectral spreading and detection performance. In [76], the spectral properties of OFDM system with phase modulation are studied. It is shown that the fractional out-of-band power of transmitted signals can be better than conventional OFDM signals. Sub-optimum PM demodulator is analyzed for BER performance and compared to the optimum receiver. It is shown that the sub-optimum receiver performs close to the optimum for small modulation index and at high SNRs.

In [77], a noncoherent CE-OFDM receiver is presented and analyzed. The matched-filter bank followed by the phase demodulator eliminates the effect of unknown phase shifts caused by the channel. The performance of this noncoherent receiver over Rayleigh and Ricean flat fading channels is also presented. It is shown that, for small modulation index and high SNR, simulation results are in good agreement with analytical approximations. In [78], a frequency-domain equalizer is proposed for CE-OFDM in multipath Rayleigh fading channel. It is shown that uncoded CE-OFDM, unlike uncoded OFDM, can exploit the frequency diversity of the channel. Compared to conventional OFDM system, CE-OFDM system is shown to offer gains in performance and in power amplifier efficiency. In [79], the influence of PM in CE-OFDM on ISI is analyzed and then a method is proposed to reduce ISI using zero-padding pattern in the transmitted OFDM symbol.

In [80], a novel receiver structure for CE-OFDM based on the Taylor series expansion is

presented. The receiver allows for a simpler implementation without the need to compute the arctangent at the receiver. It is shown that the receiver performs well compared to the conventional arctangent based receiver for small and moderate modulation indices < 0.7 , for both AWGN and multipath fading channels. In [81], spectrally precoded OFDM and CE-OFDM systems are examined. The spectrally precoded OFDM signal provides very small power spectral sidelobes and the CE-OFDM signal exhibits 0 dB PAPR. A specific CE-OFDM block signaling format is proposed to incorporate spectral precoding with an aim to suppress sidelobe power more effectively than in a conventional non-precoded CE-OFDM.

In [82], the performance of CE-OFDM system in multipath fading channels using FDE is studied. Several channel estimation techniques that use low-PAPR OFDM signals are examined in the presence of SSPA and TWTA amplifiers in the system. In [83], the application of convolutional coding to CE-OFDM is studied. A bound on the performance of convolutionally coded CE-OFDM is derived and illustrated. It is shown that channel coding with interleaving provides good performance for low to moderate modulation indices. In [84], a threshold receiver for CE-OFDM is considered. It is noted that the receiver design depends on the modulation index used in the system. In [85, 86], the performance of OFDM system with FM for digital communication over Rayleigh-fading channel is examined. In such a system, OFDM baseband signal is used to modulate the frequency of the carrier signal. Expressions are derived for the BER for QAM-mapper in the system. Some techniques for improving the performance of such a system for data communication over a Rayleigh fading channel are suggested. In [87], CE-OFDM system that uses PM in AWGN and multipath channels is explored. A theoretical approach instead of Carson's rule is used to analyze bandwidth of the system. It is shown that bandwidth requirement is determined by factors such as input data variance and modulation index of PM. The results show that the system requires the same bandwidth as that of the conventional OFDM system for low values of modulation index.

In [38], a DCT-based multicarrier system with CPM is examined over fading channel for error probability performance using simulation. Results show that a larger modulation index, h , results in better performance. However, large value of h in such a system requires proper phase detection and correction.

Based on the above literature survey, it is observed that FFT-based OFDM systems are

well examined. However, DCT-based OFDM systems have not received much attention despite the fact that such systems have several attractive properties useful in communication system. Thus, the motivation for this thesis is to investigate constant envelope OFDM signal designs for data communications. A wide range of angle modulations are considered for achieving constant envelope designs such as: i) PM; ii) FM; iii) CPM; and iv) CPCM. Both DCT- and FFT-based OFDM systems are examined. A generic system is used for examining these systems. A comprehensive study of these systems in terms of BER performance, bandwidth efficiency, complexity etc. is presented.

1.6 Thesis Objectives

There are four major objectives for this thesis. They are:

1. DCT- and FFT-OFDM Systems with PM

A system is presented to describe both DCT- and FFT-OFDM systems with PM. Expressions for bandwidth of signals in these systems are given. The detection of these signals in AWGN and fading channels (Rayleigh and Rician) is addressed and closed-form expression for BER of these systems are derived and illustrated as a function of SNR, modulation index, number of levels of MPAM mapper, and statistical parameters of noise environment. DCT-OFDM and FFT-OFDM systems with PM are compared in terms of BER, bandwidth, and structure of receivers. Also, the BER performances of DCT-OFDM system with PM and conventional DCT-OFDM system are compared as a function of IBO when TWTA amplifier is used in these systems.

2. DCT- and FFT-OFDM Systems with FM

A system description is given that can be used for both DCT- and FFT-OFDM systems with FM. The bandwidths of signals in these systems are determined. The detection of signals in these systems in AWGN and fading channels (Rayleigh and Rician) is addressed and closed-form expressions for BER are derived and illustrated. A comparison of the two systems in terms of BER, bandwidth, and structure of receivers is provided. Also, the effect of TWTA amplifier in these systems on BER performance is examined as a function of IBO.

3. DCT- and FFT-OFDM Systems with CPM

The concept of Continuous Phase Modulation (CPM) is introduced in DCT- and FFT-OFDM systems. A generic description of DCT- and FFT-OFDM systems with CPM is given and described. While these exist a wide class of CPM, in this thesis full-response CPM with rectangular pulse shaping is used. Detection of signals in these systems in AWGN and fading channels (Rayleigh and Rician) is addressed and a receiver structure that uses phase detector followed by phase correction with oversampling is suggested. Closed-form expressions for BER over AWGN and fading channels are derived and illustrated. The performances of DCT-OFDM system with CPM and conventional DCT-OFDM system are compared as a function of IBO when TWTA amplifier is used in these systems.

4. DCT- and FFT-OFDM Systems with CPCPM

Chirp (Linear FM) modulation provides attractive wideband signals suitable for application in systems where interference rejection is important. In this thesis, DCT- and FFT-OFDM systems with CPCPM are presented. The signals in these systems are described and their detection in AWGN and fading channels (Rayleigh and Rician) is addressed and a receiver structure is suggested. Closed-form expressions for BER are derived and illustrated as a function chirp modulation parameters, SNR, number of levels of MPAM mapper and noise environment parameters. The influence of TWTA amplifier in DCT-OFDM system with CPCPM and conventional DCT-OFDM system is examined as a function of IBO.

1.7 Thesis Organization

In Chapter 2, a generic description of FFT- and DCT-OFDM systems is given. The concept of guard interval/Cyclic prefix is mathematically explained in both continuous- and discrete-time. The PAPR statistics of FFT- and DCT-OFDM signals are presented. The models of HPA, both SSPA and TWTA, are described. The effect of IBO on efficiency of HPA is also illustrated.

In Chapter 3, DCT- and FFT-OFDM systems with PM are studied. The performance analyses of these systems in AWGN and fading channels are presented. The bandwidths of DCT- and FFT-OFDM signals with PM are developed. The effect of HPA on BER of

these systems is illustrated.

In Chapter 4, DCT- and FFT-OFDM systems with FM are considered. The detection of signals in these systems in AWGN and fading channels is addressed. The BER performances of both systems are derived and illustrated. Also the effect of HPA on BER of these systems is examined.

In Chapter 5, DCT- and FFT-OFDM systems with CPM are presented and their properties are studied. The detection performance of signals in these systems in AWGN and fading channels is examined. The effect of HPA on system bit error probability is also discussed.

In Chapter 6, CPCM is introduced in DCT- and FFT-OFDM systems. These systems are examined for their BER performances over AWGN and fading channels. The behaviour of these systems in the presence of HPA is illustrated.

In Chapter 7, the contributions of this thesis and the conclusions from the results obtained are summarized. Also, areas for further research in the light of the needs of modern communication systems are outlined.

1.8 Conclusions

An introduction to the thesis relevant to the objective set out for the thesis is provided. Literature survey and motivation for the problems attempted in the thesis are given. The organization of thesis is also provided.

Chapter 2

Generic FFT- and DCT-OFDM System

2.1 Introduction

In the previous Chapter some basic properties of OFDM system were identified. In this Chapter, the system is examined in more detail. A generic block diagram is presented to examine both DCT- and FFT-OFDM systems. The importance of cyclic prefix/guard interval in these systems is explained. The PAPR statistics of OFDM signals are presented and typical HPA models used in an OFDM system are examined.

2.2 Baseband OFDM System

A generic block diagram of a baseband OFDM system is shown in Figure 2.1 and can be used to study both FFT- and DCT-OFDM systems. The difference between these two systems is that, in the latter system IDCT/DCT are used for modulation/demodulation and in the former system IFFT/FFT are used for modulation/demodulation. The data source is assumed to be a sequence of binary digits $[a_0, a_1, a_2, \dots]$ where $a_l, l = 0, 1, \dots$ is either a 0 or a 1 with $P(a_l = 0) = P(a_l = 1) = 1/2$. The bit duration is assumed to be equal to T_b sec and the corresponding data rate is thus equal to $R = 1/T_b$ bps. The output of the data source is grouped into blocks of N symbols with each symbol made up of K bits and each symbol is mapped to one of $M = 2^K$ amplitude levels by an MPAM mapper. Such a mapper is referred to as a memoryless mapper, as its current output is a function of only the current input. The corresponding signal space diagrams for 2-PAM and 4-PAM mappers are shown in Figure 2.2. For the case of 2-PAM mapper $K = 1$ and hence $M = 2$. The mapper maps incoming bit 1 to $+1 V$ and bit 0 to $-1 V$. For the 4-PAM mapper, $K = 2$ and therefore $M = 4$. The mapping of symbols to amplitudes levels can be done in a number of ways. The preferred assignment is one in which the

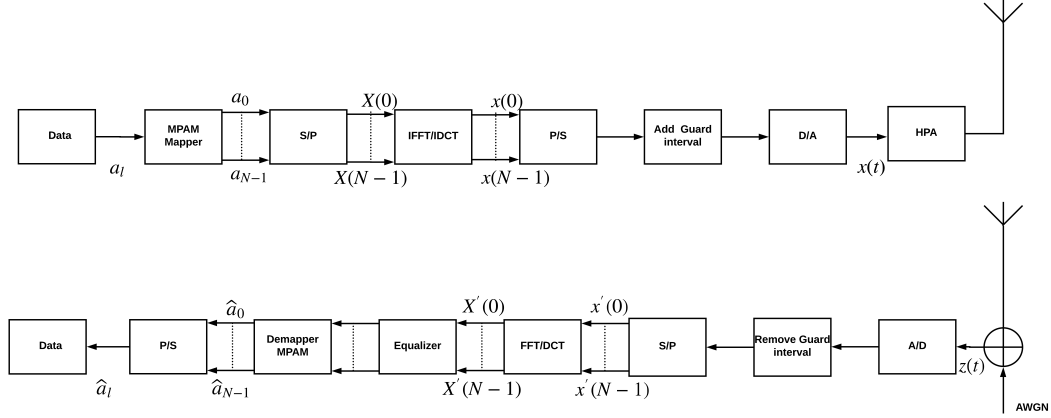


Figure 2.1: The generic block diagram of DCT- and FFT-OFDM baseband transceiver system.

adjacent signal amplitudes differ by one binary digit as illustrated in Figure 2.2 (b). This mapping is called Gray coding. By using this technique for the case of 4-PAM mapper, the mapper maps incoming symbols as given below:

$$\begin{aligned}
 00 &\rightarrow -3 \\
 01 &\rightarrow -1 \\
 11 &\rightarrow +1 \\
 10 &\rightarrow +3
 \end{aligned} \tag{2.1}$$

The output of the signal mapper, in general, can be thought of as a discrete-time real signal as shown in Figure 2.3. The S/P converter enhances the duration of each symbol by a factor of N and converts serial data to parallel data. The output of this block can be written as a vector of N real numbers given by:

$$X = [X(0), X(1), X(2), \dots, X(N-1)] \tag{2.2}$$

The discrete signal representing the data is fed to an N -point IFFT/IDCT block to obtain

$$x = [x(0), x(1), x(2), \dots, x(N-1)]. \tag{2.3}$$

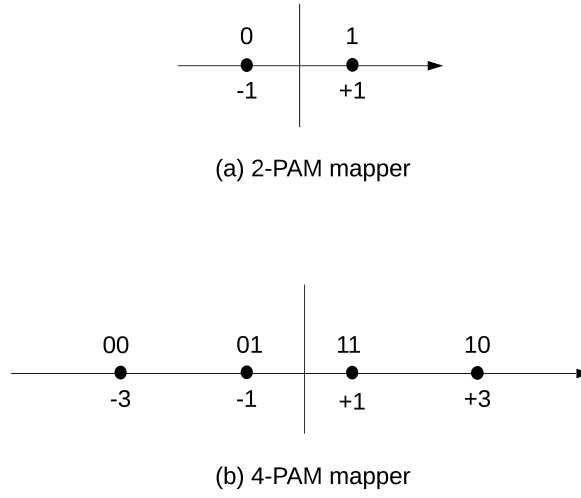


Figure 2.2: Signal space diagrams for (a) 2-PAM and (b) 4-PAM mappers.

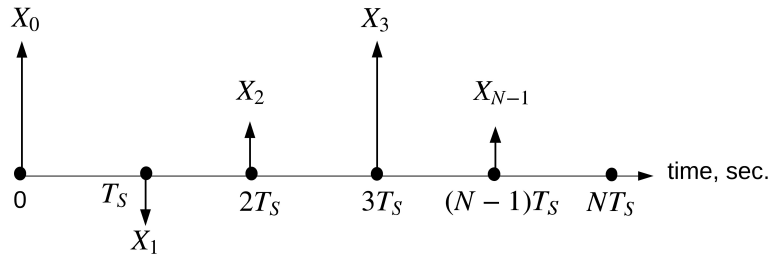


Figure 2.3: Discrete time signal at the output for MPAM mapper.

In order to differentiate samples in DCT- and FFT-OFDM systems, suffixes DCT and FFT are used, respectively

2.2.1 FFT-OFDM Signal

In this case, the relationship between (2.2) and (2.3) can be written as:

$$x_{FFT}(k) = \sum_{n=0}^{N-1} X_{FFT}(n) e^{j2\pi kn/N}, \quad k = 0, \dots, N-1, \quad (2.4)$$

The parallel signal from the IFFT block is then converted to serial signal by using the P/S converter and then fed to D/A block to obtain

$$x_{FFT}(t) = \sum_{n=0}^{N-1} X_{FFT}(n) e^{j2\pi nt/T}, \quad 0 \leq t \leq T \quad (2.5)$$

where T is the OFDM symbol duration and n/T is the frequency of the n^{th} subcarrier. For a 2-PAM mapper used in the system, $T = NT_b$, T_b is the duration of the data from the source. For a 4-PAM mapper $T = NT_s$, where $T_s = KT_b$. It is noted that $[X_{FFT}(0), X_{FFT}(1), \dots, X_{FFT}(N-1)]$ represents a block of N data symbols and the complex functions $e^{j2\pi nt/T}$, $n = 0, 1, \dots, N-1$ are referred to as the subcarriers of the system and are orthogonal to each other. It can be shown that the discrete sequence $[x_{FFT}(0), x_{FFT}(1), \dots, x_{FFT}(N-1)]$ can be obtained by sampling $x_{FFT}(t)$ at $t = (kT)/N$, $k = 0, 1, \dots, N-1$. That is,

$$x_{FFT}(k) = x_{FFT}(t) |_{t=kT/N} = \sum_{n=0}^{N-1} X_{FFT}(n) e^{j2\pi kn/N}, \quad k = 0, \dots, N-1, \quad (2.6)$$

and its frequency-domain representation is:

$$X_{FFT}(n) = \frac{1}{N} \sum_{k=0}^{N-1} x_{FFT}(k) e^{-j2\pi kn/N}, \quad n = 0, \dots, N-1 \quad (2.7)$$

It is noted that

$$\frac{1}{N} \sum_{k=0}^{N-1} e^{j2\pi pk/N} e^{-j2\pi qk/N} = \begin{cases} 1 & p = q \\ 0 & \text{otherwise} \end{cases} \quad (2.8)$$

2.2.2 DCT-OFDM Signal

The relationship between (2.2) and (2.3) can be written as:

$$x_{DCT}(k) = \sum_{n=0}^{N-1} X_{DCT}(n) \cos(\pi n(2k+1)/2N), \quad k = 0, \dots, N-1 \quad (2.9)$$

The parallel signal from the IDCT block is converted to serial signal by using the P/S converter and then fed to D/A block to obtain

$$x_{DCT}(t) = \sum_{n=0}^{N-1} X_{DCT}(n) \cos(2\pi nt/2T), \quad 0 \leq t \leq T \quad (2.10)$$

where T is OFDM symbol duration and $n/2T$ is the frequency of the n^{th} subcarrier. It is noted that $[X_{DCT}(0), X_{DCT}(1), \dots, X_{DCT}(N-1)]$ represents a block of N data symbols and the cosinusoidal functions $\cos(2\pi nt/2T), n = 0, 1, \dots, N-1$, are referred to as the subcarriers of the system and are orthogonal to each other. It can be shown that discrete sequence $[x_{DCT}(0), x_{DCT}(1), \dots, x_{DCT}(N-1)]$ can be obtain by sampling $x_{DCT}(t)$ at $t = T(2k+1)/2N, k = 0, 1, \dots, N-1$. That is,

$$x_{DCT}(k) = x_{DCT}(t) |_{t=T(2k+1)/2N} = \sqrt{\frac{2}{N}} \sum_{n=0}^{N-1} X_{DCT}(n) B(n) \cos(\pi n(2k+1)/2N), \quad k = 0, \dots, N-1 \quad (2.11)$$

where

$$B(n) = \begin{cases} \sqrt{\frac{1}{2}} & n = 0 \\ 1 & k = 1, \dots, N-1 \end{cases} \quad (2.12)$$

and the corresponding frequency-domain signal is:

$$X_{DCT}(n) = \sqrt{\frac{2}{N}} \sum_{k=0}^{N-1} x_{DCT}(k) B(n) \cos(\pi n(2k+1)/2N), \quad n = 0, \dots, N-1 \quad (2.13)$$

It is noted that:

$$\sqrt{\frac{2}{N}} \sum_{k=0}^{N-1} B(p) \cos(\pi p(2k+1)/2N) B(q) \cos(\pi q(2k+1)/2N) = \begin{cases} 1 & p = q \\ 0 & otherwise \end{cases} \quad (2.14)$$

The output of D/A converter, $x(t)$, is then amplified using HPA and transmitted over the channel.

At the receiver the received signal $x(t)+n(t)$ is fed to A/D block followed by S/P converter to obtain parallel signal. This is fed to FFT/DCT block followed by an equalizer. The output of the equalizer is fed to MPAM demapper followed by P/S block to obtain an estimate of the transmitted data sequence.

2.3 Guard Interval/Cyclic Prefix

In an OFDM system guard interval is inserted at the transmitter between successive OFDM blocks to achieve ISI-free operation at the receiver. This guard interval, T_g , is designed such that $T_g \geq \tau_{max}$ so that the effect of channel is absorbed in this guard interval. Although the introduction of guard interval results in a small reduction in spectral efficiency of the system, ISI is eliminated. This aspect is described for both DCT- and FFT-OFDM systems in the next Section.

2.3.1 FFT-OFDM System

Continuous Time Domain Description

A guard interval which is commonly called the Cyclic Prefix (CP) is added to the time-domain signal after the P/S conversion in the transmitter. The CP is a copy of the last part of the OFDM symbol, greater than or equal to the maximum delay spread of the

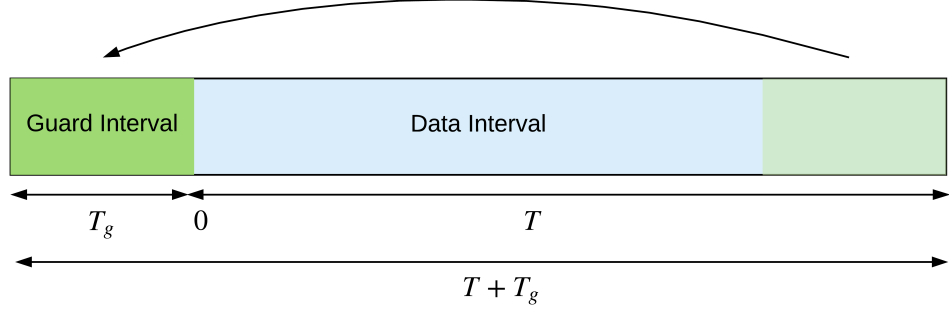


Figure 2.4: OFDM symbol with CP

channel, appended to the beginning of the symbol as shown in Figure 2.4. Thus, the OFDM signal with CP can be written as:

$$x_{FFT}(t) = \sum_{n=0}^{N-1} X_{FFT}(n) e^{j2\pi f_n t}, \quad -T_g \leq t \leq T \quad (2.15)$$

At the receiver, the received signal can be written as:

$$u(t) = x_{FFT}(t) * h(\tau) + n(t) = \int_{-\infty}^{\infty} h(\tau) x_{FFT}(t - \tau) d\tau + n(t) = \int_{-\infty}^{\tau_{max}} h(\tau) x_{FFT}(t - \tau) d\tau + n(t) \quad (2.16)$$

where $h(\tau)$ is the channel impulse response with $0 \leq \tau \leq \tau_{max}$ and $n(t)$ is the additive noise. The received signal during the guard interval, which has interference from the previous block is ignored and $u(t)$ over $0 \leq t \leq T$ is processed. The estimate of $X_{FFT}(k)$ is made by correlating $u(t)$ with the k^{th} subcarrier as shown in Figure 2.5 and the output can be expressed as:

$$u(k) = \int_0^T u(t) \varphi_k^*(t) dt, \quad k = 0, 1, \dots, N-1 \quad (2.17)$$

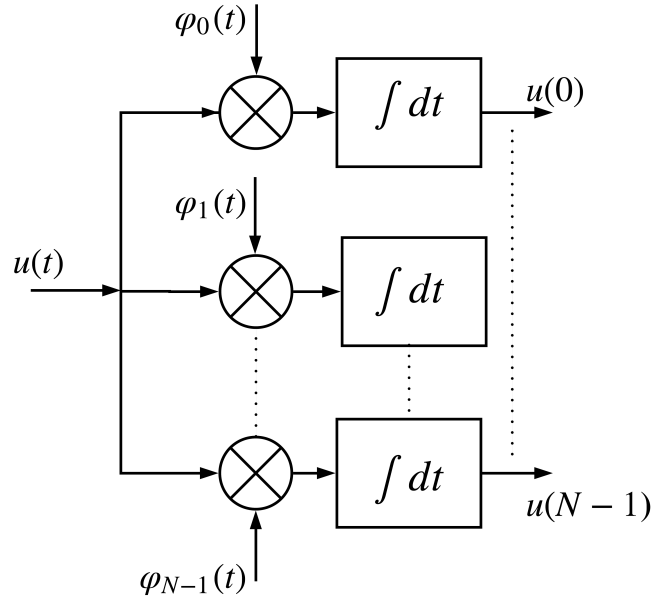


Figure 2.5: Structure of OFDM demodulator using a bank of N correlators

where

$$\varphi_k(t) = \sqrt{\frac{1}{T}} e^{j2\pi f_k t}, 0 \leq t < T, k = 0, 1, \dots, N-1 \quad (2.18)$$

and

$$\int_0^T \varphi_n(t) \varphi_k^*(t) dt = \begin{cases} 1 & n = k \\ 0 & \text{otherwise} \end{cases} \quad (2.19)$$

Thus,

$$u(k) = X_{FFT}(k) \int_0^{\tau_{max}} h(\tau) e^{-j2\pi f_k \tau} d\tau + \int_0^T n(t) \varphi_k^*(t) dt \quad (2.20)$$

$$u(k) = X_{FFT}(k) H(k) + N_u(k) \quad (2.21)$$

where $H(k)$ is Fourier transform of $h(\tau)$. From (2.21), it is noted that the system is ISI-free by virtue of using guard interval. Moreover, the channel equalization is carried out in the frequency-domain by a bank of scalars, $[H(0), H(1), \dots, H(N-1)]$.

Discrete Time Description

In this Section, ISI-free operation is explained using discrete time representation of OFDM signal. Sampling $x_{FFT}(t)$, $h(t)$ and $u(t)$ at $t = kT_s$, we obtain:

$$x_{FFT}(k) = x_{FFT}(t) |_{t=kT_s}, k = -N_g, \dots, 0, \dots, N-1 \quad (2.22)$$

$$h(k) = h(\tau) |_{\tau=kT_s}, k = 0, 1, \dots, v-1 \quad (2.23)$$

and

$$u(k) = \sum_{r=0}^{v-1} h(r)x_{FFT}(k-r) + n(k), k = -N_g, \dots, 0, \dots, N-1 \quad (2.24)$$

where N_g is the number of guard samples ($N_g \leq Tg/Ts$), v is the length of channel impulse response $v \leq \tau/T_s$ and ($v \leq N_g$) and $n(k)$ are the samples of the noise $n(t)$. Ignoring the guard samples the received signal can be written as:

$$u(k) = \sum_{r=0}^{v-1} h(r)x_{FFT}(k-r) + n(k), k = 0, \dots, N-1 \quad (2.25)$$

The transmission of CP makes the linear convolution (2.25) equivalent to a circular convolution [101]. Ignoring the noise samples, (2.25) can be written as:

$$u(k) = IFFT \{H(n)X_{FFT}(n)\} = \sum_{n=0}^{N-1} H(n)X(n)e^{j2\pi nk/N}, k = 0, \dots, N-1 \quad (2.26)$$

where

$$H(n) = \frac{1}{N} \sum_{k=0}^{N-1} h(k)e^{-j2\pi nk/N}, n = 0, \dots, N-1 \quad (2.27)$$

and

$$X_{FFT}(n) = \frac{1}{N} \sum_{k=0}^{N-1} x_{FFT}(k)e^{-j2\pi nk/N}, n = 0, \dots, N-1 \quad (2.28)$$

The channel $h(k)$ are zero-padded from $v \leq k \leq N$. It is noted that N received data symbols are equal to the transmitted symbols scaled by the value of channel gains. ISI is avoided since the k^{th} symbol is not impacted by the $N-1$ other symbols. Therefore, using CP provides ISI-free operation.

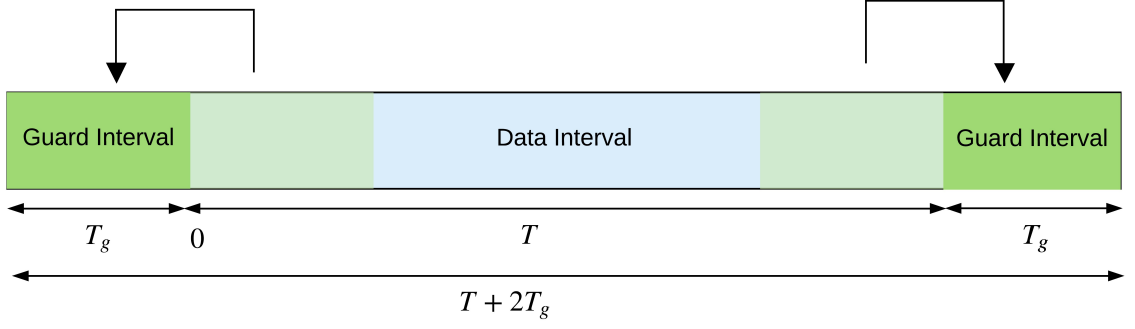


Figure 2.6: OFDM symbol with symmetric extension.

2.3.2 DCT-OFDM System

Continuous Time Domain Description

A guard interval of duration $2 T_g$ (T_g prefix + T_g suffix) which is a symmetrical extension of $x_{DCT}(t)$ is appended in the case of DCT-OFDM signal [33, 102, 103] as shown in Figure 2.6.

The signal with guard interval can be written as:

$$x_{DCT}(t) = \sum_{n=0}^{N-1} X_{DCT}(n) \cos(2\pi f_n t), \quad -T_g \leq t \leq T + T_g \quad (2.29)$$

At the receiver, a front-end prefilter that is asymmetrical extension of the channel impulse response is used to achieve ISI-free operation [33, 34]. The received signal can be written as:

$$\begin{aligned} u(t) &= x_{DCT}(t) * h(\tau) + n(t) = \int_{-\infty}^{\infty} h(\tau) x_{DCT}(t - \tau) d\tau + n(t) \\ &= \int_{-\infty}^{\tau_{max}} h(\tau) x_{DCT}(t - \tau) d\tau + n(t) \end{aligned} \quad (2.30)$$

where $h(\tau)$ is the channel impulse response with $-\tau_{max} \leq \tau \leq \tau_{max}$ and $n(t)$ is the additive noise.

The received signal during the guard interval, which has interference from the previous block is ignored and $u(t)$, $0 \leq t \leq T$, is processed. The estimate of $X_{DCT}(k)$ is made by correlating $u(t)$ with the k^{th} subcarrier as shown in Figure 2.5 and the output can be expressed as:

$$u(k) = \int_0^T u(t) \varphi_k(t) dt, k = 0, 1, \dots, N-1 \quad (2.31)$$

where

$$\varphi_k(t) = \sqrt{\frac{2}{T}} \cos(2\pi f_k t), 0 \leq t < T, k = 0, 1, \dots, N-1 \quad (2.32)$$

and

$$\int_0^T \varphi_n(t) \varphi_k(t) dt = \begin{cases} 1 & n = k \\ 0 & otherwise \end{cases} \quad (2.33)$$

Thus,

$$u(k) = X_{DCT}(k) \int_{-\tau_{max}}^{\tau_{max}} h(\tau) \cos(2\pi f_k \tau) d\tau + \int_0^T n(t) \varphi_k^*(t) dt \quad (2.34)$$

$$u(k) = X(k)H(k) + N_u(k) \quad (2.35)$$

where $H(k)$ is Fourier cosine transform of $h(\tau)$. From (2.35), it is noted that the system is ISI-free when guard interval is used. Moreover, the channel equalization is carried out in the frequency-domain by a bank of scalars, $[H(0), H(1), \dots, H(N-1)]$.

Discrete Time Description

In this Section, ISI-free operation is explained using discrete time representation of DCT-OFDM signal. Sampling $x_{DCT}(t)$, $h(t)$ and $u(t)$, we obtain:

$$x_{DCT}(k) = x_{DCT}(t) |_{t=T(2k+1)/2N}, k = -N_g, \dots, 0, \dots, N + N_g - 1 \quad (2.36)$$

$$h(k) = h(\tau) |_{\tau=kT_s}, k = 0, \dots, v-1 \quad (2.37)$$

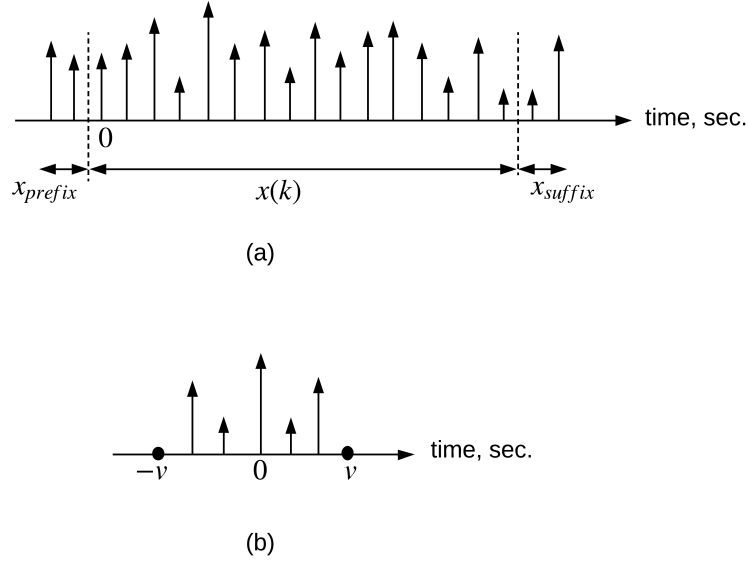


Figure 2.7: Symmetries for (a) $x(k)$ and (b) $h(k)$ to convert linear convolution into a symmetric convolution.

where v is the length of the channel impulse response. The Figure 2.7 (a) shows an example of symmetric extension of $x(k)$ using prefix and suffix. Figure 2.7 (b) illustrates an example of symmetric extension of $h(k)$. Symmetric extension of $h(k)$ can be written as:

$$h(k) = h(\tau) \big|_{\tau=kT_s}, \quad k = -v + 1, \dots, 0, \dots, v - 1 \quad (2.38)$$

The received signal samples can be expressed as:

$$u(k) = \sum_{r=-v+1}^{v-1} h(r)x_{DCT}(k-r) + n(k), \quad k = -N_g, \dots, 0, \dots, N + N_g - 1 \quad (2.39)$$

where $n(k)$ are the samples of the noise signal $n(t)$. The guard interval samples are ignored and the received signal can be written as:

$$u(k) = \sum_{r=0}^{v-1} h(r)x_{DCT}(k-r) + n(k), \quad k = 0, \dots, N - 1 \quad (2.40)$$

The transmission of a symmetrically extended guard time makes the linear convolution in (2.40) equivalent to a symmetric convolution [33, 34, 102]. Using the convolution-multiplication property of DCT [33, 102], and ignoring the noise samples, (2.40) can be written as:

$$u(k) = IDCT \{H(n)X_{DCT}(n)\} = \sqrt{\frac{2}{N}} \sum_{n=0}^{N-1} H(n)X_{DCT}(n)B(n) \cos(\pi n(2k+1)/2N),$$

$$k = 0, \dots, N-1 \quad (2.41)$$

where $IDCT \{\bullet\}$ represents IDCT operator;

$$H(n) = 2 \sum_{k=0}^N h(k)B(n) \cos(\pi nk/N), n = 0, \dots, N-1 \quad (2.42)$$

and

$$X_{DCT}(n) = \sqrt{\frac{2}{N}} \sum_{k=0}^{N-1} x_{DCT}(k)B(n) \cos(\pi n(2k+1)/2N), n = 0, \dots, N-1 \quad (2.43)$$

It is noted that N received data symbols are equal to the transmitted symbols scaled by values of channel gains. ISI is avoided since the k^{th} symbols is not affected by the $N-1$ other symbols. Therefore, using guard interval provides ISI-free operation.

2.4 PAPR of OFDM Signals

2.4.1 PAPR Statistics

The PAPR of an OFDM signal $x(t)$ is defined as the ratio of its maximum value of power to its average power. That is,

$$PAPR = \frac{\max_{0 \leq t \leq T} \{|x(t)|^2\}}{\frac{1}{T} \int_0^T |x(t)|^2 dt} \quad (2.44)$$

The computation of PAPR in (2.44) can be approximated by using samples of $x(t)$ and the reasons for this approach are: i) most systems are implemented in discrete-time; ii)

computation in continuous-time is too complex as closed-form expression is difficult to arrive at; and iii) when an oversampling rate of 4 times that of Nyquist rate is used, it closely approximates continuous-time PAPR given by (2.44). The PAPR of J -times oversampled signal $x(t)$ is given by:

$$PAPR = \frac{\max \left\{ |x(k)|^2, k = 0, 1, \dots, JN - 1 \right\}}{\frac{1}{JN} \sum_{k=0}^{JN-1} |x(k)|^2} \quad (2.45)$$

For FFT- and DCT-OFDM signals $x(k)$ are given by:

$$x_{FFT}(k) = \sum_{n=0}^{N-1} X_{FFT}(n) e^{j2\pi kn/JN}, \quad k = 0, \dots, JN - 1, \quad (2.46)$$

and

$$x_{DCT}(k) = \sqrt{\frac{2}{N}} \sum_{n=0}^{N-1} X_{DCT}(n) B(n) \cos(\pi n(2k+1)/2JN), \quad k = 0, \dots, JN - 1 \quad (2.47)$$

The Complementary Cumulative Distribution Function (CCDF) of the PAPR is used to estimate the PAPR of a given OFDM system. The CCDF denotes the probability that the PAPR of an OFDM data block exceeds a given threshold, $PAPR_0$. An approximate lower bound on PAPR for an OFDM system with N subcarriers can be obtained [104] and is given by:

$$Pr(PAPR > PAPR_0) \approx 1 - \left(1 - e^{(-PAPR_0)}\right)^N \quad (2.48)$$

Figures 2.8 shows CCDFs of PAPR for an OFDM signal for $N = 32, 64, 128, 256, 512$, and 1024. It is noted that PAPR increases as the number of subcarriers (N) in the system. The CCDFs of PAPR of DCT- and FFT-OFDM systems with QPSK mapper for $N = 32$ are shown in Figure 2.9. It is noted that PAPR bound for $N = 32$, also shown in Figure 2.8, closely matches with simulation results.

The significance of PAPR of a modulated signal is that it significantly affects the ability of the signal to be processed by HPA used in the transmitted of the system. The high PAPR of OFDM signal requires HPA with a large linear range capable of accommodating the dynamic range of the signal. Otherwise, the nonlinear distortion caused by the HPA

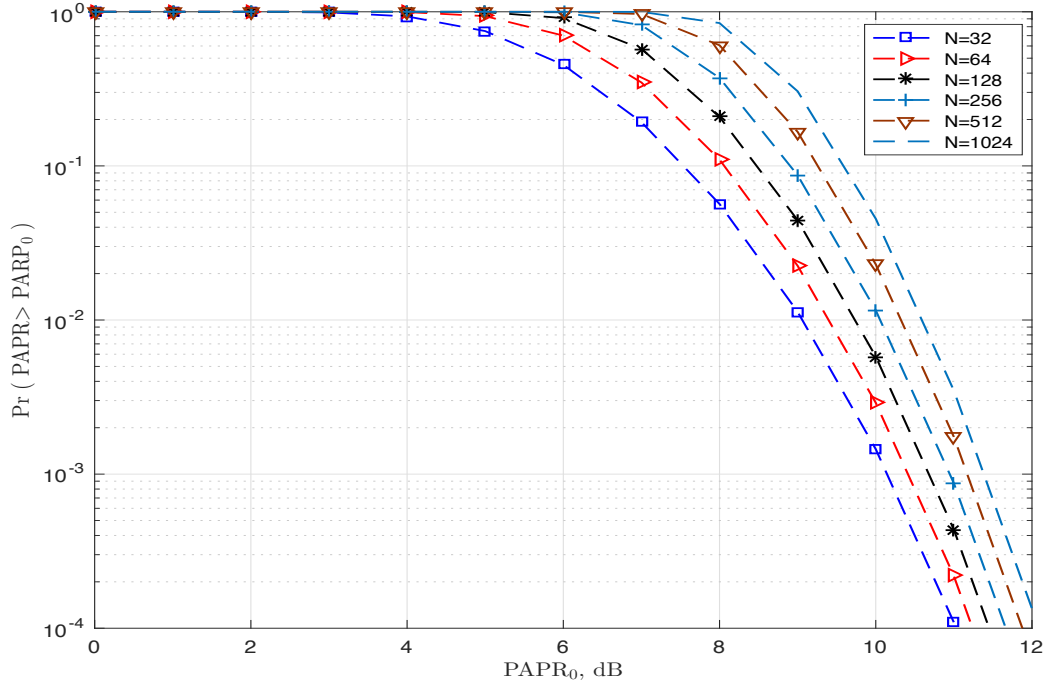


Figure 2.8: CCDF of PAPR of an OFDM signal for $N = 32, 64, 128, 256, 512$, and 1024.

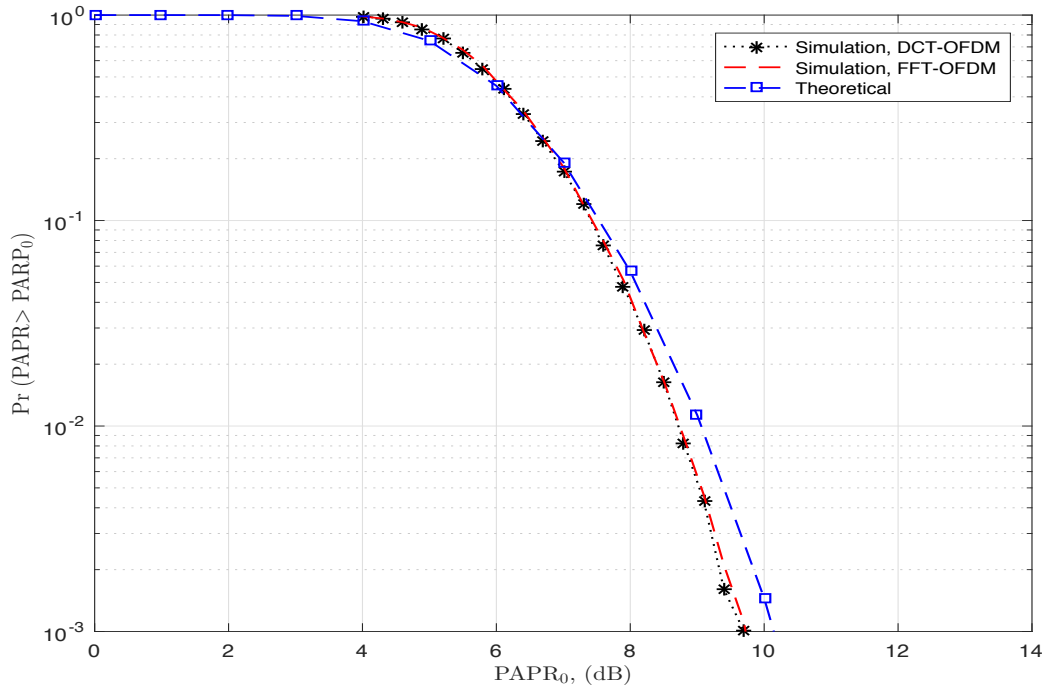


Figure 2.9: CCDFs of PAPR of DCT- and FFT-OFDM signals for $N = 32$.

results in the loss of subcarrier orthogonality and hence degrades BER performance of the system. To determine the effect of PAPR on OFDM system performance, nonlinear HPA models must be defined. These models and their impact on OFDM signals with high PAPR are discussed in the next Section.

2.4.2 Models of HPA and their effects

HPA is a necessary stage in most communication systems, as signals must be equipped with enough power to reach required distances with good fidelity. The HPA is typically modeled as a memory-less nonlinear device. The output of HPA can be written as:

$$x_{out}(t) = G(A(t)) e^{j[\phi(t)+\Theta(A(t))]} \quad (2.49)$$

where $A(t)e^{j[\phi(t)]}$ is the input to HPA, $G[A(t)]$ and $\Theta[A(t)]$ are the AM/AM and the AM/PM distortion functions, respectively. In practice two models of HPA are used. They are: i) Solid State Power Amplifier (SSPA) and ii) Traveling-Wave Tube Amplifier (TWT). The characteristics of these amplifiers are described below:

Solid State Power Amplifier

The SSPA is the most commonly used HPA in wireless communication systems. The functions $G[A(t)]$ and $\Theta[A(t)]$ for this model can be written as [105]:

$$G[A(t)] = \frac{G_0 A(t)}{\left[1 + \left(\frac{A(t)}{A_{sat}}\right)^{2p}\right]^{1/2p}} \quad (2.50)$$

and

$$\Theta[A(t)] = 0 \quad (2.51)$$

where G_0 is the amplifier gain, p controls the sharpness of the saturation region and A_{sat} is the input saturation level. Using (2.50) and (2.51) in (2.49), the output of SSPA can be written as:

$$x_{out}(t) = \frac{G_0 A(t)}{\left[1 + \left(\frac{A(t)}{A_{sat}}\right)^{2p}\right]^{1/2p}} e^{j[\phi(t)]} \quad (2.52)$$

Traveling-Wave Tube Amplifier

The TWTA is a wideband amplifier widely used in communication systems [106]. The AM/AM and AM/PM functions for this amplifier can be written as [107]:

$$G[A(t)] = \frac{G_0 A(t)}{1 + \left(\frac{A(t)}{A_{sat}}\right)^2} \quad (2.53)$$

and

$$\Theta[A(t)] = \frac{\alpha_\phi A(t)^2}{1 + \beta_\phi A(t)^2} \quad (2.54)$$

where α_ϕ and β_ϕ are nonzero constants. It is noted that TWTA model is relatively more nonlinear than the SSPA model. Using (2.53) and (2.54) in (2.49), the output of TWTA can be written as:

$$x_{out}(t) = \frac{G_0 A(t)}{1 + \left(\frac{A(t)}{A_{sat}}\right)^2} e^{j[\phi(t) + \frac{\alpha_\phi A(t)^2}{1 + \beta_\phi A(t)^2}]} \quad (2.55)$$

As a comparison, the AM/AM functions for SSPA (for $p = 3, 10$) and TWTA are shown in Figure 2.10. The AM/PM function for TWTA is shown in Figure 2.11.

In order to minimize the nonlinear distortion caused by the HPA in an OFDM system, an input power backoff (IBO) is required and is given by [108]:

$$IBO = \frac{A_{sat}^2}{P_{in}} \quad (2.56)$$

where P_{in} is the average power of the input signal.

In Figures 2.12 and 2.13, results of computer simulations of BER performance of DCT-OFDM ($N = 64$) system with 8-PSK mapper are shown for HPA with various IBO levels. The BER performance for the SSPA model for $0 \leq IBO \leq 10$ dB is shown in Figure 2.12. It is noted that there exist irreducible error for $IBO = 0$ dB. However, when $IBO = 10$ dB this error can be overcome. For the TWTA model BER performance is shown in Figure 2.13 for $0 \leq IBO \leq 18$ dB. It is noted that the irreducible error exists for $IBO = 0$ dB. To overcome this an IBO of 18 dB is required, which is 8 dB more than that required in the case of SSPA. In addition it is noted that the TWTA model is more

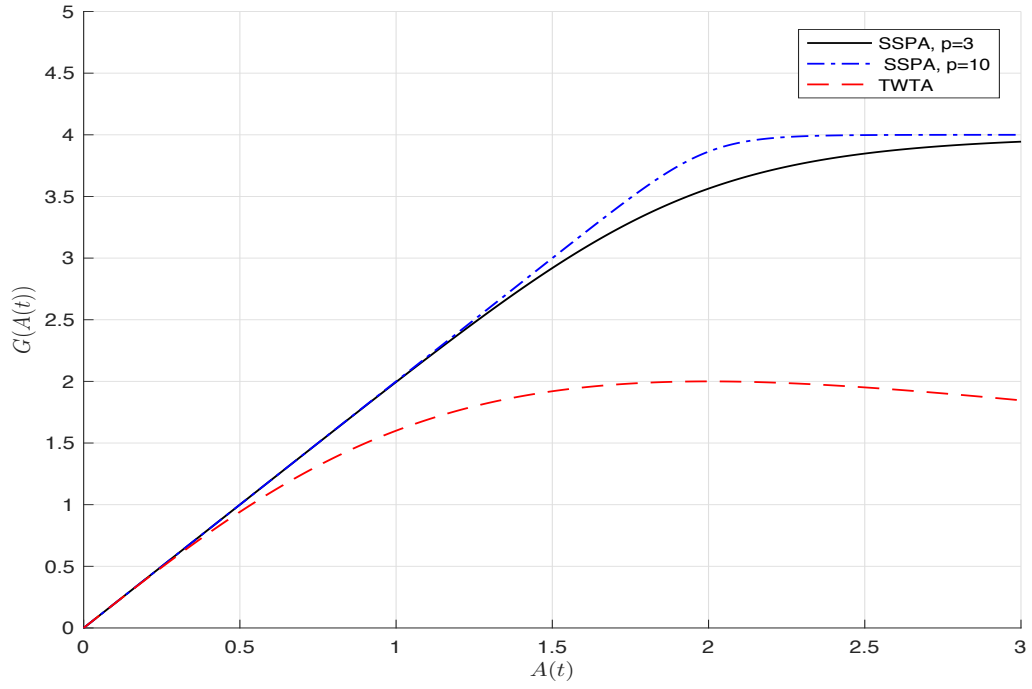


Figure 2.10: AM/AM functions for SSPA (for $p = 3, 10$) and TWTA for $A_{sat} = 2$.

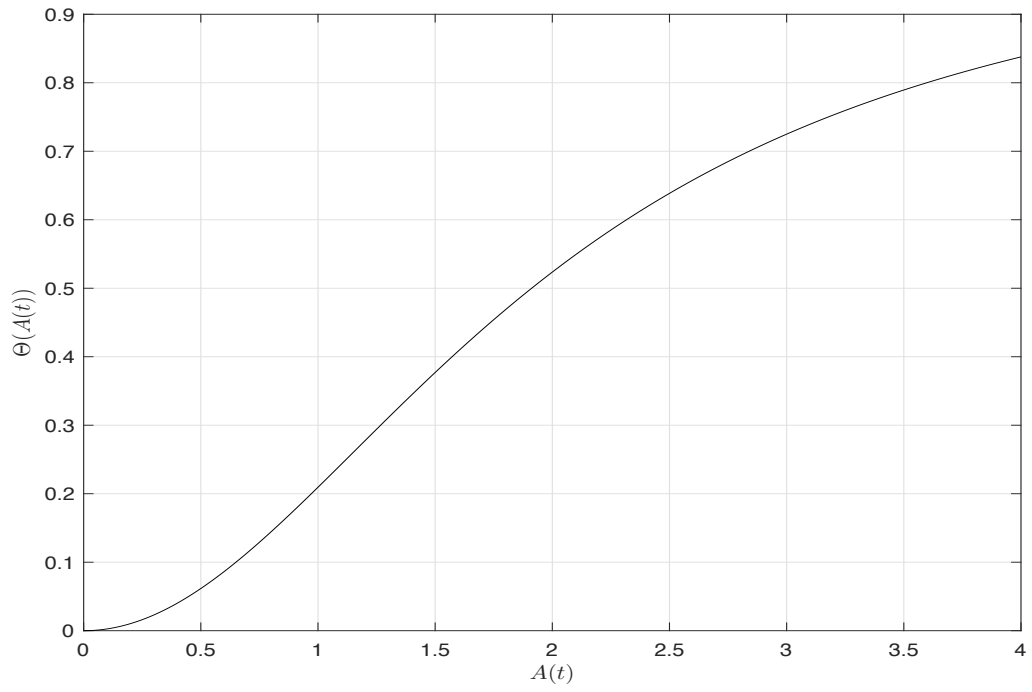


Figure 2.11: AM/PM function for TWTA for $\alpha_\phi = \pi/12$ and $\beta_\phi = 0.25$.

nonlinear than the SSPA model.

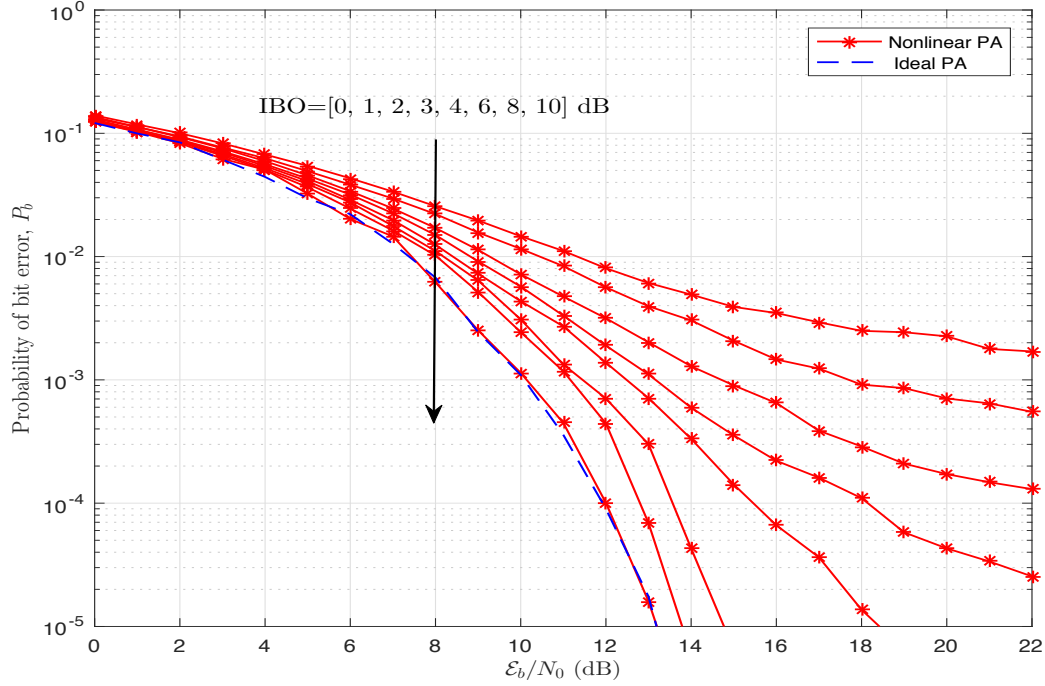


Figure 2.12: BER performance of DCT-OFDM (8-PSK, $N = 64$) system with SSPA for various values of IBO.

The relationship between efficiency and IBO for a Class A HPA is given by [52, 53]:

$$\eta_A = \frac{.5}{IBO} \times 100\% , IBO \geq 1 \quad (2.57)$$

The efficiency of Class A HPA as a function of IBO is shown in Figures 2.14. it is observed that the efficiency is inversely proportional to IBO. The maximum efficiency, (50 %) occurs at $IBO = 0$ dB.

It is noted that the undesirable effects of HPA nonlinearities can be reduced by increasing IBO, which is an unsatisfactory solution, since HPA efficiency reduces with IBO. The amount of IBO required is a function of the PAPR of the input OFDM signal to the HPA and a large PAPR leads to an increased value of IBO thereby reducing the HPA efficiency which is undesirable particularly for battery-powered systems. Therefore, increasing the IBO is not a good solution to overcome the problem of PAPR. Constant envelope OFDM signal design provides a good solution to this problem, as such a signal design offers 0

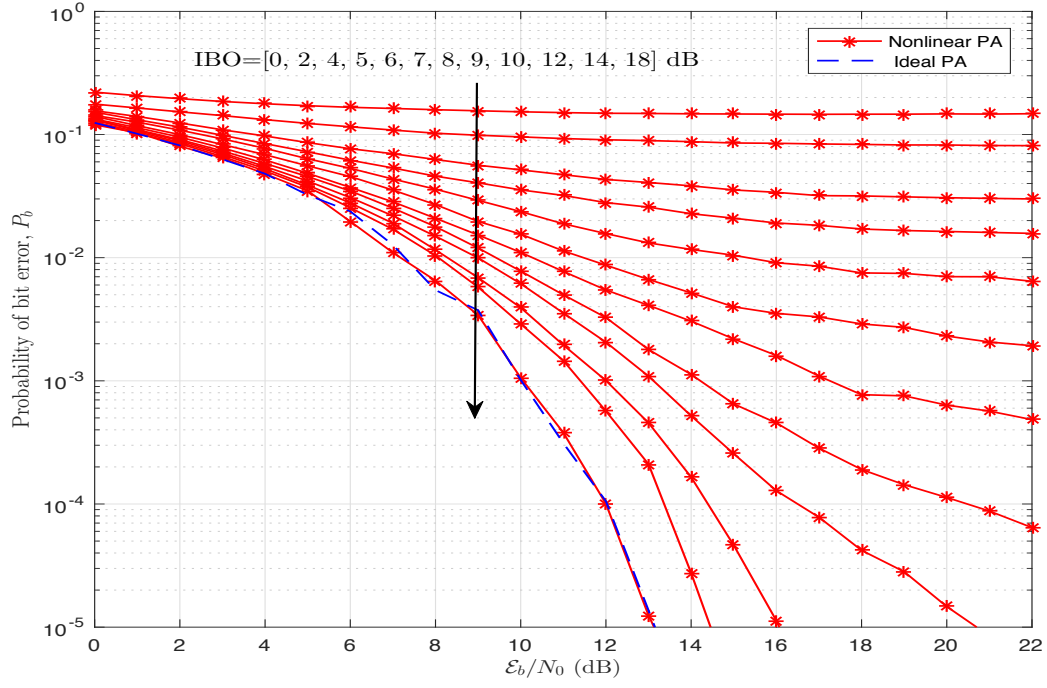


Figure 2.13: BER performance of DCT-OFDM (8-PSK, $N = 64$) system with TWTA for various values of IBO.

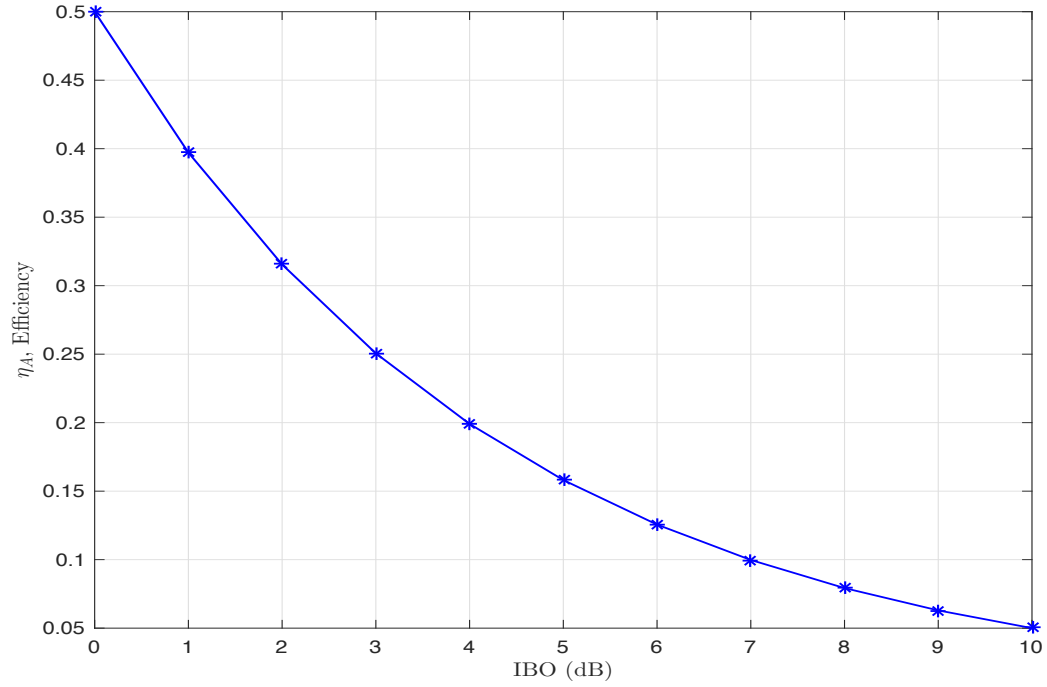


Figure 2.14: Efficiency (η_A) of Class A HPA as a function of IBO.

dB PAPR and hence does not require IBO and provides high efficiency of HPA in the system.

2.5 Conclusions

In this Chapter, a generic description of FFT- and DCT-OFDM systems is given. The concept of guard interval/Cyclic prefix is mathematically explained in both continuous- and discrete-time for these systems and it is shown that ISI-free operation is possible with the appropriate use of guard interval/Cyclic prefix. The PAPR statistics of FFT- and DCT-OFDM signals are presented and it is shown that PAPR increases as the number of subcarriers in the system. The models of HPA, both SSPA and TWAT, are described. The effect of IBO on the efficiency of HPA is illustrated. It is noted that by using CE-OFDM signals, it is possible to reduce IBO to 0 dB and increase the efficiency of HPA in the system.

Chapter 3

Constant Envelope DCT- and FFT-OFDM Systems with PM^{1,2,3}

3.1 Introduction

A generalized OFDM system with PM (CE-DCT- and CE-FFT-OFDM systems) is presented for data transmission. In the system, MPAM mapper is used. The system is described, illustrated, and examined for its properties. The detection of signals in this system in AWGN and fading channels is addressed. It is shown that the receiver structure consists of phase demodulator followed by the optimum OFDM detector. Expressions for bandwidth of CE-DCT and CE-FFT-OFDM systems are developed and presented. Closed-form expressions for BER performance of the receiver are derived and illustrated as a function of E_b/N_0 , M , h_p , and statistical parameters of densities of noise environment. The effect of TWTA amplifier on BER of the system is also presented.

-
1. Rayan H. Alsisi and Raveendra K. Rao, "Performance Comparison of Constant Envelope DCT- and FFT-based OFDM Systems with Phase Modulation over Frequency-Nonselective Fading Channels," 2017 IEEE 28th Annual International Symposium on Personal, Indoor, and Mobile Radio Communications (PIMRC), Montreal, Canada, October 2017, pp. 1-6.
 2. Rayan H. Alsisi and Raveendra K. Rao, "Performance of constant envelope DCT based OFDM system with M-ary PAM mapper in AWGN channel," 2017 Annual IEEE International Systems Conference (SysCon 2017), Montreal, Canada, April 2017, pp. 1-7.
 3. Rayan H. Alsisi and Raveendra K. Rao, "Discrete Cosine Transform Based Orthogonal Frequency Division Multiplexing with Phase Modulation and Constant Envelope," International Conference on Electronics, Information, and Communication (ICEIC 2017), Phuket, Thailand, January 2017, pp. 35-40.

3.2 Signals in DCT- and FFT-OFDM Systems with PM

A phase modulated OFDM bandpass signal can be written as:

$$s(t) = A_c \cos(2\pi f_c t + \phi(t)), \quad 0 \leq t \leq T \quad (3.1)$$

where A_c and f_c are the carrier amplitude and frequency of the signal and $\phi(t)$ is the information carrying phase and is given by:

$$\phi(t) = k_p x(t) \quad (3.2)$$

where k_p is the phase sensitivity constant of the modulator and $x(t)$, $0 \leq t \leq T$, is the real-valued OFDM signal carrying information about data to be transmitted. It is noted that $s(t)$ is a constant envelope signal. The information carrying phase $\phi(t)$ in CE-FFT- and CE-DCT-OFDM systems are given by:

$$\phi_{FFT}(t) = k_p x_{FFT}(t) = k_p \sqrt{\frac{2}{T\sigma_s^2}} \sum_{n=0}^{N-1} X_{FFT}(n) \cos(2\pi n t / T) \quad (3.3)$$

and

$$\phi_{DCT}(t) = k_p x_{DCT}(t) = k_p \sqrt{\frac{2}{T\sigma_s^2}} \sum_{n=0}^{N-1} X_{DCT}(n) \cos(\pi n t / T) \quad (3.4)$$

where $x_{FFT}(t)$ and $x_{DCT}(t)$ represent real signals of DCT- and FFT-OFDM systems with MPAM mapper. In the case of FFT-OFDM system $x_{FFT}(t)$ is obtained using conjugate symmetry of input data vector as explained in Chapter 1 and in the case of DCT-OFDM system, $x_{DCT}(t)$ is real-valued

3.3 CE-OFDM Transmitter

The block diagram of CE-OFDM transmitter is shown in Figure 3.1. A block of N symbols from a high rate data rate source is first passed through S/P converter to obtain a set of N low rate parallel data streams. These symbols are then passed to an MPAM

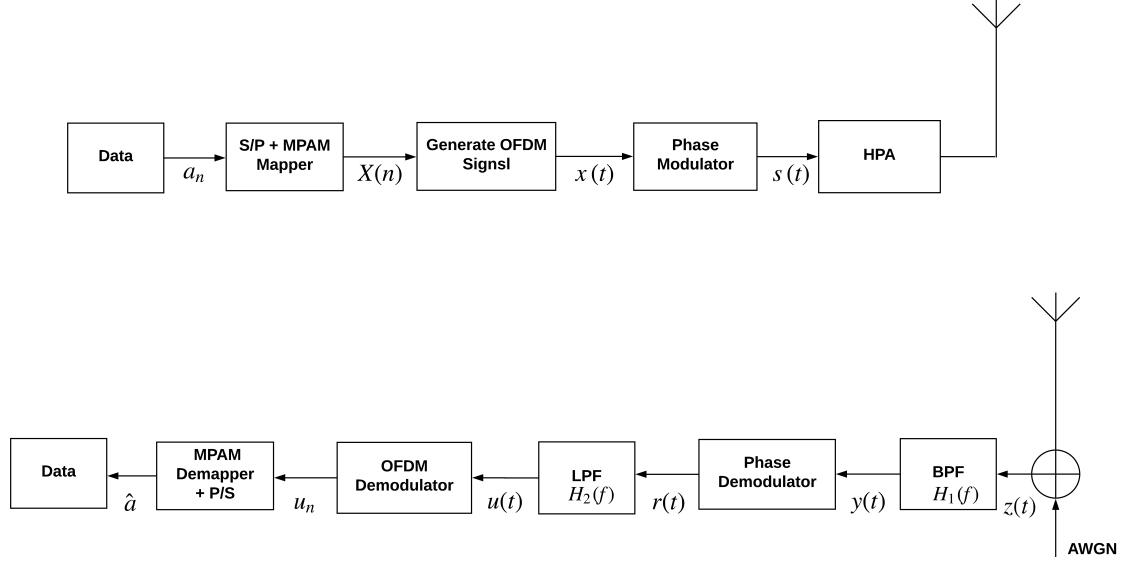


Figure 3.1: Transmitter and receiver structures for CE-OFDM system with PM

mapper whose output is a vector $[X(0), X(1), \dots, X(N-1)]^T$ consisting of N symbols. For an MPAM mapper, $X(n), n = 0, 1, \dots, N-1, \in \{\pm 1, \pm 3, \dots, \pm(M-1)\}$ and is used to generate the OFDM signal $x(t)$ which is fed to a phase modulator to obtain CE-OFDM signal $s(t)$. This signal is amplified by HPA and transmitted using an antenna over the communication channel.

Using (3.2) and (3.3) in (3.1), CE-FFT-OFDM signal can be written as:

$$s(t) = A_c \cos \left(2\pi f_c t + \sqrt{\frac{2}{T\sigma_s^2}} k_p \sum_{n=0}^{N-1} X_{FFT}(n) \cos(2\pi n t / T) \right) \quad (3.5)$$

Using (3.2) and (3.4) in (3.1), CE-DCT-OFDM signal can be written as:

$$s(t) = A_c \cos \left(2\pi f_c t + \sqrt{\frac{2}{T\sigma_s^2}} k_p \sum_{n=0}^{N-1} X_{DCT}(n) \cos(\pi n t / T) \right) \quad (3.6)$$

where σ_s^2 is the variance of data symbols and is given by:

$$\sigma_s^2 = E[|X_n|^2] = \frac{1}{M} \sum_{i=1}^M (2i - 1 - M)^2 = \frac{M^2 - 1}{3}$$

The average power and energy of signals in (3.5) and (3.6) are:

$$P_s = \frac{1}{T} \int_0^T s(t)^2 dt = \frac{A_c^2}{2}$$

and

$$E_s = P_s T = \frac{A_c^2 T}{2}$$

For N information symbols per transmission, the average bit energy is $E_b = A_c^2 T / (2N \log_2 M)$.

Bandwidth of CE-OFDM Signals

PM is a nonlinear modulation technique and its bandwidth is complex to analyze. However, a rough estimate of bandwidth can be obtained using Maclaurin series expansion of PM signal in (3.1). That is,

$$s(t) = A_c [\cos(2\pi f_c t) - \phi(t) \sin(2\pi f_c t) - \frac{1}{2!} \phi^2(t) \cos(2\pi f_c t) + \dots] \quad (3.7)$$

For $\phi(t) \ll 1$, the first two terms in the series are sufficient to represent the signal. That is,

$$s(t) \approx A_c \cos 2\pi f_c t - A_c \phi(t) \sin 2\pi f_c t \quad (3.8)$$

This represents the narrowband case and the bandwidth of such a signal is at least $2W$ Hz, where W is the bandwidth of the modulating OFDM signal $x(t)$. As $\phi(t)$ becomes larger, the bandwidth of the signal broadens. A useful expression for bandwidth in such a case is given by the Root Mean Square (RMS) bandwidth of the signal [109], and is equal to $\max(2h_p, 2)W$ Hz, where $h_p = k_p \max |x(t)|$, is the modulation index. For the case of FFT-OFDM message signal $W = N/T$ Hz and for DCT-OFDM message signal

$$W = N/2T \text{ Hz} [44, 38].$$

3.4 CE-OFDM Receiver: Signal Detection and Performance

The block diagram of CE-OFDM receiver is shown in Figure 3.1 and consists of cascade of Band Pass Filter (BPF), phase demodulator, Low Pass Filter (LPF), OFDM demodulator, MPAM demapper, and P/S converter blocks.

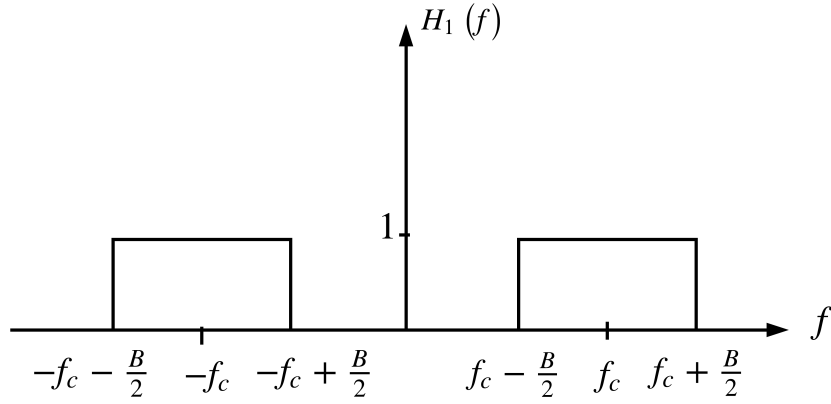


Figure 3.2: Ideal bandpass filter characteristic

The received signal ($z(t) = s(t) + w(t)$) is first passed through a BPF, $H_1(f)$, with characteristic as shown in Figure 3.2, where B is the bandwidth of CE-OFDM signal $s(t)$. The bandwidth B is in excess of twice the OFDM message signal bandwidth $W \text{ Hz}$ by an amount that depends on the modulation index of the PM signal $s(t)$. The noise $w(t)$ is modelled as AWGN with zero mean and PSD of $N_0/2 \text{ Watts/Hz}$. The input to the phase demodulator can be written as

$$y(t) = s(t) + n(t), 0 \leq t \leq T \quad (3.9)$$

where $n(t)$ represents the output of BPF due to the input $w(t)$ and can be represented in terms of its in-phase and quadrature components. Thus, the output of the phase

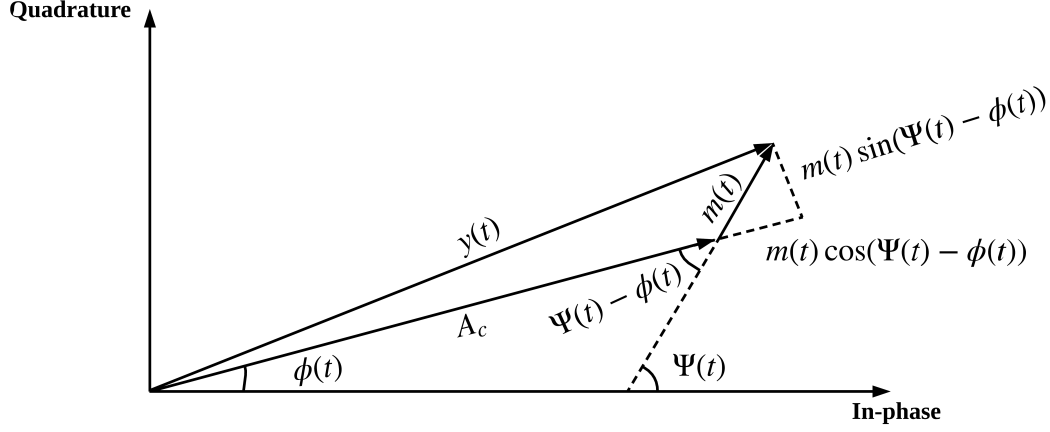


Figure 3.3: Phasor diagram of $y(t)$

demodulator is a low pass signal with bandwidth equal to message signal, W Hz. The LPF output is then fed to the OFDM demodulator followed by the MPAM demapper and P/S converter to get an estimate of transmitted data.

3.4.1 Phase Demodulator

The phase demodulator consists of arctangent block to detect the phase of the received signal, using $\arctan \left\{ \frac{y_Q(t)}{y_I(t)} \right\}$, where $y_Q(t)$ and $y_I(t)$ are quadrature and in-phase components of $y(t)$, followed by a phase unwrapper [110]. The noise, $n(t)$ at the input of the phase demodulator can be expressed as

$$n(t) = n_I(t)\cos 2\pi f_c t - n_Q(t)\sin 2\pi f_c t \quad (3.10)$$

where $n_I(t)$ and $n_Q(t)$ are the in-phase and quadrature components of filtered $w(t)$. In polar form (3.10) can be written as

$$n(t) = m(t)\cos[2\pi f_c t + \Psi] \quad (3.11)$$

where the envelope $m(t)$ and phase $\Psi(t)$ are given by:

$$m(t) = \sqrt{[n_I^2(t) + n_Q^2(t)]} \quad (3.12)$$

and

$$\Psi(t) = \arctan \left\{ \frac{n_Q(t)}{n_I(t)} \right\} \quad (3.13)$$

Thus, the input to the phase demodulator can be written as

$$y(t) = A_c \cos[2\pi f_c t + \phi(t)] + m(t) \cos[2\pi f_c t + \Psi(t)], \quad (3.14)$$

which, in polar form, can be written as:

$$y(t) = v(t) \cos[2\pi f_c t + \theta(t)] \quad (3.15)$$

where $v(t)$ represents the envelope and $\theta(t)$ the phase angle of $y(t)$ in (3.14). The phase diagram of $y(t)$ is shown in Figure 3.3. Ignoring $m(t)$, as its variation is restricted by the limiter in the phase demodulator, it is evident from Figure 3.3 that the phase of $y(t)$ is given by [109, 110]:

$$\theta(t) = \phi(t) + \varepsilon(t) \quad (3.16)$$

where

$$\varepsilon(t) = \arctan \left\{ \frac{m(t) \sin[\Psi(t) - \phi(t)]}{A_c + m(t) \cos[\Psi(t) - \phi(t)]} \right\} \quad (3.17)$$

is the phase noise. For high value of Carrier-to-Noise Ratio (CNR), $A_c \gg m(t)$, (3.16) can be approximated by:

$$\theta(t) \approx \phi(t) + \frac{m(t)}{A_c} \sin[\Psi(t) - \phi(t)] \quad (3.18)$$

The output of the phase demodulator is proportional to $\theta(t)$ and is given by

$$r(t) = \frac{1}{k_p} \theta(t) \quad (3.19)$$

Using (3.18) in (3.19), we get

$$r(t) = x(t) + n_d(t) \quad (3.20)$$

where

$$n_d(t) = \frac{m(t)}{k_p A_c} \sin[\Psi(t) - \phi(t)] \quad (3.21)$$

The PSD, $S_{N_d}(f)$, of $n_d(t)$ is related to the PSD, $S_{N_Q}(f)$, of $n_Q(t)$ [110, 111] and is given by

$$S_{N_d}(f) = \left\{ \frac{1}{k_p A_c} \right\}^2 S_{N_Q}(f) \quad (3.22)$$

where

$$S_{N_Q}(f) = \begin{cases} N_0, & |f| \leq \frac{B}{2} \\ 0, & \text{otherwise} \end{cases} \quad (3.23)$$

The phase demodulator output is applied to LPF of bandwidth equal to that of message signal $x(t)$, W Hz. The LPF allows the message signal $x(t)$ to pass through and rejects out-of-band noise due to $n_d(t)$. The transfer function of LPF is

$$H_2(f) = \begin{cases} 1, & |f| \leq W \\ 0, & \text{otherwise} \end{cases} \quad (3.24)$$

The output of LPF can be written as

$$u(t) = x(t) + n_u(t) \quad (3.25)$$

The PSD, $S_{N_u}(f)$, of $n_u(t)$ at the output of LPF is given by

$$S_{N_u}(f) = \begin{cases} N_0/k_p^2 A_c^2, & |f| \leq W \\ 0, & \text{otherwise} \end{cases} \quad (3.26)$$

and, thus, the average power of $n_u(t)$ is:

$$\int_{-W}^W \frac{N_0 k_d^2}{A_c} df = \frac{2W N_0}{k_p^2 A_c^2} \quad (3.27)$$

3.4.2 OFDM Demodulator

The OFDM demodulator block shown in Figure 3.4 consists of two stages, a demodulator followed by a detector. The demodulator projects the incoming signal $u(t)$ on to an N -dimensional orthogonal signal space and the detector outputs are applied to MPAM demappers to estimate the transmitted information symbols based on the projected co-

ordinates. The N outputs of the demodulator are $u(0), u(1), \dots, u(N-1)$. The j^{th} of

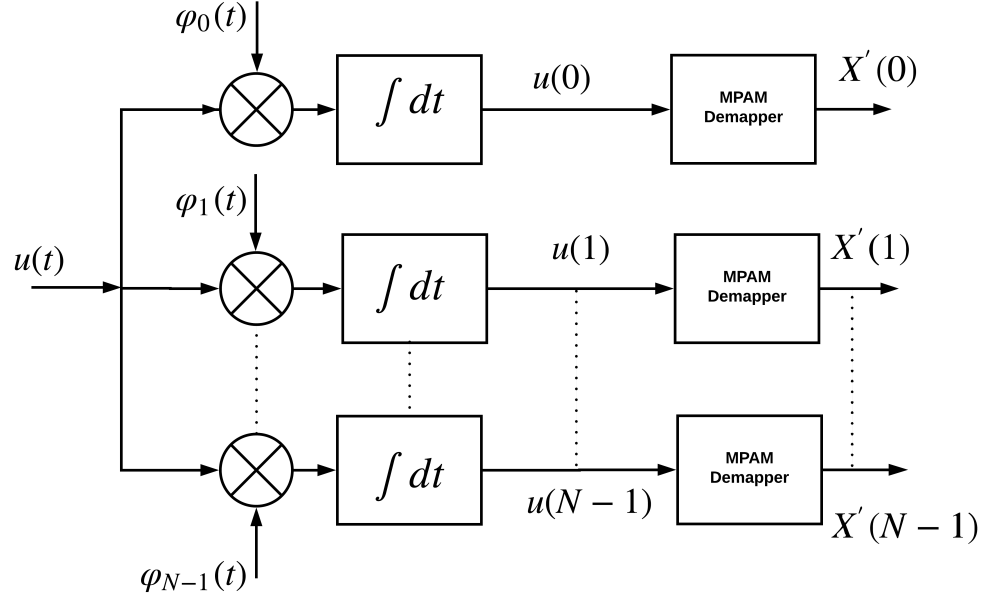


Figure 3.4: Structure of OFDM demodulator

these outputs is given by:

$$u(j) = \int_0^T u(t) \varphi_j^*(t) dt \quad (3.28)$$

where $\varphi_j(t)$, $j = 0, 1, \dots, N-1$ are given in (1.5) and (1.6) for FFT- and DCT-OFDM systems. Using (3.25) in (3.28), $u(j)$ can be written as:

$$u(j) = X(j)/\sqrt{\sigma_s^2} + N_u(j); j = 0, 1, \dots, N-1 \quad (3.29)$$

The mean of $u(j)$ is,

$$E[u(j)] = E[X(j)/\sqrt{\sigma_s^2} + N_u(j)] = E[X(j)/\sqrt{\sigma_s^2}] \quad (3.30)$$

where $X(j) \in \{\pm 1, \pm 3, \dots, \pm(M-1)\}$. It is noted that the mean is independent of the noise $n_u(t)$. However, the variance of $u(j)$ is dependent on the characteristic of the noise

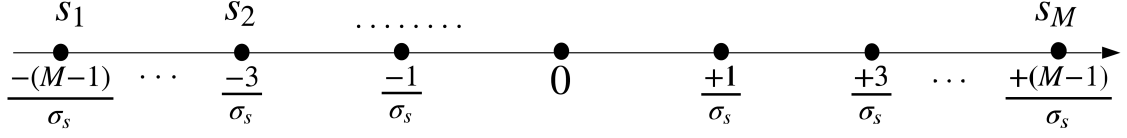


Figure 3.5: Signal constellation of MPAM demapper

$n_u(t)$. and is given by:

$$\text{Var}[u(j)] = \sigma_u^2(j) = E \left\{ [u(j) - E \{u(j)\}]^2 \right\} \quad (3.31)$$

The variance can be shown to be given by:

$$\text{Var}[u(j)] = \sigma_u^2 = \frac{2WN_0}{k_p^2 A_c^2}, \quad j = 0, 1, \dots, N-1 \quad (3.32)$$

3.4.3 BER Probability of CE-OFDM system

In this Section, the BER performance of the CE-OFDM receiver is derived. Consider the output of the j^{th} correlator fed to the MPAM demapper as shown in Figure 3.4. That is,

$$u(j) = \frac{X(j)}{\sqrt{\sigma_s^2}} + N_u(j)$$

where $X(j) \in \{\pm 1, \pm 3, \dots, \pm(M-1)\}$, $\sigma_s^2 = ((M^2 - 1)/3)$ is the variance of data symbols, and $N_u(j)$ is a zero Gaussian random variable with variance σ_u^2 given by (3.32). The signal constellation of MPAM demapper is shown in Figure 3.5. It is noted that there exist two types of points in the constellation. There are $M - 2$ inner points and 2 outer points (s_1 and s_M) in the constellation. If an inner point is transmitted, there will be an error in detection if $|N_u(j)| > \frac{1}{2}d_{\min}$, where $d_{\min} = \frac{2}{\sqrt{\sigma_s^2}}$. For the outer points, the probability of error is one-half of the error probability of an inner points since noise can cause error in only one direction. Since $N_u(j)$ is a zero-mean Gaussian random variable with variance given by (3.32), the error probability of inner points is given by:

$$P_{inner} = Prob. \left[|N_u(j)| > \frac{1}{2}d_{min} \right] = 2Prob. \left[N_u(j) > \frac{1}{2}d_{min} \right] \quad (3.33)$$

$$= 2 \int_{1/\sqrt{\sigma_s^2}}^{\infty} \frac{1}{\sqrt{2\pi\sigma_u^2}} e^{(-x^2/2\sigma_u^2)} dx \quad (3.34)$$

$$P_{inner} = 2Q \left(\sqrt{\frac{A_c^2 h_p^2}{2W N_0 \sigma_s^2}} \right) \quad (3.35)$$

where

$$Q(x) = \frac{1}{\sqrt{2\pi}} \int_x^{\infty} e^{-y^2/2} dy \quad (3.36)$$

and for the outer points, the probability of error is

$$P_{outer} = \frac{1}{2}P_{inner} \quad (3.37)$$

Therefore, the symbol error probability for the j^{th} MPAM mapper can be written as:

$$\begin{aligned} P_s &= \frac{1}{M} \sum_{i=1}^M Prob. [error \mid s_i \text{ sent}] \\ &= \frac{1}{M} [(M-2) P_{inner} + 2P_{outer}] \\ &= 2 \left(\frac{M-1}{M} \right) Q \left(\sqrt{\frac{A_c^2 h_p^2}{2W N_0 \sigma_s^2}} \right) \end{aligned} \quad (3.38)$$

Using the values of W for message signals DCT- and FFT-OFDM systems, the symbol error probabilities for the CE-FFT- and CE-DCT-OFDM systems are given by:

$$P_{s_{FFT}} = 2 \left(\frac{M-1}{M} \right) Q \left(\sqrt{\frac{3h_p^2 \log_2(M) E_b}{(M^2-1)N_0}} \right) \quad (3.39)$$

and

$$P_{s_{DCT}} = 2 \left(\frac{M-1}{M} \right) Q \left(\sqrt{\frac{6h_p^2 \log_2(M) E_b}{(M^2-1)N_0}} \right) \quad (3.40)$$

In the receiver, there are N demappers and each has the same symbol error probability

given by (3.39) and (3.40). The average of N symbol error is simply given by (3.39) and (3.40). It is noted that for $h_p = 1$, (3.40) reduces to the well-known expression symbol error rate of MPAM system [6]. Converting the symbol error rate to Bit Error Rate (BER), we get

$$P_b \approx \frac{P_s}{\log_2(M)} \quad (3.41)$$

The BER for the CE-FFT- and CE-DCT-OFDM systems are given by:

$$P_{b_{FFT}} \approx 2 \left(\frac{M-1}{M \log_2(M)} \right) Q \left(\sqrt{\frac{3h_p^2 \log_2(M) E_b}{(M^2-1)N_0}} \right) \quad (3.42)$$

and

$$P_{b_{DCT}} \approx 2 \left(\frac{M-1}{M \log_2(M)} \right) Q \left(\sqrt{\frac{6h_p^2 \log_2(M) E_b}{(M^2-1)N_0}} \right) \quad (3.43)$$

The BER given by (3.42) and (3.43) are functions of h_p , modulation index, M , number of amplitude levels in MPAM mapper, and E_b/N_0 , signal-to-noise ratio.

3.5 Performance of CE-OFDM system over Fading Channels

Wireless channel introduces various impairments and effects that cause degradation of SNR leading to poor BER performance. In this study, slow frequency non-selective fading channels are considered, as they represent many practical wireless channel environment. There are several statistical models available to describe fading effects; however, Rayleigh and Rician models are used in our study. Also, the BER performance of CE-OFDM system over flat Rayleigh and Rician channels is evaluated.

3.5.1 Frequency Non-Selective Fading Channel

The received CE-OFDM signal over a frequency non-selective fading channel can be modeled as:

$$\int_{-\infty}^{\infty} h(\tau) s(t-\tau) d\tau + w(t) \quad (3.44)$$

where $s(t)$ is the transmitted signal, $w(t)$ is AWGN and $h(t)$ is the impulse response of the channel and is given by

$$h(t) = \alpha e^{j\phi_0} \delta(t) \quad (3.45)$$

Using (3.45) in (3.44), the received signal can be written as:

$$z(t) = \alpha e^{j\phi_0} s(t) + n(t) \quad (3.46)$$

where α and ϕ_0 are the channel amplitude and phase, respectively. In the frequency domain, the channel is described by $H(f) = \mathcal{F}[h(t)] = \alpha e^{j\phi_0}$ denoting that it is constant at all frequencies and hence the channel is frequency non-selective. Such a channel is referred to as flat-fading channel. The channel amplitude is treated as a random quantity. When it is a zero-mean complex-valued Gaussian process, its envelope is Rayleigh distributed. The pdf of Rayleigh distributed random variable α is given by:

$$p_\alpha(\alpha; \sigma) = \frac{\alpha}{\sigma^2} e^{-\alpha^2/2\sigma^2}, \quad \alpha \geq 0 \quad (3.47)$$

where σ is the scale parameter of the distribution

Another pdf that is commonly used to model the envelope is the Rice distribution. The pdf of Rician random variable can be expressed as:

$$p_\alpha(\alpha; a, \sigma) = \frac{\alpha}{\sigma^2} e^{-\frac{\alpha^2 + a^2}{2\sigma^2}} I_0 \left[\frac{\alpha a}{\sigma^2} \right], \quad a \geq 0, \alpha \geq 0 \quad (3.48)$$

where $I_0(z)$ is the modified Bessel function of the first kind with order zero. The pdfs of Rayleigh and Rice random variables are shown in Figures 3.6 and 3.7, respectively.

3.5.2 BER performance of CE-OFDM system

The instantaneous SNR and the average SNR per bit can be represented as $\gamma = \alpha^2 E_b / N_0$ and $\bar{\gamma} = E \{ \alpha^2 \} E_b / N_0$, respectively. To obtain the bit error rate (P_b) of CE-OFDM system over a fading channel, the conditional BER is averaged over the pdf of γ and can be written as [112]:

$$P_b = \int_0^\infty P_b(\gamma) p_\gamma(\gamma) d\gamma \quad (3.49)$$

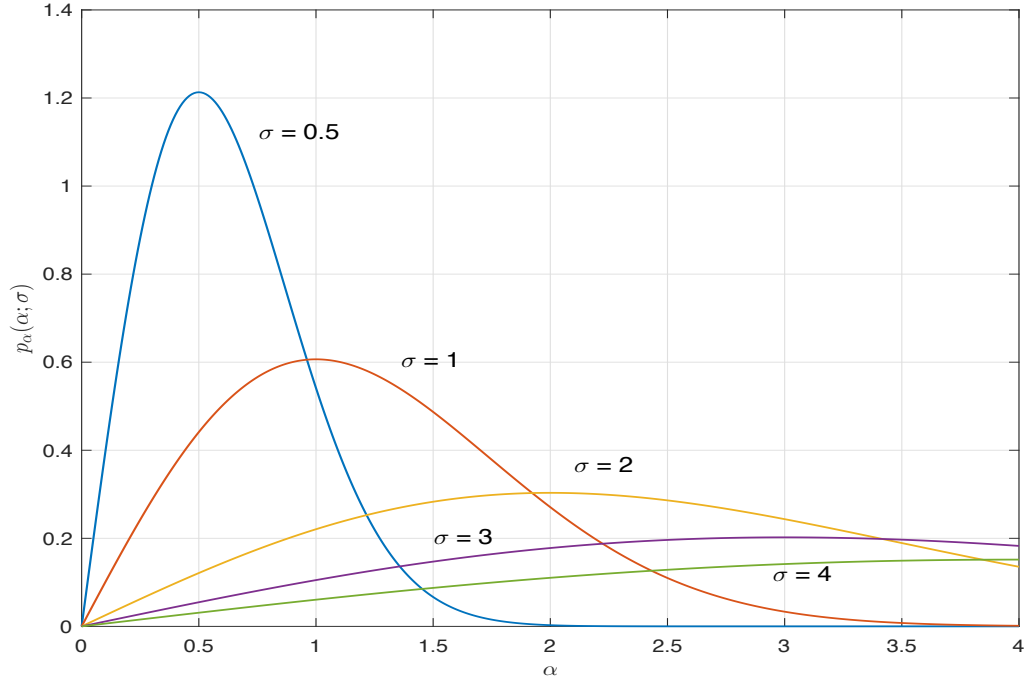


Figure 3.6: Probability density function of Rayleigh random variable as a function of σ .

where $P_b(\gamma)$ from (3.42) and (3.43) is given by:

$$P_b(\gamma) = 2 \left(\frac{M-1}{M \log_2(M)} \right) Q \left(\sqrt{q \alpha^2 \frac{E_b}{N_0}} \right) = 2 \left(\frac{M-1}{M \log_2(M)} \right) Q(\sqrt{q\gamma}) \quad (3.50)$$

where $q = \frac{3h_p^2 \log_2(M)}{M^2-1}$, for FFT-OFDM system and for DCT-OFDM system $q = \frac{6h_p^2 \log_2(M)}{M^2-1}$.

3.5.3 Rayleigh Fading Channel

The Rayleigh channel is characterized with no direct LOS path. Since α is Rayleigh distributed, α^2 has a chi-square pdf with two degrees of freedom. Consequently, the pdf of γ can be shown to be given by [112]:

$$p_\gamma(\gamma) = \frac{1}{\bar{\gamma}} \exp\left(-\frac{\gamma}{\bar{\gamma}}\right), \gamma \geq 0 \quad (3.51)$$

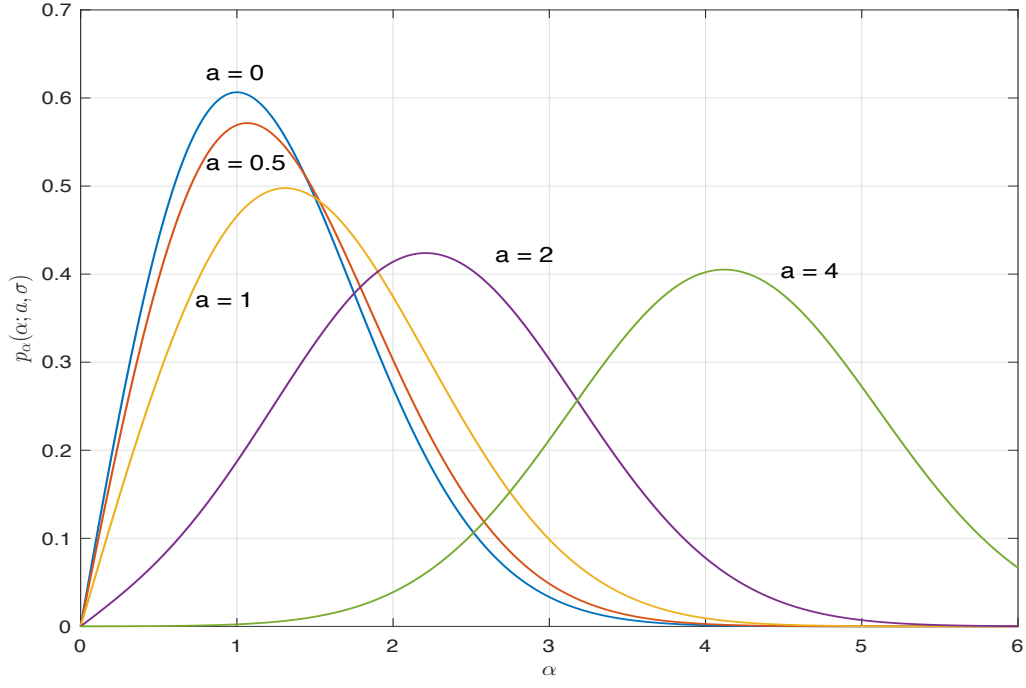


Figure 3.7: Probability density function for Rice random variable for $\sigma = 1$ and various values of a .

Using (3.50) and (3.51) in (3.49), P_b is given by

$$P_b = 2 \left(\frac{M-1}{M \log_2(M)} \right) \frac{1}{\pi \bar{\gamma}} \int_0^{\pi/2} \int_0^{\infty} \exp \left(-\frac{q\gamma}{2 \sin^2(\theta)} - \frac{\gamma}{\bar{\gamma}} \right) d\gamma d\theta \quad (3.52)$$

where an alternate expression for $Q(z)$ has been used and is given by:

$$Q(z) = \frac{1}{\pi} \int_0^{\pi/2} \exp \left(-\frac{z^2}{2 \sin^2(\theta)} \right) d\theta \quad (3.53)$$

Upon simplification of (3.52) [113], the bit error rate can be written as:

$$P_b = \left(\frac{M-1}{M \log_2(M)} \right) \left[1 - \sqrt{\frac{1}{1 + \frac{1}{q\bar{\gamma}/2}}} \right] \quad (3.54)$$

The BER given by (3.54) is a function of h_p , modulation index, M , and $\bar{\gamma}$, the average SNR of the received signal over Rayleigh fading channel. In deriving (3.54), it is assumed that the channel phase shift ϕ_0 is estimated from the received signal without error and remains constant during the observation interval.

3.5.4 Rician Fading Channel

The Rician channel has one strong direct LOS component and many indirect weaker components. Since α is Rice distributed, γ is noncentral chi-square distributed and is given by [112]:

$$p_\gamma(\gamma) = \frac{(1+K)e^{-K}}{\bar{\gamma}} \exp\left[-\frac{(1+K)\gamma}{\bar{\gamma}}\right] I_0\left[2\sqrt{\frac{(K+K^2)\gamma}{\bar{\gamma}}}\right], \gamma \geq 0 \quad (3.55)$$

where K is the Rice factor expressed in dB as:

$$K = 10 \log \frac{a^2}{2\sigma^2} \text{ dB}$$

where a^2 represents the power of signal from LOS path and σ^2 is the power of signals from non LOS paths. For the special case when the $K = 0$, the Rician density reduces to Rayleigh density. Using (3.50) and (3.55) in (3.49), we get

$$P_b = \frac{2}{\pi} \left(\frac{M-1}{M \log_2(M)} \right) \frac{(1+K)e^{-K}}{\bar{\gamma}} \int_0^{\pi/2} \int_0^\infty \exp\left[-\frac{q\gamma}{2\sin^2(\theta)} - \frac{(1+K)\gamma}{\bar{\gamma}}\right] I_0\left[2\sqrt{\frac{(K+K^2)\gamma}{\bar{\gamma}}}\right] d\gamma d\theta \quad (3.56)$$

where $Q(z)$ given in (3.53) has been used. Upon simplification of (3.56) [113], the bit error rate can be written as:

$$P_b = \frac{2}{\pi} \left(\frac{M-1}{M \log_2(M)} \right) \int_0^{\pi/2} \frac{(1+K)\sin^2(\theta)}{(1+K)\sin^2(\theta) + q\bar{\gamma}/2} \exp\left[-\frac{Kq\bar{\gamma}/2}{(1+K)\sin^2(\theta) + q\bar{\gamma}/2}\right] d\theta \quad (3.57)$$

It is noted that BER is a function of h_p , modulation index, M , K , Rice factor and $\bar{\gamma}$, average SNR of received signal over Rician channel. In deriving (3.57), it is assumed that the channel phase shift ϕ_0 is estimated from the received signal without error and remain constant during the observation interval.

3.6 Numerical Results and Discussion

In this Section numerical results of probability of bit error performances of CE-DCT- and CE-FFT-OFDM systems are presented and discussion of these results is also included. The effect of HPA on BER performances of these systems is also persented.

3.6.1 Performance in AWGN Channel

The expressions for BER in AWGN channel for CE-DCT- and CE-FFT-OFDM systems are given by (3.42) and (3.43), respectively. They are functions of h_p , modulation index, M , number of amplitude levels in MPAM mapper, and E_b/N_0 , signal-to-noise ratio. The BER performances of these systems are shown in Figure 3.8 as a function of h_p and E_b/N_0 for a 2-PAM mapper. It is observed that CE-DCT-OFDM system performs better than the corresponding CE-FFT-OFDM system. For example at $P_b = 10^{-5}$, $h_p = 0.6$, E_b/N_0 required for CE-DCT-OFDM system is nearly 3 dB less than that required for CE-FFT-OFDM system. Also, it is observed that BER decreases as h_p increases for a fixed value of E_b/N_0 . For example, at $P_b = 10^{-5}$, E_b/N_0 required for $h_p = 0.2$ is 9.5 dB more than that required for $h_p = 0.6$. Table 3.1 summarizes E_b/N_0 required at $P_b = 10^{-5}$ for both systems as a function of h_p . In Figure 3.9, probability of bit error performances

Table 3.1: Comparison of CE-DCT- and CE-FFT-OFDM systems (2-PAM mapper) at $P_b = 10^{-5}$ as a function of h_p

h_p	CE-DCT-OFDM	CE-FFT-OFDM
	E_b/N_0 (dB)	E_b/N_0 (dB)
1.2	8.004	11.016
1.0	9.588	12.598
0.8	11.526	14.536
0.6	14.025	17.035
0.4	17.547	20.557
0.2	23.567	26.578

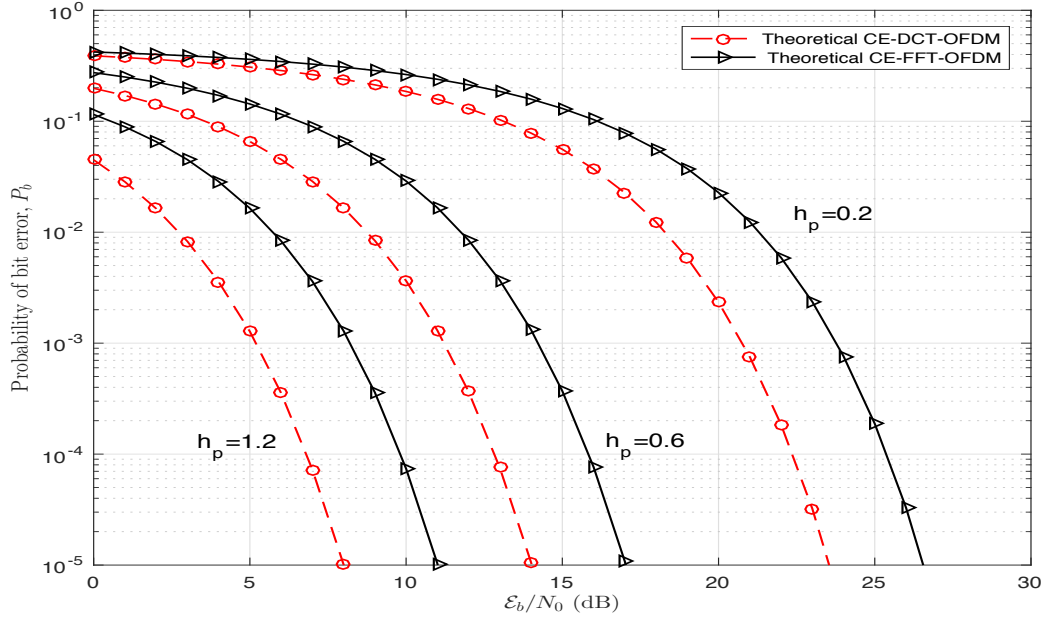


Figure 3.8: Probability of bit error performances of CE-DCT- and CE-FFT-OFDM systems for (2-PAM mapper) over AWGN channel.

of CE-DCT- and CE-FFT-OFDM systems are shown, for 4-PAM mapper in the system. Table 3.2 summarizes E_b/N_0 required at $P_b = 10^{-5}$ for both systems as a function of h_p . It is observed that BER decreases as h_p increases for a fixed value of E_b/N_0 .

Table 3.2: Comparison of CE-DCT- and CE-FFT-OFDM systems (4-PAM mapper) at $P_b = 10^{-5}$ as a function of h_p

h_p	CE-DCT-OFDM	CE-FFT-OFDM
	E_b/N_0 (dB)	E_b/N_0 (dB)
1.2	11.851	14.561
1.0	13.435	16.445
0.8	15.373	18.383
0.6	17.872	20.882
0.4	21.393	24.404
0.2	27.414	30.424

Figure 3.10. shows BER performance of CE-DCT-OFDM system for 8-PAM mapper as a function of h_p and E_b/N_0 . In the same figure, BER performance of CE-FFT-OFDM is also shown. Table 3.3 summarizes E_b/N_0 required at $P_b = 10^{-5}$ for both systems as a function of h_p . The probability of bit error performances of CE-DCT- and CE-FFT-OFDM systems with $h_p = 0.6$ for various values of M are illustrated in Figures 3.11 and

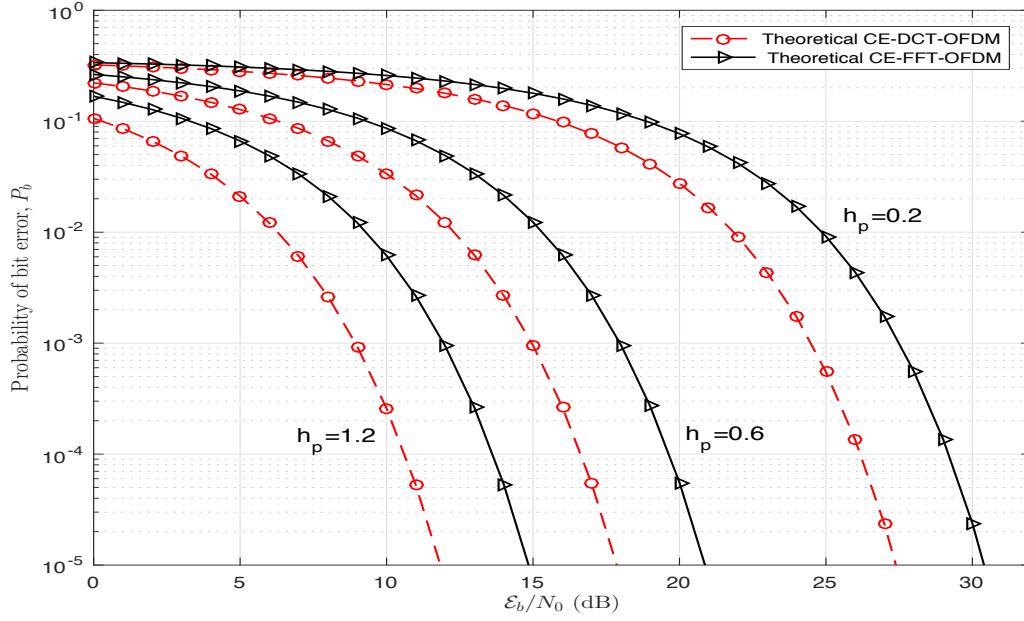


Figure 3.9: Probability of bit error performances of CE-DCT- and CE-FFT-OFDM systems for (4-PAM mapper) over AWGN channel.

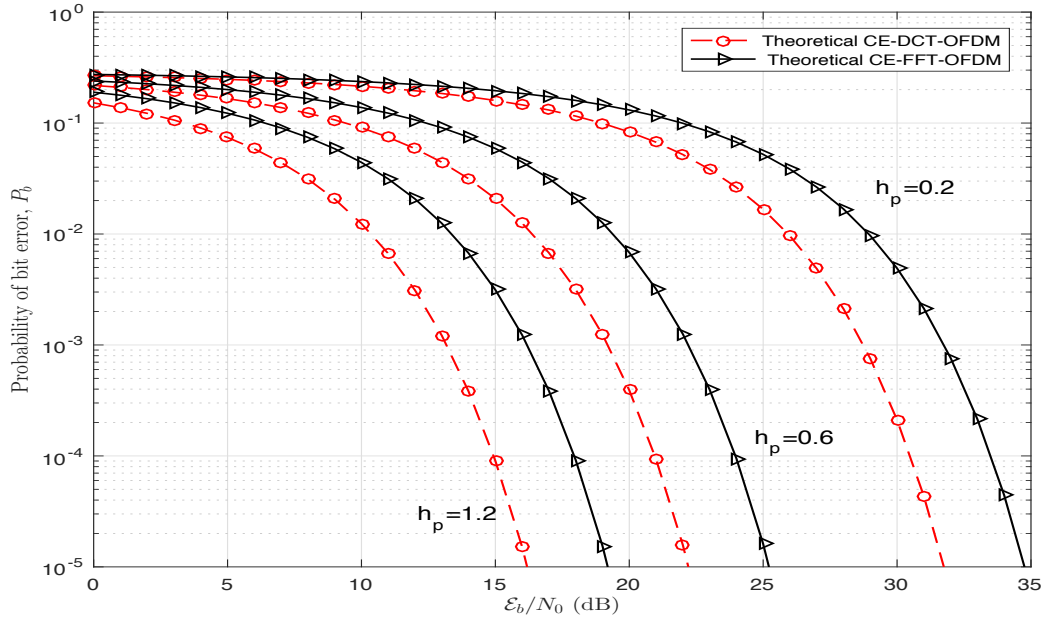


Figure 3.10: Probability of bit error performances of CE-DCT- and CE-FFT-OFDM systems for (8-PAM mapper) over AWGN channel.

Table 3.3: Comparison of CE-DCT- and CE-FFT-OFDM systems (8-PAM mapper) at $P_b = 10^{-5}$ as a function of h_p

h_p	CE-DCT-OFDM	CE-FFT-OFDM
	E_b/N_0 (dB)	E_b/N_0 (dB)
1.2	16.203	19.213
1.0	17.787	20.797
0.8	19.725	22.734
0.6	22.224	25.234
0.4	25.746	28.756
0.2	31.766	34.776

3.12, respectively. For both systems, it is noted that BER increases as the modulation order M increases. For example, for CE-DCT-OFDM system ($M = 4, h_p = 0.6$) at $\text{BER} = 10^{-5}$, $E_b/N_0 = 14.025 \text{ dB}$ is required, whereas for $M = 4$ and $M = 8$, $E_b/N_0 = 17.872 \text{ dB}$ and 22.224 dB are required, respectively. At $P_b = 10^{-5}$, the systems with $M = 4$ and 8 are worse than the system with $M = 2$ by 3.8 and 8.2 dB, respectively. However, spectral efficiency improves with increased value of M in the system.

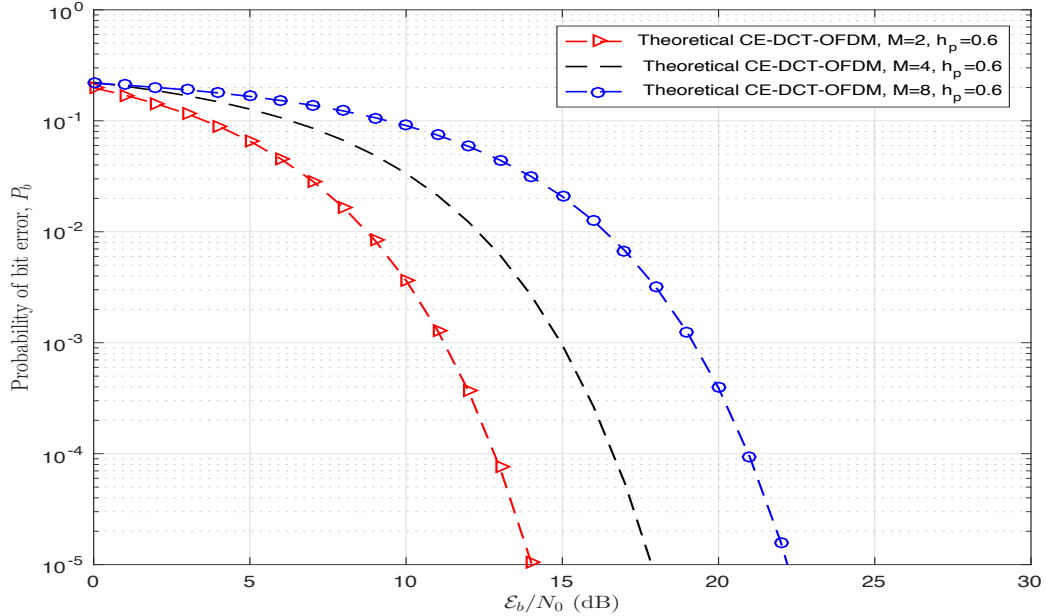


Figure 3.11: Probability of bit error performance of CE-DCT-OFDM system as a function of M for $h_p = 0.6$ over AWGN channel.

The BER performances of both systems can be controlled by appropriately choosing h_p and M as shown in Figures 3.13 and 3.14. For example, CE-DCT-OFDM system with

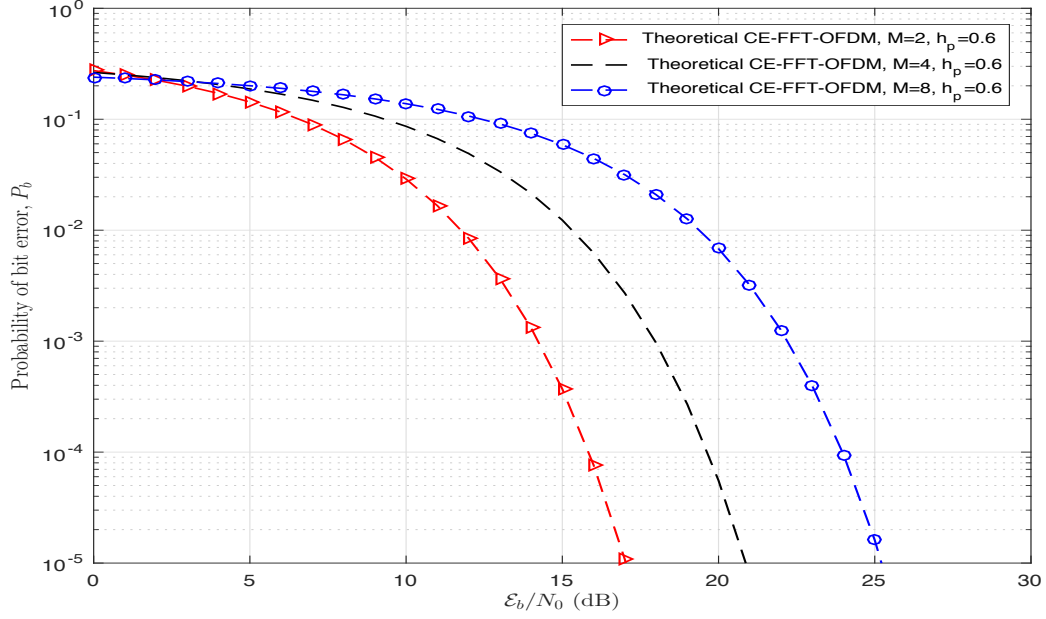


Figure 3.12: Probability of bit error performance of CE-FFT-OFDM system as a function of M for $h = 0.6$ over AWGN channel.

$M = 8$ and $h_p = 1.2$ outperforms corresponding system with $M = 2$ and $h_p = 0.2$ by 7.4 dB at BER = 10^{-5} .

Figures 3.15 and 3.16 show comparison of simulation and theoretical BER results for CE-DCT-OFDM system ($N = 64$ subcarriers) for $M = 4$ and $M = 8$, respectively. It is noted that simulation and theoretical results are nearly the same.

3.6.2 Performance over Fading Channels

The expression for BER over Rayleigh fading channel is given by (3.54). Figures 3.17, 3.18, and 3.19 show P_b of CE-DCT- and CE-FFT-OFDM systems for $M = 2, 4$, and 8, respectively. Figures 3.8 and 3.17 show the probability of bit error performances of both systems for 2-PAM mapper for AWGN and flat Rayleigh fading channels, respectively. It is noted that, the presence of signal fading causes a large increase in the E_b/N_0 required to achieve the same level of BER as that for the AWGN channel. For example, at $h_p = 0.6$ to achieve BER equal to 10^{-5} over AWGN channel CE-DCT-OFDM system requires 14.025 dB. However, the same system over Rayleigh fading channel requires, 48.105 dB to achieve the same BER. The reason for this large increase in E_b/N_0 required can be

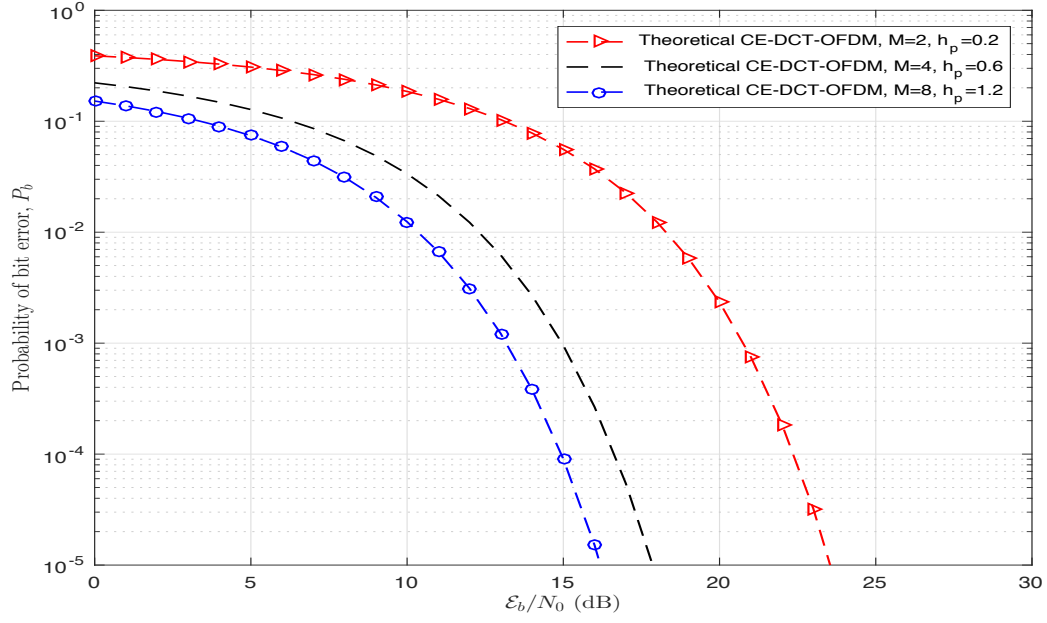


Figure 3.13: Probability of bit error performance of CE-DCT-OFDM system as a function of h_p and M over AWGN channel.

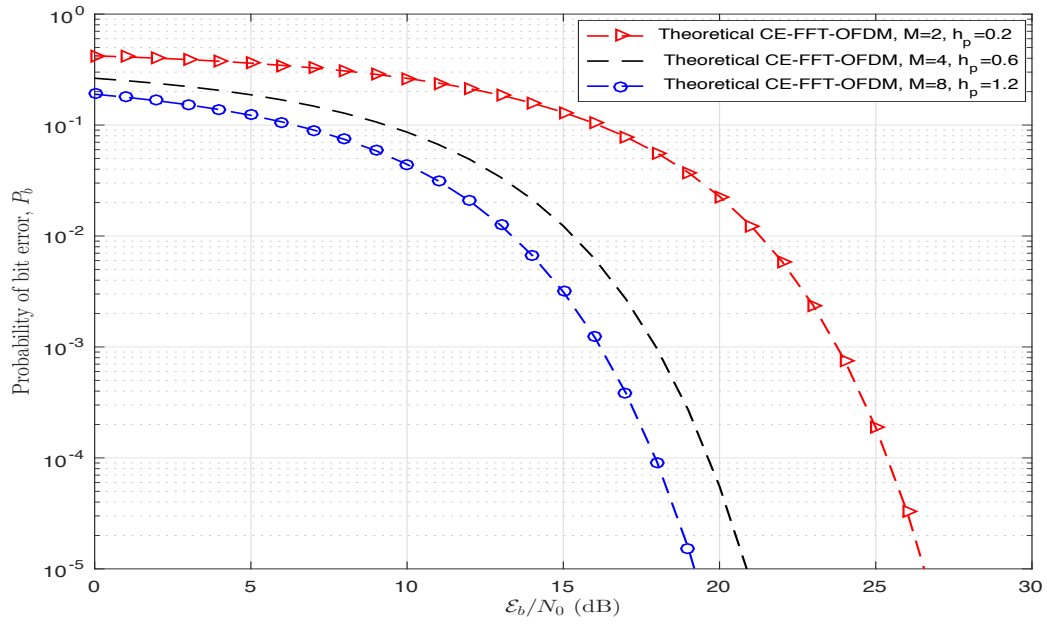


Figure 3.14: Probability of bit error performance of CE-FFT-OFDM system as a function of h_p and M over AWGN channel.

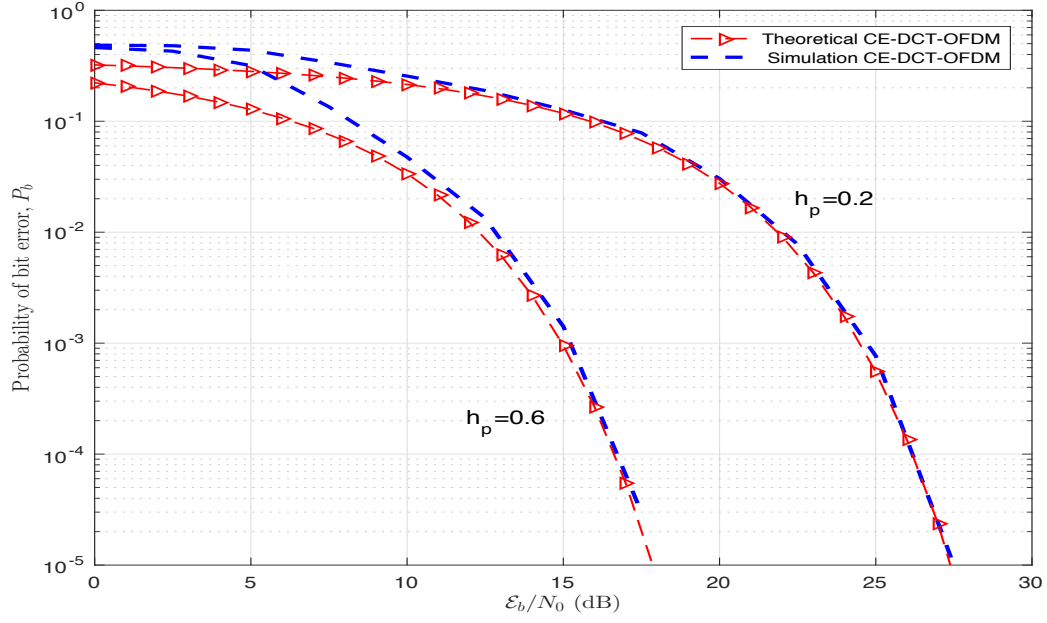


Figure 3.15: Comparison of analytical and simulation results for CE-DCT-OFDM system (4-PAM mapper) over AWGN channel.

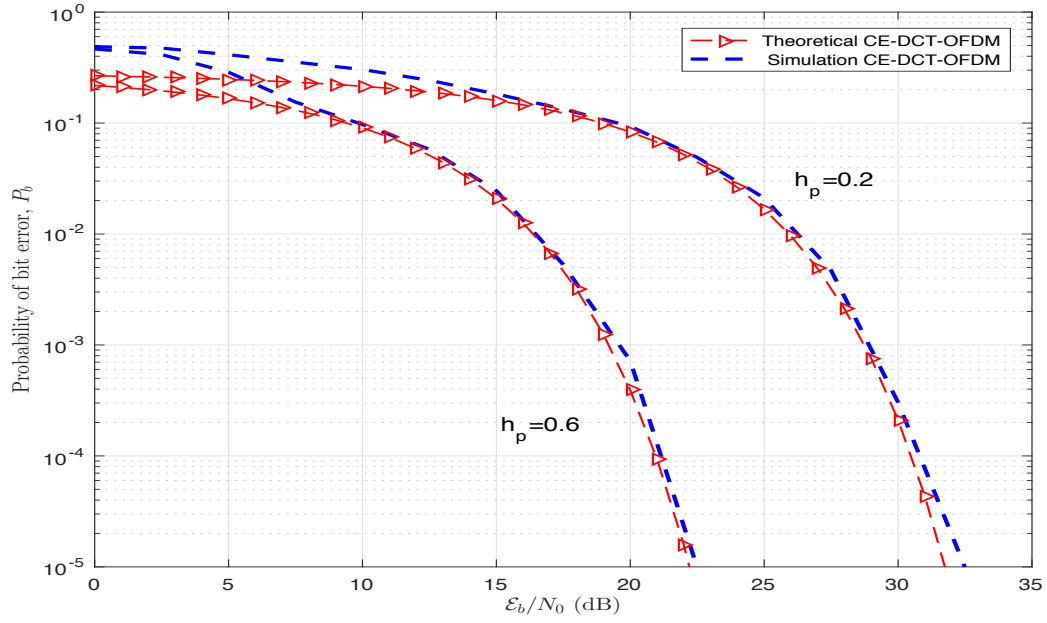


Figure 3.16: Comparison of analytical and simulation results for CE-DCT-OFDM system (8-PAM mapper) over AWGN channel.

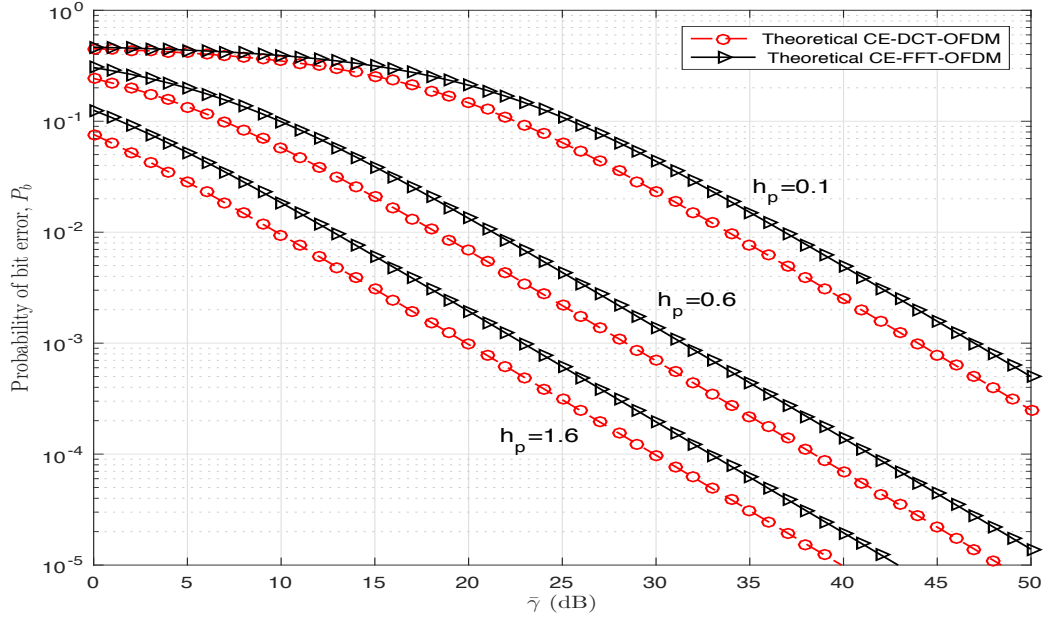


Figure 3.17: Probability of bit error performances of CE-DCT- and CE-FFT-OFDM systems (2-PAM mapper) over Rayleigh fading channel.

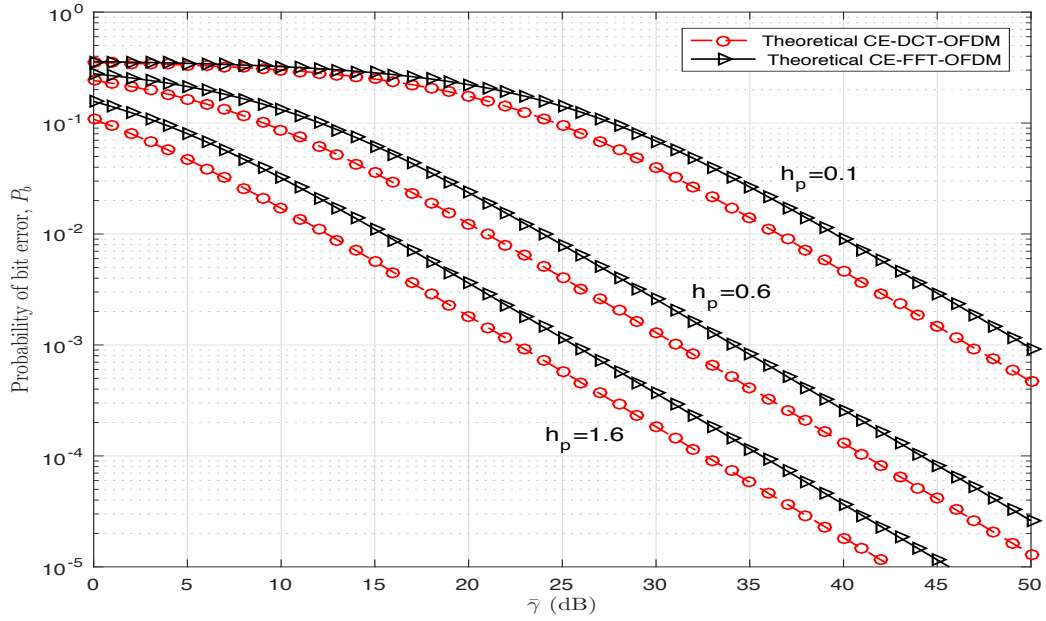


Figure 3.18: Probability of bit error performances of CE-DCT- and CE-FFT-OFDM systems (4-PAM mapper) over Rayleigh fading channel.

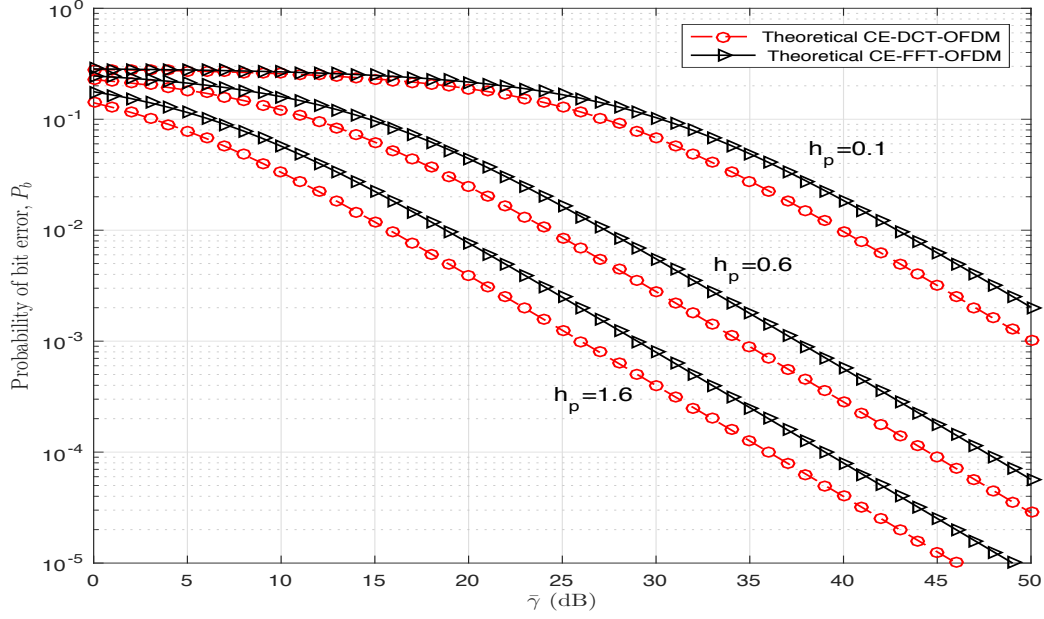


Figure 3.19: Probability of bit error performances of CE-DCT- and CE-FFT-OFDM systems (8-PAM mapper) over Rayleigh fading channel.

understood by examining the density function of SNR of the received signal, given by (3.51), where the exponential form places some values of signal power at very low levels. For higher values of signal power, the error rates are negligible. Therefore, the average BER is dominated by the intervals over which the SNR is low and BER is high. As a result, a large increase in average signal power, which greatly widens the density of SNR given (3.51), is needed to reduce the probability that the instantaneous signal power lies in the region of high BER.

The expression for BER for Rician fading channel is given by (3.57). The BER is not only a function of h_p , M and $\bar{\gamma}$, but also depends on K , Rice factor. Figures 3.20, 3.21 and 3.22 depict P_b vs $\bar{\gamma}$, average SNR, of CE-DCT- and CE-FFT-OFDM systems for $M = 2, 4$ and 8 , for Rician fading channel with $K = 6$ dB, respectively. The comparison of probability of bit error performances of CE-DCT- and CE-FFT-OFDM systems for $M = 2$ and $h_p = 1$ over AWGN, Rician and Rayleigh channels as a function of average SNR are shown in Figures 3.23 and 3.24, respectively. It is noted that there is a penalty in SNR that must be paid as consequence of fading. Tables 3.4 and 3.5 summarize SNR required at $P_b = 10^{-3}, 10^{-4}$ and 10^{-5} for CE-DCT- and FFT-OFDM

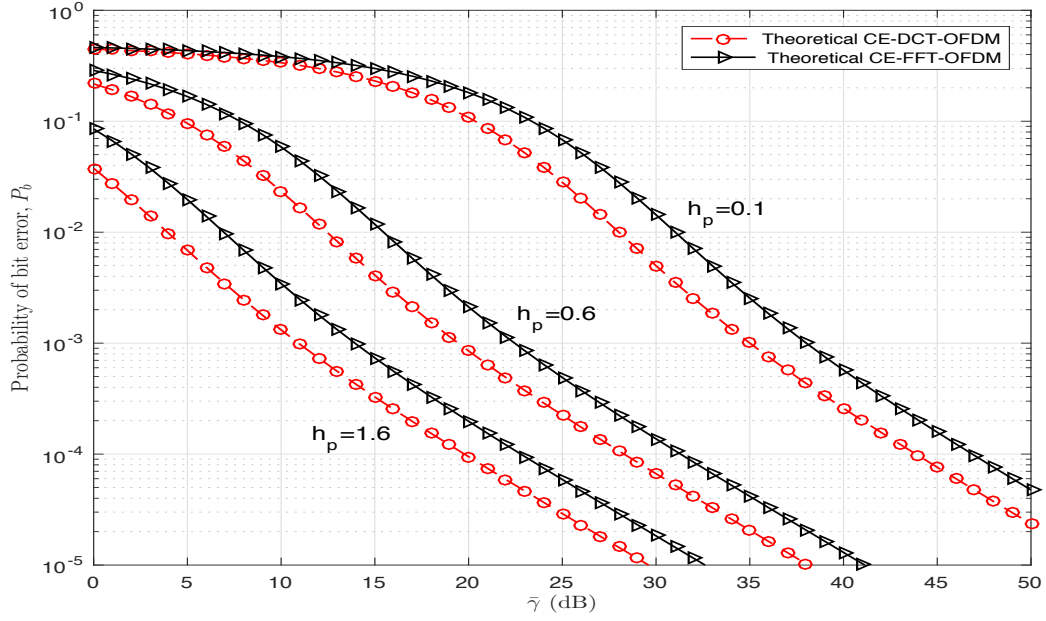


Figure 3.20: Probability of bit error performances of CE-DCT- and CE-FFT-OFDM systems (2-PAM mapper) over Rician fading channel ($K = 6$ dB).

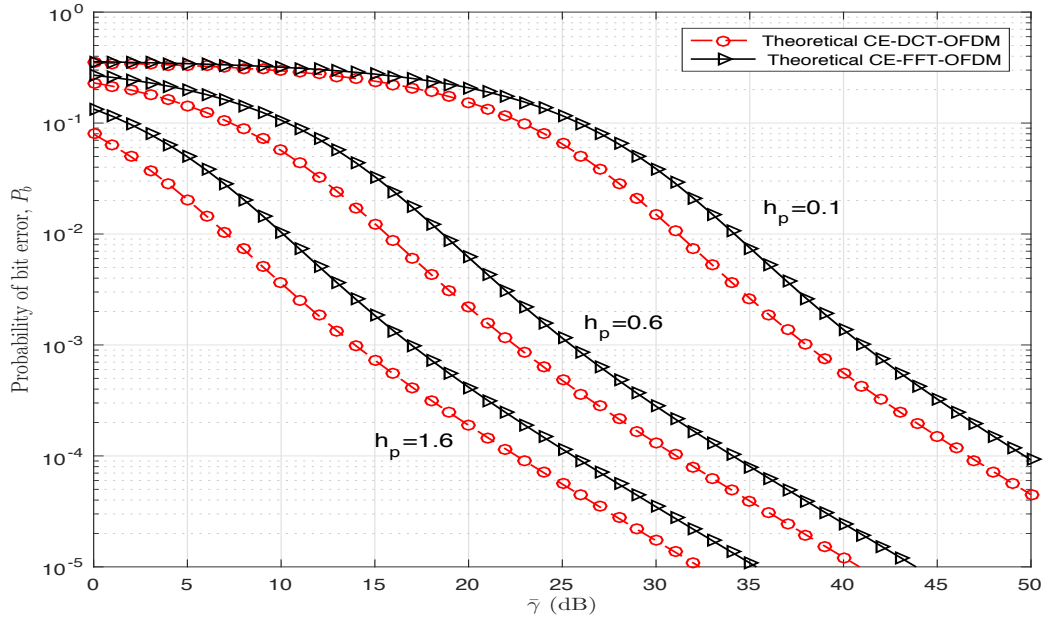


Figure 3.21: Probability of bit error performances of CE-DCT- and CE-FFT-OFDM systems (4-PAM mapper) over Rician fading channel ($K = 6$ dB).

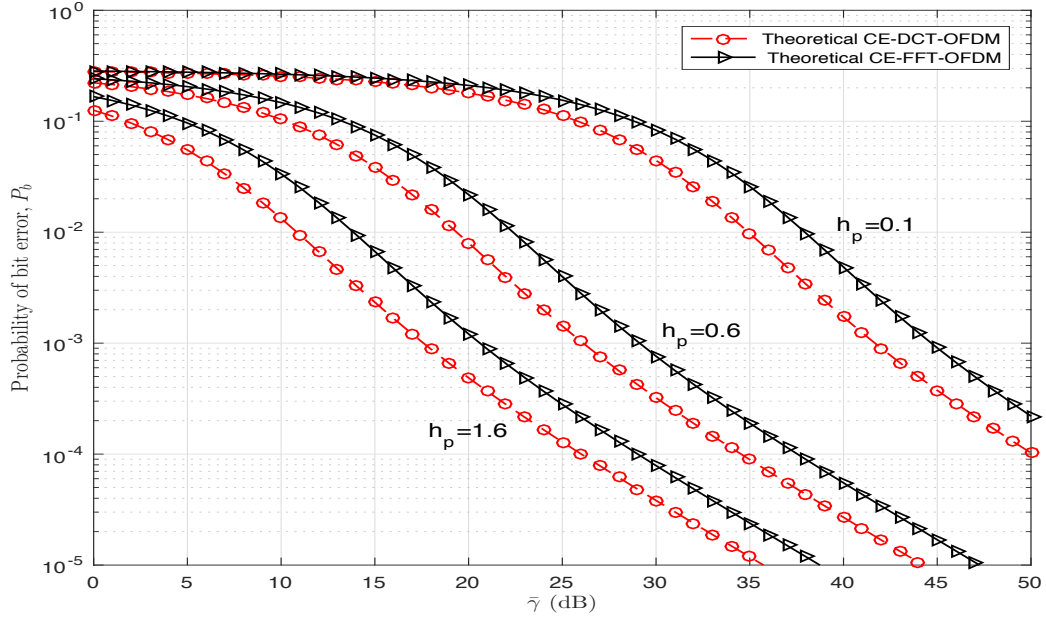


Figure 3.22: Probability of bit error performances of CE-DCT- and CE-FFT-OFDM systems (8-PAM mapper) over Rician fading channel ($K = 6$ dB).

systems over AWGN, Rician and Rayleigh channels, respectively.

Table 3.4: Comparison of probability of bit error performances of CE-DCT-OFDM system over AWGN, Rician and Rayleigh channels.

P_b	Average SNR (dB)		
	AWGN	Rician	Raleigh
10^{-3}	6.789	15.118	24.162
10^{-4}	8.398	23.873	34.851
10^{-5}	9.588	34.851	43.542

Table 3.5: Comparison of probability of bit error performances of CE-FFT-OFDM system over AWGN, Rician and Rayleigh channels.

P_b	Average SNR (dB)		
	AWGN	Rician	Raleigh
10^{-3}	9.799	18.132	27.111
10^{-4}	11.409	27.861	36.851
10^{-5}	12.598	36.674	46.655

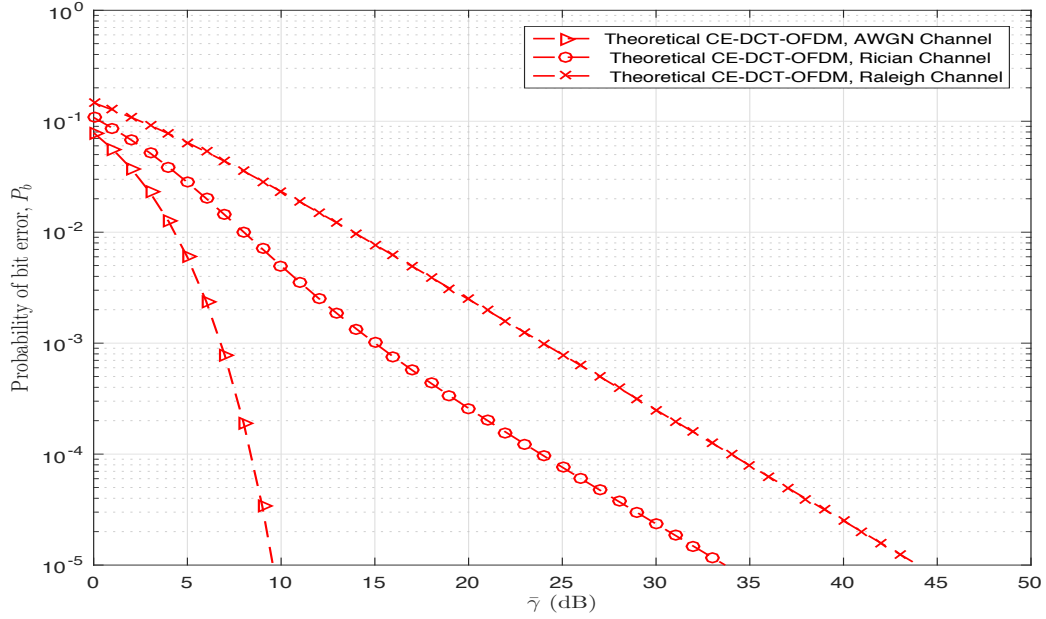


Figure 3.23: Comparison of probability of bit error performances of CE-DCT-OFDM system (2-PAM mapper, $h_p = 1$) over AWGN, Rician ($K = 6$ dB) and Rayleigh channels.

Figure 3.25 illustrates the effect of K on BER performances for CE-DCT- and CE-FFT-OFDM systems for $M = 4$ and $h_p = 0.5$. It is evident that BER decreases as the value of K increases. For example at BER of 10^{-4} , the average SNR required for $K = 18$ dB is nearly by 30 dB less than that required for $K = 2$ dB. It is well known that as $K \rightarrow \infty$, Rician density approaches that of Gaussian density.

3.7 CE-DCT- and DCT-OFDM Systems with TWTA Amplifier

The undesirable effects of nonlinear HPA in an OFDM system can be mitigated by increasing IBO, as discussed in Chapter 2. For the DCT-OFDM system, one needs to adjust the average input power so that the peaks of the signal are rarely clipped. That is, one needs to apply an IBO to the signal prior to amplification. In the case of CE-DCT-OFDM system with power amplifier, the input and output signals can be written

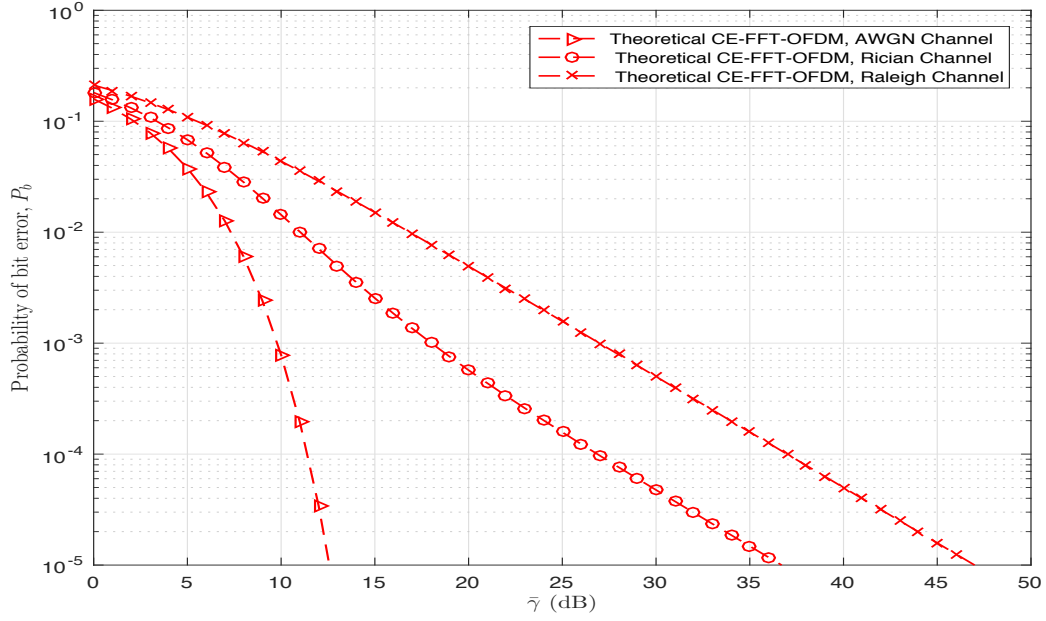


Figure 3.24: Comparison of probability of bit error performances of CE-FFT-OFDM system (2-PAM mapper, $h_p = 1$) over AWGN, Rician ($K = 6$ dB) and Rayleigh channels as a function of SNR.

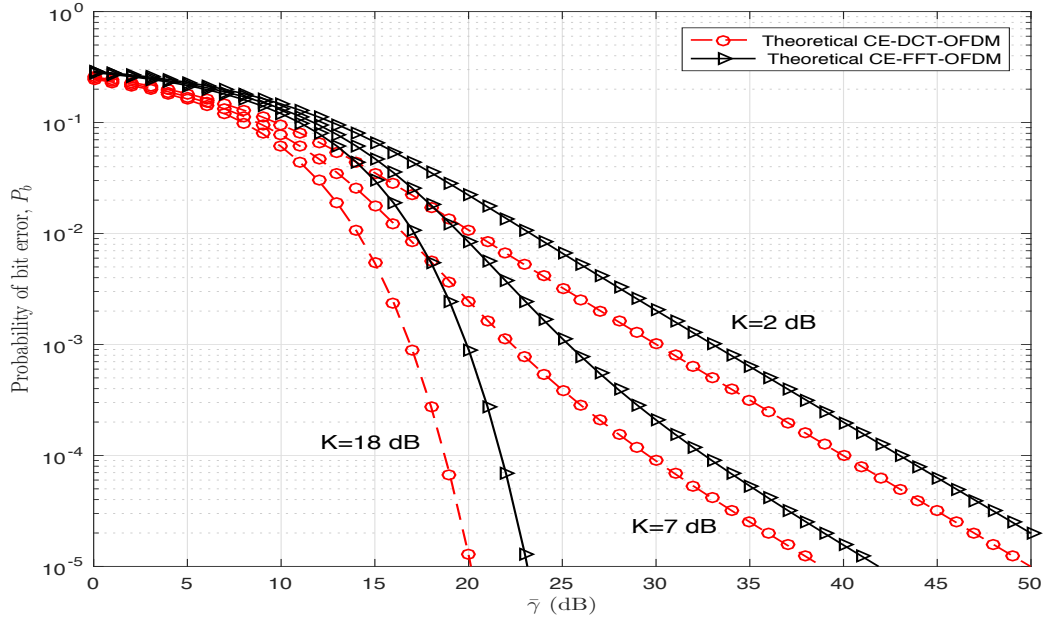


Figure 3.25: Probability of bit error performances of CE-DCT- and CE-FFT-OFDM systems (4-PAM mapper, $h_p = 0.5$) as function of Rice factor for Rician Channel.

as:

$$x_{in}(t) = A e^{j\phi(t)} \quad (3.58)$$

and

$$x_{out}(t) = G(A) e^{j[\phi(t)+\Theta(A)]} \quad (3.59)$$

It is noted from (3.58) and (3.59) that the power amplifier has no impact on the performance of CE-DCT-OFDM system, as no IBO is needed since the instantaneous nonlinearity results in a constant amplitude and a constant phase shift. Computer simulations have been used to study the BER performances of both CE-DCT-OFDM and DCT-OFDM systems with TWTA amplifier in the them, as a function of the IBO. Figure 3.26 compares BER performances of CE-DCT-OFDM system (64 subcarriers, 4-PAM mapper, $h_p = 1.2, 1.5$) and DCT-OFDM system (64 subcarriers, QPSK mapper) for IBO= 0 dB and 4 dB, for TWTA amplifier model with $\alpha_\phi = \pi/12$ $\beta_\phi = 0.25$. The DCT-OFDM system with IBO= 0 dB has an error floor of nearly 3.20×10^{-2} . At BER = 10^{-3} , the IBO required for the DCT-OFDM system is 4 dB, with $E_b/N_0 = 13.8$ dB. However, the CE-DCT-OFDM system with IBO= 0 dB and $h_p = 1.5$ achieves a BER of 10^{-3} at $E_b/N_0 = 12.8$ dB.

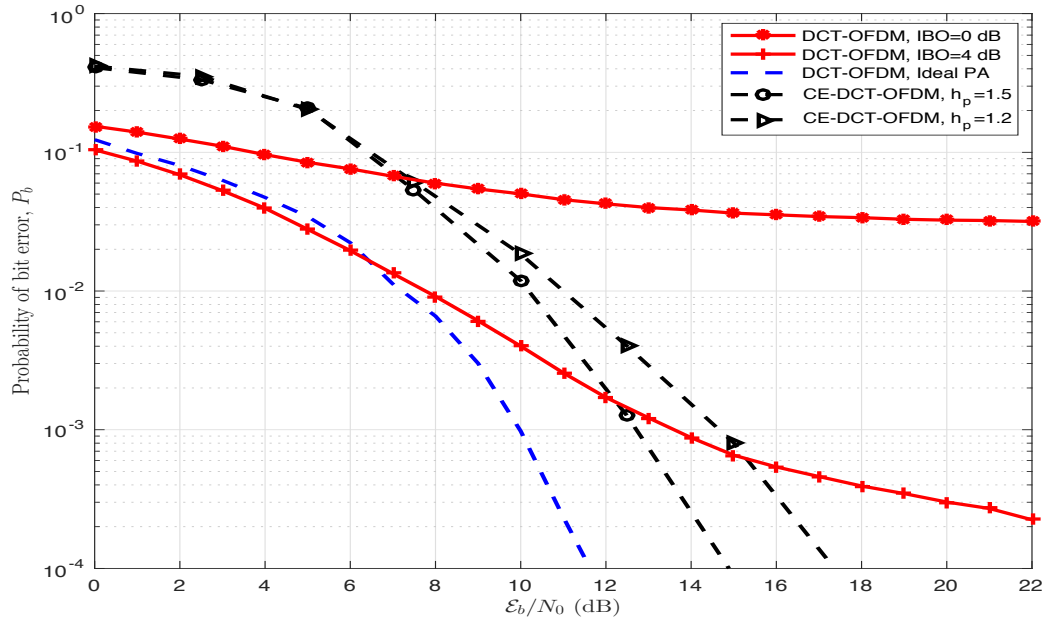


Figure 3.26: Probability of bit error performances of CE-DCT-OFDM and performance of DCT-OFDM systems as a function of IBO for TWTA.

3.8 Conclusions

A generic description of DCT- and FFT-OFDM systems with PM is presented. These systems are referred to as CE-DCT- and CE-FFT-OFDM systems. In these systems the transmitted signals have 0 dB PAPR due to the use of PM and, therefore, costly PAPR mitigation techniques are not required. The BER performance analyses of these systems over AWGN and flat fading channels are presented and closed-form expressions for BER have been derived. The results show that the CE-DCT-OFDM system outperforms the CE-FFT-OFDM system by nearly 3 dB. It is also observed that BER performances of these systems can be controlled by appropriately choosing h_p and the numbers of levels in MPAM mapper in these systems. The BER simulation results are nearly the same as that of theoretical BER results. BER performances of CE-DCT- and CE-FFT-OFDM systems over AWGN, Rician and Rayleigh channels, as a function of system and noise environment parameters are presented. The power penalty required as consequence of fading has been estimated for both Rayleigh and Rician channels. It is observed that power penalty required is higher for Rayleigh than for Rician channel, as in the latter there exist direct LOS path while in former there is no LOS path. BER performances of CE-DCT-OFDM and DCT-OFDM systems with nonlinear TWTA amplifier in them are compared as a function of IBO. The results show CE-DCT-OFDM system is attractive compared to DCT-OFDM system, as no IBO is required in the former system.

Chapter 4

Constant Envelope DCT- and FFT-OFDM Systems with FM^{4,5}

4.1 Introduction

In this Chapter, DCT- and FFT-OFDM systems with FM are considered. These systems with MPAM mapper are described, illustrated, and examined for transmission of data. Detection and performance of signals in these systems are addressed. The receiver structure consists of an FM demodulator followed by the optimum OFDM demodulator. Closed-form expressions for BER of these systems over AWGN and fading channels are derived and illustrated as a function of E_b/N_0 , M , and modulation index h_f . Expressions for bandwidth of CE-DCT and CE-FFT-OFDM systems with FM are developed and given. A comparison of DCT- and FFT-OFDM systems with FM and PM is also provided. The effect of TWTA amplifier on BER performances of conventional DCT-OFDM and CE-DCT-OFDM systems is also presented

-
4. Rayan H. Alsisi and Raveendra K. Rao, "Constant Envelope DCT- and FFT-based OFDM Systems with Frequency Modulation in Flat Fading Channels," 2017 8th IEEE Annual Information Technology, Electronics and Mobile Communication Conference (IEMCON), Vancouver, Canada, October 2017, pp. 576-581.
 5. Rayan H. Alsisi and Raveendra K. Rao, "Performance Comparison of Constant Envelope DCT and FFT Based OFDM Frequency Modulation," 2017 IEEE International Conference on Signal Processing, Informatics, Communication and Energy Systems (SPICES), Kollam, India, August 2017.

4.2 DCT- and FFT-OFDM Signals with FM

An FM modulated OFDM bandpass signal can be written as:

$$s(t) = A_c \cos(2\pi f_c t + \phi(t)), 0 \leq t \leq T \quad (4.1)$$

where A_c and f_c are carrier amplitude and frequency, T is the duration of OFDM symbol and $\phi(t)$ is the information carrying phase and can be written as:

$$\phi(t) = 2\pi k_f \int_0^t x(\varepsilon) d\varepsilon \quad (4.2)$$

where $x(t)$ is the real-valued OFDM signal carrying information about data to be transmitted and k_f is frequency deviation constant.

In the case of FFT-OFDM system, the information carrying phase can be written as:

$$\phi_{FFT}(t) = 2\pi k_f \int_0^t x_{FFT}(\varepsilon) d\varepsilon = 2\pi k_f \int_0^t \sum_{n=0}^{N-1} \sqrt{\frac{2}{T\sigma_s^2}} X_{FFT}(n) \cos(2\pi n\varepsilon/T) d\varepsilon. \quad (4.3)$$

and in the case of DCT-OFDM system, it is given by:

$$\phi_{DCT}(t) = 2\pi k_f \int_0^t x_{DCT}(\varepsilon) d\varepsilon = 2\pi k_f \int_0^t \sum_{n=0}^{N-1} \sqrt{\frac{2}{T\sigma_s^2}} X_{DCT}(n) \cos(\pi n\varepsilon/T) d\varepsilon \quad (4.4)$$

where $x_{FFT}(t)$ and $x_{DCT}(t)$, given by (1.22) and (1.6), respectively, represent real signals of DCT- and FFT-OFDM systems with MPAM mapper.

4.3 CE-OFDM Transmitter

The transmitter of an OFDM system with FM is shown in Figure 4.1. A block of N symbols from a data source is first passed through S/P converter to obtain a set of N low rate parallel data symbols. These are then passed to an MPAM mapper, whose output can be represented by a vector $[X(0), X(1), \dots, X(N-1)]^T$ consisting of N symbols.

For an MPAM mapper in the system, $X(n), n = 0, 1, \dots, N-1$ take values from the set $\{\pm 1, \pm 3, \dots, \pm(M-1)\}$ and is used to generate the OFDM signal $x(t)$ which is then fed to the FM modulator to obtain CE-OFDM signal $s(t)$. This signal is fed to HPA whose output is transmitted using an antenna over the communication channel.

Using (4.3) in (4.1), CE-FFT-OFDM signal can be written as:

$$s(t) = A_c \cos \left(2\pi f_c t + 2\pi k_f \sqrt{\frac{2}{T\sigma_s^2}} \left[X_{FFT}(0)t + \frac{T}{2\pi} \sum_{n=1}^{N-1} \frac{X_{FFT}(n)}{n} \sin(2\pi n t/T) \right] \right) \quad (4.5)$$

Using (4.4) in (4.1), CE-DCT-OFDM signal can be written as:

$$s(t) = A_c \cos \left(2\pi f_c t + 2\pi k_f \sqrt{\frac{2}{T\sigma_s^2}} \left[X_{DCT}(0)t + \frac{T}{\pi} \sum_{n=1}^{N-1} \frac{X_{DCT}(n)}{n} \sin(\pi n t/T) \right] \right) \quad (4.6)$$

The average power of $s(t)$ is $A_c^2/2$ and its energy is $A_c^2 T/2$. For $N \log_2(M)$ bits of information per transmission, the average bit energy is $E_b = A_c^2 T/2N \log_2(M)$. The variance of the data symbols, σ_s^2 is equal to $((M^2 - 1)/3)$. The bandwidths of signals in (4.5) and (4.6) are given by $\max(2h_f, 2)W$ Hz [109], where W is the bandwidth of message signal. For the FFT-OFDM system, the message signal bandwidth is $W = N/T$ Hz and for DCT-OFDM system, $W = N/2T$ Hz [38, 44], where h_f is the modulation index and is given by $h_f = \frac{k_f \max|x(t)|}{W}$.

4.4 CE-OFDM Receiver: Signal Detection and Performance

The CE-OFDM receiver, shown in Figure 4.1, consists of cascade of BPF, FM demodulator, LPF, OFDM demodulator, MPAM demapper, and P/S converter blocks. The additive white Gaussian noise $w(t)$ with two-sided PSD $N_0/2$ Watts/Hz is added to $s(t)$ and the received signal $z(t) = s(t) + w(t)$ is passed through BPF, $H_1(f)$, with characteristic as shown in Figure 3.2. The input to the FM demodulator can be written as: $y(t) = s(t) + n(t), 0 \leq t \leq T$, where $n(t)$ represents the output of BPF due to the input $w(t)$. The signal at the output of the FM demodulator is then passed through

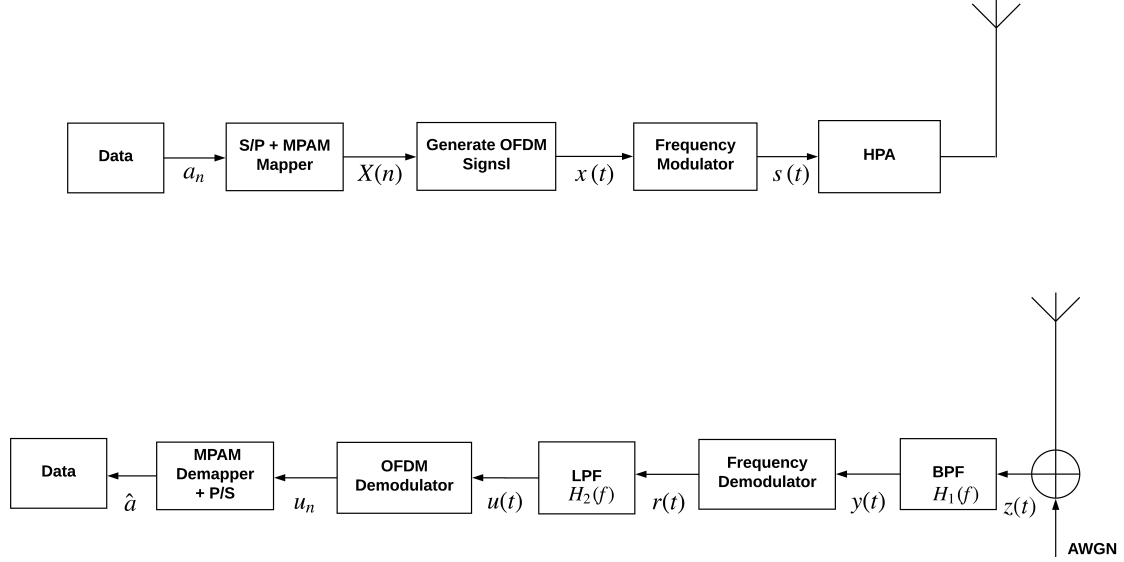


Figure 4.1: Transmitter and receiver structures for DCT- and FFT-OFDM systems with FM

LPF with bandwidth equal to message bandwidth W . The LPF output is then fed to OFDM demodulator followed by MPAM demapper and P/S block to get an estimate of information transmitted.

4.4.1 FM Demodulation

FM demodulation consists of arctangent block, phase unwrapper and differentiator. Arc-tangent block is used to detect the phase of the received signal by taking arctangent of the ratio of quadrature and in phase components of the received signal as explained in Chapter 3. The phase unwrapper is used to unwrap the demodulated phase of the signal. Differentiator is used to recover the modulating signal.

As explained in Chapter 3, the phase of $y(t)$ is given by (3.18) as:

$$\theta(t) \approx \phi(t) + \frac{m(t)}{A_c} \sin[\Psi(t) - \phi(t)] \quad (4.7)$$

where $m(t)$ is given by (3.12) represents the envelope of $n(t)$ and $\Psi(t)$ is given by (3.13)

represents the phase of $n(t)$. The output of the FM demodulator is given by,

$$r(t) = \frac{1}{k_f} \cdot \frac{1}{2\pi} \frac{d\theta(t)}{dt} \quad (4.8)$$

Using (4.7) in (4.8), we get

$$r(t) = x(t) + n_d(t) \quad (4.9)$$

where

$$n_d(t) = \frac{1}{k_f} \cdot \frac{1}{2\pi A_c} \frac{d(m(t) \sin[\Psi(t) - \phi(t)])}{dt} \quad (4.10)$$

The PSD of $S_{N_d}(f)$ is related to the PSD of $\frac{d n_Q(t)}{dt}$ [110, 111] and is given by:

$$S_{N_d}(f) = \left\{ \frac{1}{2\pi A_c k_f} \right\}^2 |j2\pi f|^2 S_{N_Q}(f) \quad (4.11)$$

The above step follows from the fact that $\frac{d n_Q(t)}{dt}$ can be obtained by passing $n_Q(t)$ through a differentiator with the transfer function $j2\pi f$. Thus,

$$S_{N_d}(f) = \left\{ \frac{f}{A_c k_f} \right\}^2 S_{N_Q}(f) \quad (4.12)$$

where

$$S_{N_Q}(f) = \begin{cases} N_0, & |f| \leq \frac{B}{2} \\ 0, & \text{otherwise} \end{cases} \quad (4.13)$$

In (4.13), B represents the bandwidth of $s(t)$ in (4.1). The FM demodulator output is applied to LPF of bandwidth W Hz which passes the message signal $x(t)$ and rejects out-of-band noise due to $n_d(t)$. The output of LPF can be written as:

$$u(t) = x(t) + n_u(t) \quad (4.14)$$

The PSD $S_{N_u}(f)$ of $n_u(t)$ is given by:

$$S_{N_u}(f) = \begin{cases} N_0 \left(\frac{f}{A_c k_f} \right)^2, & |f| \leq W \\ 0, & \text{otherwise} \end{cases} \quad (4.15)$$

and its average noise power is

$$\int_{-W}^W \frac{N_0}{A_c k_f} f^2 df = \frac{2W^3 N_0}{3k_f^2 A_c^2} \quad (4.16)$$

4.4.2 OFDM Demodulator

The signal $u(t)$ is then passed to the OFDM demodulator. As discussed in Chapter 3, Section 3.4.2, the input to the j^{th} correlator in the demodulator can be written as:

$$u(j) = \int_0^T u(t) \varphi_j(t) dt = X(j)/\sqrt{\sigma_s^2} + N_u(j); j = 0, 1, \dots, N-1 \quad (4.17)$$

with mean

$$E[u(j)] = E[X(j)/\sqrt{\sigma_s^2} + N_u(j)] = E[X(j)/\sqrt{\sigma_s^2}] \quad (4.18)$$

and variance

$$Var[u(j)] = \sigma_u^2 = \frac{2W^3 N_0}{3k_f^2 A_c^2} \quad j = 0, 1, \dots, N-1 \quad (4.19)$$

The BER performance of the CE-OFDM receiver can be derived by observing the output of the j^{th} correlator fed to the MPAM demapper is given by:

$$u(j) = \frac{X(j)}{\sqrt{\sigma_s^2}} + N_u(j)$$

where $X(j) \in \{\pm 1, \pm 3, \dots, \pm(M-1)\}$, $\sigma_s^2 = ((M^2 - 1)/3)$ is the variance of data symbols, and $N_u(j)$ is a zero Gaussian random variable with variance σ_u^2 given by (4.19). The symbol error probability can then be written as [Section 3.4.3]:

$$\begin{aligned}
P_s &= \frac{1}{M} \sum_{i=1}^M \text{Prob.}[\text{error} \mid s_i \text{ sent}] \\
&= \frac{1}{M} [(M-2) P_{inner} + 2P_{outer}] \\
&= 2 \left(\frac{M-1}{M} \right) \int_{1/\sqrt{\sigma_s^2}}^{\infty} \frac{1}{\sqrt{2\pi\sigma_u^2}} e^{(-x^2/2\sigma_u^2)} dx
\end{aligned} \tag{4.20}$$

Simplifying (4.20), the probability of symbol error probability of j^{th} demapper in the demodulator can be written as

$$P_s = 2 \left(\frac{M-1}{M} \right) Q \left(\sqrt{\frac{3A_c^2 h_f^2}{2W N_0 \sigma_s^2}} \right) \tag{4.21}$$

Since, $W = N/T$ and $W = N/2T$ for FFT- and DCT-OFDM signals, respectively, the symbol error probability P_s for the j^{th} demapper of CE-FFT- and CE-DCT-OFDM systems are given by:

$$P_{s_{FFT}} = 2 \left(\frac{M-1}{M} \right) Q \left(\sqrt{\frac{9h_f^2 \log_2(M) E_b}{(M^2-1)N_0}} \right) \tag{4.22}$$

and

$$P_{s_{DCT}} = 2 \left(\frac{M-1}{M} \right) Q \left(\sqrt{\frac{18h_f^2 \log_2(M) E_b}{(M^2-1)N_0}} \right) \tag{4.23}$$

In the receiver, there are N demappers and each has the same symbol error probability. The average of symbol error probabilities of N demapper is simply given by (4.22) and (4.23), as all are equally likely. Converting the symbol error rate to bit error rate, we get

$$P_b \approx \frac{P_s}{\log_2(M)} \tag{4.24}$$

The BER for CE-FFT- and CE-DCT-OFDM systems are thus given by:

$$P_{b_{FFT}} \approx 2 \left(\frac{M-1}{M \log_2(M)} \right) Q \left(\sqrt{\frac{9h_f^2 \log_2(M) E_b}{(M^2-1)N_0}} \right) \quad (4.25)$$

and

$$P_{b_{DCT}} \approx 2 \left(\frac{M-1}{M \log_2(M)} \right) Q \left(\sqrt{\frac{18h_f^2 \log_2(M) E_b}{(M^2-1)N_0}} \right) \quad (4.26)$$

The bit error rates given by (4.25) and (4.26) are functions of E_b/N_0 , h_f , modulation index, and M .

4.5 Performance of CE-OFDM System over Fading Channels

The performance of CE-OFDM receiver over flat Rayleigh and Rician fading channels can be determined by modeling the received signal over the fading channel as:

$$\int_{-\infty}^{\infty} h(\tau) s(t-\tau) d\tau + w(t) \quad (4.27)$$

where $s(t)$ is the transmitted signal, $w(t)$ is AWGN and $h(t) = \alpha e^{j\phi_0} \delta(t)$. The instantaneous SNR and the average SNR per bit are $\gamma = \alpha^2 E_b/N_0$ and $\bar{\gamma} = E \{ \alpha^2 \} E_b/N_0$, respectively. To obtain the bit error rate (P_b) of CE-OFDM system over a fading channel, the conditional BER is averaged over the Probability Density Function (pdf) of γ and can be written as [112]:

$$P_b = \int_0^{\infty} P_b(\gamma) p_{\gamma}(\gamma) d\gamma \quad (4.28)$$

where $P_b(\gamma)$ represents the bit error probability of CE-OFDM system at the instantaneous SNR γ . Using (4.25) and (4.26) a generalized expression for $P_b(\gamma)$ can be written as

$$P_b(\gamma) = 2 \left(\frac{M-1}{M \log_2(M)} \right) Q \left(\sqrt{L h_f^2 \alpha^2 \frac{E_b}{N_0}} \right) = 2 \left(\frac{M-1}{M \log_2(M)} \right) Q \left(\sqrt{L h_f^2 \gamma} \right) \quad (4.29)$$

where $L = \frac{9\log_2(M)}{M^2-1}$ for CE-FFT-OFDM system and $L = \frac{18\log_2(M)}{M^2-1}$ for CE-DCT-OFDM system.

BER Expression for Rayleigh Fading Channel

For Rayleigh fading channel, the pdf of γ is given by[112]:

$$P_\gamma(\gamma) = \frac{1}{\bar{\gamma}} \exp\left(-\frac{\gamma}{\bar{\gamma}}\right), \gamma \geq 0 \quad (4.30)$$

Using (4.29) and (4.30) in (4.28), and using $Q(z)$ given in (3.53), P_b can be shown to be given by

$$P_b = 2 \left(\frac{M-1}{M \log_2(M)} \right) \frac{1}{\pi \bar{\gamma}} \int_0^{\pi/2} \int_0^\infty \exp\left(-\frac{Lh_f^2 \gamma}{2 \sin^2(\theta)} - \frac{\gamma}{\bar{\gamma}}\right) d\gamma d\theta \quad (4.31)$$

Integrating (4.31) [113], the bit error rate expression for CE-OFDM system can be shown to be given by:

$$P_b = \left(\frac{M-1}{M \log_2(M)} \right) \left[1 - \sqrt{\frac{Lh_f^2 \bar{\gamma}/2}{1 + Lh_f^2 \bar{\gamma}/2}} \right] \quad (4.32)$$

It is noted that BER is a function of h_f , modulation index, M , and $\bar{\gamma}$, average SNR per bit of the received signal. In deriving (4.32), it is assumed that the channel phase shift ϕ_0 is estimated from the received signal without error and remains constant during the observation interval.

BER Expression for Rician Fading Channel

For Rician fading channel, the pdf of γ is given by [112] as:

$$p_\gamma(\gamma) = \frac{(1+K)e^{-K}}{\bar{\gamma}} \exp\left[-\frac{(1+K)\gamma}{\bar{\gamma}}\right] I_0 \left[2\sqrt{\frac{(K+K^2)\gamma}{\bar{\gamma}}} \right], \gamma \geq 0 \quad (4.33)$$

Using (4.29) and (4.33) in (4.28), and using $Q(z)$ given in (3.53), P_b can be written as:

$$P_b = \frac{2}{\pi} \left(\frac{M-1}{M \log_2(M)} \right) \frac{(1+K)e^{-K}}{\bar{\gamma}} \int_0^{\pi/2} \int_0^\infty \exp \left[-\frac{Lh_f^2 \gamma}{2 \sin^2(\theta)} - \frac{(1+K)\gamma}{\bar{\gamma}} \right] I_0 \left[2 \sqrt{\frac{(K+K^2)\gamma}{\bar{\gamma}}} \right] d\gamma d\theta \quad (4.34)$$

Simplifying (4.34) [113], the expression for bit error rate can be written as:

$$P_b = \frac{2}{\pi} \left(\frac{M-1}{M \log_2(M)} \right) \int_0^{\pi/2} \frac{(1+K) \sin^2(\theta)}{(1+K) \sin^2(\theta) + Lh_f^2 \bar{\gamma}/2} \exp \left[-\frac{KLh_f^2 \bar{\gamma}/2}{(1+K) \sin^2(\theta) + Lh_f^2 \bar{\gamma}/2} \right] d\theta \quad (4.35)$$

The BER is a function of h_f , M , K , Rice factor, and $\bar{\gamma}$, average SNR per bit of the received signal. Again, it is assumed that ϕ_0 is estimated without error and remains constant during the observation interval.

4.6 Numerical Results and Discussion

In this Section numerical results of probability of bit error rate performances of CE-DCT- and CE-FFT-OFDM systems are presented. A comparison of these systems in terms of BER and bandwidth is also provided. The effect of TWTA amplifier on system BER is also discussed .

4.6.1 Performance in AWGN Channel

The expressions for probability of bit error, P_b , in AWGN channel for CE-DCT- and CE-FFT-OFDM systems are given by (4.25) and (4.26), respectively. The CE-DCT-OFDM system performs better than CE-FFT-OFDM system by nearly 3 dB. Figure 4.2 depicts P_b as a function of h_f ($= 0.1, 0.2$, and 0.6) and E_b/N_0 for 2-PAM mapper for both systems. It is observed that BER increases as h_f decreases for a fixed value of SNR. For example, at $E_b/N_0 = 8$ dB the BER for CE-DCT-OFDM system with $h_f = 0.2$ is

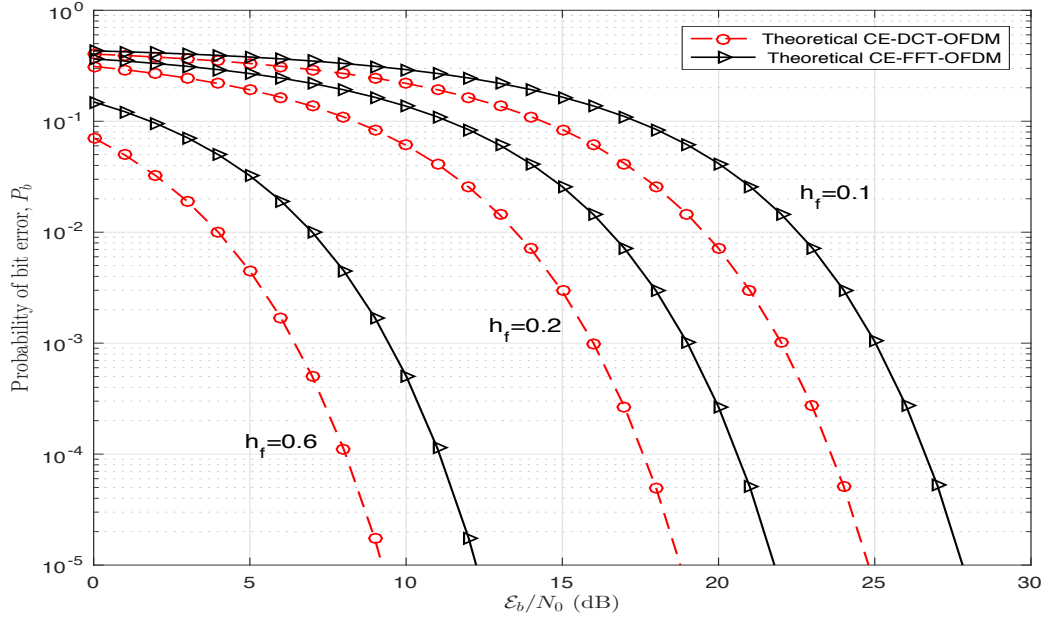


Figure 4.2: Probability of bit error performances of CE-DCT- and CE-FFT-OFDM systems (2-PAM mapper) over AWGN channel.

Table 4.1: Comparison of CE-DCT- and CE-FFT-OFDM systems (2-PAM mapper) at $P_b = 10^{-5}$ as a function of h_f

h_f	CE-DCT-OFDM	CE-FFT-OFDM
	E_b/N_0 (dB)	E_b/N_0 (dB)
0.7	7.915	10.925
0.6	9.254	12.264
0.5	10.837	13.848
0.4	12.775	15.786
0.3	15.274	18.285
0.2	18.7960	21.806

1.09×10^{-1} , and at $h_f = 0.6$ it is 1.114×10^{-4} . Table 4.1 summarizes E_b/N_0 required at 10^{-5} for CE-DCT- and CE-FFT-OFDM systems as a function of h_f .

The probability of bit error performances of CE-DCT- and CE-FFT-OFDM systems for 4-PAM and 8-PAM mappers as a function of h_f ($= 0.1, 0.2$ and 0.6) are shown in Figures 4.3 and 4.4, respectively. Tables 4.2 and 4.3 summarize E_b/N_0 required at $P_b = 10^{-5}$ as a function h_f for both CE-OFDM systems.

The probability of bit error performances of the two CE-OFDM systems for $h_f = 0.6$ are plotted as a function of number of levels in the MPAM mapper ($M = 2, 4, 8, 16$,

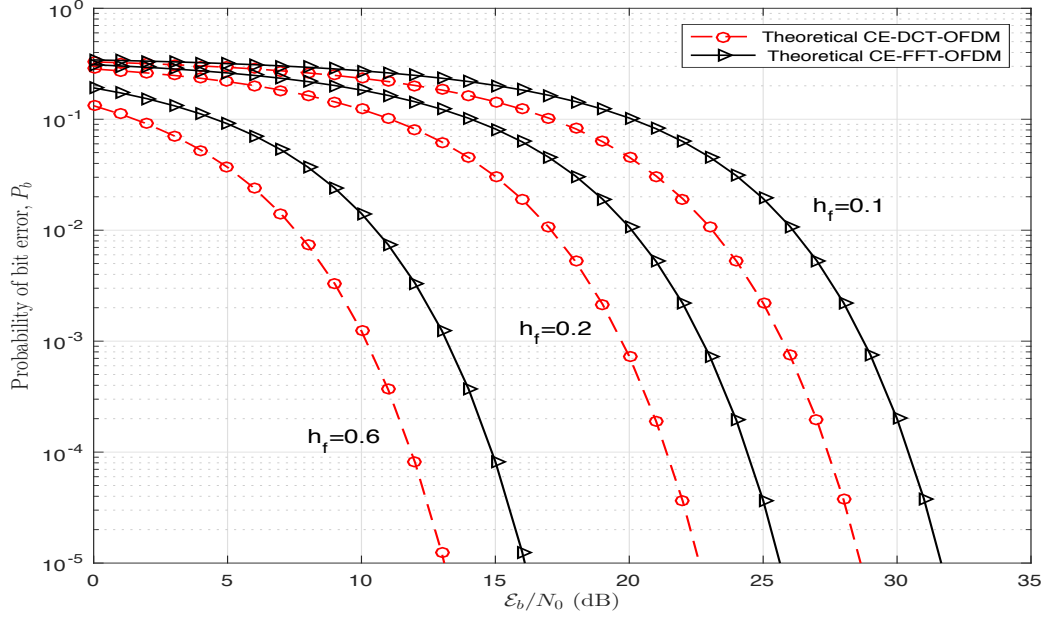


Figure 4.3: Probability of bit error performances of CE-DCT- and CE-FFT-OFDM systems (4-PAM mapper) over AWGN channel.

Table 4.2: Comparison of CE-DCT- and CE-FFT-OFDM systems (4-PAM mapper) at $P_b = 10^{-5}$ as a function of h_f

h_f	CE-DCT-OFDM	CE-FFT-OFDM
	E_b/N_0 (dB)	E_b/N_0 (dB)
0.7	11.761	14.772
0.6	13.100	16.111
0.5	14.684	17.694
0.4	16.622	19.632
0.3	19.121	22.131
0.2	22.643	25.653

and 32) in Figures 4.5 and 4.6. It is observed that BER increases as M increases for a fixed value of E_b/N_0 . It can also be observed that at $P_b = 10^{-5}$, E_b/N_0 required for 8-PAM mapper is 8.2 dB more than that required for 2-PAM mapper for both CE-OFDM systems. However, OFDM systems with 8-PAM mapper are more spectrally efficient than systems with 2-PAM mapper. The data rate and spectral efficiency of CE-OFDM system are given by:

$$R_r = \frac{N \log_2(M)}{T} \text{ b/s}$$

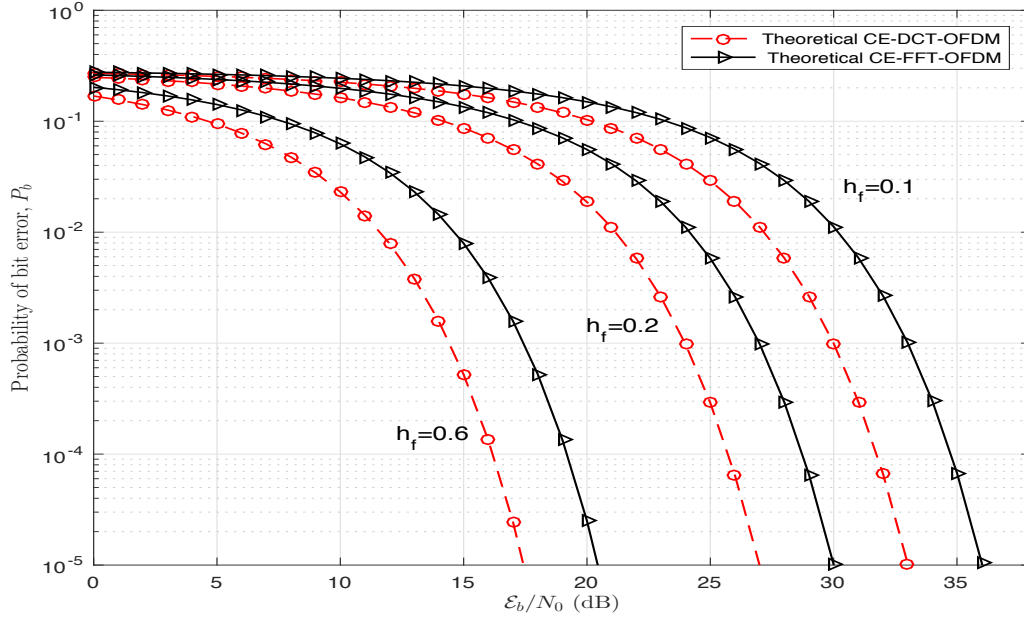


Figure 4.4: Probability of bit error performances of CE-DCT- and CE-FFT-OFDM systems (8-PAM mapper) over AWGN channel.

Table 4.3: Comparison of CE-DCT- and CE-FFT-OFDM systems (8-PAM mapper) at $P_b = 10^{-5}$ as a function of h_f

h_f	CE-DCT-OFDM	CE-FFT-OFDM
	E_b/N_0 (dB)	E_b/N_0 (dB)
0.7	16.114	19.124
0.6	17.453	20.463
0.5	19.036	22.046
0.4	20.976	23.985
0.3	23.473	26.484
0.2	26.995	30.005

and

$$\eta = \frac{R_r}{B} = \frac{N \log_2(M)}{T[\max(2h_f, 2)W]} \text{ b/s/Hz}$$

Since, $W = N/T$ and $W = N/2T$ for FFT- and DCT-OFDM systems, the spectral efficiencies of these systems are thus given by:

$$\eta_{CE-FFT-OFDM} = \frac{\log_2(M)}{\max(2h_f, 2)}$$

and

$$\eta_{CE-DCT-OFDM} = \frac{2 \log_2(M)}{\max(2h_f, 2)}$$

In order to understand the tradoff between M and h_f in CE-OFDM system, P_b as a function of h_f and M as are plotted in Figures 4.7 and 4.8 for CE-DCT- and CE-FFT-OFDM systems, respectively. It is apparent that P_b improves for higher values of M and h_f . The CE-DCT-OFDM system with $M = 8$ and $h_f = 0.6$ outperforms a corresponding system with $M = 4$ and $h_f = 0.2$ by nearly 5.2 dB at BER = 10^{-5} .

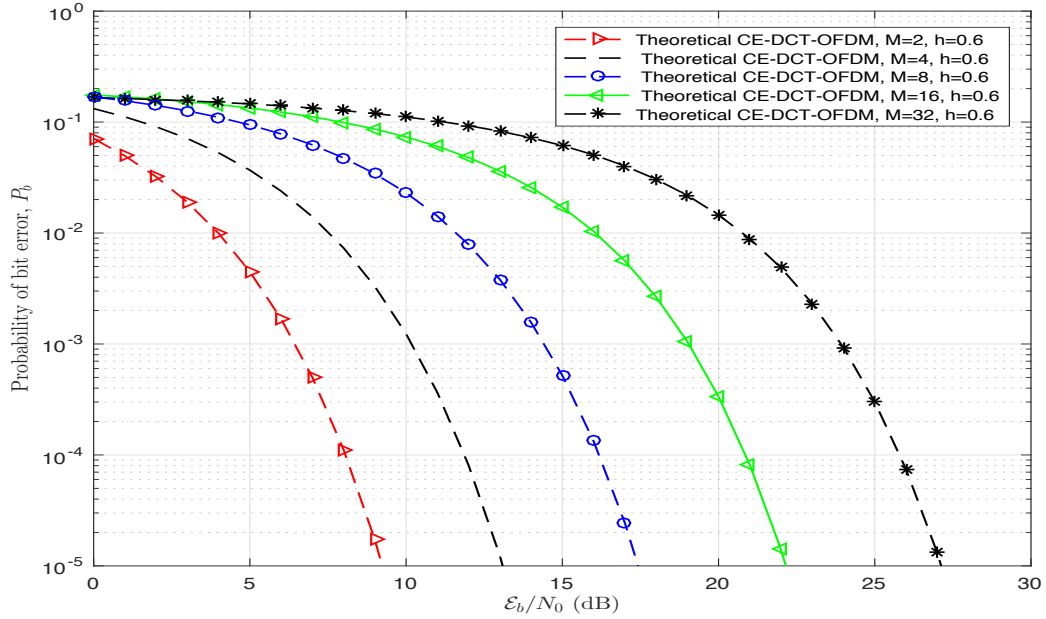


Figure 4.5: Probability of bit error performance of CE-DCT-OFDM system as a function of M for $h_f = 0.6$ over AWGN channel.

Figure 4.9 compares simulation results and theoretical P_b for CE-DCT-OFDM system ($N = 64$ subcarriers) with $M = 4$ for $h_f = 0.2$ and 0.4 . It is noted that for $h_f = 0.2$, simulation result is nearly the same as theoretical result and for $h_f = 0.4$, the theoretical BER is not as accurate as simulation result but still is within 1 dB of the former. It is observed that for smaller value of h_f theoretical results are nearly the same as that of simulations, whereas for larger values of modulation index simulation results are not as accurate as theoretical results.

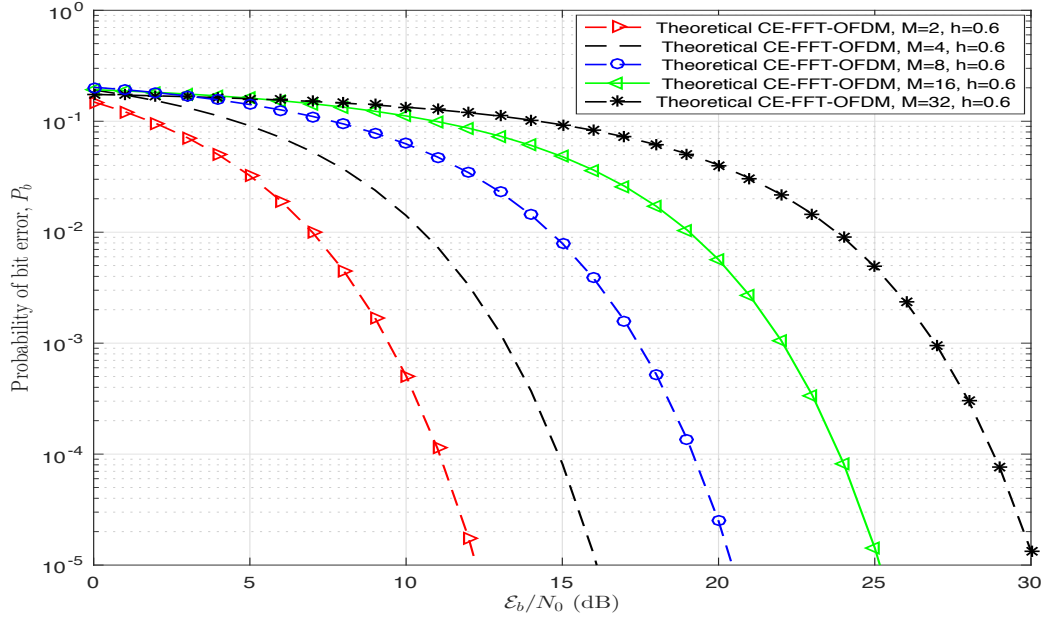


Figure 4.6: Probability of bit error performance of CE-FFT-OFDM system as a function of M for $h_f = 0.6$ over AWGN channel.

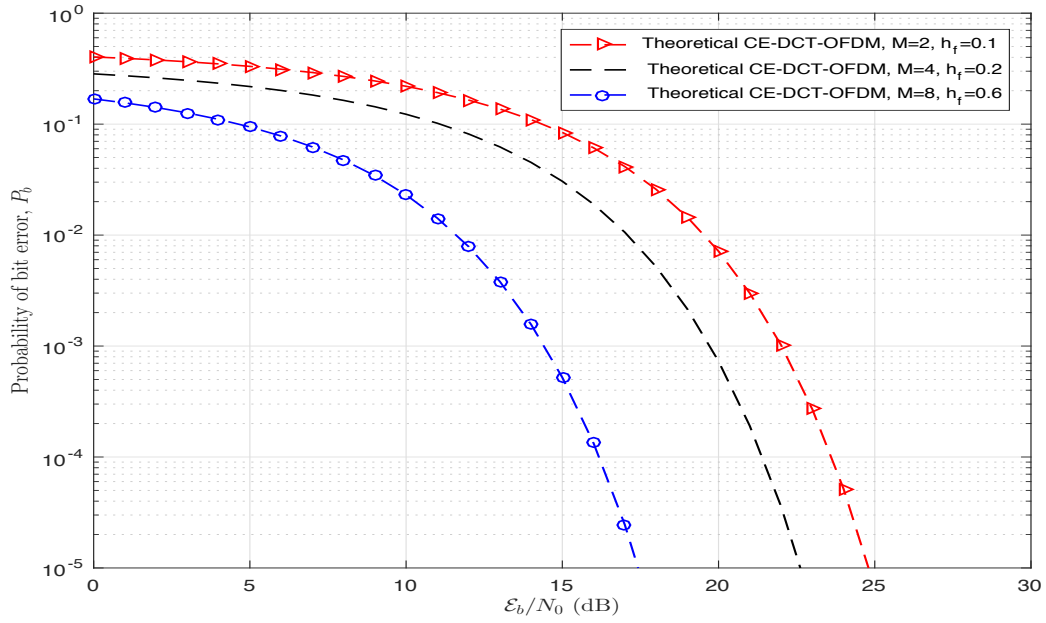


Figure 4.7: Probability of bit error performance of CE-DCT-OFDM system as a function of h_f and M over AWGN channel.

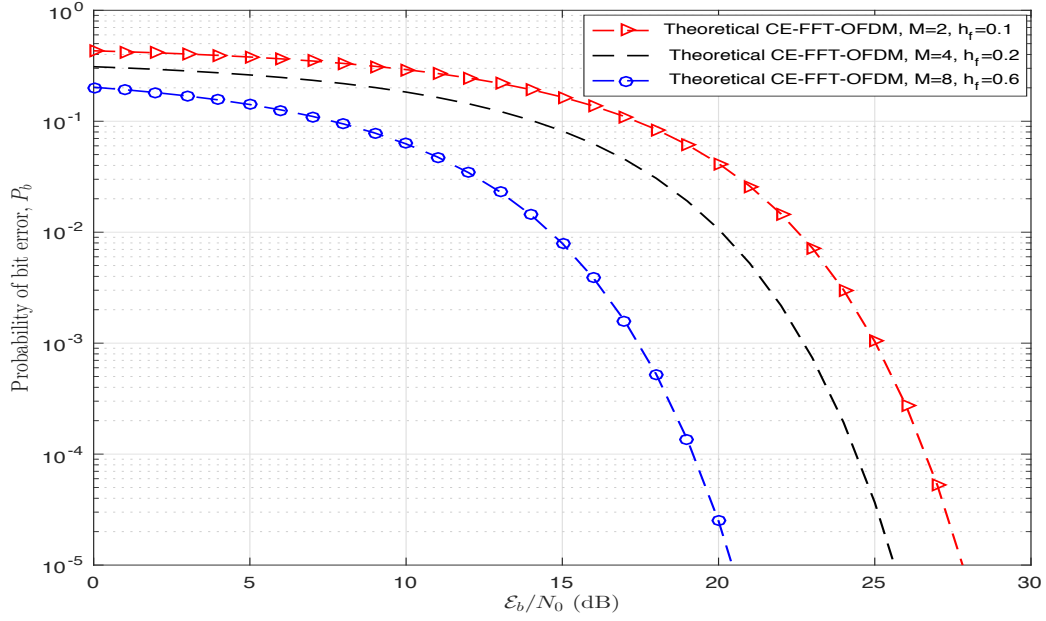


Figure 4.8: Probability of bit error performance of CE-FFT-OFDM system as a function of h_f and M over AWGN channel.

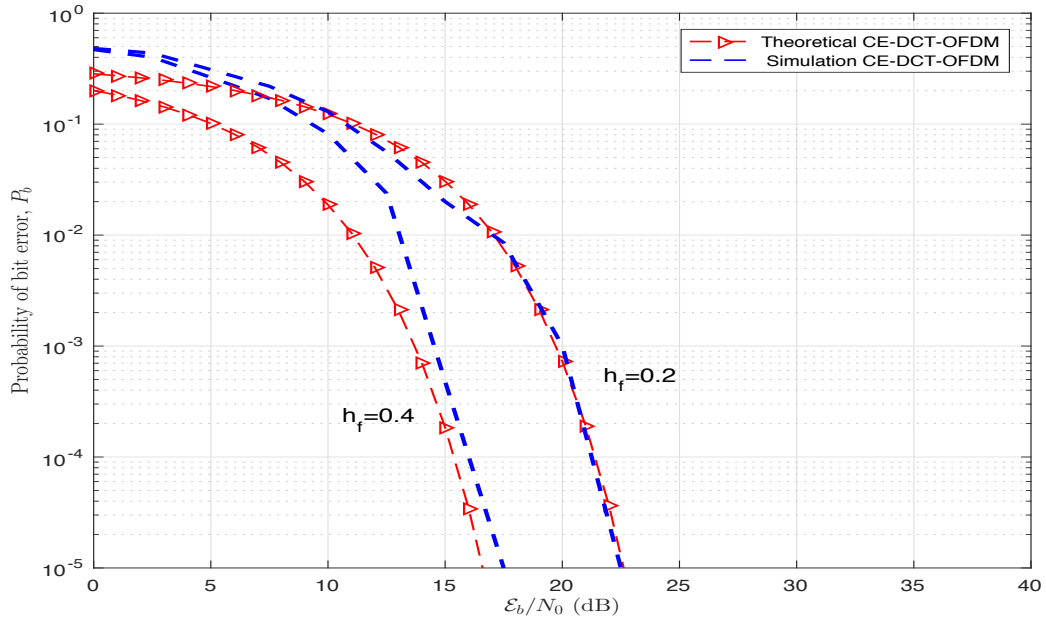


Figure 4.9: Comparison of analytical and simulation results of BER for EC-DCT-OFDM system (4-PAM mapper) over AWGN channel.

4.6.2 Performance in Fading Channels

The expression for P_b over Rayleigh fading channel is given by (4.32). Figures 4.10, 4.11, and 4.12 show P_b of CE-DCT- and CE-FFT-OFDM systems for $M = 2, 4$, and 8 respectively, for $h_f = 0.1, 0.6$ and 1.6. It is noted that, the presence of signal fading requires a large increases in E_b/N_0 to achieve same levels of BER that can be achieved over AWGN channel. In order to achieve BER equal to 10^{-5} , CE-DCT-OFDM system ($h_f = 0.6, M = 2$) requires $E_b/N_0 = 9.254 \text{ dB}$ on an AWGN channel. However, when the same system is operated over Rayleigh channel, to achieve the same BER an average SNR of 43.112 dB is required.

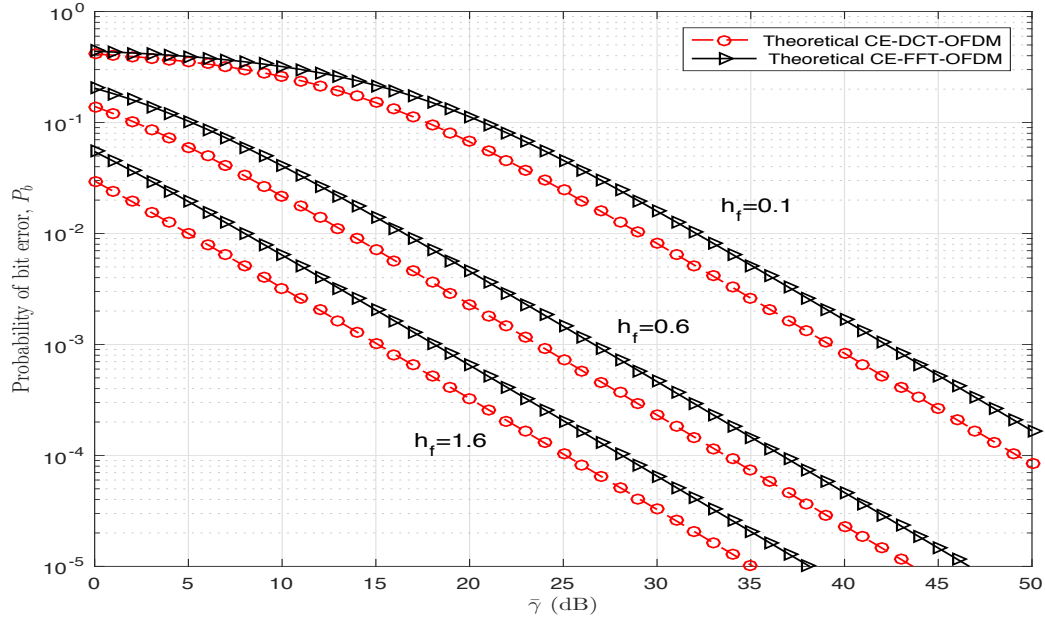


Figure 4.10: Probability of bit error performances of CE-DCT- and CE-FFT-OFDM systems (2-PAM mapper) over Rayleigh fading channel.

The expression for BER for Rician fading channel is given by (4.35). The BER is not only a function of h_f , M and $\bar{\gamma}$, but also depends on K , Rice factor. P_b vs. $\bar{\gamma}$ for $M = 2, 4$ and 8 CE-DCT- and CE-FFT-OFDM systems for $K = 6 \text{ dB}$ are illustrated in Figures 4.13, 4.14 and 4.15, respectively, as a function of $h_f (= 0.1, 0.6, \text{ and } 1.6)$.

In order to compare probability of bit error performances of CE-OFDM systems over AWGN, Rician and Rayleigh channels, P_b vs. $\bar{\gamma}$ are plotted for $M = 2$ and $h_f = 0.7$ in Figures 4.16 and 4.17. Tables 4.4 and 4.5 summarize average SNR required at $P_b =$

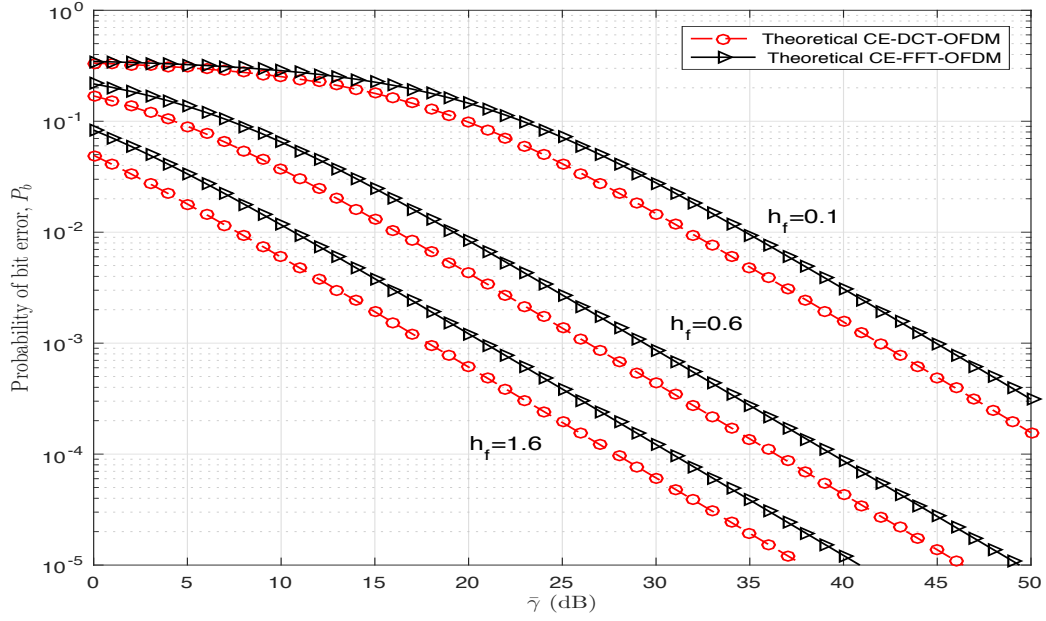


Figure 4.11: Probability of bit error performances of CE-DCT- and CE-FFT-OFDM systems (4-PAM mapper) over Rayleigh fading channel.

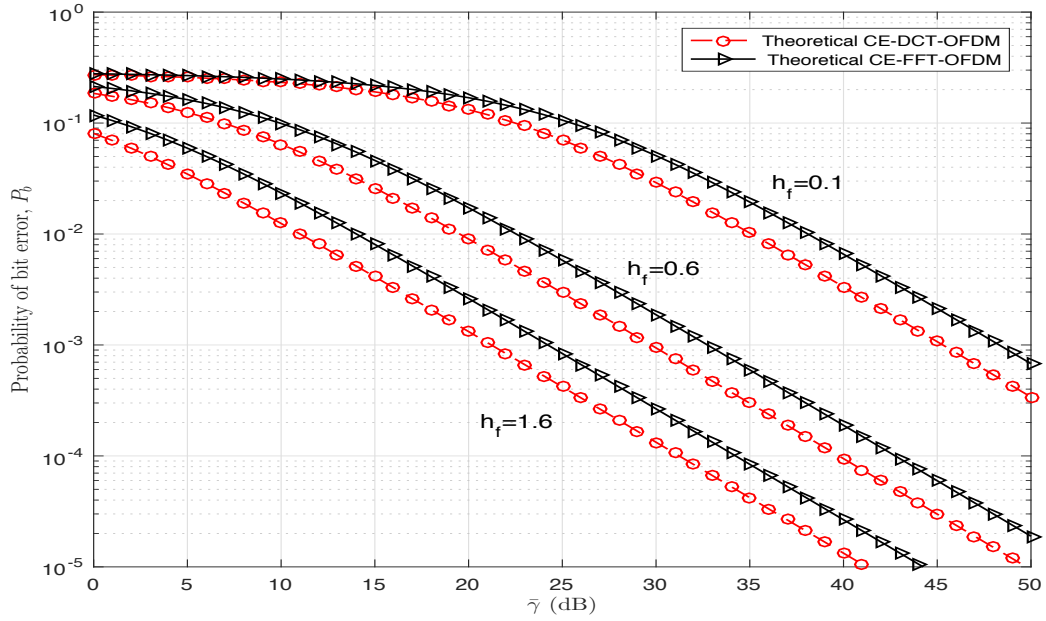


Figure 4.12: Probability of bit error performances of CE-DCT- and CE-FFT-OFDM systems (8-PAM mapper) over Rayleigh fading channel.

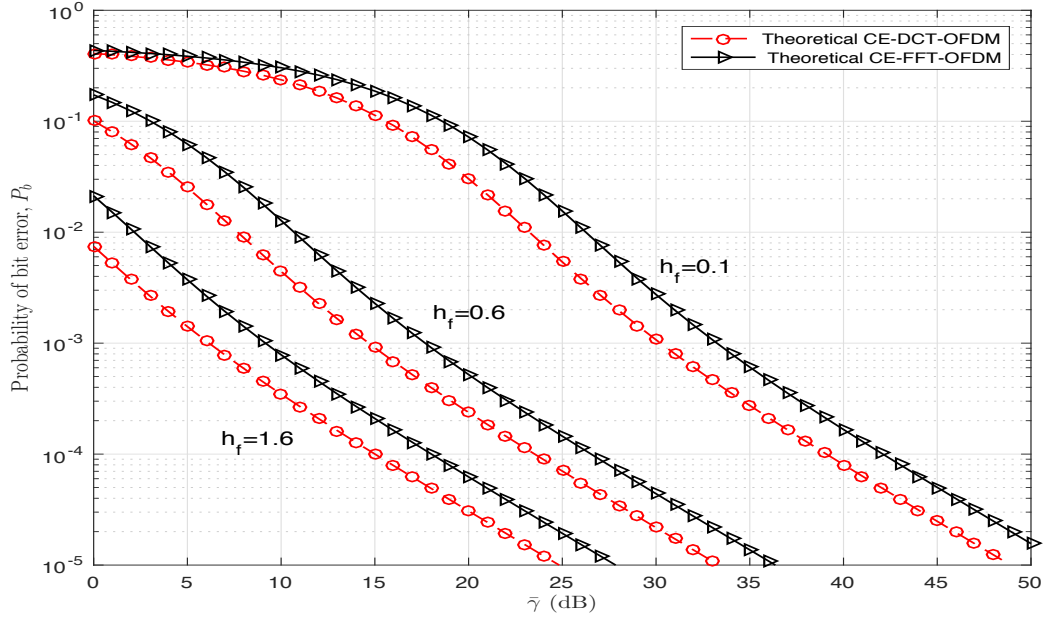


Figure 4.13: Probability of bit error performances of CE-DCT- and CE-FFT-OFDM systems (2-PAM mapper) over Rician fading channel ($K = 6$ dB).

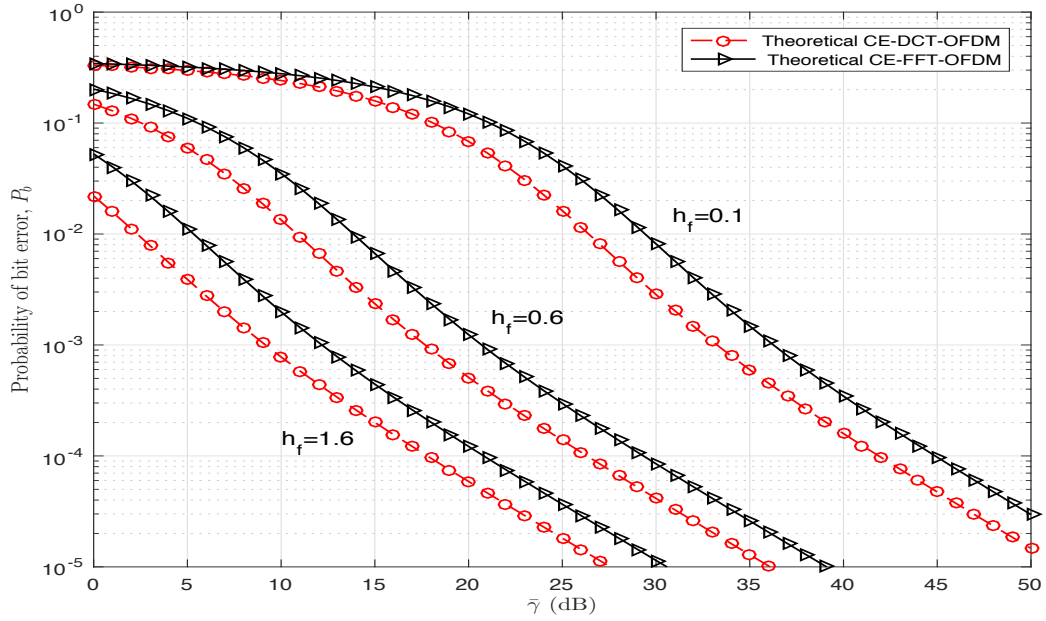


Figure 4.14: Probability of bit error performances of CE-DCT- and CE-FFT-OFDM systems (4-PAM mapper) over Rician fading channel ($K = 6$ dB).

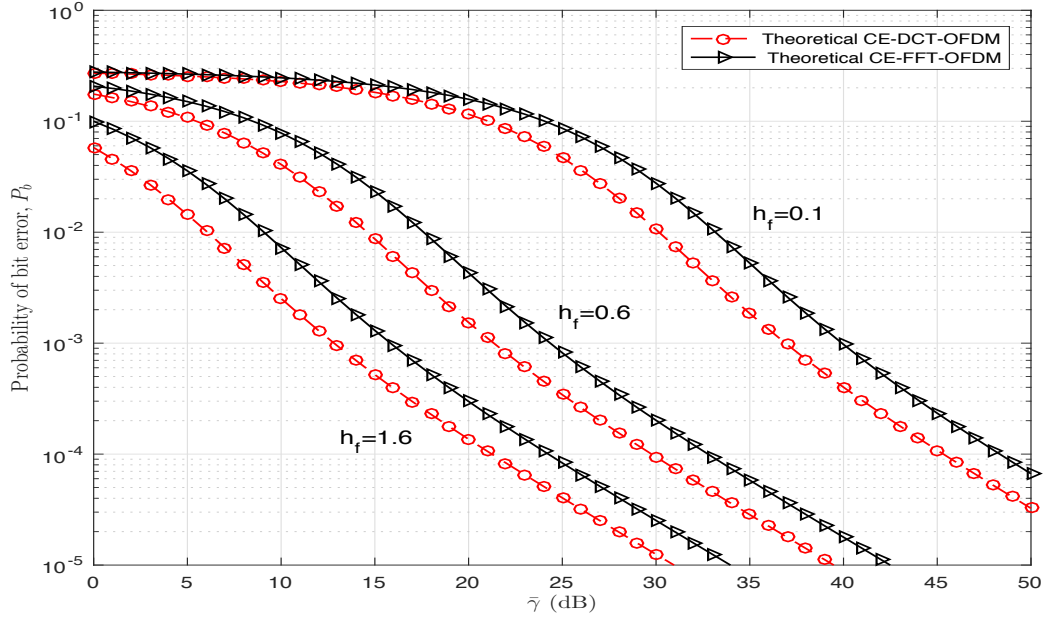


Figure 4.15: Probability of bit error performances of CE-DCT- and CE-FFT-OFDM systems (8-PAM mapper) over Rician fading channel ($K = 6$ dB).

10^{-3} , 10^{-4} and 10^{-5} for CE-DCT- and CE-FFT-OFDM systems over AWGN, Rician and Rayleigh channels, respectively.

Table 4.4: Comparison of probability of bit error performances of CE-DCT-OFDM system ($M = 2, h_f = 0.7$) over AWGN, Rician ($K = 6$ dB) and Rayleigh channels

P_b	Average SNR dB		
	AWGN	Rician	Raleigh
10^{-3}	5.116	13.118	22.163
10^{-4}	6.725	22.221	32.251
10^{-5}	7.915	32.151	42.242

Table 4.5: Comparison of probability of bit error performances of CE-FFT-OFDM system ($M = 2, h_f = 0.7$) over AWGN, Rician ($K = 6$ dB) and Rayleigh channels

P_b	Average SNR dB		
	AWGN	Rician	Raleigh
10^{-3}	8.127	16.142	25.111
10^{-4}	9.735	25.222	35.251
10^{-5}	10.925	35.156	45.155

The effect of Rice factor K on probability of bit error of CE-OFDM system (4-PAM

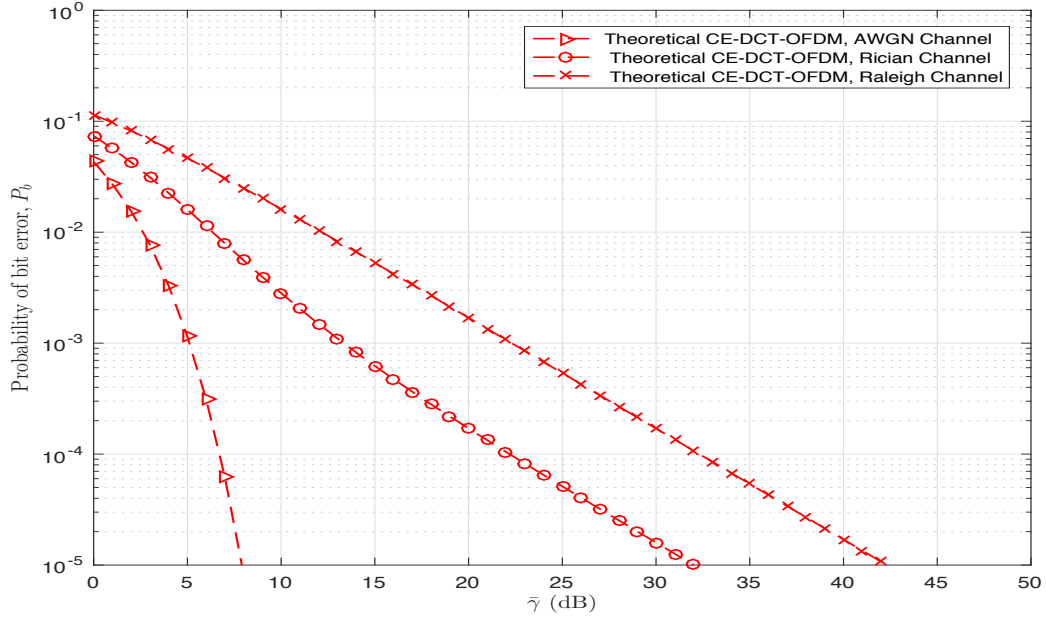


Figure 4.16: Comparison of probability of bit error performances of CE-DCT-OFDM system (2-PAM mapper, $h_f = 0.7$) over AWGN, Rician ($K = 6$ dB) and Rayleigh channels.

mapper, $h_f = 0.5$) is illustrated in Figure 4.18. It is noted that the BER decreases as K increases. For example, at $\text{BER} = 10^{-5}$ the average SNR required for $K = 18$ dB is nearly 30 dB less than that required for $K = 2$ dB. It is well known that as $K \rightarrow \infty$, Rician density approaches that of Gaussian density.

4.6.3 Effect of TWTA Amplifier on System Performance

To understand the effect of TWTA amplifier on the system BER performance, two systems are considered; DCT-OFDM system with QPSK mapper and DCT-OFDM system (4-PAM mapper) with FM (CE-DCT-OFDM system). While in the former system signals are non-constant envelope, in the latter system signals are constant-envelope and hence have 0 dB PAPR. The BER performances over AWGN channel of these systems with TWTA amplifier in them have been simulated and are shown in Figure 4.19. It is observed that DCT-OFDM system with IBO= 0 dB performs quite poorly compared to the performance of the same system with IBO=4 dB. Also, it can be observed that DCT-OFDM system with 0 dB IBO has an error floor at BER of nearly 3.20×10^{-2} .

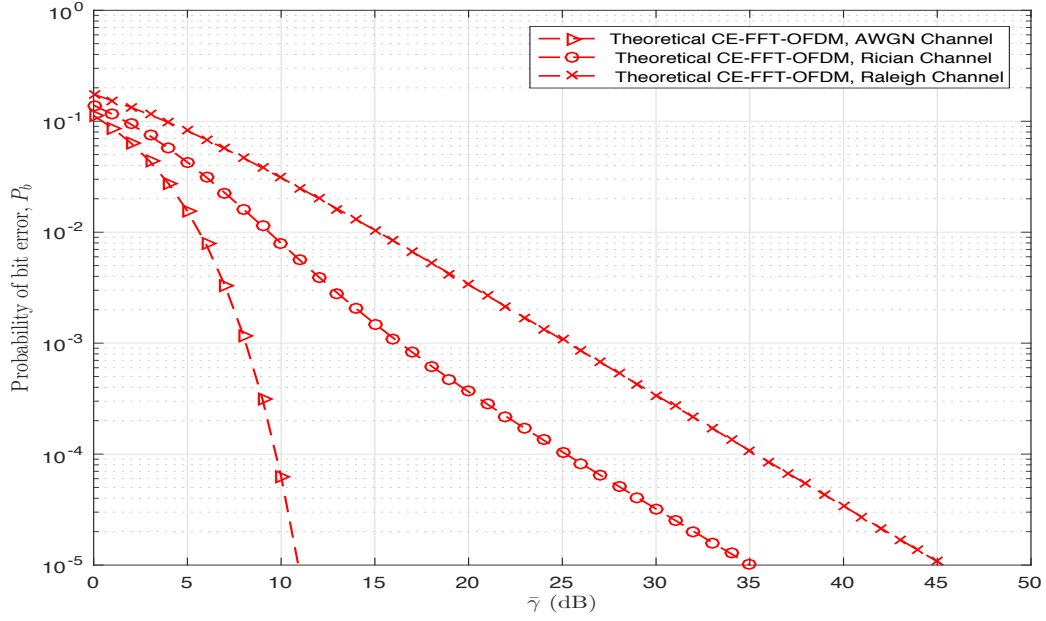


Figure 4.17: Comparison of probability of bit error performances of CE-FFT-OFDM system (2-PAM mapper, $h_f = 0.7$) over AWGN, Rician ($K = 6$ dB) and Rayleigh channels.

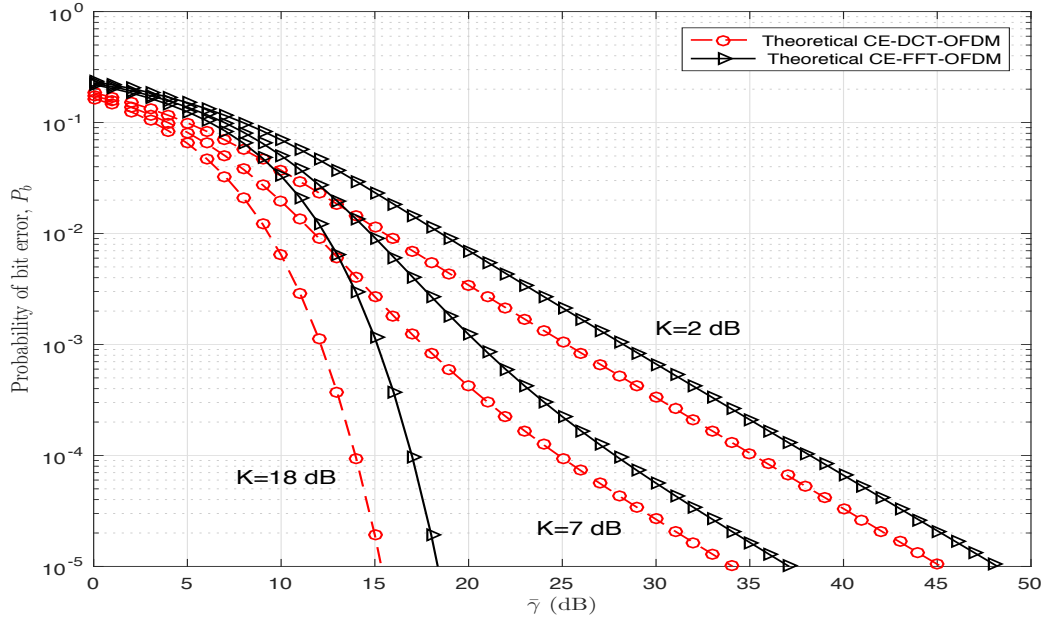


Figure 4.18: Probability of bit error performances of CE-DCT- and CE-FFT-OFDM systems (4-PAM mapper, $h_f = 0.5$) as a function of Rice factor for Rician Channel.

At $\text{BER} = 10^{-4}$, the IBO required for DCT-OFDM system exceeds 4 dB, whereas CE-DCT-OFDM system ($h_f = 0.4$) achieves this BER with IBO=0 dB

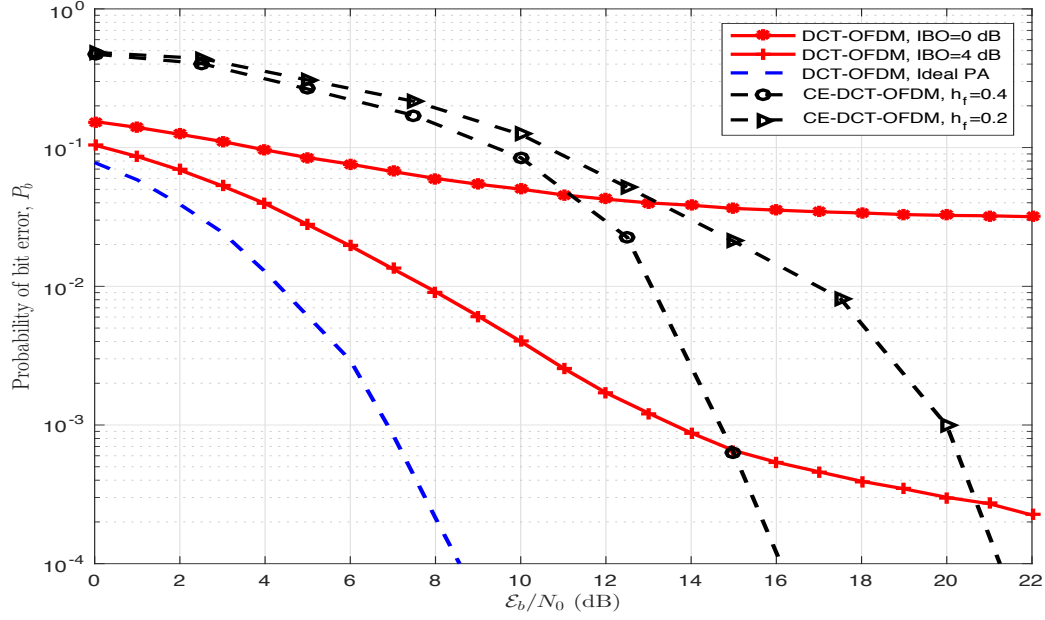


Figure 4.19: Probability of bit error performances of CE-DCT-OFDM and DCT-OFDM systems as a function of IBO for TWTA.

4.6.4 Comparison of PM and FM with DCT- and FFT-OFDM

In this Section, comparison of probability of bit error performances of CE-OFDM systems with PM and FM is presented. For this purpose, probability of bit error performances of DCT-OFDM system ($M = 4$) with PM ($h_p = 0.6$) and DCT-OFDM system ($M = 4$) with FM ($h_f = 0.6$) are compared. For these systems, P_b vs. average SNR are plotted in Figure 4.20 for AWGN, Rayleigh, and Rician ($K = 6$ dB) channels. Similar plots are shown in Figure 4.21 for FFT-OFDM system with PM and FM. It is noted that FM performs better than PM in OFDM systems. For example at $P_b = 10^{-5}$, over AWGN channel, average SNR required for DCT-OFDM system with FM is nearly 4.8 dB less than that required for DCT-OFDM system with PM. The bandwidths of DCT-OFDM system with PM and FM are given by $\max(2h_p, 2)W$ and $\max(2h_f, 2)W$, respectively. It is noted that DCT-OFDM system with FM can offer better BER performance than DCT-OFDM system with PM at the same bandwidths.

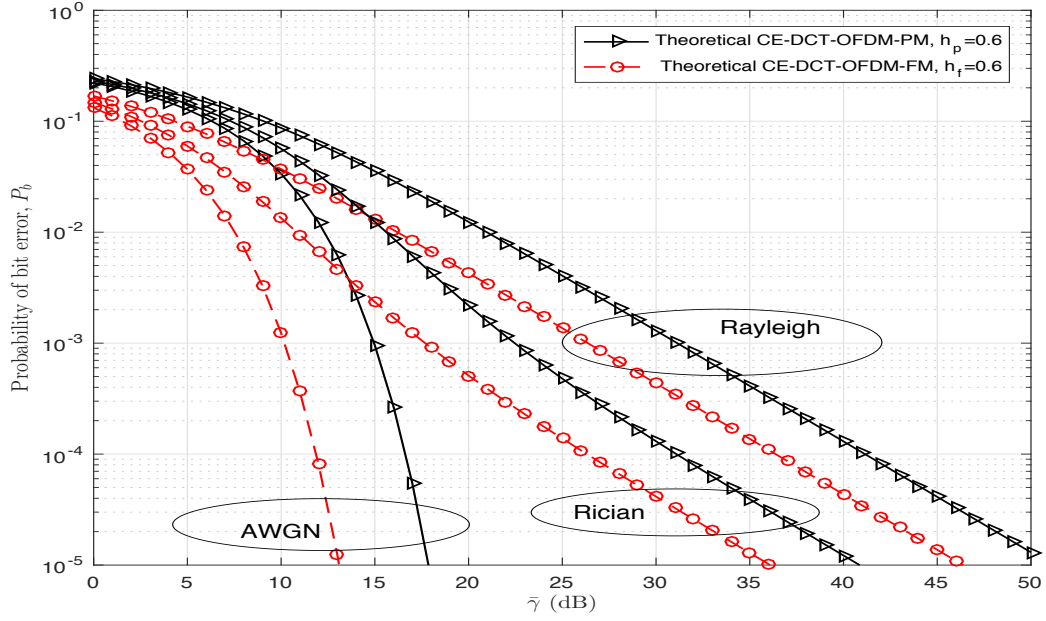


Figure 4.20: Probability of bit error performances of DCT-OFDM system (4-PAM mapper) with PM ($h_p = 0.6$) and FM ($h_f = 0.6$) over AWGN, Rician ($K = 6$ dB) and Rayleigh channels.

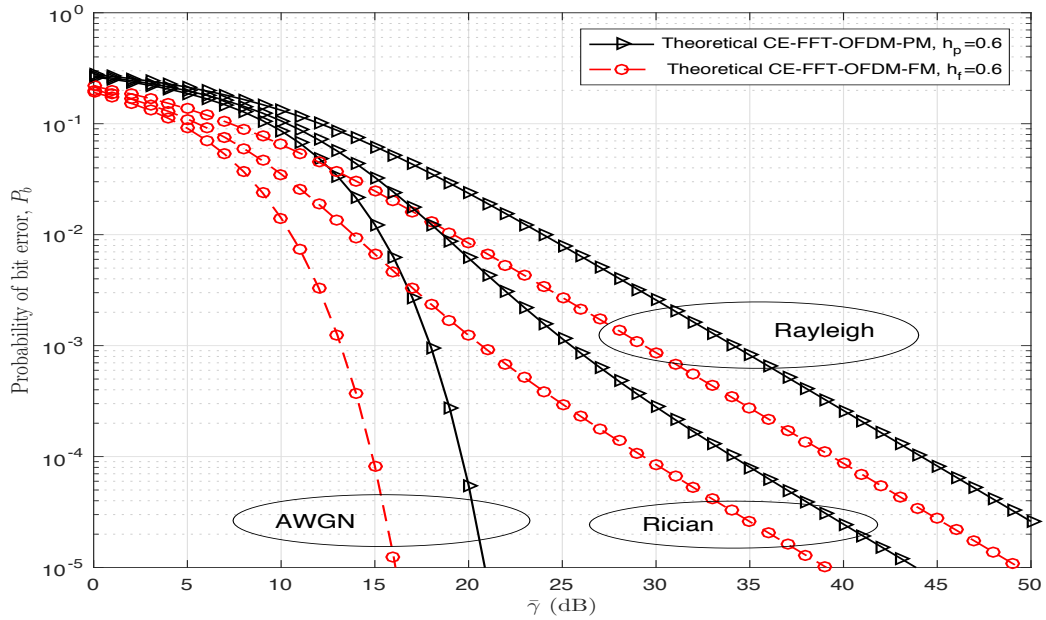


Figure 4.21: Probability of bit error performances of FFT-OFDM systems (4-PAM mapper) with PM ($h_p = 0.6$) and FM ($h_f = 0.6$) over AWGN, Rician ($K = 6$ dB) and Rayleigh channels.

4.7 Conclusions

A generalized description of constant envelope DCT- and FFT-OFDM systems, with MPAM mapper, with FM is given and signals in these systems are mathematically described. Performance analysis of these systems over AWGN and fading channels are carried out and closed-form expressions for BER are derived and illustrated as a function of system parameters such as modulation index of FM, SNR, number of levels of M-PAM mapper and parameters of channel environment. It is observed that CE-DCT-OFDM system is superior to CE-FFT-OFDM system by nearly 3 *dB*. Power penalty required for these systems over fading channels is assessed and tabulated. The effect of TWTA amplifier in DCT-OFDM system on BER performance is also presented as function of IBO and compared with performance of CE-DCT-OFDM system with IBO= 0 *dB*. Comparison of DCT-OFDM system with PM and FM is also provided.

Chapter 5

Constant Envelope DCT- and FFT-OFDM Systems with CPM⁶

5.1 Introduction

As discussed in the previous Chapters 3 and 4, in an OFDM system with angle modulation signals have 0 dB PAPR, which permits HPA to operate near saturation level achieving maximum power efficiency. Continuous Phase Modulation (CPM) is a manifestation of PM used in communication systems for its attractive bandwidth and power properties [54, 55]. It is possible to introduce systematic correlation among adjacent data samples in an OFDM system with CPM, which can be exploited to better BER performance of the system. Moreover signals in such a system are constant envelope and, hence, require no costly PAPR reduction techniques [54]. The intent of this Chapter is to introduce CPM in DCT- and FFT-OFDM systems and examine their BER performances over Gaussian and fading channels. Also expressions for effective bandwidth of two systems are developed and presented.

6. Rayan H. Alsisi and Raveendra K. Rao ,”DCT- and FFT-based OFDM Systems with Continuous Phase Modulation over Flat Fading Channels,” 2017 International Conference on Electrical and Computing Technologies and Applications (ICECTA), Ras Al Khaimah, UAE, November 2017, pp. 1-6.

5.2 Signals in DCT- and FFT-OFDM Systems with CPM

The OFDM-CPM signal can be written as:

$$s(t) = A_c \cos(2\pi f_c t + \phi(t) + \phi_0), \quad 0 \leq t \leq T \quad (5.1)$$

where A_c and f_c represent carrier amplitude and frequency, ϕ_0 is the starting phase assumed zero without loss of generality, and $\phi(t)$ is the information carrying phase and is given by:

$$\phi(t) = 2\pi h \sum_{k=0}^{N-1} x(k) q(t - kT_s) \quad 0 \leq t \leq T \quad (5.2)$$

where h is the modulation index, $T = NT_s$ is the OFDM symbol duration, and $x(k)$, $k = 0, \dots, N-1$, are the real-valued OFDM message signal. $x_{FFT}(k)$ and $x_{DCT}(k)$, respectively, are used to denote message signals in DCT- and FFT-OFDM systems. The phase function $q(t)$ is the integral of some frequency shaping pulse $f(t)$, i.e.,

$$q(t) = \int_0^t f(\tau) d\tau \quad 0 \leq t \leq T_s \quad (5.3)$$

If $f(t) = 0$, $t < 0$ and $t > T_s$ the signal is referred to as full-response CPM. Several frequency shaping pulses for $f(t)$ can be used [54]. When a rectangle pulse shape is used, $f(t)$ and $q(t)$ are given by

$$f(t) = \begin{cases} \frac{1}{2T_s} & 0 \leq t \leq T_s \\ 0 & \text{Otherwise} \end{cases} \quad (5.4)$$

and

$$q(t) = \begin{cases} \frac{t}{2T_s} & 0 \leq t \leq T_s \\ \frac{1}{2} & T_s \leq t \end{cases} \quad (5.5)$$

In Figure 5.1 and 5.2, $f(t)$ and $q(t)$ are shown for rectangular pulse shaping function.

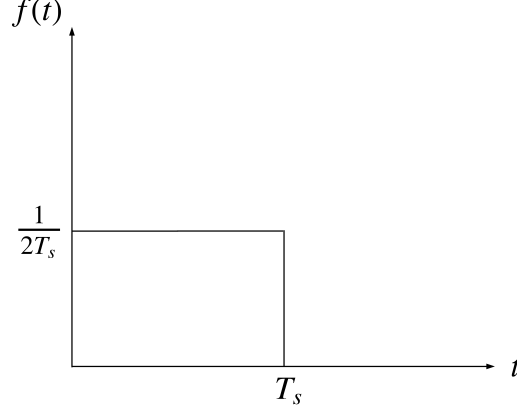


Figure 5.1: Rectangular frequency pulse shaping function $f(t)$

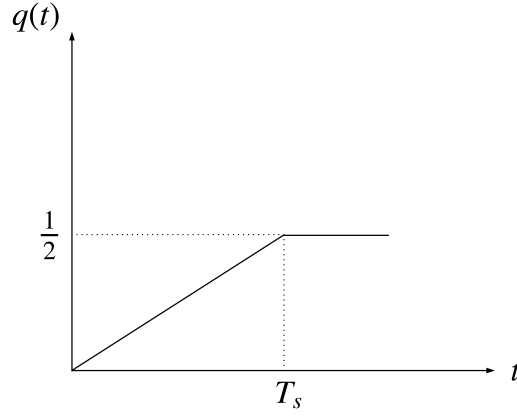


Figure 5.2: Phase function $g(t)$ for rectangular frequency pulse function

Using (5.5) in (5.2), The information carrying phase can be written as

$$\phi(t) = \frac{\pi h x(k)}{T_s} (t - kT_s) + \pi h \sum_{j=0}^{k-1} x(j), \quad kT_s \leq t \leq (k+1)T_s, \quad k = 0, 1, \dots, N-1 \quad (5.6)$$

In (5.6), $\sum_{j=0}^{-1} x(j) = 0$. It is noted that during the k^{th} information symbol, the phase is a function of not only $x(k)$ but also is a function of $x(k-1), x(k-2), \dots, x(0)$. The quantity $\pi h \sum_{j=0}^{k-1} x(j)$ is referred to as the accumulated phase and is always modulo 2π . In the case of FFT-OFDM system with MPAM mapper, real-valued $x_{FFT}(k)$ can be obtained by using conjugate symmetric data vector, $[0, X_{FFT}(0), \dots, X_{FFT}(N-1), 0, X_{FFT}^*(N-1), \dots, X_{FFT}^*(0)]$, as input to the IFFT block and it is given by (1.21). In the case of corresponding DCT-OFDM system with MPAM mapper, $x(k)$'s are real and is given by

(2.11). Figure 5.3 shows $\phi(t)$ as a function of t for a CE-DCT-OFDM system (2-PAM mapper) with number of subcarriers $N = 8$.

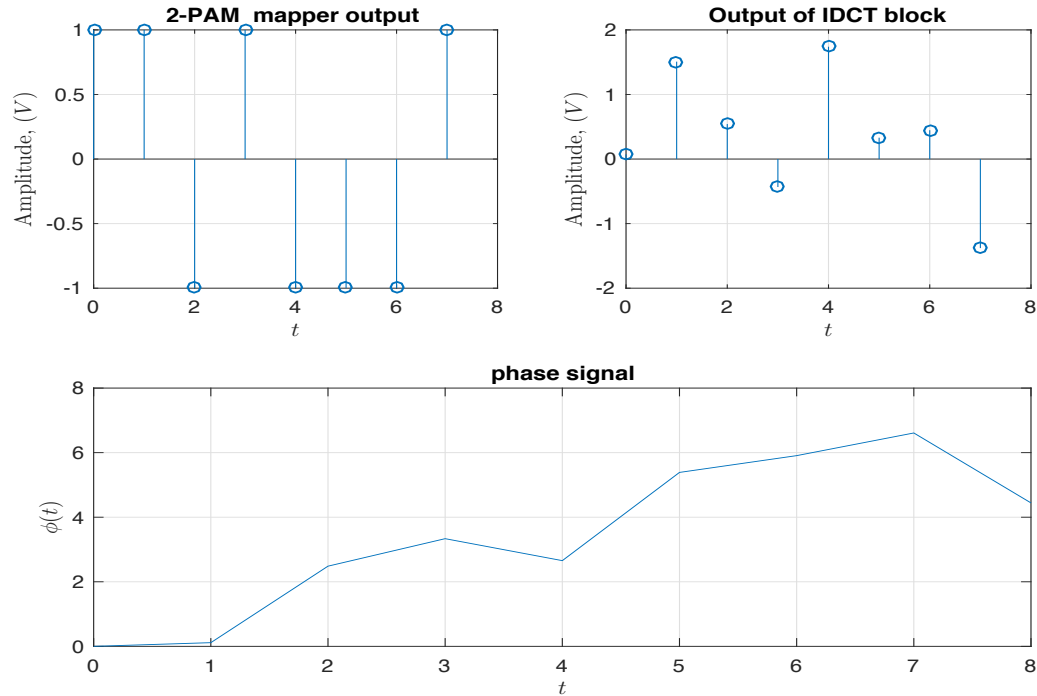


Figure 5.3: Phase $\phi(t)$ in a CE-DCT-OFDM system (2-PAM mapper) with 8 subcarriers.

5.3 OFDM System with CPM: Transmitter

The block diagram of transmitter in an OFDM system with CPM is shown in Figure 5.4. A block of N serial symbols from a data source goes into a S/P converter. The output of this block is fed to an MPAM mapper whose output is a vector $[X(0), X(1), \dots, X(N-1)]^T$ of N elements. For an MPAM mapper in the system, $X(n), n = 0, 1, \dots, N-1 \in \{\pm 1, \pm 3, \dots, \pm(M-1)\}$ are used to generate $x(k)$. In the case of an FFT-OFDM system, $x_{FFT}(k)$ is obtained by using conjugate symmetric data vector, $[0, X_{FFT}(0), \dots, X_{FFT}(N-1), 0, X_{FFT}^*(N-1), \dots, X_{FFT}^*(0)]$ as input to IFFT block. In a DCT-OFDM system the input to IDCT block is $[X(0), X(1), \dots, X(N-1)]$. The $x(k)$, $k = 0, \dots, N-1$, are then fed to a CPM modulator to obtain modulated signal $s(t)$, which is transmitted after amplification by HPA over the communication channel. Using

(5.5) in (5.2), the CPM modulated signals in FFT- and DCT-OFDM systems can be written as:

$$s(t) = A_c \cos(2\pi f_c t + \phi_{FFT}(t)) \quad 0 \leq t \leq T \quad (5.7)$$

and

$$s(t) = A_c \cos(2\pi f_c t + \phi_{DCT}(t)) \quad 0 \leq t \leq T \quad (5.8)$$

The average power and energy of $s(t)$ are $A_c^2/2$ and $A_c^2 T/2$. For $N \log_2(M)$ bits per OFDM symbol the average bit energy is $E_b = A_c^2 T / 2N \log_2(M)$. The variance of the data symbols, σ_s^2 , is equal to $((M^2 - 1)/3)$.

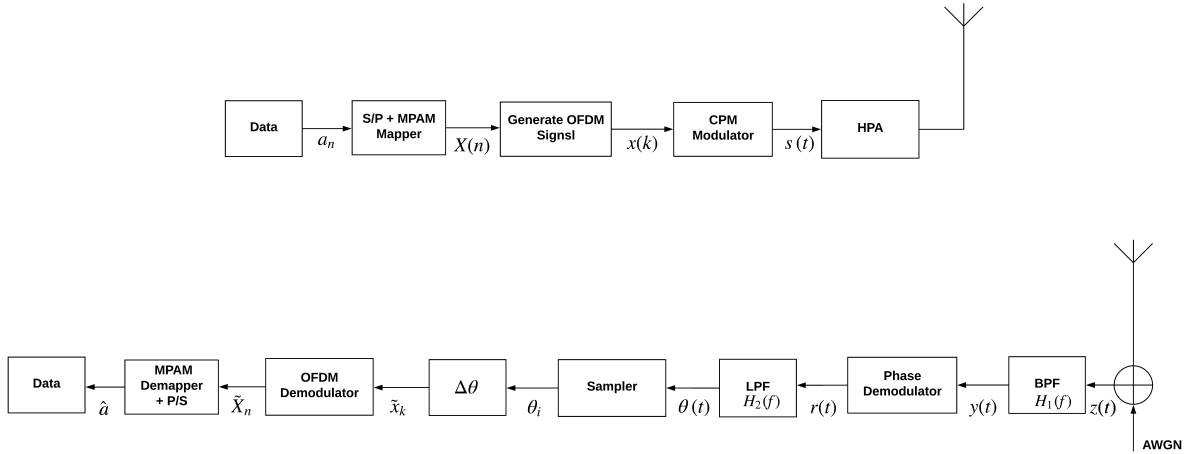


Figure 5.4: Transmitter and receiver structures of OFDM system with CPM

Bandwidth of CPM Modulated OFDM Signals

The effective bandwidth of the modulated signal in (5.1) can be written as: [114, 115]:

$$B = \sqrt{\frac{4 \int_0^\infty [(f - f_0) P(f)] df}{\int_0^\infty P(f) df}} \quad (5.9)$$

where $P(f)$ is the positive frequency part of the spectral density of the signal in (5.1)

and (5.9) can be approximated by [114]:

$$B = \sqrt{\frac{4h^2}{T_s} \int_0^{T_s} f^2(t) dt} \quad (5.10)$$

where $f(t)$ is the frequency pulse. For rectangular pulse shaping considered in this work, $B = hW \text{ Hz}$, where for FFT-OFDM message signal $W = N/T \text{ Hz}$ and for DCT-OFDM message signal $W = N/2T \text{ Hz}$

5.4 OFDM System with CPM: Receiver

The receiver block diagram of OFDM system with CPM is shown in Figure 5.4 and consists of Band Pass Filter (BPF), phase demodulator, Low Pass Filter (LPF), sampler, phase difference, OFDM demodulator, MPAM demapper, and P/S converter blocks.

The received signal ($z(t) = s(t) + w(t)$) goes through a BPF, $H_1(f)$, with characteristic as shown in Figure 3.2, where B is the bandwidth of $s(t)$ and is in excess of twice the message signal bandwidth $W \text{ Hz}$ by an amount that depends on the modulation index h of the CPM signal $s(t)$. The noise $w(t)$ is modelled as AWGN with zero mean and PSD of $N_0/2 \text{ Watts/Hz}$. The input to the phase demodulator is given by:

$$y(t) = s(t) + n(t), 0 \leq t \leq T \quad (5.11)$$

where $n(t)$ represents the output of BPF due to input $w(t)$. The output of the phase demodulator is a low pass signal with bandwidth equal to message signal, $W \text{ Hz}$. The LPF output is then fed to the sampler to obtain JN samples of the demodulated phase signal, where J is the oversampling factor, which are fed to phase difference block to get the phase difference of neighbor samples. The output of this block is fed to OFDM demodulator followed by the MPAM demapper and P/S converter to get an estimate of transmitted data.

5.4.1 Phase Demodulation and OFDM Demodulator

As explained in Chapter 3, the phase demodulator consists of arctangent block to detect the phase of the received signal, using $\arctan \left\{ \frac{y_Q(t)}{y_I(t)} \right\}$, where $y_Q(t)$ and $y_I(t)$ are the quadrature and in-phase components of $y(t)$, followed by a phase unwrapper. The phase of $y(t)$ can be written as:

$$\theta(t) \approx \phi(t) + \frac{m(t)}{A_c} \sin[\Psi(t) - \phi(t)] \quad (5.12)$$

where $m(t)$ is given by (3.12), $\Psi(t)$ is given by (3.13). The output of LPF can be written as:

$$\theta(t) = \phi(t) + \Phi(t) \quad (5.13)$$

The PSD of noise at the output of LPF is:

$$S(f) = \begin{cases} N_0/A_c^2, & |f| \leq W \\ 0, & \text{otherwise} \end{cases} \quad (5.14)$$

and its average power is

$$\int_{-W}^W \frac{N_0}{A_c^2} df = \frac{2WN_0}{A_c^2} \quad (5.15)$$

The signal $\theta(t)$ is fed to sampler to obtain JN samples of $\theta(t)$, J being the oversampling factor. That is,

$$\theta[i] = \theta(t) \big|_{t=\frac{i}{J}T_s}, \quad i = 0, \dots, JN - 1 \quad (5.16)$$

The phase difference between adjacent samples is then given by:

$$\Delta\tilde{\theta} = \tilde{\theta}_{i+1} - \tilde{\theta}_i \quad (5.17)$$

which can be written as:

$$\Delta\tilde{\theta} = (\phi_{i+1} - \phi_i) + (\Phi_{i+1} - \Phi_i) \quad (5.18)$$

The estimated value of $\tilde{x}(k)$ can be shown to be equal to:

$$\tilde{x}(k) = \frac{1}{h\pi} \sum_{l=0}^{J-1} \left(\phi_{(Jk+1)+l} - \phi_{(Jk)+l} \right) + \left(\Phi_{(Jk+1)+l} - \Phi_{(Jk)+l} \right) \quad (5.19)$$

That is,

$$\tilde{x}(k) = x(k) + \frac{1}{h\pi} \left(\Phi_{J(k+1)} - \Phi_{(Jk)} \right) \quad (5.20)$$

$\tilde{x}(k)$'s are then fed to OFDM demodulator (FFT or DCT block) to get $\tilde{X}(n)$ and can be written as:

$$\tilde{X}(n) = X(n)/\sqrt{\sigma_s^2} + N(n); \quad n = 0, 1, \dots, N-1 \quad (5.21)$$

where

$$N(n) = \frac{1}{h\pi} \sum_{k=0}^{N-1} \left(\Phi_{n,J(k+1)} - \Phi_{n,Jk} \right) \varphi_k \quad (5.22)$$

are Gaussian. The mean and variance of $\tilde{X}(n)$ are given by:

$$E[\tilde{X}(n)] = E[X(n)/\sqrt{\sigma_s^2} + N(n)] = E[X(n)/\sqrt{\sigma_s^2}] \quad (5.23)$$

and

$$Var[\tilde{X}(n)] = \sigma^2 = \frac{4WN_0}{h^2\pi^2A_c^2}; \quad n = 0, 1, \dots, N-1 \quad (5.24)$$

5.4.2 BER Probability of OFDM system with CPM

Consider the output of the n^{th} correlator of OFDM demodulator fed to the MPAM demapper. That is,

$$\tilde{X}(n) = \frac{X(n)}{\sqrt{\sigma_s^2}} + N(n)$$

where $X(n) \in \{\pm 1, \pm 3, \dots, \pm(M-1)\}$, $\sigma_s^2 = ((M^2 - 1)/3)$ is the variance of data symbols, and $N(n)$ are zero Gaussian random variables with variance σ^2 given by (5.24). Using the technique explained in Chapter 3, the symbol error probability of the n^{th} demapper can be written as:

$$\begin{aligned}
P_s &= \frac{1}{M} \sum_{i=1}^M \text{Prob.}[\text{error} \mid s_i \text{ sent}] \\
&= \frac{1}{M} [(M-2) P_{\text{inner}} + 2P_{\text{outer}}] \\
&= 2 \left(\frac{M-1}{M} \right) \int_{1/\sqrt{\sigma_s^2}}^{\infty} \frac{1}{\sqrt{2\pi\sigma^2}} e^{(-x^2/2\sigma^2)} dx
\end{aligned} \tag{5.25}$$

Simplifying (5.25), the probability of symbol error can be written as

$$P_s = 2 \left(\frac{M-1}{M} \right) Q \left(\sqrt{\frac{(\pi h)^2 A_c^2}{4W N_0 \sigma_s^2}} \right) \tag{5.26}$$

Since, $W = N/T$ and $N/2T$ for FFT- and DCT-OFDM signals, respectively. The symbol error probabilities for CE-FFT- and CE-DCT-OFDM systems are given by:

$$P_{s_{FFT}} = 2 \left(\frac{M-1}{M} \right) Q \left(\sqrt{(\pi h)^2 \frac{3 \log_2(M) E_b}{2(M^2-1)N_0}} \right) \tag{5.27}$$

and

$$P_{s_{DCT}} = 2 \left(\frac{M-1}{M} \right) Q \left(\sqrt{(\pi h)^2 \frac{3 \log_2(M) E_b}{(M^2-1)N_0}} \right) \tag{5.28}$$

By observing that in the receiver, there are N demappers and each has the same symbol error probability, the average symbol error probability is simply given by (5.26). Converting the symbol error rate to BER, the BER for CE-FFT- and CE-DCT-OFDM systems are given by:

$$P_{b_{FFT}} \approx 2 \left(\frac{M-1}{M \log_2(M)} \right) Q \left(\sqrt{(\pi h)^2 \frac{3 \log_2(M) E_b}{2(M^2-1)N_0}} \right) \tag{5.29}$$

and

$$P_{b_{DCT}} \approx 2 \left(\frac{M-1}{M \log_2(M)} \right) Q \left(\sqrt{(\pi h)^2 \frac{3 \log_2(M) E_b}{(M^2-1)N_0}} \right) \tag{5.30}$$

The BER performances given by (5.29) and (5.30) are a functions of E_b/N_0 , signal-to-noise ratio, h , modulation index, and M .

5.5 Performance over Fading Channels

Using (5.26) and following the approach presented in Section 3.5.2, a generalized expression for $P_b(\gamma)$ can be written as

$$P_b(\gamma) = 2 \left(\frac{M-1}{M \log_2(M)} \right) Q \left(\sqrt{I(\pi h)^2 \alpha^2 \frac{E_b}{N_0}} \right) = 2 \left(\frac{M-1}{M \log_2(M)} \right) Q \left(\sqrt{I(\pi h)^2 \gamma} \right) \quad (5.31)$$

where $I = 3 \frac{\log_2(M)}{M^2-1}$ and $\frac{3}{2} \frac{\log_2(M)}{M^2-1}$ for CE-DCT- and CE-FFT-OFDM systems. In (5.31), γ represents the instantenus SNR of the received signal over the fading channel.

BER Expression for Rayleigh Fading Channel

Using (5.31) and (3.51) in (3.49), and using $Q(z)$ given in (3.53), P_b for Rayleigh fading channel can be shown to be given by

$$P_b = 2 \left(\frac{M-1}{M \log_2(M)} \right) \frac{1}{\pi \bar{\gamma}} \int_0^{\pi/2} \int_0^\infty \exp \left(-\frac{I(\pi h)^2 \gamma}{2 \sin^2(\theta)} - \frac{\gamma}{\bar{\gamma}} \right) d\gamma d\theta \quad (5.32)$$

Integrating (5.32) [113], the bit error rate can be shown to be given by:

$$P_b = \left(\frac{M-1}{M \log_2(M)} \right) \left[1 - \sqrt{\frac{1}{1 + \frac{1}{I(\pi h)^2 \bar{\gamma}/2}}} \right] \quad (5.33)$$

It is noted that BER is a function of h , modulation index, M , and $\bar{\gamma}$, average SNR of received signal over Rayleigh channel.

BER Expression for Rician Fading Channel

For the Rician channel, the pdf of γ is given by (3.55). Using (5.31) and (3.55) in (3.49), and using $Q(z)$ given in (3.53), P_b for Rician channel can be shown to be given by

$$P_b = \frac{2}{\pi} \left(\frac{M-1}{M \log_2(M)} \right) \frac{(1+K)e^{-K}}{\bar{\gamma}} \int_0^{\pi/2} \int_0^\infty \exp \left[-\frac{I(\pi h)^2 \gamma}{2 \sin^2(\theta)} - \frac{(1+K)\gamma}{\bar{\gamma}} \right] I_0 \left[2 \sqrt{\frac{(K+K^2)\gamma}{\bar{\gamma}}} \right] d\gamma d\theta \quad (5.34)$$

Upon simplification of (5.34) [113], we get:

$$P_b = \frac{2}{\pi} \left(\frac{M-1}{M \log_2(M)} \right) \int_0^{\pi/2} \frac{(1+K) \sin^2(\theta)}{(1+K) \sin^2(\theta) + I(\pi h)^2 \bar{\gamma}/2} \exp \left[-\frac{KI(\pi h)^2 \bar{\gamma}/2}{(1+K) \sin^2(\theta) + I(\pi h)^2 \bar{\gamma}/2} \right] d\theta \quad (5.35)$$

Again, it is noted that BER is a function of h_p , modulation index, M , and $\bar{\gamma}$, average SNR of received signal over Rician channel. Also, BER is a function of K , Rice factor of the density function.

5.6 Numerical Results and Discussion

Numerical results of probability of bit error performances of DCT- and FFT-OFDM systems with CPM are presented and discussed next.

5.6.1 Performance in AWGN Channel

The expressions for BER in AWGN channel for both systems are given by (5.29) and (5.30). The P_b vs. E_b/N_0 plots for CE-DCT- and CE-FFT-OFDM systems for 2-PAM mapper are shown in Figure 5.5 for $h = 0.1, 0.2$ and 0.6 . Table 5.1 summarizes E_b/N_0 required at $P_b = 10^{-5}$ for both systems as a function of h . It is noted that CE-DCT-OFDM system performs better than the corresponding CE-FFT-OFDM system. For

example at $P_b = 10^{-5}$, $h = 0.4$, E_b/N_0 required for CE-DCT-OFDM system is nearly 3 dB less than that required for CE-FFT-OFDM system. Also, it is observed that BER decreases as h increases. The probability of bit error performances of CE-DCT- and

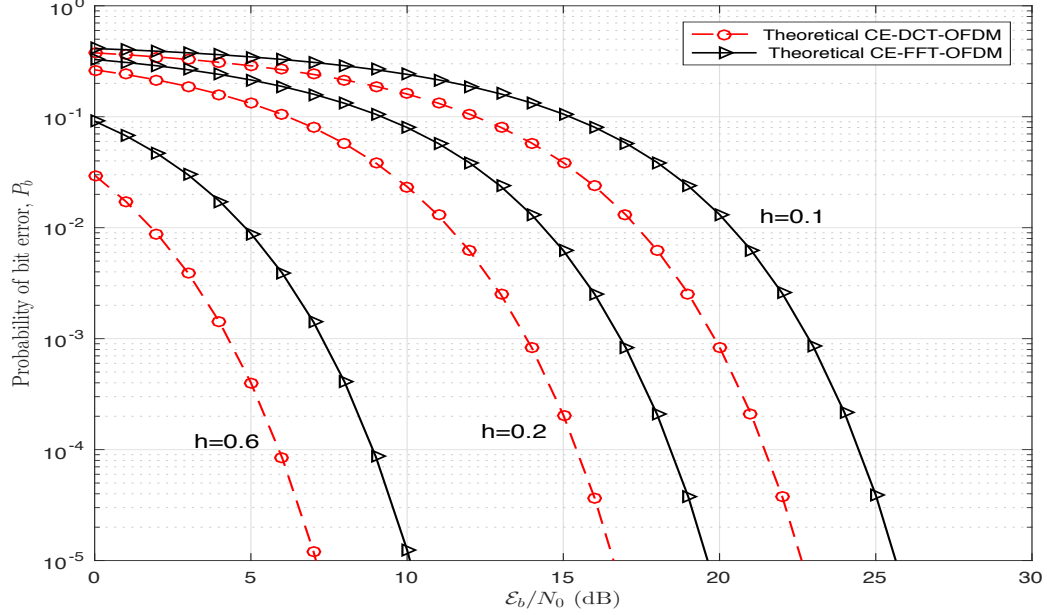


Figure 5.5: Probability of bit error performances of CE-DCT- and CE-FFT-OFDM systems (2-PAM mapper) over AWGN channel.

Table 5.1: Comparison of CE-DCT- and CE-FFT-OFDM systems (2-PAM mapper) at $P_b = 10^{-5}$ as a function of h

h	CE-DCT-OFDM	CE-FFT-OFDM
	E_b/N_0 (dB)	E_b/N_0 (dB)
0.7	5.753	8.766
0.6	7.092	10.102
0.5	8.676	11.686
0.4	10.614	13.624
0.3	13.113	16.123
0.2	16.635	19.645

CE-FFT-OFDM systems for 4-PAM and 8-PAM mappers are shown in Figures 5.6 and 5.7, respectively. Tables 5.2 and 5.3 summarize E_b/N_0 required at $P_b = 10^{-5}$ for both systems as a function of h .

The BER performances of CE-DCT- and CE-FFT-OFDM systems with $h = 0.6$ for various values of M are shown in Figures 5.8 and 5.9, respectively. For both systems, it is

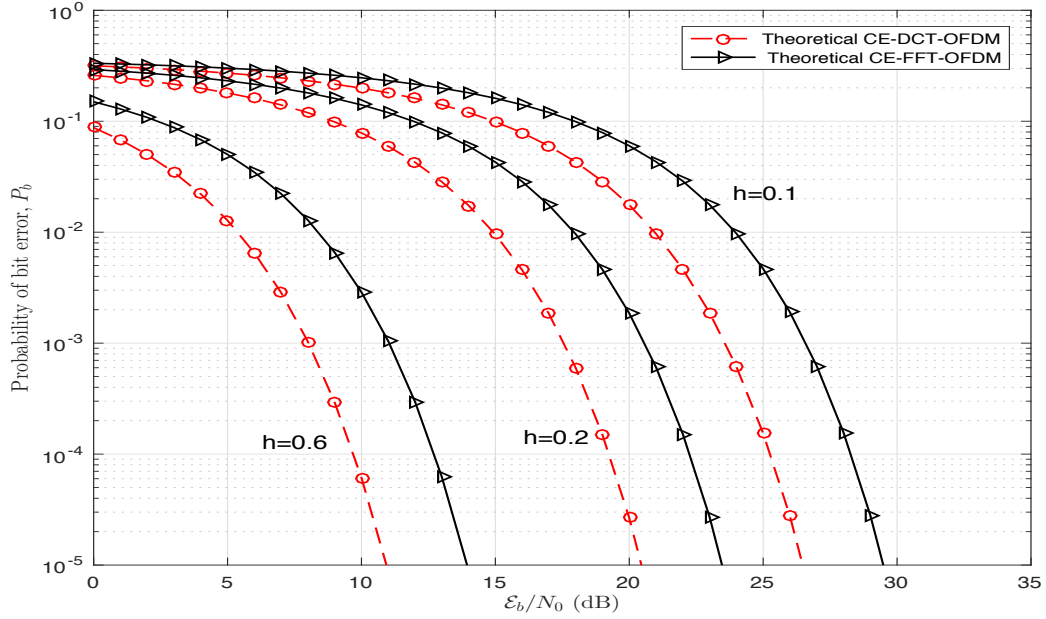


Figure 5.6: Probability of bit error performances of CE-DCT- and CE-FFT-OFDM systems (4-PAM mapper) over AWGN channel.

Table 5.2: Comparison of CE-DCT- and CE-FFT-OFDM systems (4-PAM mapper) at $P_b = 10^{-5}$ as a function of h

h	CE-DCT-OFDM	CE-FFT-OFDM
	E_b/N_0 (dB)	E_b/N_0 (dB)
0.7	9.599	12.610
0.6	10.939	13.949
0.5	12.522	15.533
0.4	14.461	17.471
0.3	16.959	19.969
0.2	20.481	23.492

noted that BER increases as M increases. For CE-DCT-OFDM system with $h = 0.6$ and $M = 2$, to achieve $\text{BER} = 10^{-5}$, $E_b/N_0 = 8.676 \text{ dB}$ is required, whereas for $M = 4$ and $M = 8$ systems to achieve the same error rate, $E_b/N_0 = 12.522 \text{ dB}$ and $E_b/N_0 = 16.875 \text{ dB}$ are required, respectively. At $P_b = 10^{-5}$, systems with $M = 4$ and $M = 8$ are worse than the system with $M = 2$ by 3.8 and 8.2 dB, respectively. However, the spectral efficiency of the system improves with increased value of M . The BER performances of both systems can be controlled by varying h and M as shown in Figures 5.10 and 5.11. The CE-DCT-OFDM system with $M = 8$ and $h = 0.6$ outperforms corresponding

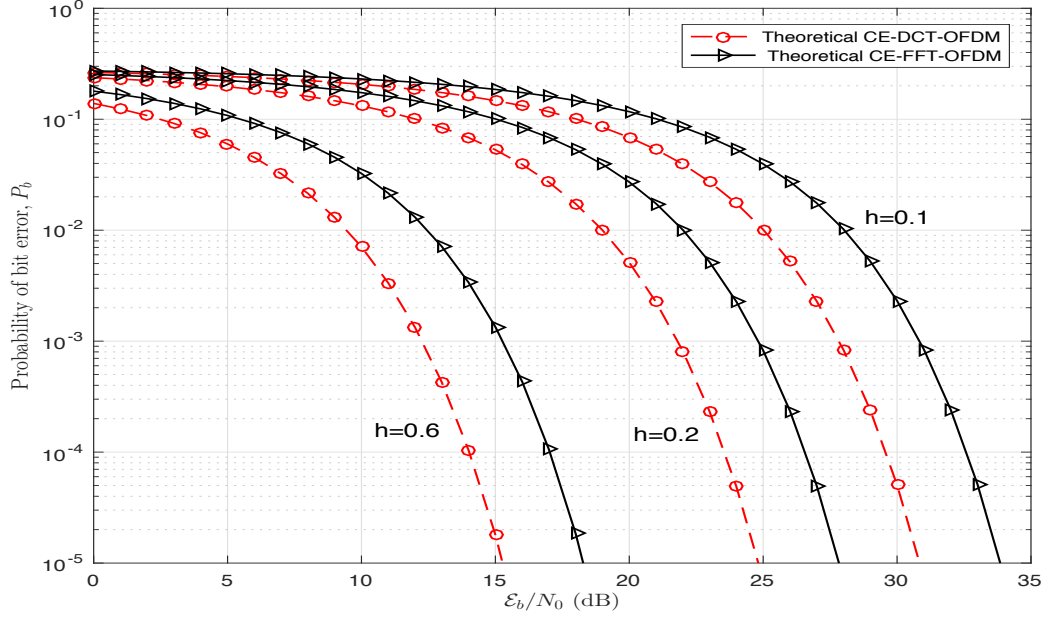


Figure 5.7: Probability of bit error performances of CE-DCT- and CE-FFT-OFDM systems (8-PAM mapper) over AWGN channel.

Table 5.3: Comparison of CE-DCT- and CE-FFT-OFDM systems (8-PAM mapper) at $P_b = 10^{-5}$ as a function of h

h_p	CE-DCT-OFDM	CE-FFT-OFDM
	E_b/N_0 (dB)	E_b/N_0 (dB)
0.7	13.952	16.963
0.6	15.291	18.302
0.5	16.875	19.885
0.4	18.813	21.823
0.3	21.312	24.322
0.2	24.834	27.844

system with $M = 2$ and $h = 0.1$ by 7.4 dB at BER = 10^{-5} .

Figure 5.12 and 5.13 compare simulation results with those of theoretical BER results given by (5.29) for CE-DCT-OFDM system ($N = 64$) for $M = 2$ and $M = 4$, respectively.

5.6.2 Performance over Fading Channels

The expression for BER over Rayleigh fading channel is given by (5.33). Figures 5.14, 5.15, and 5.16 show P_b of CE-DCT- and CE-FFT-OFDM systems for $M = 2, 4$, and 8 over Rayleigh channel, respectively. It is noted that P_b decreases as h increases for a

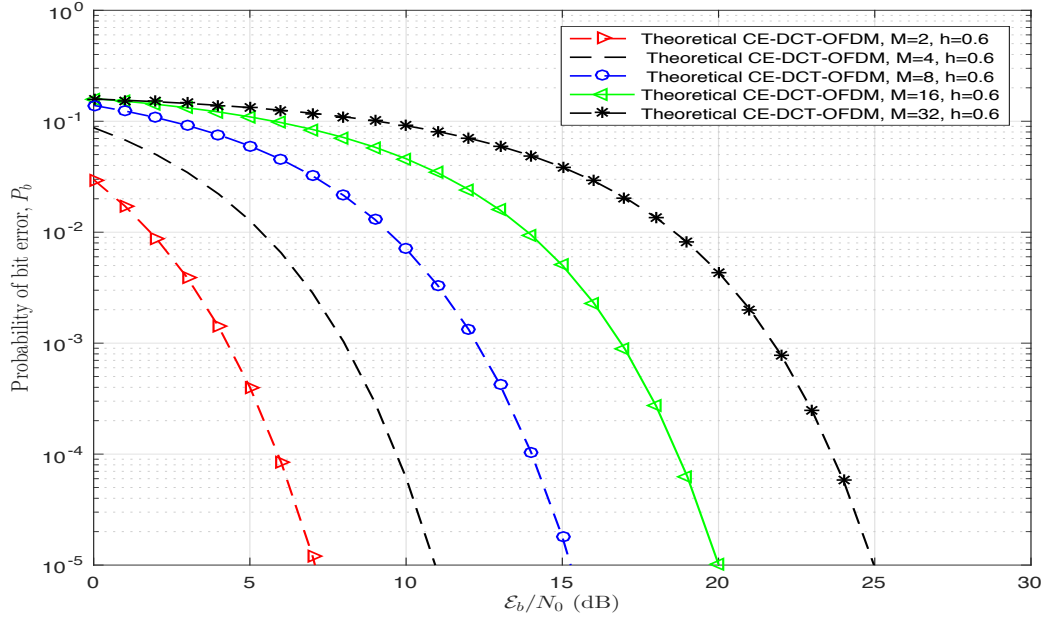


Figure 5.8: Probability of bit error performance of CE-DCT-OFDM system as a function of M for $h = 0.6$ over AWGN channel.

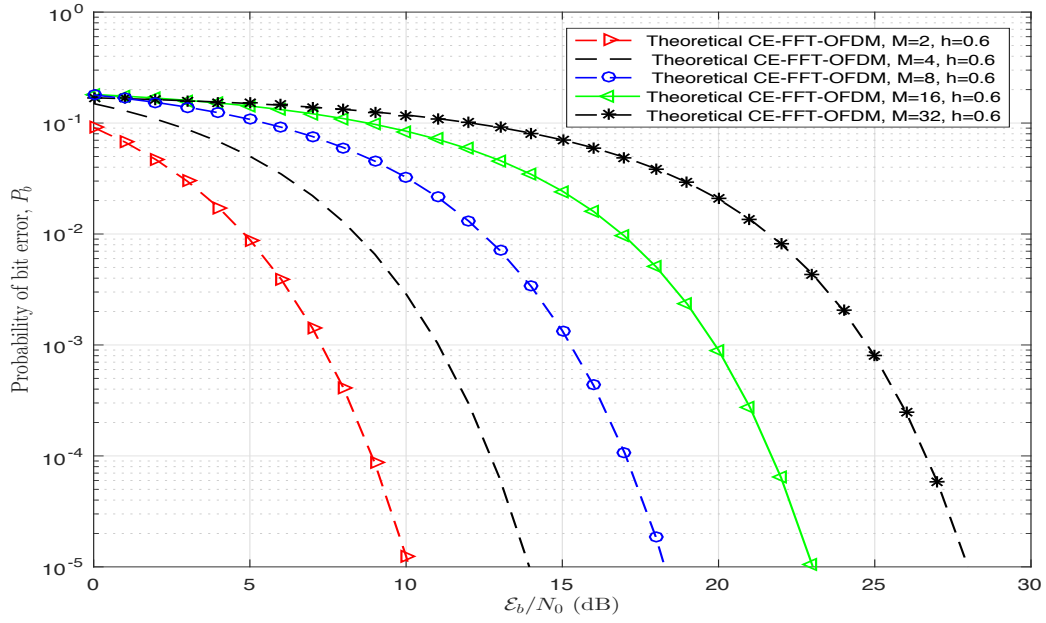


Figure 5.9: Probability of bit error performance of CE-FFT-OFDM system as a function of M for $h = 0.6$ over AWGN channel.

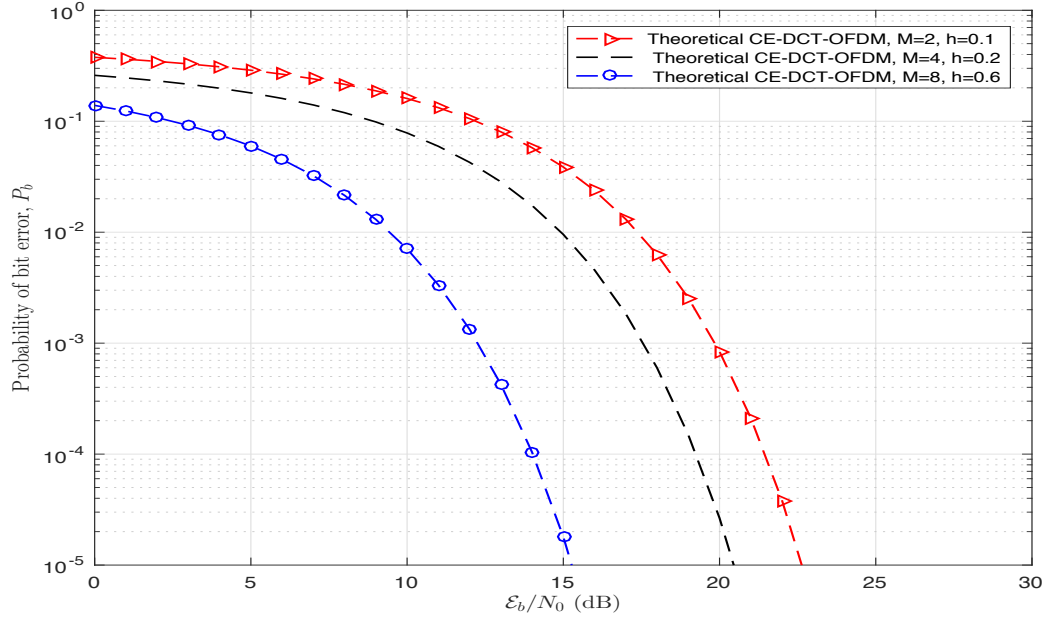


Figure 5.10: Probability of bit error performance of CE-DCT-OFDM system as a function of h and M over AWGN channel.

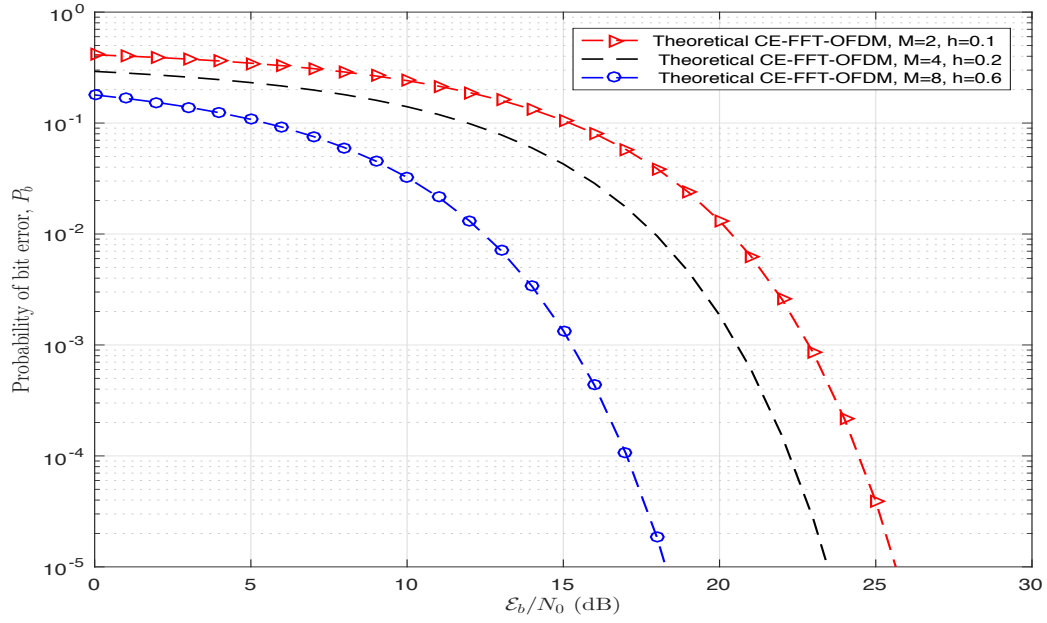


Figure 5.11: Probability of bit error performance of CE-FFT-OFDM system as a function of h and M over AWGN channel.

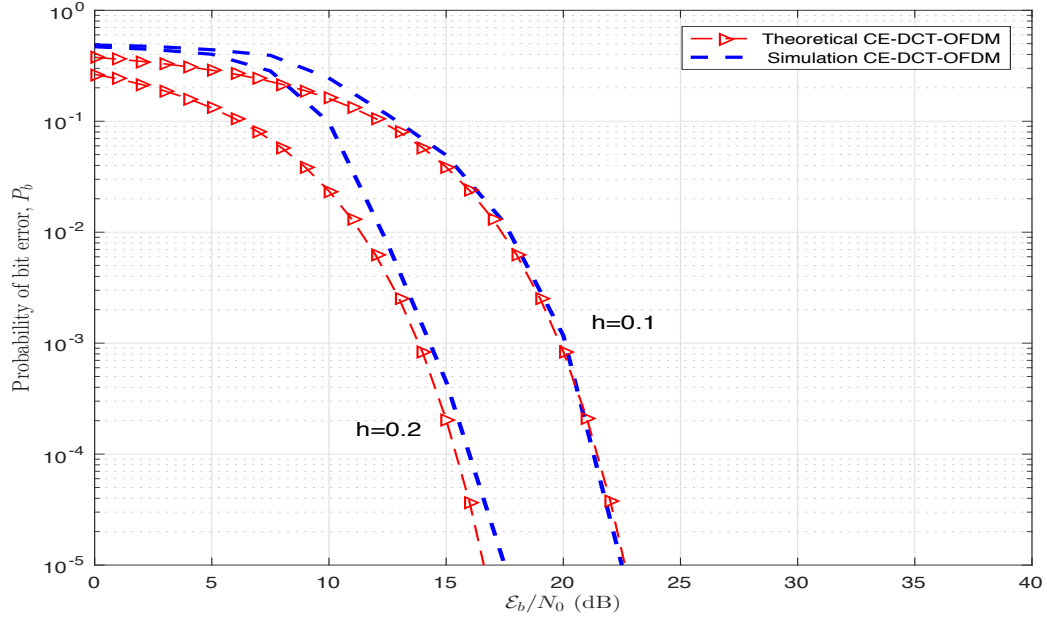


Figure 5.12: Comparison of analytical and simulation results for CE-DCT-OFDM system (2-PAM mapper) over AWGN channel.

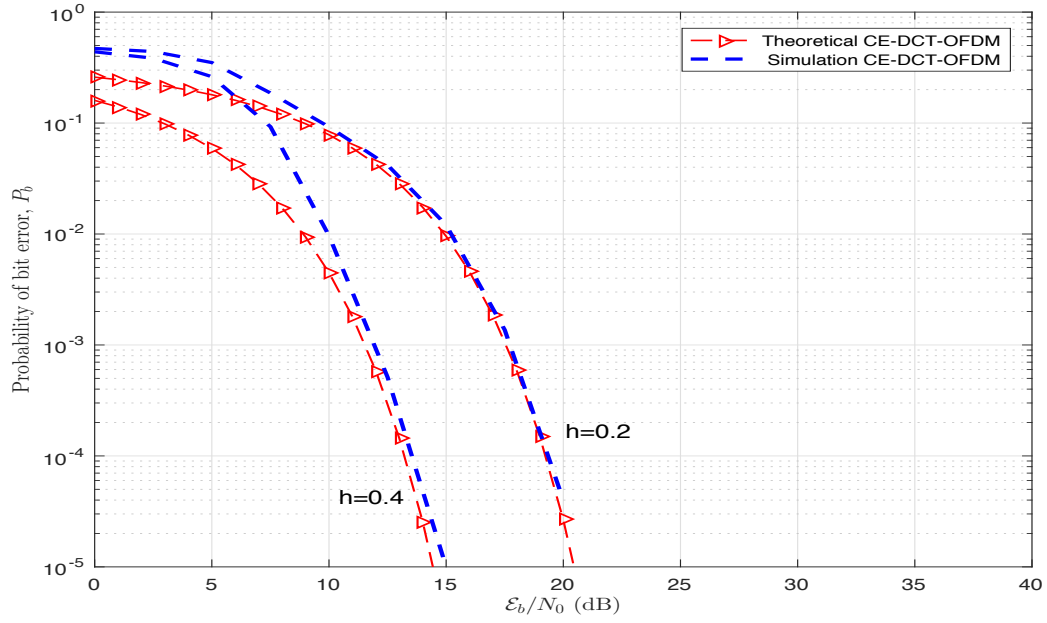


Figure 5.13: Comparison of analytical and simulation results for CE-DCT-OFDM system (4-PAM mapper) over AWGN channel.

fixed value of SNR. Also, it is observed that CE-DCT-OFDM system performs better than CE-FFT-OFDM system. The expression for BER for Rician fading channel is

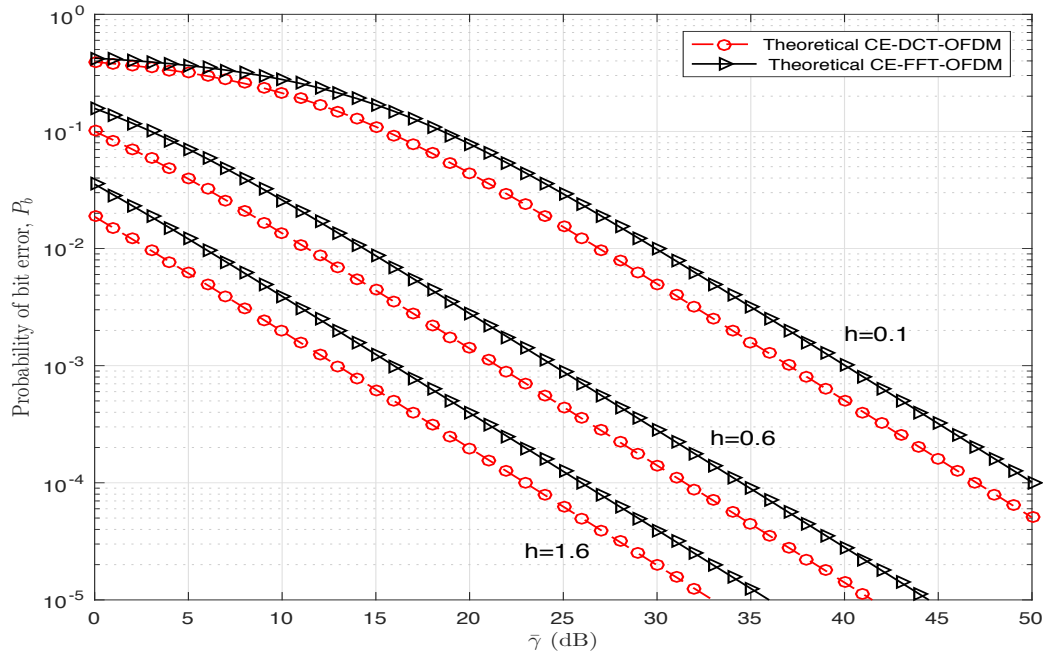


Figure 5.14: Probability of bit error performances of CE-DCT- and CE-FFT-OFDM systems (2-PAM mapper) over Rayleigh fading channel.

given by (5.35). The BER is not only a function of h , M and $\bar{\gamma}$, but also depends on K , Rice factor. Figures 5.17, 5.18 and 5.19 depict P_b of CE-DCT- and CE-FFT-OFDM systems for Rician channel for $M = 2, 4$ and 8 , respectively, for $K = 6$ dB. It is noted that CE-DCT-OFDM system performs better than CE-FFT-OFDM system.

The comparison of P_b performances of CE-DCT- and CE-FFT-OFDM systems, for $M = 2$ and $h = 0.7$, over AWGN, Rician and Rayleigh channels as a function of average SNR are shown in Figures 5.20 and 5.21, respectively. Tables 5.4 and 5.5 summarize average SNR required at $P_b = 10^{-3}, 10^{-4}$ and 10^{-5} for CE-DCT- and CE-FFT-OFDM systems over these channels.

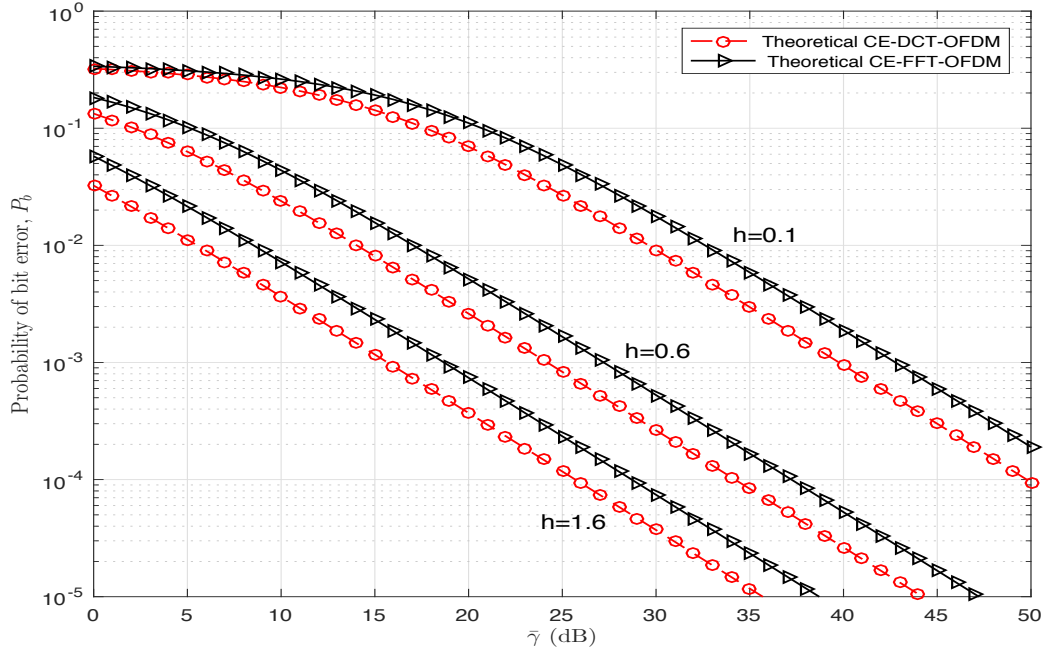


Figure 5.15: Probability of bit error performances of CE-DCT- and CE-FFT-OFDM systems (4-PAM mapper) over Rayleigh fading channel.

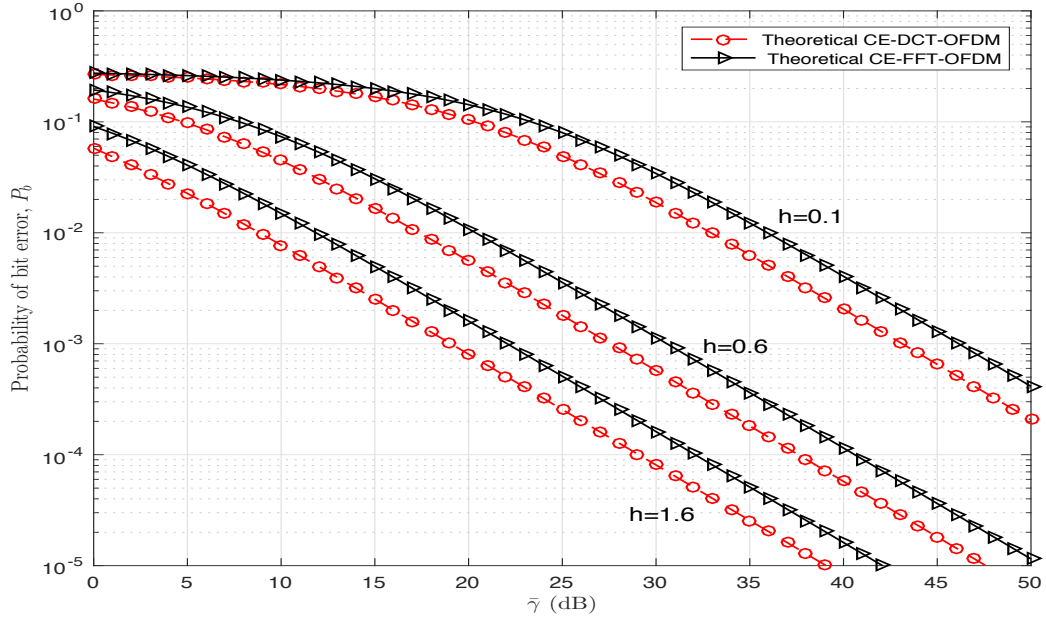


Figure 5.16: Probability of bit error performances of CE-DCT- and CE-FFT-OFDM systems (8-PAM mapper) over Rayleigh fading channel.

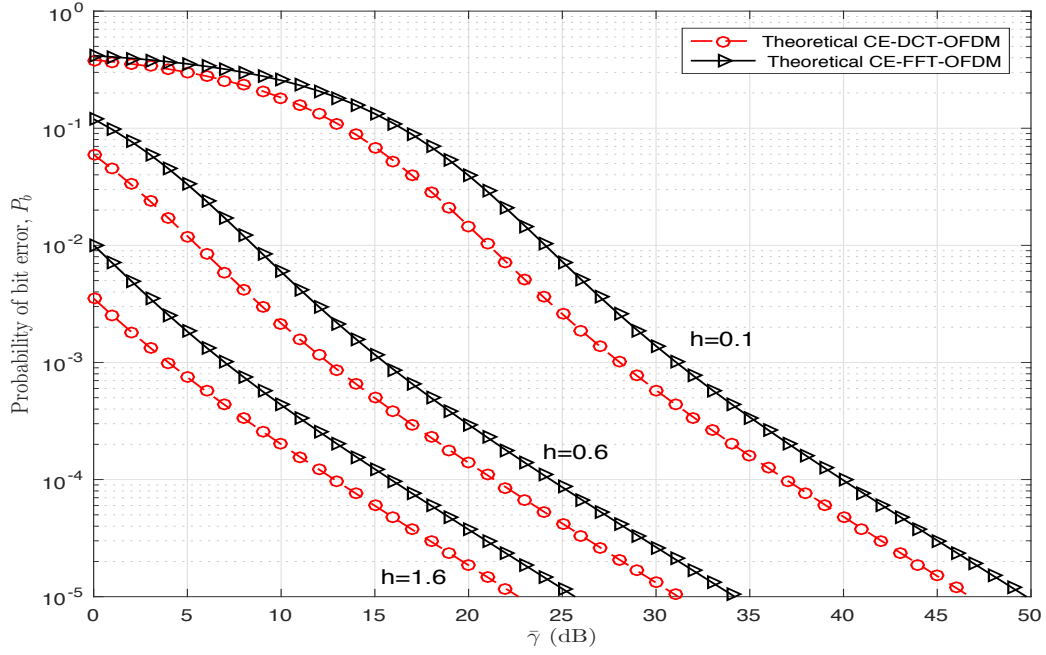


Figure 5.17: Probability of bit error performances of CE-DCT- and CE-FFT-OFDM systems (2-PAM mapper) over Rician fading channel ($K = 6$ dB).

Table 5.4: Comparison of probability of bit error performances of CE-DCT-OFDM system over AWGN, Rician and Rayleigh channels.

P_b	Average SNR (dB)		
	AWGN	Rician	Raleigh
10^{-3}	2.954	11.128	20.165
10^{-4}	4.564	20.165	30.215
10^{-5}	5.753	29.851	40.532

Table 5.5: Comparison of probability of bit error performances of CE-FFT-OFDM system over AWGN, Rician and Rayleigh channels.

P_b	Average SNR (dB)		
	AWGN	Rician	Raleigh
10^{-3}	5.965	14.151	23.112
10^{-4}	7.574	23.111	33.151
10^{-5}	8.764	32.774	43.555

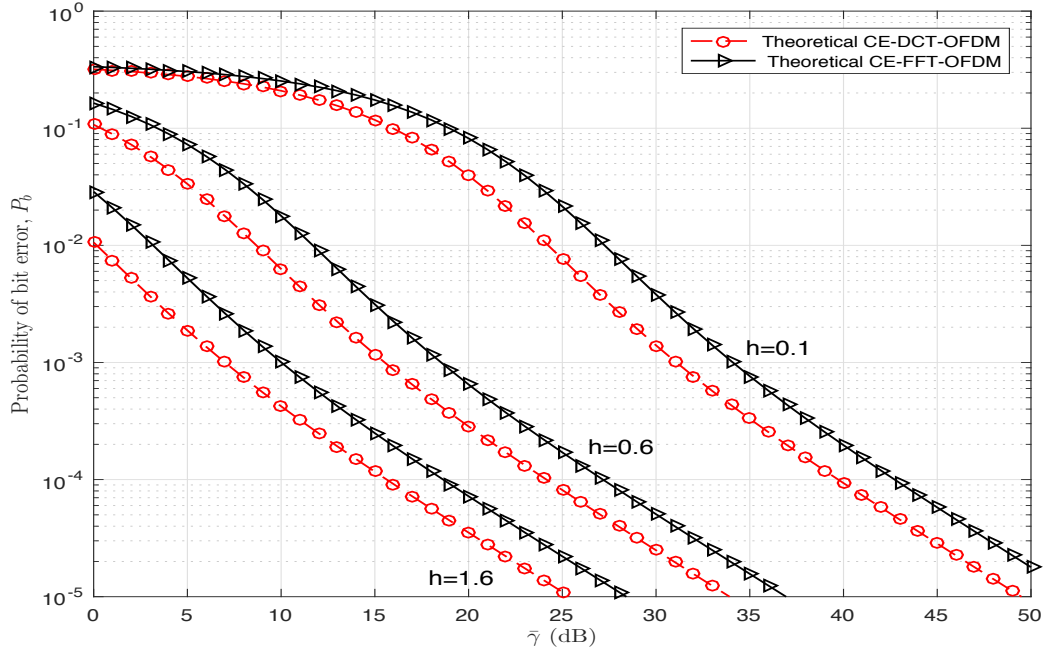


Figure 5.18: Probability of bit error performances of CE-DCT- and CE-FFT-OFDM systems (4-PAM mapper) over Rician fading channel ($K = 6$ dB).

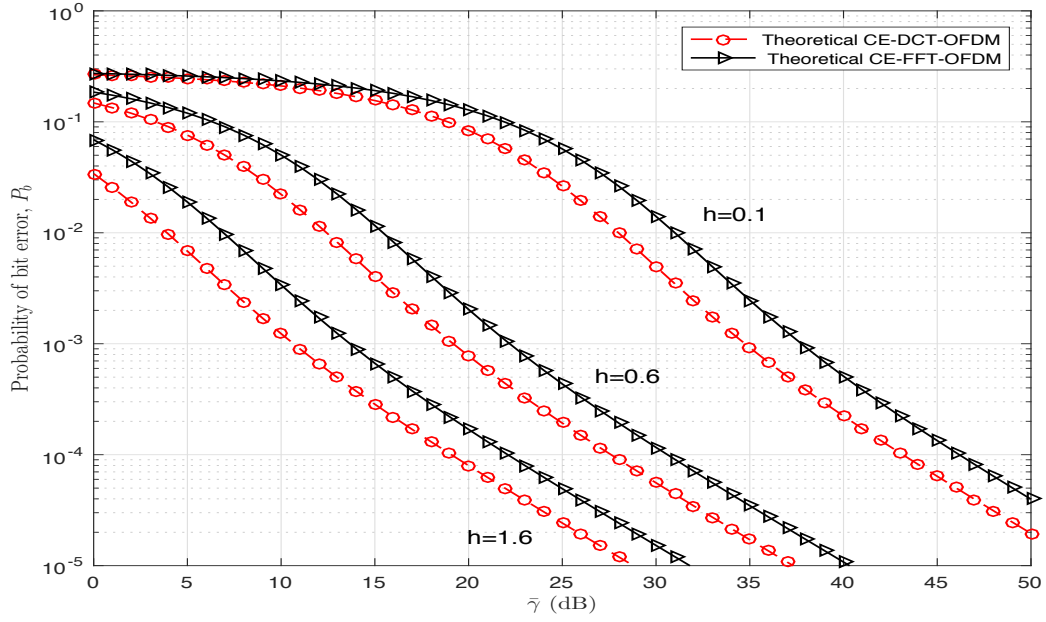


Figure 5.19: Probability of bit error performances of CE-DCT- and CE-FFT-OFDM systems (8-PAM mapper) over Rician fading channel ($K = 6$ dB).

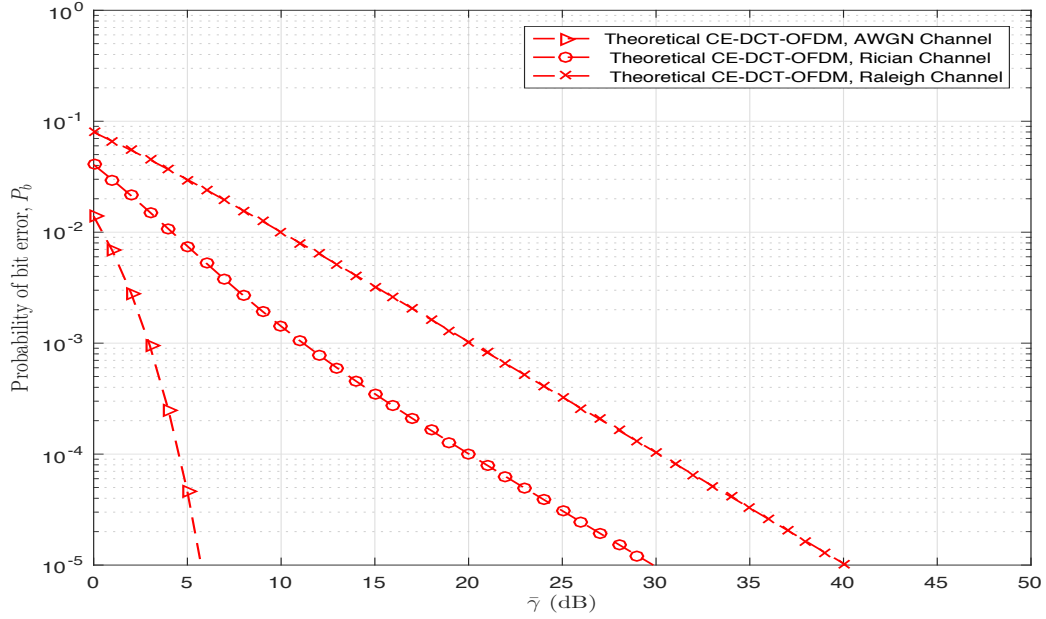


Figure 5.20: Comparison of probability of bit error performances of CE-DCT-OFDM system (2-PAM mapper, $h = 0.7$) over AWGN, Rician ($K = 6$ dB) and Rayleigh channels.

Figure 5.22 shows the effect of K on P_b . The results were obtained for CE-DCT- and CE-FFT-OFDM systems with $M = 4$ and $h = 0.5$ for various values of K . It is noted that the P_b decreases as the value of K increases. It is well known that as $K \rightarrow \infty$, Rician density approaches that of Gaussian density.

5.7 CE-DCT- and DCT-OFDM Systems with TWTA Amplifier

Figure 5.23 compares the P_b performances of CE-DCT-OFDM system with 4-PAM mapper with IBO = 0 dB and DCT-OFDM system with QPSK mapper with IBO = 0 dB and 4 dB for TWTA amplifier model. It is observed that CE-DCT-OFDM system is far superior compared to DCT-OFDM system. The DCT-OFDM system with 0 dB IBO has an error floor at a bit error rate of nearly 3.20×10^{-2} . At BER equal to 10^{-3} , the IBO required for DCT-OFDM system is more than 4 dB. However, the CE-DCT-OFDM system with ($h = 0.4$) achieves this BER = 10^{-3} with 0 dB IBO.

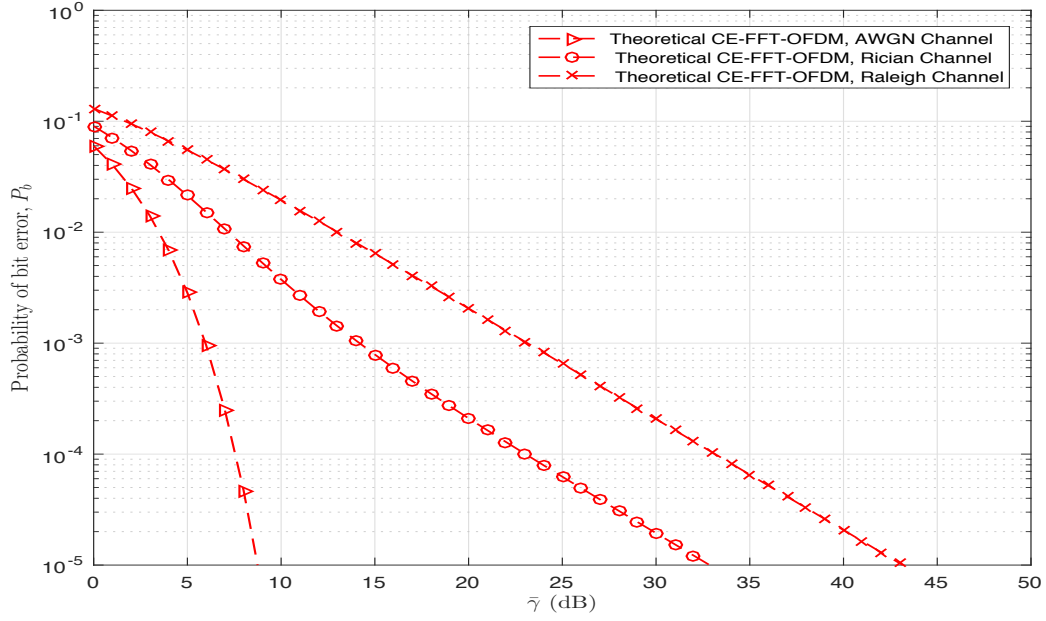


Figure 5.21: Comparison of probability of bit error performances of CE-FFT-OFDM system (2-PAM mapper, $h = 0.7$) over AWGN, Rician ($K = 6$ dB) and Rayleigh channels.

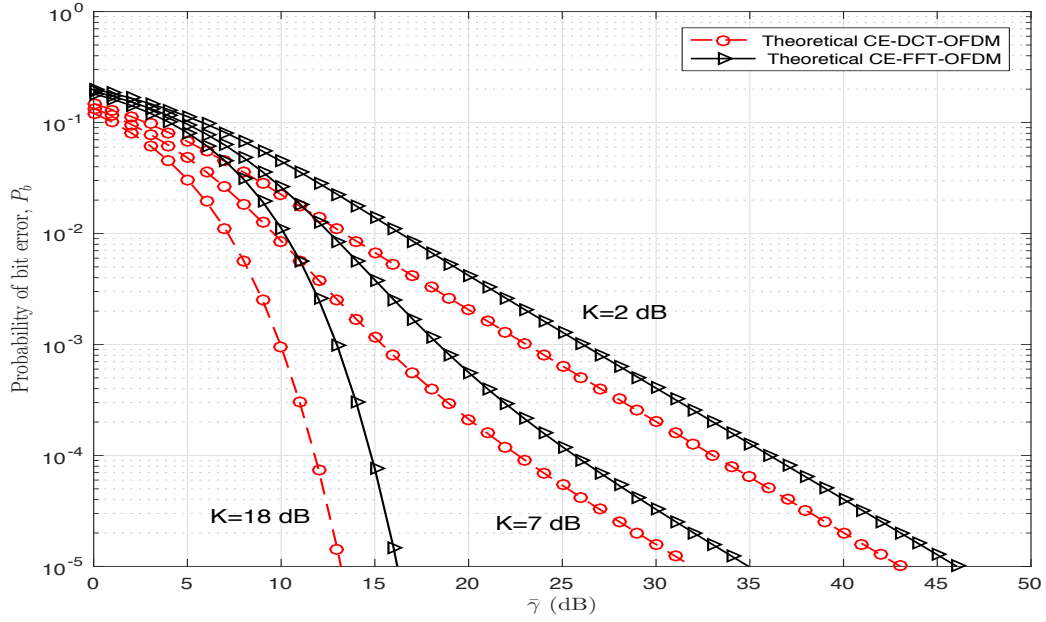


Figure 5.22: Probability of bit error performances of CE-DCT- and CE-FFT-OFDM systems as function of Rice factor.

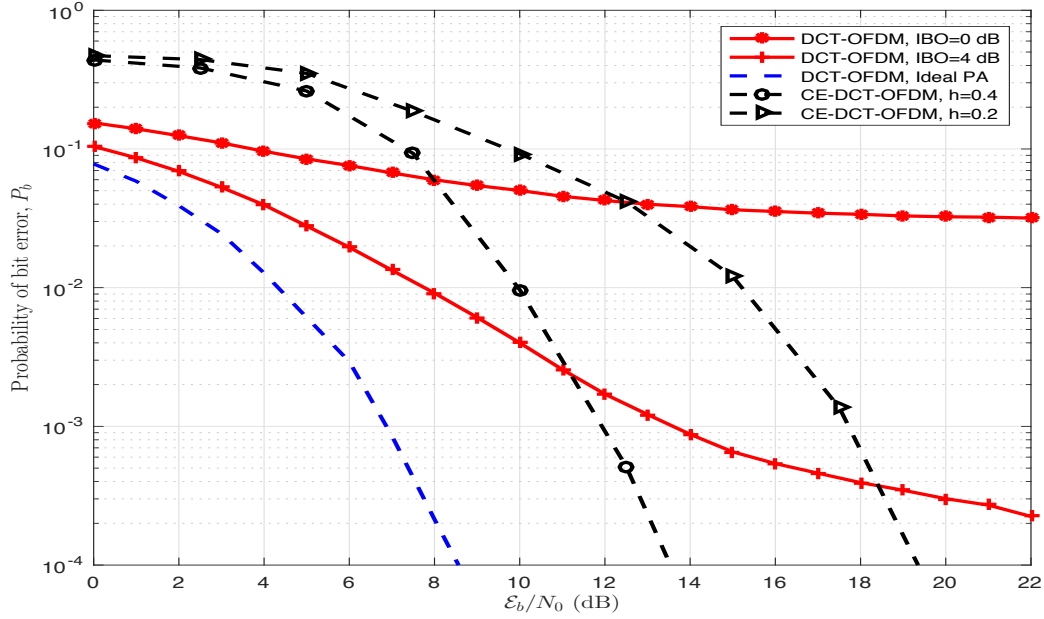


Figure 5.23: Probability of bit error performances of CE-DCT- and of DCT-OFDM systems as a function of IBO for TWTA model.

5.7.1 Comparison of BER of OFDM System with FM, PM and CPM

In this Section, comparison of probability of bit error performances of DCT- and FFT-OFDM systems with PM, FM and CPM are presented as a function of SNR. In these systems, 4-PAM mapper is used with $h_p = 0.6$, $h_f = 0.6$ and $h = 0.6$ for PM, FM, and CPM, respectively. Figures 5.24 and 5.25, respectively, depict these results for DCT- and FFT-OFDM systems over AWGN, Rician and Rayleigh channels. It is noted that DCT- and FFT-OFDM systems with CPM perform better than the corresponding systems with FM and PM. For example at $P_b = 10^{-5}$ over AWGN channel, E_b/N_0 required for CPM system is nearly 6.9 dB and 2.2 dB less than E_b/N_0 required for PM and FM systems, respectively.

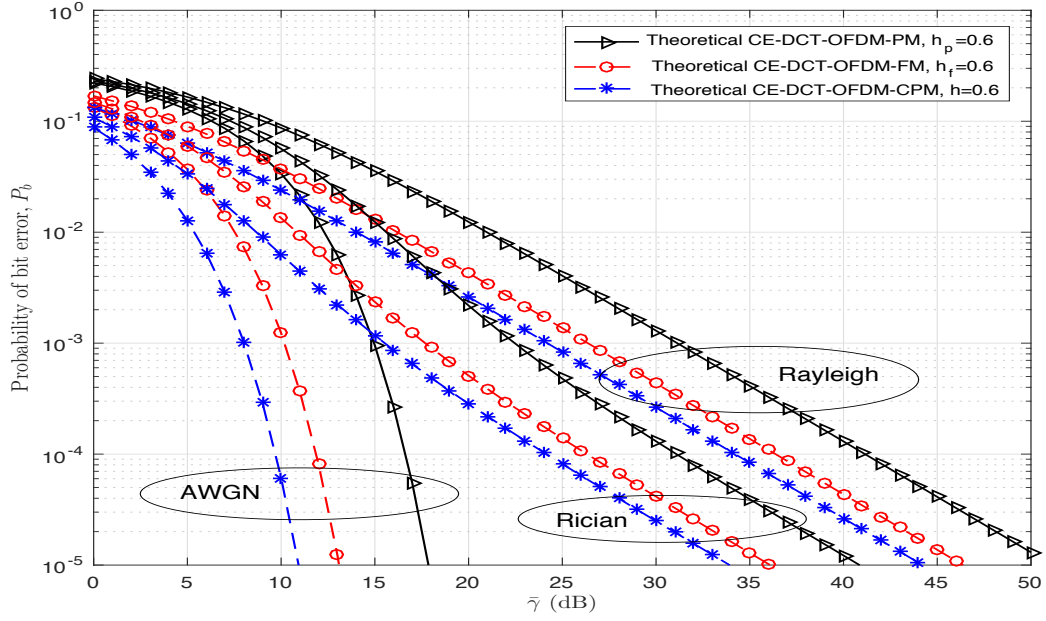


Figure 5.24: Comparison of probability of bit error performances of DCT-OFDM system (4-PAM) with PM ($h_p = 0.6$), FM ($h_f = 0.6$) and CPM ($h = 0.6$) over AWGN, Rician ($K = 6$ dB) and Rayleigh channels.

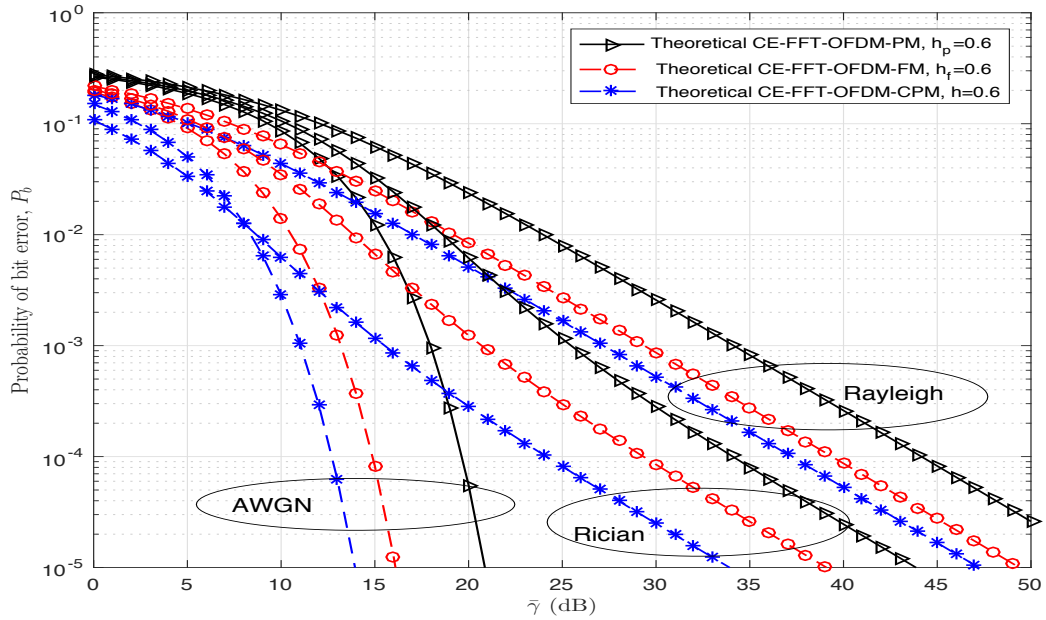


Figure 5.25: Comparison of probability of bit error performances of FFT-OFDM system (4-PAM) with PM ($h_p = 0.6$), FM ($h_f = 0.6$) and CPM ($h = 0.6$) over AWGN, Rician ($K = 6$ dB) and Rayleigh channels.

5.8 Conclusion

In this Chapter, CPM is introduced in DCT- and FFT-OFDM systems. Structures of transmitter and receiver are given and BER analyses are presented over AWGN and fading channels. Closed-form expressions for BER are obtained and illustrated. A comparison of DCT- and FFT-OFDM systems with PM, FM, and CPM in terms of BER is presented. It is shown that CPM can be gainfully employed to achieve better BER compared to FM and PM in OFDM system.

Chapter 6

Constant Envelope DCT- and FFT-OFDM Systems with CPCM⁷

6.1 Introduction

Continuous Phase Chirp Modulation (CPCM) is used for data communication due to its attractive properties such as: anti-eavesdropping, anti-interference capability and low-Doppler sensitivity. It produces a transmitted signal bandwidth much greater than the bandwidth of the information signal being sent. CPCM can be used in an OFDM system to correlate data samples at the transmitter and this correlation can be exploited to achieve better bit error rate (BER) performance of the system. It is noted that CPCM be viewed as a subclass of CPM and produce constant envelope signals, which are attractive in OFDM systems with HPA in them [116, 117]. In this Chapter, OFDM system with CPCM is considered. Both DCT- and FFT- OFDM systems are considered and their BER performances are analysed over AWGN and fading channels. Closed-form expressions for BER over these channels are derived and illustrated. Effective bandwidth expressions of these systems are developed and presented.

7. Rayan H. Alsisi and Raveendra K. Rao,” Constant Envelope DCT- and FFT-based OFDM Systems with Continuous Phase Chirp Modulation over Fading Channels,” 2017 2nd International conferences on Information Technology, Information Systems and Electrical Engineering (ICITISEE), Yogyakarta, Indonesia, November 2017, pp.211-216.

6.2 Signals in DCT- and FFT-OFDM Systems with CPCM

The general expression for OFDM-CPCM signal can be written as:

$$s(t) = A_c \cos(2\pi f_c t + \phi(t) + \phi_0), \quad 0 \leq t \leq T \quad (6.1)$$

where A_c and f_c are the carrier amplitude and frequency, ϕ_0 is the starting phase assumed to be zero without loss of generality, and $\phi(t)$ is the information carrying phase given by:

$$\phi(t) = x(k)g(t - kT_s) + \pi q \sum_{i=0}^{k-1} x(i), \quad kT_s \leq t \leq (k+1)T_s \quad (6.2)$$

where the data symbol duration is T_s , and $x(k), k = 0, \dots, N-1$, are the real-valued OFDM signal carrying the message signal. The phase function $g(t)$ in (6.2) is given by

$$g(t) = \begin{cases} 0 & t \leq 0, t > T_s \\ 2\pi \int_0^t f(\tau) d\tau, & 0 \leq t \leq T_s \\ \pi q = \pi(h - w) & t = T_s \end{cases} \quad (6.3)$$

where $f(t)$ for chirp signalling is given by:

$$f(t) = \begin{cases} 0 & t \leq 0, t > T_s \\ \frac{h}{2T_s} - \frac{w}{T_s^2} t & 0 \leq t \leq T_s \end{cases} \quad (6.4)$$

Using (6.4) in (6.3), the phase function can be written as:

$$g(t) = \begin{cases} 0 & t \leq 0, t > T_s \\ \pi \left[h \frac{t}{T_s} - w \left(\frac{t}{T_s} \right)^2 \right] & 0 \leq t \leq T_s \\ \pi q = \pi(h - w) & t = T_s \end{cases} \quad (6.5)$$

In (6.5) h and w represent the peak-to-peak frequency deviation divided by $1/T_s$, and the frequency sweep width divided by $1/T_s$, respectively. It is noted that h and w are dimensionless parameters. Since $q = (h - w)$, the pair (h, w) is chosen to be the

independent signal modulation parameters. In Figure 6.1 and 6.2 $f(t)$ and $g(t)$ are shown for arbitrary values of (h, w) . The phase during $kT_s \leq t \leq (k+1)T_s$ is a function of not only $x(k)$, but also is a function of $x(k-1), x(k-2), \dots, x(0)$. The quantity $\pi q \sum_{i=0}^{k-1} x(i)$ in (6.2) is the accumulated phase and phase is always modulo 2π .

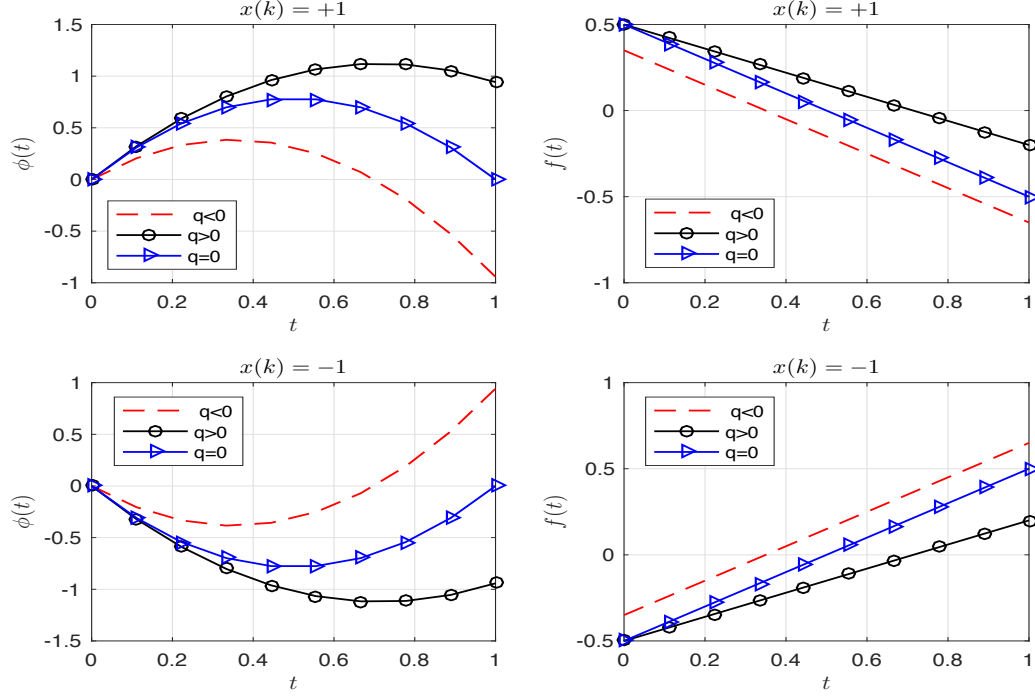


Figure 6.1: Phase and frequency as a function of time for $x(k) = \pm 1$

In the case of an FFT-OFDM system, real-valued message signal ($x_{FFT}(k)$) is obtained by using conjugate symmetric data vector, $[0, X(0), \dots, X(N-1), 0, X^*(N-1), \dots, X^*(0)]$, as input to the IFFT block. Unlike in FFT-OFDM system, in DCT-OFDM system the modulating signal ($x_{DCT}(k)$) is always real valued; when MPAM mapper is used in the system.

6.3 OFDM System with CPCM: Transmitter

The block diagram of transmitter is shown in Figure 6.2. As explained in Chapter 5, a block of N data symbols goes through an S/P converter. The parallel data from this block is fed to an MPAM mapper to obtain a vector $[X(0), X(1), \dots, X(N-1)]^T$ of N elements which are used to generate signal $x(k)$. After passing this signal through

P/S converter, the signal is fed to CPCM modulator to generate the modulated signal $s(t)$. This signal is fed to HPA whose its output is transmitted over the communication channel.

Using (6.2) in (6.1), the signals in FFT- and DCT-OFDM systems with CPCM can be written as:

$$s(t) = A_c \cos(2\pi f_c t + \phi_{FFT}(t)) \quad (6.6)$$

and

$$s(t) = A_c \cos(2\pi f_c t + \phi_{DCT}(t)) \quad (6.7)$$

The average power and energy of $s(t)$ are $A_c^2/2$ and $A_c^2 T/2$. For $N \log_2(M)$ bits per OFDM symbol, the average bit energy is $E_b = A_c^2 T/2N \log_2(M)$. and the variance of the data symbols, σ_s^2 , is $((M^2 - 1)/3)$. The bandwidth of $s(t)$ can be found using the approach used for CPM in Chapter 5. For both FFT- and DCT-OFDM systems, the bandwidth is given by $\left[2\sqrt{\frac{h^2}{4} - \frac{hw}{4} + \frac{w^2}{3}}\right] W$ Hz, where W is the bandwidth of message signal. For FFT and DCT-OFDM systems the message bandwidths (W) are N/T Hz and $N/2T$ Hz, respectively.

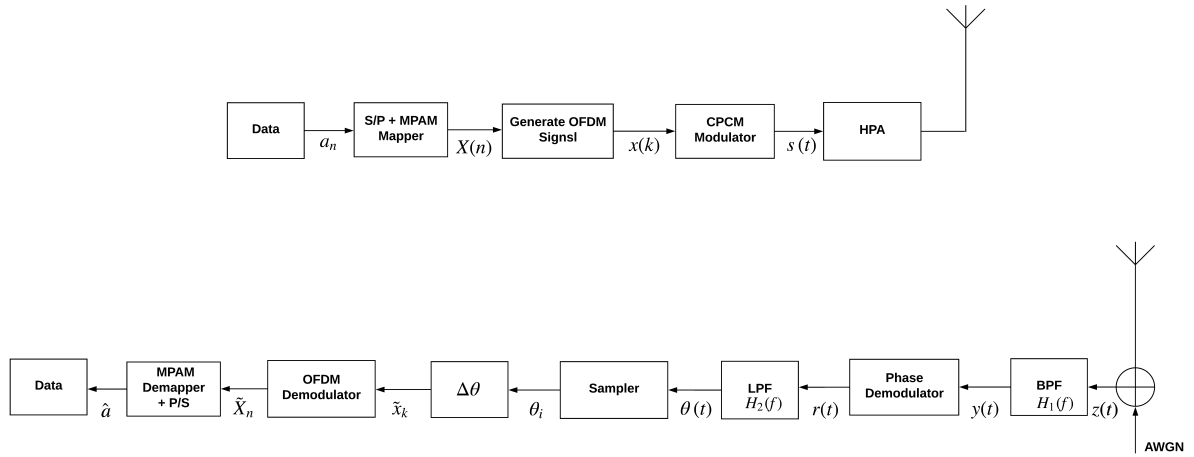


Figure 6.2: Block diagram of CE-OFDM system with CPCM

6.4 OFDM Sytem with CPCMC: Receiver

The receiver structure is shown in Figure 6.2 and consists of cascade of BPF, PM demodulator, LPF, sampler, phase difference, OFDM demodulator, MPAM demapper, and P/S converter blocks. The received signal $(s(t) + w(t))$ is passed through a bandpass filter $H_1(f)$ with characteristic as shown in Figure 3.2, where B is the bandwidth of $s(t)$. The noise $w(t)$ is modelled as AWGN with zero mean and power spectral density of $N_0/2 \text{ Watts/Hz}$. The input to the PM demodulator can be written as $y(t) = s(t) + n(t), 0 \leq t \leq T$, where $n(t)$ represents the output of the BPF due to the input $w(t)$. The output of phase demodulator is fed to LPF and then to sampler to obtain JN samples of the phase signal, where J is the oversampling factor. The output of sampler is fed to phase difference block to get the phase difference of neighbor samples. OFDM demodulator is then used followed by the MPAM demapper and P/S converter to get an estimate of transmitted data.

6.4.1 Analysis over AWGN Channel

The signal $z(t)$ is passed through an ideal bandpass filter whose output can be written as:

$$y(t) = s(t) + n(t) \quad (6.8)$$

where $n(t)$ can be represented in terms of in-phase and quadrature components. Following the steps used in Chapter 5, the power spectral density of the noise at the output of LPF is given by [110, 111]:

$$S(f) = \begin{cases} N_0/A_c^2, & |f| \leq W \\ 0, & \text{otherwise} \end{cases} \quad (6.9)$$

and its average power is

$$\int_{-W}^W \frac{N_0}{A_c^2} df = \frac{2WN_0}{A_c^2} \quad (6.10)$$

The signal from the LPF is then passed to the a sampler to obtain samples of $\theta(t)$ given by:

$$\theta[i] = \theta(t) \big|_{t=\frac{i}{J}T_s}, \quad i = 0, \dots, JN - 1 \quad (6.11)$$

where J denotes the oversampling factor. The phase difference between adjacent samples is given by:

$$\Delta\tilde{\theta} = \tilde{\theta}_{i+1} - \tilde{\theta}_i \quad (6.12)$$

Equation (6.12) can be written as:

$$\Delta\tilde{\theta} = (\phi_{i+1} - \phi_i) + (\Phi_{i+1} - \Phi_i) \quad (6.13)$$

The signal $\tilde{x}(k)$ can be shown to be given by:

$$\tilde{x}(k) = \frac{1}{(h-w)\pi} \sum_{J=0}^{J-1} \left(\phi_{(Jk+1)+l} - \phi_{(Jk)+l} \right) + \left(\Phi_{(Jk+1)+l} - \Phi_{(Jk)+l} \right) \quad (6.14)$$

Simplifying (6.14), we get:

$$\tilde{x}(k) = x(k) + \frac{1}{(h-w)\pi} \left(\Phi_{J(k+1)} - \Phi_{(Jk)} \right) \quad (6.15)$$

which is fed to the OFDM demodulator to obtain $\tilde{X}(n)$. That is

$$\tilde{X}(n) = X(n)/\sqrt{\sigma_s^2} + N(n); \quad n = 0, 1, \dots, N-1 \quad (6.16)$$

where

$$N(n) = \frac{1}{(h-w)\pi} \sum_{k=0}^{N-1} \left(\Phi_{n,J(k+1)} - \Phi_{n,Jk} \right) \varphi_k \quad (6.17)$$

By observing that $\tilde{X}(n)$ are Gaussian its mean and variance are given by:

$$E[\tilde{X}(n)] = E[X(n)/\sqrt{\sigma_s^2} + N(n)] = E[X(n)/\sqrt{\sigma_s^2}] \quad (6.18)$$

with

$$Var[\tilde{X}(n)] = \sigma^2 = \frac{4WN_0}{(h-w)^2\pi^2 A_c^2}; \quad n = 0, 1, \dots, N-1 \quad (6.19)$$

The BER performances of the DCT and FFT-OFDM systems with CPCPM can be determined by feeding the output of OFDM demodulator to the MPAM demapper. That

is,

$$\tilde{X}(n) = \frac{X(n)}{\sqrt{\sigma_s^2}} + N(n)$$

where $X(n) \in \{\pm 1, \pm 3, \dots, \pm(M-1)\}$, $\sigma_s^2 = ((M^2 - 1)/3)$, and $N(n)$ are a zero mean Gaussian random variables with variance σ^2 given by (6.19). The symbol error probability for the j^{th} MPAM mapper, following the steps given in Section 3.4.3, can be written as:

$$P_s = 2 \left(\frac{M-1}{M} \right) Q \left(\sqrt{(h-w)^2 \pi^2 \frac{A_c^2}{4W N_0 \sigma_s^2}} \right) \quad (6.20)$$

Since, $W = N/T$ and $N/2T$ for FFT- and DCT-OFDM signals, respectively, the symbol error probabilities for CE-FFT- and CE-DCT-OFDM system are given by:

$$P_{s_{FFT}} = 2 \left(\frac{M-1}{M} \right) Q \left(\sqrt{(h-w)^2 \pi^2 \frac{3 \log_2(M) E_b}{2(M^2 - 1) N_0}} \right) \quad (6.21)$$

and

$$P_{s_{DCT}} = 2 \left(\frac{M-1}{M} \right) Q \left(\sqrt{(h-w)^2 \pi^2 \frac{3 \log_2(M) E_b}{(M^2 - 1) N_0}} \right) \quad (6.22)$$

In the receiver, there are N demappers and each has the same symbol error probability given by (6.21) and (6.22). The average of N symbol error probabilities is simply given by (6.21) and (6.22). The symbol error rate is related BER and is given by

$$P_b \approx \frac{P_s}{\log_2(M)} \quad (6.23)$$

Using (6.23) and symbol error rate expressions, the BER expressions for CE-FFT- and CE-DCT-OFDM systems with CPCM are given by:

$$P_{b_{FFT}} \approx 2 \left(\frac{M-1}{M \log_2(M)} \right) Q \left(\sqrt{(h-w)^2 \pi^2 \frac{3 \log_2(M) E_b}{2(M^2 - 1) N_0}} \right) \quad (6.24)$$

and

$$P_{b_{DCT}} \approx 2 \left(\frac{M-1}{M \log_2(M)} \right) Q \left(\sqrt{(h-w)^2 \pi^2 \frac{3 \log_2(M) E_b}{(M^2 - 1) N_0}} \right) \quad (6.25)$$

The BER for both systems are function of (h, w) , modulation parameters, E_b/N_0 , signal-to-noise ratio, and M , the number of amplitude levels in PAM mapper.

6.5 Performance over Fading Channels

The performances of DCT- and FFT-OFDM systems with CPCM over Rayleigh and Rician fading channels can be derived following steps given in Chapter 3, Section 3.5.2. A generalized expression for $P_b(\gamma)$ over fading channels can be written as

$$P_b(\gamma) = 2 \left(\frac{M-1}{M \log_2(M)} \right) Q \left(\sqrt{I(h-w)^2 \pi^2 \alpha^2 \frac{E_b}{N_0}} \right) \\ = 2 \left(\frac{M-1}{M \log_2(M)} \right) Q \left(\sqrt{I(h-w)^2 \pi^2 \gamma} \right) \quad (6.26)$$

where $I = 3 \frac{\log_2(M)}{M^2-1}$, and $\frac{3}{2} \frac{\log_2(M)}{M^2-1}$ for DCT- and FFT-OFDM systems with CPCM, respectively.

BER Expressions for Rayleigh Fading Channel

Using (6.26) and averaging over the density of γ , given by (3.51), the bit error rate for Rayleigh fading channel is given by:

$$P_b = \left(\frac{M-1}{M \log_2(M)} \right) \left[1 - \sqrt{\frac{1}{1 + \frac{1}{I \pi^2 (h-w)^2 \bar{\gamma}/2}}} \right] \quad (6.27)$$

The BER given by (6.27) is a function of (h, w) , modulation parameters, M , and $\bar{\gamma}$, average SNR per bit of the received signal.

BER Performance over Rician Fading Channel

Using (6.26) and averaging over the density of γ , given by (3.55), the bit error rate expression for Rician fading channel is given by:

$$P_b = \frac{2}{\pi} \left(\frac{M-1}{M \log_2(M)} \right) \int_0^{\pi/2} \frac{(1+K) \sin^2(\theta)}{(1+K) \sin^2(\theta) + I \pi^2 (h-w)^2 \bar{\gamma}/2} \\ \exp \left[-\frac{K I \pi^2 (h-w)^2 \bar{\gamma}/2}{(1+K) \sin^2(\theta) + I \pi^2 (h-w)^2 \bar{\gamma}/2} \right] d\theta \quad (6.28)$$

As (6.28) shows, the BER is a function of (h, w) , modulation parameters, M , K , Rice factor, and $\bar{\gamma}$, average SNR per bit of the received signal.

6.6 Numerical Results and Discussion

The numerical results of probability of bit error performances of DCT- and FFT-OFDM systems with CPCM are presented and discussed.

6.6.1 Performance over AWGN Channel

The BER expressions given by (6.24) and (6.25) are functions of (h, w) , modulation parameters, E_b/N_0 , and M . In order to understand the effect of modulation parameters on bit error rate, P_b vs. E_b/N_0 are plotted as a function of (h, w) , in Figure 6.3, 6.4, and 6.5 for both DCT- and FFT-OFDM systems with CPCM, for $M = 2, 4$, and 8. Tables 6.1, 6.2 and 6.3 summarize E_b/N_0 required at $P_b = 10^{-5}$ as a function of $(h, 0.15)$ for these systems.

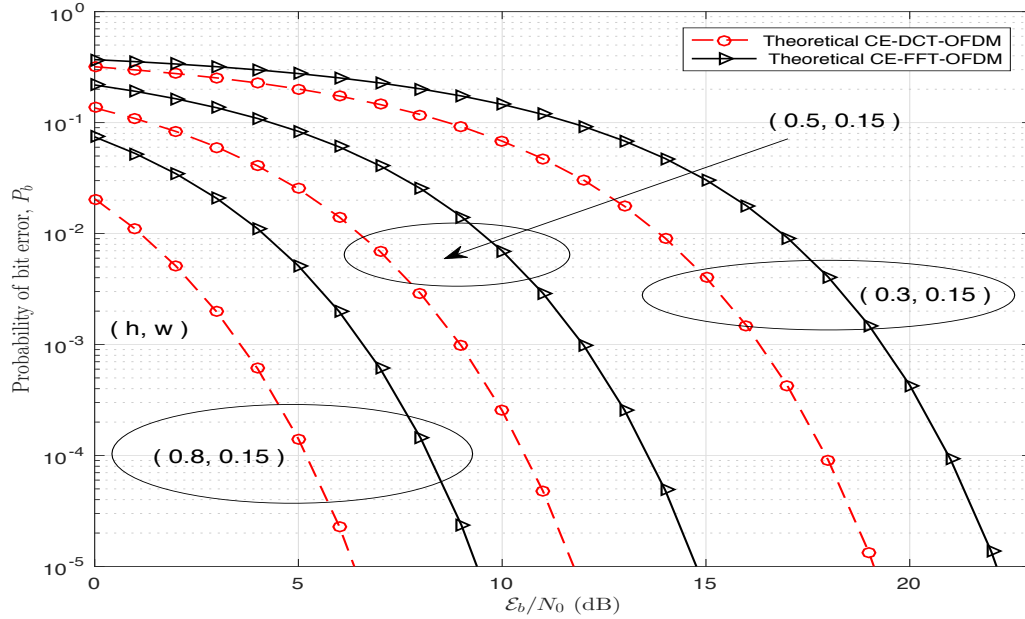


Figure 6.3: Probability of bit error performances of CE-DCT- and CE-FFT-OFDM systems (2-PAM mapper) as a function of $(h, 0.15)$ over AWGN channel.

Table 6.1: Comparison of CE-DCT- and CE-FFT-OFDM systems (2-PAM mapper) at $P_b = 10^{-5}$ as a function of $(h, 0.15)$

(h, w)	CE-DCT-OFDM	CE-FFT-OFDM
	E_b/N_0 (dB)	E_b/N_0 (dB)
(0.9, 0.15)	5.154	8.164
(0.8, 0.15)	6.397	9.407
(0.7, 0.15)	7.848	10.858
(0.6, 0.15)	9.591	12.601
(0.5, 0.15)	11.774	14.784
(0.4, 0.15)	14.696	17.707

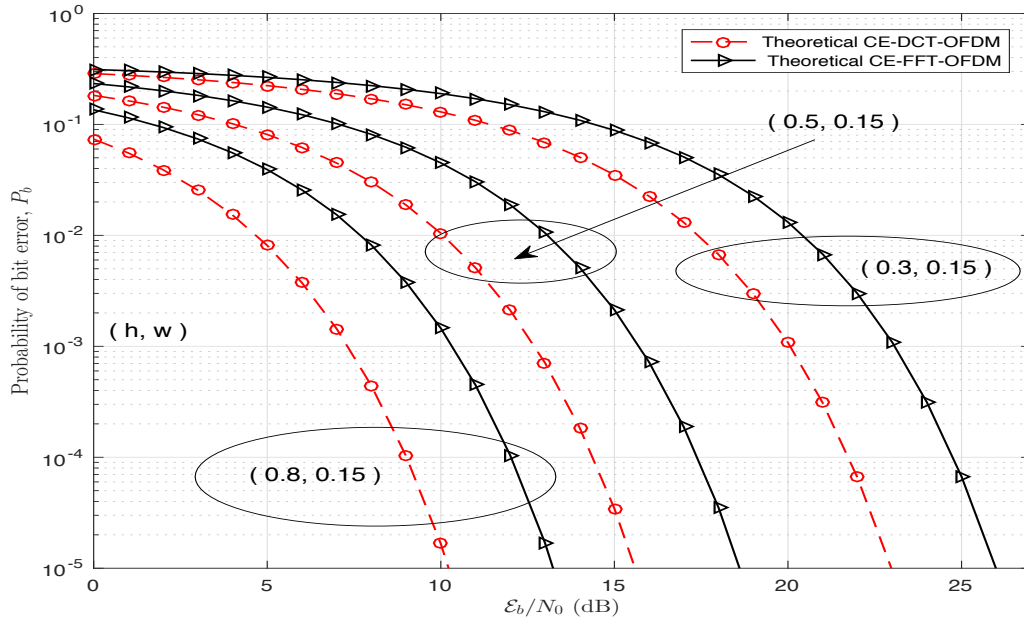


Figure 6.4: Probability of bit error performances of CE-DCT- and CE-FFT-OFDM systems (4-PAM mapper) as a function of $(h, 0.15)$ over AWGN channel.

In Figures 6.6, 6.7 and 6.8, P_b for both systems ($M = 2, 4$, and 8) are plotted as a function of $(1, w)$. Tables 6.4, 6.5 and 6.6 summarize E_b/N_0 required at $P_b = 10^{-5}$ as a function of $(1, w)$. It is evident from these figures that P_b decreases as h increases for fixed value of w , and also P_b increases as w increases for fixed value of h . Also, it is observed that CE-DCT-OFDM system performs better than corresponding CE-FFT-OFDM system by nearly 3 dB.

It can also be observed that for both CE-OFDM systems (8-PAM mapper, $(0.6, 0.15)$), at $P_b = 10^{-5}$, E_b/N_0 required are 4.351 and 8.198 dB more than that required for cor-

Table 6.2: Comparison of CE-DCT- and CE-FFT-OFDM systems (4-PAM mapper) at $P_b = 10^{-5}$ as a function of $(h, 0.15)$

(h, w)	CE-DCT-OFDM	CE-FFT-OFDM
	E_b/N_0 (dB)	E_b/N_0 (dB)
(0.9, 0.15)	9.001	12.011
(0.8, 0.15)	10.244	13.254
(0.7, 0.15)	11.695	14.705
(0.6, 0.15)	13.438	16.448
(0.5, 0.15)	15.621	18.631
(0.4, 0.15)	18.543	21.553

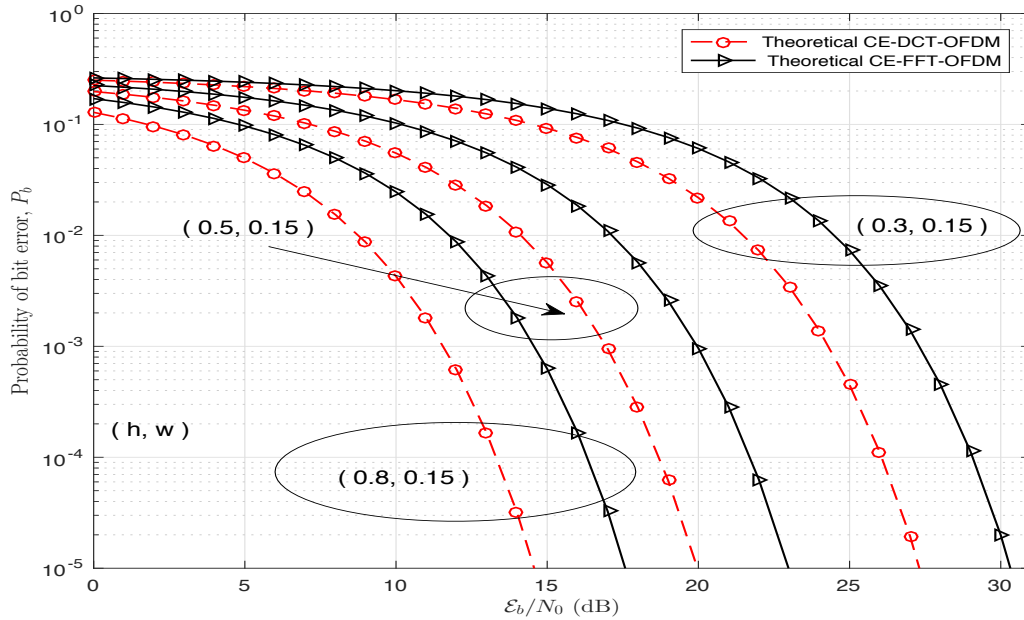


Figure 6.5: Probability of bit error performances of CE-DCT- and CE-FFT-OFDM systems (8-PAM mapper) as a function of $(h, 0.15)$ over AWGN channel.

responding systems with 4-PAM and 2-PAM mappers, respectively. However, OFDM systems with 8-PAM mapper are more spectrally efficient than systems with 4-PAM and 2-PAM mappers.

It is also apparent that CE-DCT-OFDM system (8-PAM mapper, and $(1, 0.3)$) outperforms a corresponding system (4-PAM mapper, and $(1, 0.9)$) by nearly 8.7 dB, at BER = 10^{-5} .

Figure 6.9 compares simulation and theoretical results of P_b for CE-DCT-OFDM system (4-PAM mapper) with $N = 64$ subcarriers, for two sets of modulation parameters, $(0.7,$

Table 6.3: Comparison of CE-DCT- and CE-FFT-OFDM systems (8-PAM mapper) at $P_b = 10^{-5}$ as a function of $(h, 0.15)$

(h, w)	CE-DCT-OFDM	CE-FFT-OFDM
	E_b/N_0 (dB)	E_b/N_0 (dB)
(0.9, 0.15)	13.353	16.363
(0.8, 0.15)	14.596	17.606
(0.7, 0.15)	16.047	19.057
(0.6, 0.15)	17.789	20.800
(0.5, 0.15)	19.973	22.983
(0.4, 0.15)	22.8895	25.906

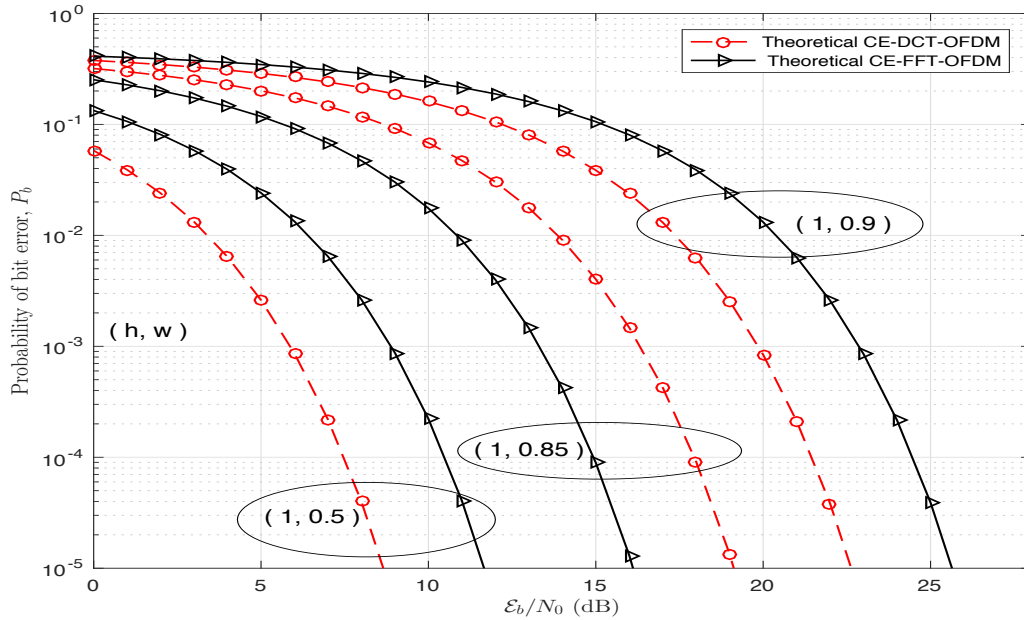


Figure 6.6: Probability of bit error performances of CE-DCT- and CE-FFT-OFDM systems (2-PAM mapper) as a function of $(1, w)$ over AWGN channel.

0.25) and (0.5, 0.2). It is noted that for (0.5, 0.2), simulation result is nearly the same as theoretical result and for (0.7, 0.25), the theoretical BER is not as accurate as simulation result but still is within 2 dB of the former. It is observed that for smaller values of h and w theoretical results are nearly the same as that of simulations, whereas for larger values of modulation parameters simulation results are not as accurate as theoretical results.

Table 6.4: Comparison of CE-DCT- and CE-FFT-OFDM systems (2-PAM mapper) at $P_b = 10^{-5}$ as a function of $(1, w)$

(h, w)	CE-DCT-OFDM	CE-FFT-OFDM
	E_b/N_0 (dB)	E_b/N_0 (dB)
(1, 0.3)	5.753	8.764
(1, 0.5)	8.676	11.686
(1, 0.6)	10.614	13.624
(1, 0.7)	13.113	16.123
(1, 0.8)	16.635	19.645
(1, 0.9)	22.655	25.666

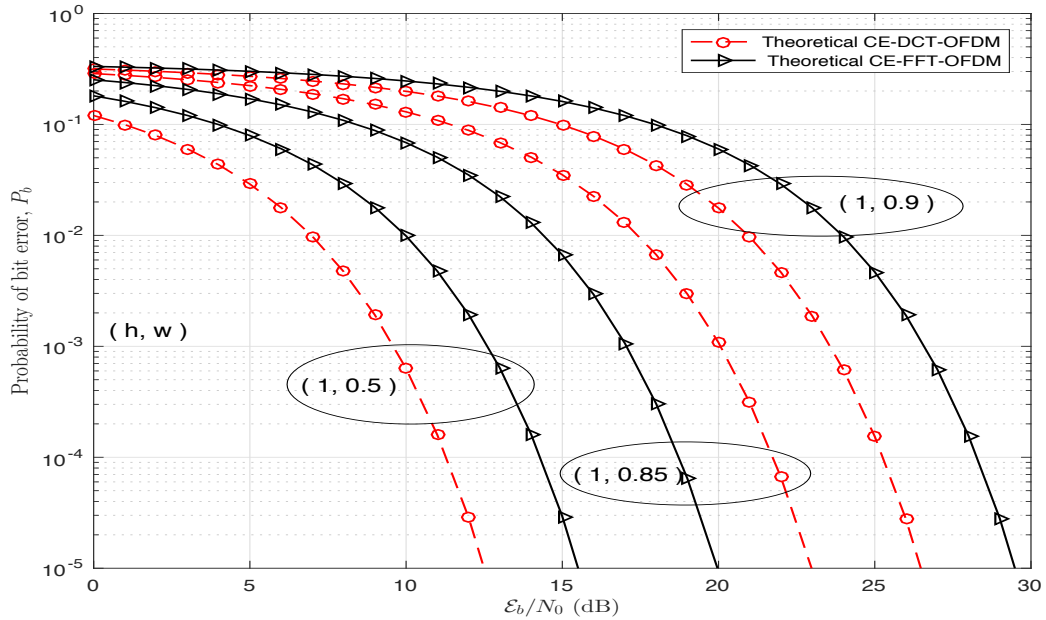


Figure 6.7: Probability of bit error performances of CE-DCT- and CE-FFT-OFDM systems (4-PAM mapper) as a function of $(1, w)$ over AWGN channel.

6.6.2 Performance over Fading Channels

The expression for P_b over Raleigh fading channel is given by (6.27). Figures 6.10, 6.11, and 6.12 show P_b of DCT- and FFT-OFDM systems with CPCPM for $M = 2, 4$, and 8, respectively, as a function of (h, w) . It is noted that, the presence of signal fading requires a large increases in E_b/N_0 to achieve same levels of BER that can be achieved over AWGN channel. In order to achieve BER equal to 10^{-5} , CE-DCT-OFDM system ($h = 0.9, w = 0.15, M = 2$) requires $E_b/N_0 = 5.154$ dB on an AWGN channel, whereas over Rayleigh channel, to achieve the same BER an average SNR of 39.143 dB is required.

Table 6.5: Comparison of CE-DCT- and CE-FFT-OFDM systems (4-PAM mapper) at $P_b = 10^{-5}$ as a function of $(1, w)$

(h, w)	CE-DCT-OFDM	CE-FFT-OFDM
	E_b/N_0 (dB)	E_b/N_0 (dB)
(1, 0.3)	9.599	12.610
(1, 0.5)	12.522	15.533
(1, 0.6)	14.461	17.471
(1, 0.7)	16.959	19.969
(1, 0.8)	20.481	23.491
(1, 0.9)	26.502	29.512

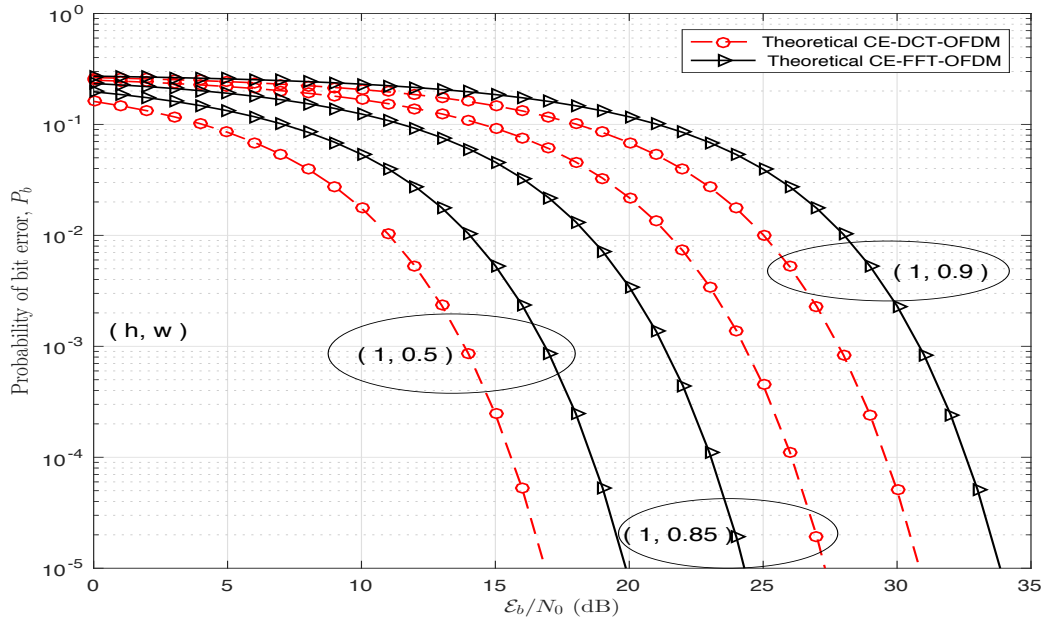


Figure 6.8: Probability of bit error performances of CE-DCT- and CE-FFT-OFDM systems (8-PAM mapper) as a function of $(1, w)$ over AWGN channel.

The expression for BER for Rician fading channel is given by (6.28). The BER is not only a function of (h, w) , M and $\bar{\gamma}$, but also depends on K , Rice factor. P_b vs. $\bar{\gamma}$ for $M = 2, 4$ and 8 for DCT- and FFT-OFDM systems with CPCM for $K = 6$ dB are illustrated in Figures 6.13, 6.14 and 6.15, respectively, as a function of (h, w) .

In order to compare probability of bit error performances of CE-OFDM systems over AWGN, Rician and Rayleigh channels, P_b vs. $\bar{\gamma}$ are plotted for $M = 2$ and $(0.9, 0.15)$ in Figures 6.16 and 6.17. Tables 6.6 and 6.7 summarize average SNR required at $P_b = 10^{-3}, 10^{-4}$ and 10^{-5} for CE-DCT- and CE-FFT-OFDM systems over AWGN, Rician

Table 6.6: Comparison of CE-DCT- and CE-FFT-OFDM systems (8-PAM mapper) at $P_b = 10^{-5}$ as a function of $(1, w)$

(h, w)	CE-DCT-OFDM	CE-FFT-OFDM
	E_b/N_0 (dB)	E_b/N_0 (dB)
(1, 0.3)	13.952	16.963
(1, 0.5)	16.875	19.885
(1, 0.6)	18.813	21.823
(1, 0.7)	21.311	24.322
(1, 0.8)	24.834	27.844
(1, 0.9)	30.854	33.865

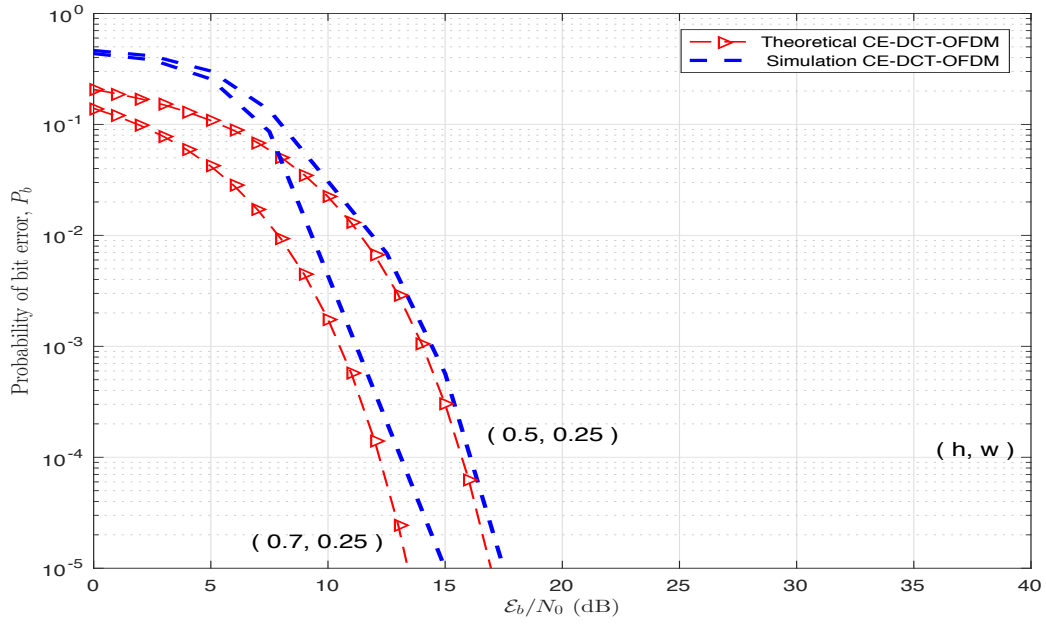


Figure 6.9: Comparison of analytical and simulation results of BER for CE-DCT-OFDM system (4-PAM mapper) over AWGN channel.

and Rayleigh channels, respectively.

Table 6.7: Comparison of CE-DCT-OFDM system ($M = 2, (0.9, 0.15)$) over AWGN, Rician ($K = 6$ dB) and Rayleigh channels

P_b	Average SNR dB		
	AWGN	Rician	Raleigh
10^{-3}	2.356	10.405	19.313
10^{-4}	3.964	19.121	29.232
10^{-5}	5.154	29.126	39.143

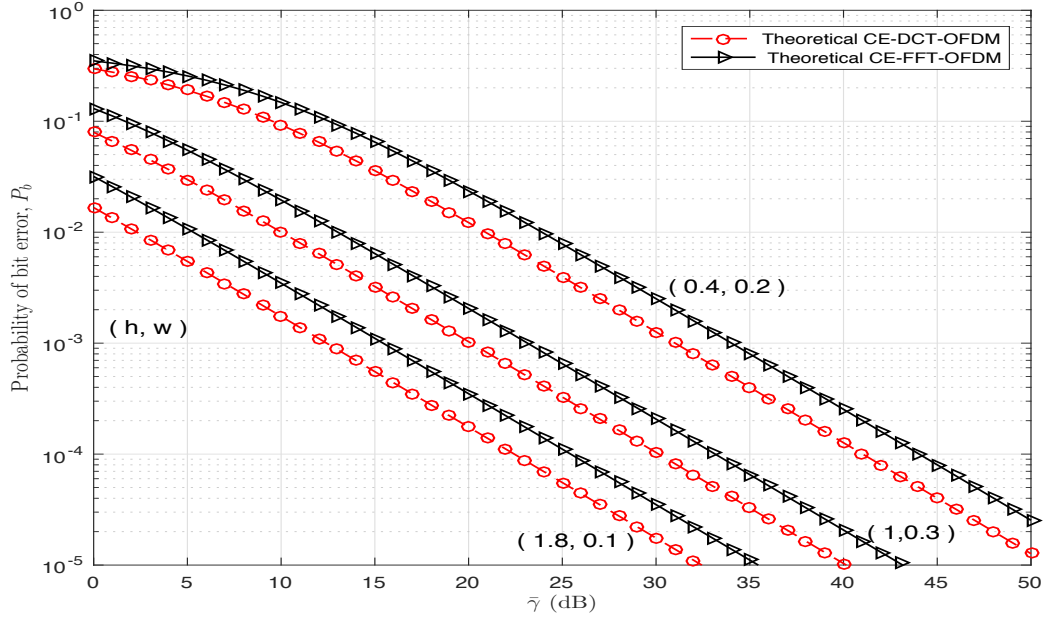


Figure 6.10: Probability of bit error performances of CE-DCT- and CE-FFT-OFDM systems (2-PAM mapper) over Rayleigh fading channel.

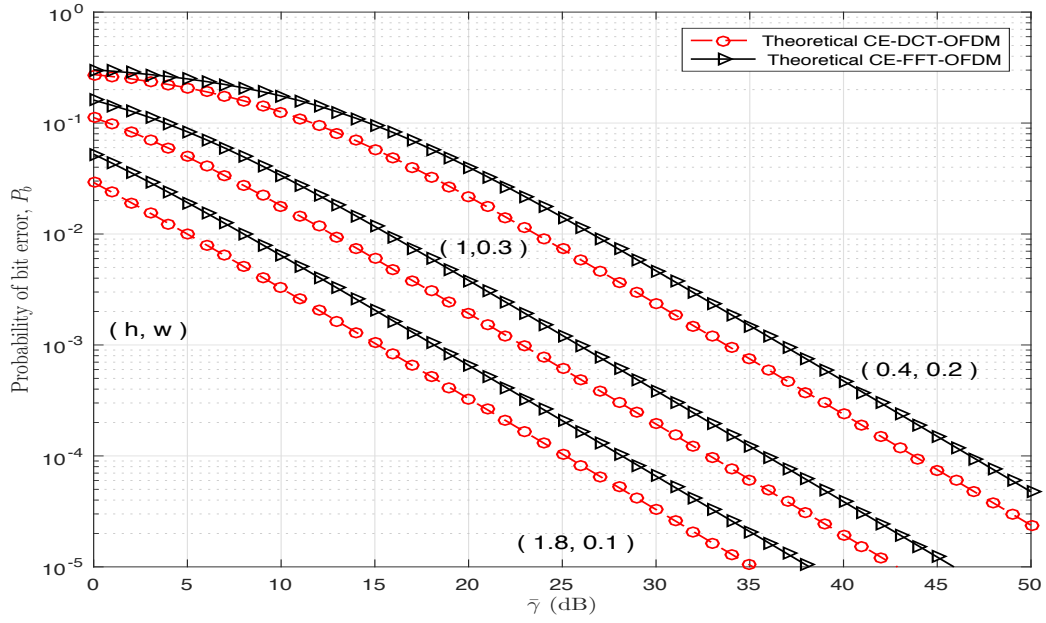


Figure 6.11: Probability of bit error performances of CE-DCT- and CE-FFT-OFDM systems (4-PAM mapper) over Rayleigh fading channel.

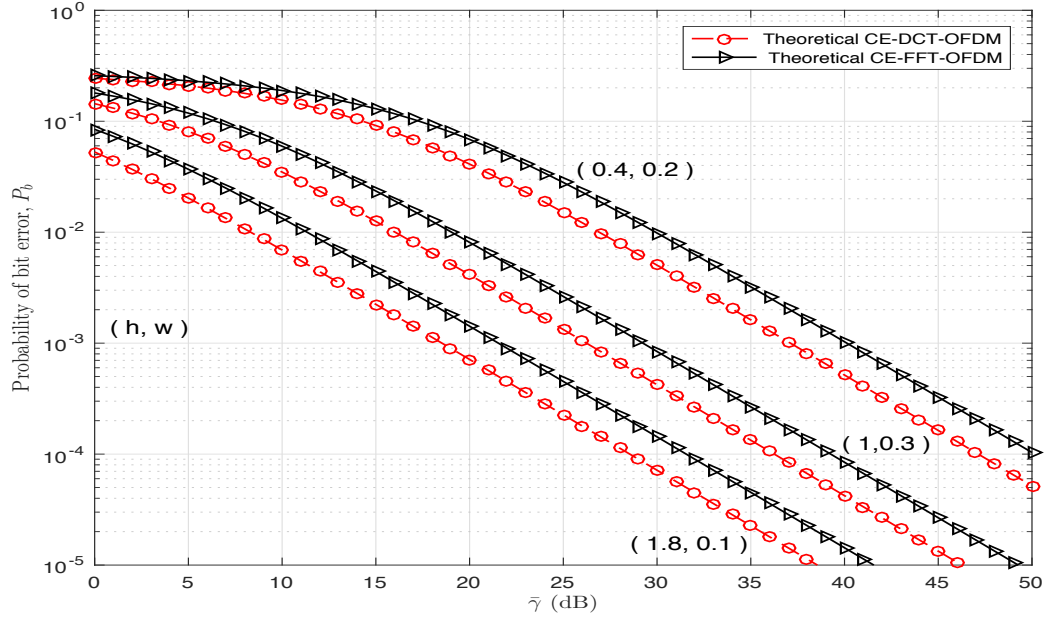


Figure 6.12: Probability of bit error performances of CE-DCT- and CE-FFT-OFDM systems (8-PAM mapper) over Rayleigh fading channel.

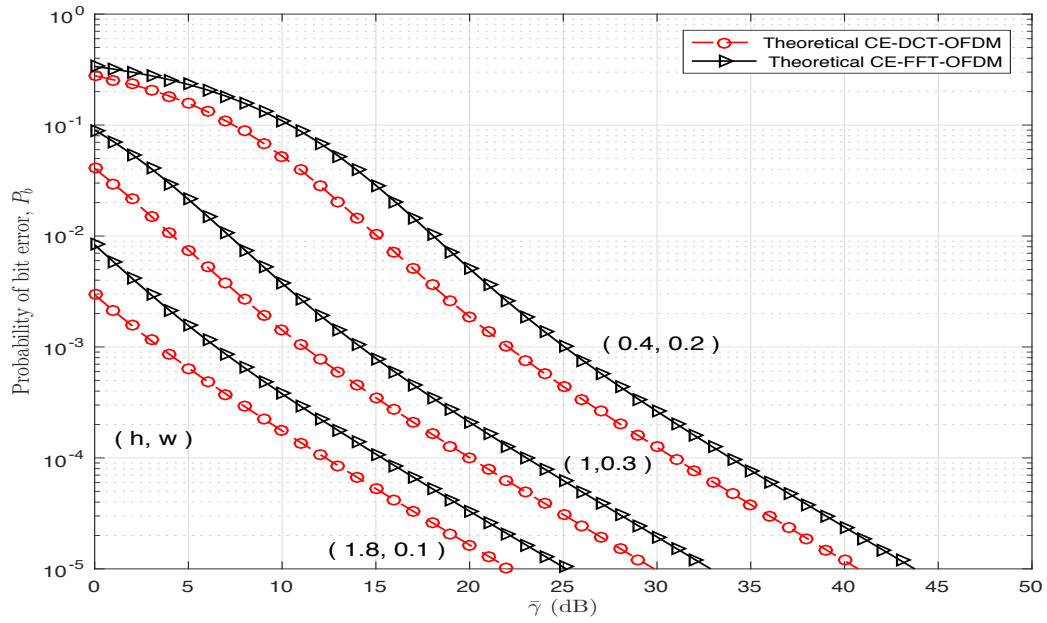


Figure 6.13: Probability of bit error performances of CE-DCT- and CE-FFT-OFDM systems (2-PAM mapper) over Rician fading channel ($K = 6$ dB).

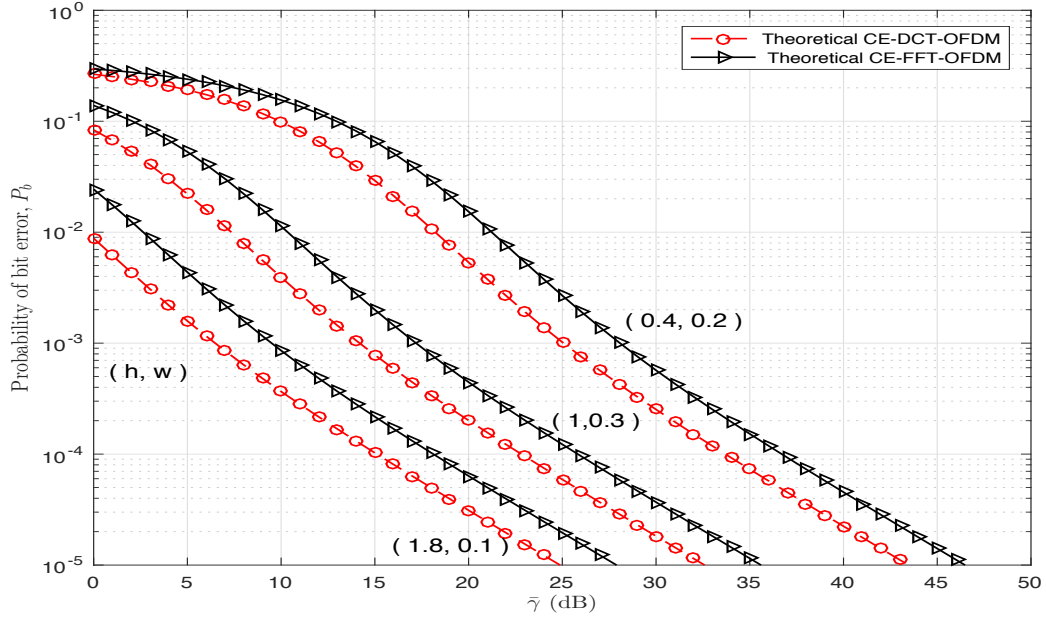


Figure 6.14: Probability of bit error performances of CE-DCT- and CE-FFT-OFDM systems (4-PAM mapper) over Rician fading channel ($K = 6$ dB).

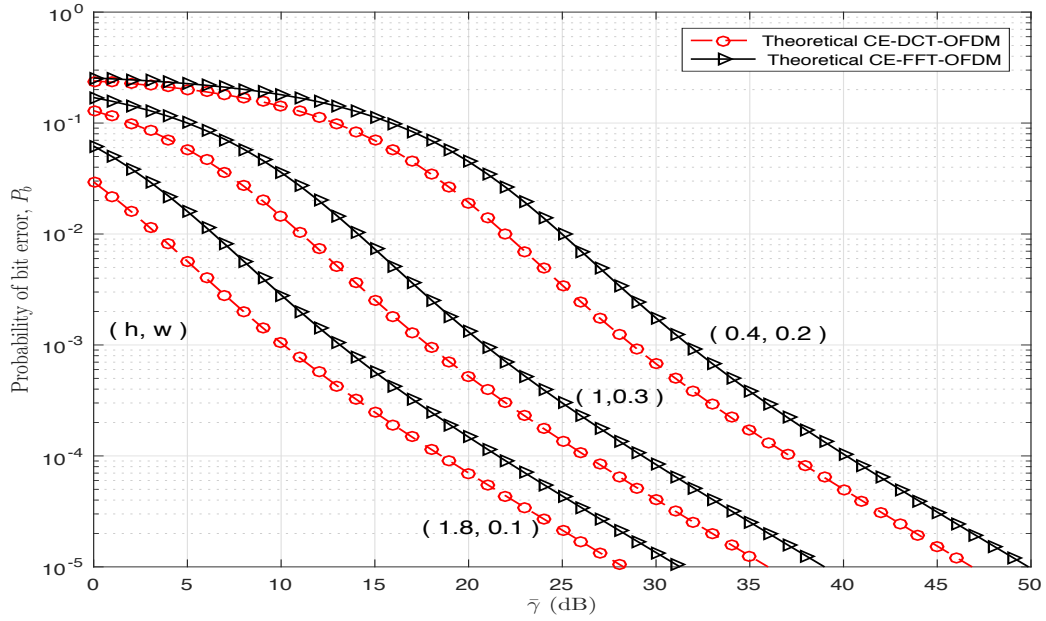


Figure 6.15: Probability of bit error performances of CE-DCT- and CE-FFT-OFDM systems (8-PAM mapper) over Rician fading channel ($K = 6$ dB).

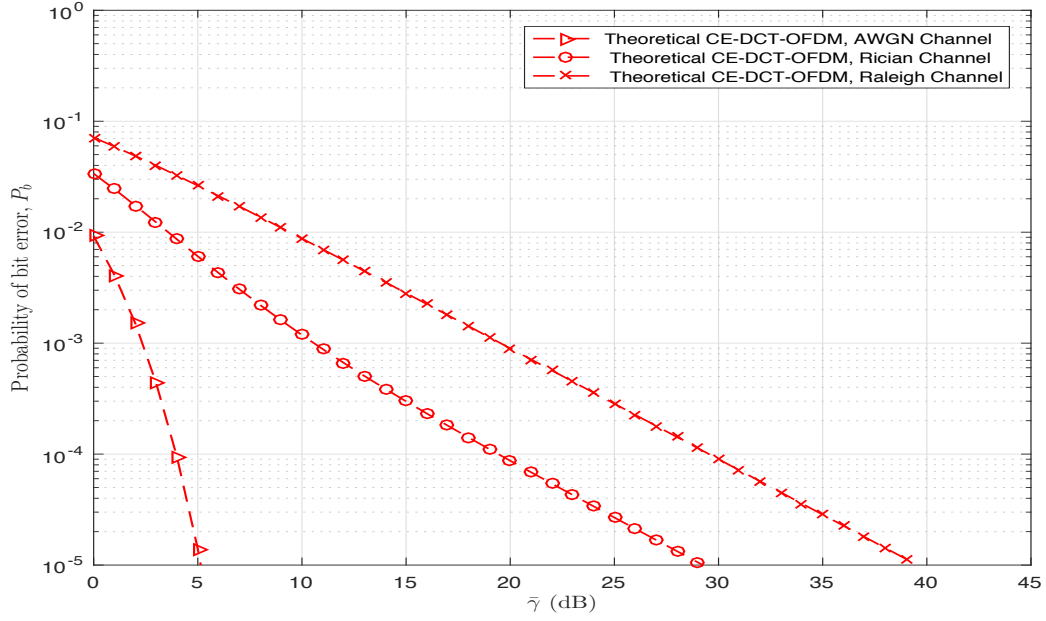


Figure 6.16: Comparison of probability of bit error performances of CE-DCT-OFDM system ($M = 2, (0.9, 0.15)$) over AWGN, Rician ($K = 6$ dB) and Rayleigh channels.

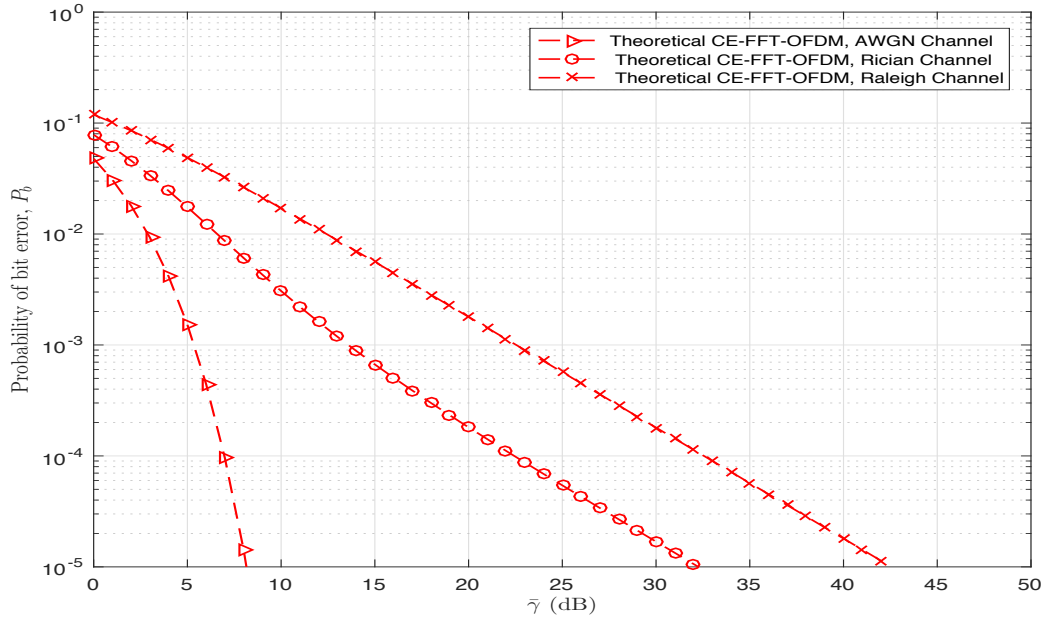


Figure 6.17: Comparison of probability of bit error performances of CE-FFT-OFDM system ($M = 2, (0.9, 0.15)$) over AWGN, Rician ($K = 6$ dB) and Rayleigh channels.

Table 6.8: Comparison of CE-FFT-OFDM system ($M = 2, (0.9, 0.15)$) over AWGN, Rician ($K = 6$ dB) and Rayleigh channels

P_b	Average SNR dB		
	AWGN	Rician	Raleigh
10^{-3}	5.366	13.915	22.141
10^{-4}	6.975	22.152	32.149
10^{-5}	8.164	32.154	42.143

The effect of Rice factor K on probability of bit error performance of CE-OFDM system (4-PAM mapper, $(0.9, 0.2)$) is illustrated in Figure 6.18. It is noted that BER decreases as K increases. For example, at $\text{BER} = 10^{-5}$ the average SNR required for $K = 18$ dB is nearly 30 dB less than that required for $K = 2$ dB. It is well known that as $K \rightarrow \infty$, Rician density approaches that of Gaussian density.

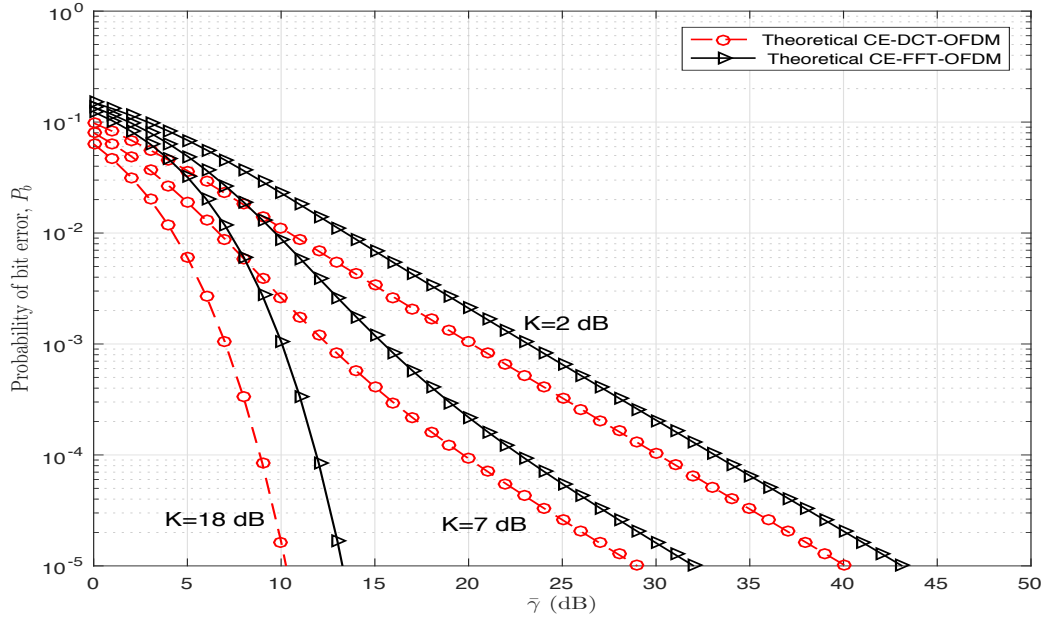


Figure 6.18: Probability of bit error performances of CE-DCT- and CE-FFT-OFDM systems (4-PAM mapper, $(0.9, 0.2)$) as a function of Rice factor.

6.6.3 Effect of TWTA Amplifier on System Performance

The effect of TWTA amplifier on the system BER performance is examined for two systems: DCT-OFDM system with QPSK mapper and DCT-OFDM system (4-PAM

mapper) with CPCM. While in the former system signals are non-constant envelope, in the latter system signals are constant-envelope. The BER performances over AWGN channel of these systems with TWTA amplifier in them have been simulated and are shown in Figure 6.19. It is noted that DCT-OFDM system with 0 dB IBO has an error floor at BER of nearly 3.20×10^{-2} . At BER= 10^{-4} , the IBO required for DCT-OFDM system exceeds 4 dB, whereas CE-DCT-OFDM system with modulation parameters (0.7, 0.25) achieves this BER with IBO=0 dB

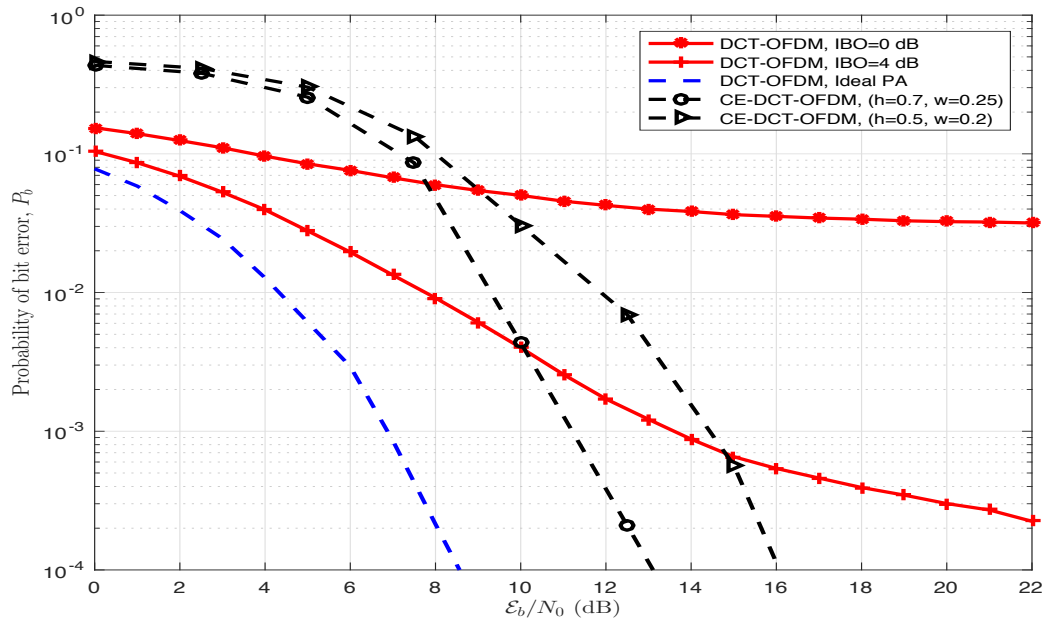


Figure 6.19: Probability of bit error performances of CE-DCT-OFDM and DCT-OFDM systems as a function of IBO for TWTA.

6.6.4 Comparison of DCT- and FFT-OFDM system with FM, CPM, and CPCM

Comparison of probability of bit error performances of DCT- and FFT-OFDM systems with CPCM, CPM and FM is presented. For this purpose, probability of bit error performances of DCT-OFDM system ($M = 4$) with CPCM ($h = 0.8, w = 0.1$), DCT-OFDM system ($M = 4$) with CPM ($h = 0.6$) and DCT-OFDM systems with FM ($h_f = 0.6$) are compared. P_b vs. average SNR for these systems are shown in Figure 6.20, for AWGN, Rayleigh, and Rician ($K = 6$ dB) channels. Similar plots are shown in

Figure 6.21 for FFT-OFDM system with CPCM, CPM and FM. It is observed that by controlling h and w , CPCM system can be designed to perform better than CPM and FM in OFDM systems. The use of CPCM in OFDM systems can provide attractive trade off between bandwidth and BER performance.

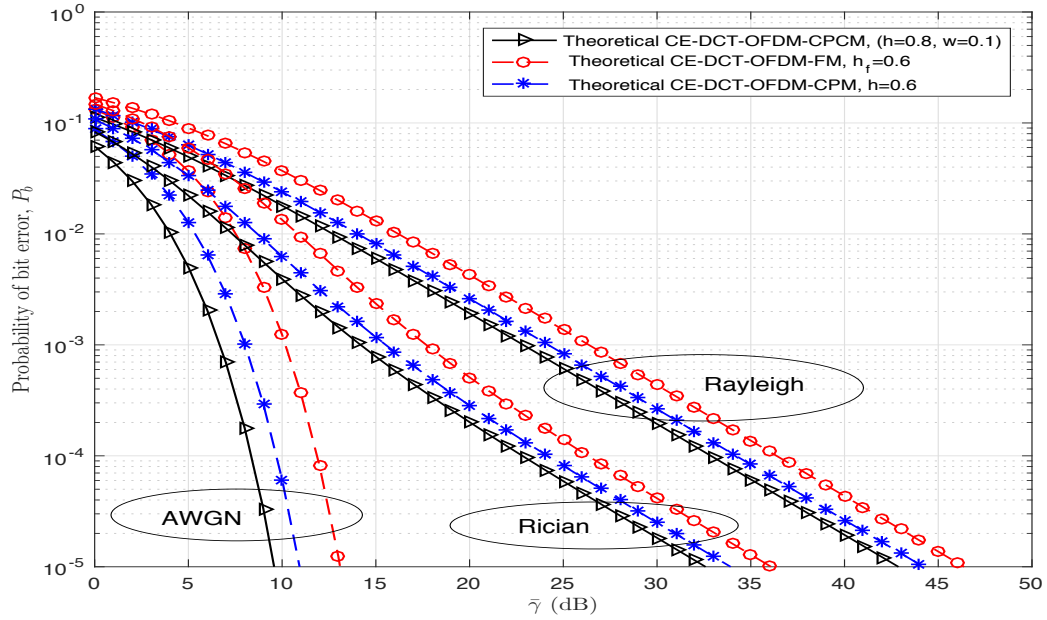


Figure 6.20: Probability of bit error performances of DCT-OFDM system (4-PAM mapper) with CPCM ($h = 0.8, w = 0.1$), CPM ($h = 0.6$) and FM ($h_f = 0.6$) over AWGN, Rician ($K = 6$ dB) and Rayleigh channels.

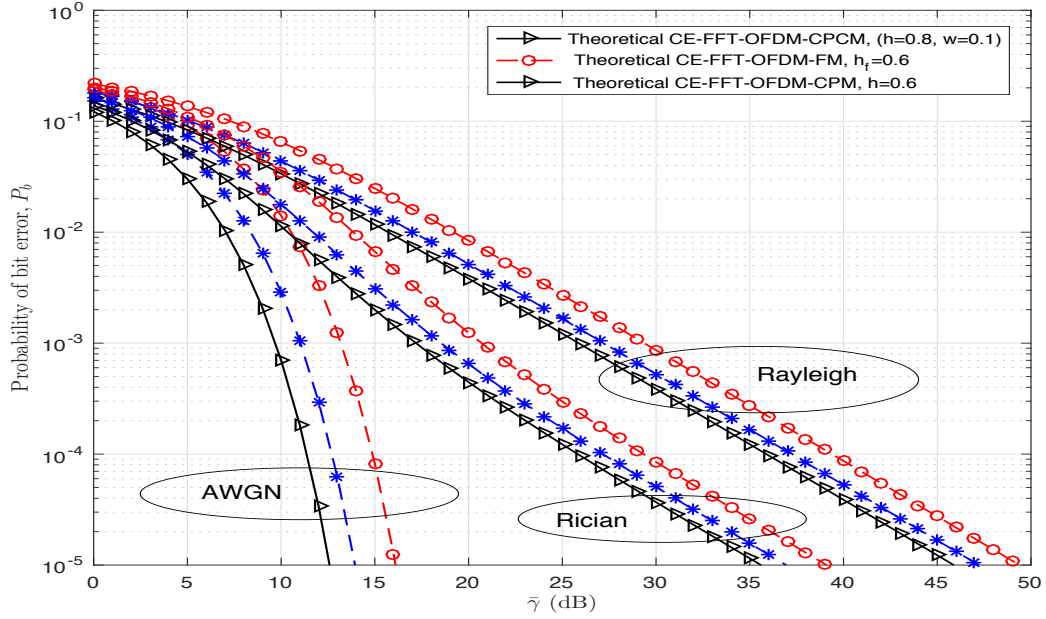


Figure 6.21: Probability of bit error performances of FFT-OFDM systems (4-PAM mapper) with CPCM ($h = 0.8, w = 0.1$), CPM ($h = 0.6$) and FM ($h_f = 0.6$) over AWGN, Rician ($K = 6$ dB) and Rayleigh channels.

6.7 Conclusion

DCT- and FFT-OFDM systems with CPCM is introduced. The transmitted signals in these systems are constant envelope and are highly suitable in systems with HPA in them. Block diagrams of transmitter and receiver in these systems are given and explained. BER analyses over AWGN and flat fading channels are presented and closed-form expressions for BER have been obtained. The results show that BER performance of CE-DCT-OFDM system is better than CE-FFT-OFDM system. It also noted that by appropriately choosing modulation parameters (h, w) system can be designed to perform better than CPM, FM and PM in OFDM systems.

Chapter 7

Conclusions

7.1 Introduction

In this Chapter, a summary of contributions of this thesis is provided and suggestions are made for further research in the light of the results obtained.

7.2 Summary of Contributions

A class of multicarrier systems called CE-OFDM is proposed and examined. Both FFT- and DCT-based systems with MPAM mapper in them are considered. The signals in these systems have constant envelope and, hence, have 0 *dB* PAPR. This property of signals in these systems eliminate the need for costly and complex PAPR reduction techniques in them thereby enhancing their energy efficiency, particularly, when HPA is employed. To achieve constant envelope signals in OFDM systems four well-known modulations, typically employed in single-carrier communication systems, are used. They are: i) PM, ii) FM, iii) CPM, and iv) CPCPM. While the first two are memoryless modulations, the other two are modulations with memory. The latter two modulations are proposed in an OFDM system to purposely introduce systematic memory among the data samples at the output of IFFT/IDCT block so that the memory introduced can be exploited at the receiver to better BER performance of the system. The CE-OFDM systems are examined for their transmitter and receiver structures, bandwidths, and BER performances over AWGN, Rayleigh, and Rician channels. The influence of HPA in these systems on system BER performance is also examined. Based on the work presented in the thesis, following are the chief contributions and observations:

1. Generic descriptions of transmitter and receiver structures are given that can be used to examine both DCT- and FFT-based OFDM systems with angle modulations. These systems are referred to as CE-DCT-OFDM and CE-FFT-OFDM

systems. The receiver structure for memoryless modulations such as FM and PM consists of arctangent demodulation followed by optimum OFDM receiver. However, when modulations with memory are used in OFDM systems, a modified receiver is required to exploit the inherent memory in modulated signal. In this thesis a receiver structure is presented that consists of arctangent demodulator followed by oversampling with correction block prior to the optimum OFDM receiver.

2. The detection of CE-OFDM signals in AWGN channel is addressed and closed-form expressions for BER are derived and extensively illustrated. The BER of CE-OFDM system, in general, is a function of E_b/N_0 , Signal-to-Noise-Ratio, modulation parameters, h_p for PM, h_f for FM, h for CPM and (h, w) for CPCPM, and numbers of amplitude levels of M-PAM mapper. Table 7.1 provides a comparison of BER performances of DCT- and FFT-OFDM systems as a function of various angle modulations.

Table 7.1: E_b/N_0 required at $P_b = 10^{-5}$ for various modulations in an OFDM system (2-PAM mapper).

Modulation Type	E_b/N_0 (dB)	
	DCT-OFDM system	FFT-OFDM system
PM, $h_p = 0.7$	12.686	15.696
FM, $h_f = 0.7$	7.915	10.925
CPM, $h = 0.7$	5.753	8.766
CPCPM, $(h = 0.9, w = 0.15)$	5.154	8.164

3. It is shown that, in general, CE-DCT-OFDM system outperforms CE-FFT-OFDM system by nearly 3 dB, for identical system and modulation parameters. The DCT- and FFT-OFDM systems with CPM and CPCPM are far superior, in terms of BER, compared to systems with PM or FM. However, the receivers are more complex with the former compared to latter systems. Thus, it is observed that there exist tradeoffs among power, complexity, and bandwidth in CE-OFDM systems. In general, CE-OFDM system BER decreases as a function of increasing value of modulation parameters such as h_p , h_f , h and (h, w) . However, an increase in the value of modulation parameters increases the bandwidth of the system. Finally, it is noted that as the number of levels in the MPAM mapper in CE-OFDM system is increased, the system BER increases; however, spectral efficiency of the system

increases with the increases in the number of levels in the mapper. Therefore, in the design of a CE-OFDM system appropriate choice of system and modulation parameters must be made depending on the needs of the communication system.

4. Closed-form expressions for BER of CE-OFDM systems have been derived and extensively illustrated as a function of system and modulation parameters and parameters of densities of Rayleigh and Rician environment. In general, severe power penalty must be paid due to signal fading over these channels. It is observed that power penalty needed over Rayleigh channel is higher than that required over Rician channel. This is due to the fact that over Rayleigh channel there is no direct LOS path between the transmitter and receiver, whereas over Rician channel there exist such as path. Table 7.2 compares power penalties for various modulations for Rayleigh and Rician channels.

Table 7.2: Power penalty required for various modulations in an OFDM system (2-PAM mapper) over fading channels at $P_b = 10^{-5}$.

Modulation Type	E_b/N_0 (dB)			
	Rician		Rayleigh	
	DCT-OFDM	FFT-OFDM	DCT-OFDM	FFT-OFDM
PM , $h_p = 0.7$	24.011	24.021	34.254	34.427
FM , $h_f = 0.7$	24.236	24.231	34.327	34.239
CPM , $h = 0.7$	24.098	24.019	34.779	34.791
CPCM , (0.9, 0.15)	23.972	23.991	33.989	33.979

5. The effect of TWTA amplifier on the BER of CE-OFDM systems is presented. It is shown that without appropriate IBO conventional OFDM systems perform very poorly. However, it is shown that CE-OFDM systems are far superior in terms of BER and require absolutely no IBO.
6. Easy-to-compute expressions for bandwidth of CE-OFDM systems have been determined. They are summarized in Table 7.3. In Figure 7.1 are shown bandwidth as function of modulation parameters for PM, FM, CPM and CPCM in an OFDM system. The spectral efficiency of a communication system is the number of bits/sec that can be transmitted per unit Hz of bandwidth and is an important metric used to characterize the system. The spectral efficiencies of an OFDM system with PM,

FM, CPM, and CPCPM are depicted in Figure 7.2 as function of modulation parameters.

The bandwidth of CE-OFDM system, when modulation parameters are small ($h_p, h_f, h, (h, w)$), is nearly the same as that of non-constant envelope OFDM system that uses I-Q modulation technique. However, as the modulation parameters increase in value in CE-OFDM system, the bandwidth of the system increases. For example, CE-OFDM system with FM with $h_f = 2$ requires twice the bandwidth of non-constant envelope OFDM system with I-Q modulation. It is noted that non-constant envelope OFDM signals when passed through HPA results in spectral broadening if sufficient IBO is not employed. However, CE-OFDM signals when passed through HPA do not suffer from spectral broadening.

Table 7.3: Expressions for bandwidth of transmitted signal in CE-OFDM system for various modulation.

Modulation Type	$BW(Hz)$
PM	$\max(2h_p, 2) W$
FM	$\max(2h_f, 2) W$
CPM	$\max(h, 2) W$
CPCPM	$\max\left(\left\lceil 2\sqrt{\frac{h^2}{4} - \frac{hw}{4} + \frac{w^2}{3}} \right\rceil, 2\right) W$

There exist a variety of communication situation where CE-OFDM systems presented in this thesis can be deployed. For example, over power-limited satellite communication channels CE-OFDM system is highly attractive compared to single-carrier systems that require complex techniques to over come the effect of multipath. Also, CE-OFDM systems are highly desirable over such channels, as signal in them are constant envelope. Also, CE-OFDM system can be used as a standalone system to replace the existing conventional OFDM system, particularly over channels that kill the performance due to insufficient power backoff.

7.3 Suggestion for Further Research

It is important to translate theoretical research into practical systems that can be implemented . In this context, further research is needed to develop prototype of CE-OFDM

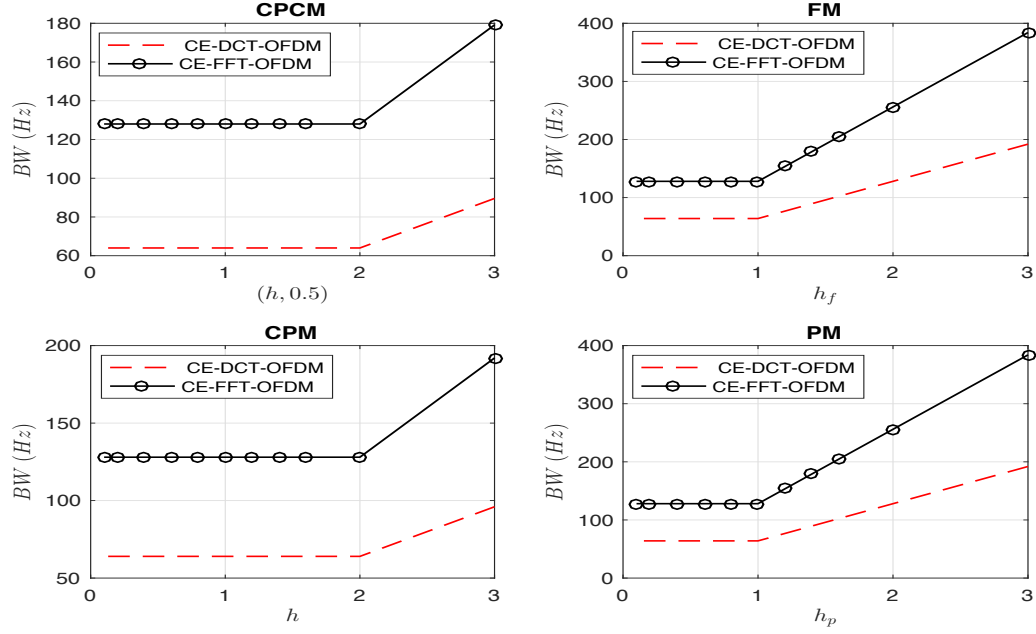


Figure 7.1: Bandwidth as a function of modulation parameters ($N = 64$, $T = 1$) for various angle modulation in an OFDM system.

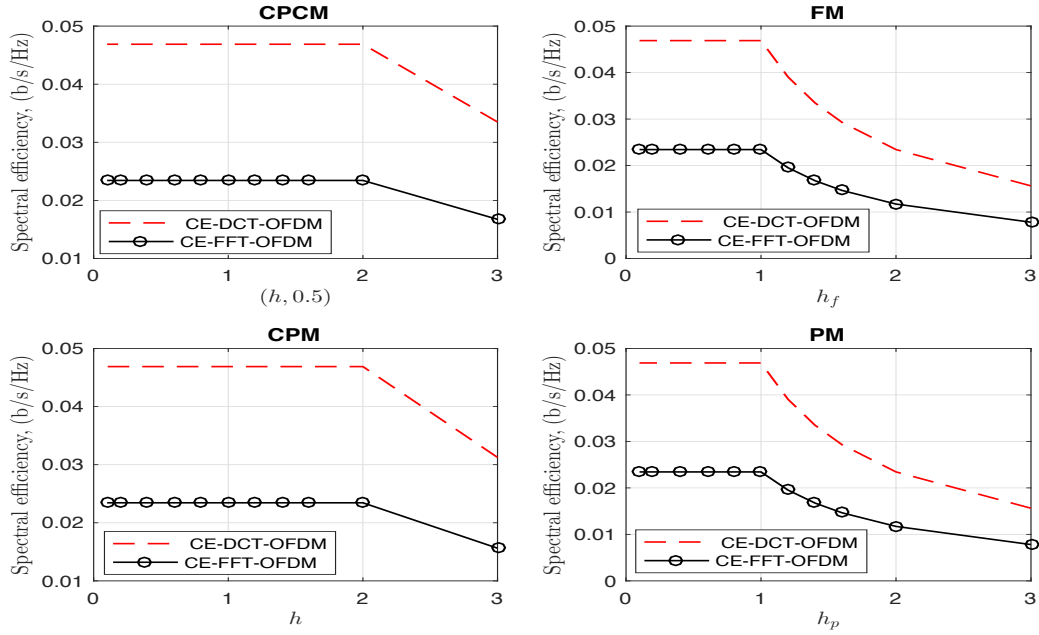


Figure 7.2: Spectral efficiency as a function of modulation parameters (8PAM mapper, $T = 1$, and $N = 64$) for various angle modulation in an OFDM system.

system presented in this thesis.

One of the observation in the thesis is that severe power penalty is needed when operating CE-OFDM systems over fading channels. Therefore, techniques are needed to reduce this power penalty. It is well-known that channel coding and interleaving techniques can be used to better performance over fading channels. It would be interesting to examine CE-OFDM systems using these techniques.

In the thesis, performance of CE-OFDM system over non-frequency selective fading channels was considered. It is important to examine CE-OFDM system over frequency-selective channels. Also, the system needs to be examined in imperfect channel state information.

There has been an increasing attention given to communication at high frequencies including the 60 GHz band. A study of how CE-OFDM systems can be designed to function at these frequencies requires further research.

References

- [1] Cisco visual networking index: Forecast and methodology 2009-2014, Cisco White Paper, Tech. Rep., June 2010.
- [2] K. S. Jacobsen, "Methods of upstream power backoff on very high speed digital subscriber lines," in IEEE Communications Magazine, vol. 39, no. 3, pp. 210-216, March 2001.
- [3] A. Leshem and E. Zehavi, "Game theory and the frequency selective interference channel," in IEEE Signal Processing Magazine, vol. 26, no. 5, pp. 28-40, September 2009.
- [4] J. G. Proakis, Digital Communications, 4th ed., New York: McGraw- Hill, 2001.
- [5] G. Forney, "Maximum-likelihood sequence estimation of digital sequences in the presence of intersymbol interference," in IEEE Transactions on Information Theory, vol. 18, no. 3, pp. 363-378, May 1972.
- [6] S. Haykin, Adaptive Filter Theory, Prentice-Hall, Upper Saddle River, New Jersey, USA, Fourth edition, September 2001.
- [7] J. M. Cioffi, G. P. Dudevoir, M. Vedat Eyuboglu and G. D. Forney, "MMSE decision-feedback equalizers and coding. I. Equalization results," in IEEE Transactions on Communications, vol. 43, no. 10, pp. 2582-2594, October 1995.
- [8] D. L. Goeckel and G. Ananthaswamy, "On the design of multidimensional signal sets for OFDM systems," in IEEE Transactions on Communications, vol. 50, no. 3, pp. 442-452, March 2002.
- [9] Kay SM, Fundamentals of Statistical Signal Processing: Estimation Theory. Prentice-Hall, Englewood Cliffs, NJ, USA, 1993

- [10] I. Kalet, "The multitone channel," in IEEE Transactions on Communications, vol. 37, no. 2, pp. 119-124, February 1989.
- [11] A. Ruiz, J. M. Cioffi and S. Kasturia, "Discrete multiple tone modulation with coset coding for the spectrally shaped channel," in IEEE Transactions on Communications, vol. 40, no. 6, pp. 1012-1029, June 1992.
- [12] L. Cimini, "Analysis and Simulation of a Digital Mobile Channel Using Orthogonal Frequency Division Multiplexing," in IEEE Transactions on Communications, vol. 33, no. 7, pp. 665-675, July 1985.
- [13] W.C.Y. Lee, Mobile Cellular Telecommunications Systems, McGraw Hill Publications, New York, USA, December 1989.
- [14] M. Speth, S. A. Fechtel, G. Fock and H. Meyr, "Optimum receiver design for wireless broad-band systems using OFDM. I," in IEEE Transactions on Communications, vol. 47, no. 11, pp. 1668-1677, November 1999.
- [15] J. A. C. Bingham, "Multicarrier modulation for data transmission: an idea whose time has come," in IEEE Communications Magazine, vol. 28, no. 5, pp. 5-14, May 1990.
- [16] S. Weinstein and P. Ebert, "Data Transmission by Frequency-Division Multiplexing Using the Discrete Fourier Transform," in IEEE Transactions on Communication Technology, vol. 19, no. 5, pp. 628-634, October 1971.
- [17] R. W. Chang, "Synthesis of band-limited orthogonal signals for multichannel data transmission," in The Bell System Technical Journal, vol. 45, no. 10, pp. 1775-1796, December 1966.
- [18] B. Saltzberg, "Performance of an Efficient Parallel Data Transmission System," in IEEE Transactions on Communication Technology, vol. 15, no. 6, pp. 805-811, December 1967.
- [19] S. Weinstein and P. Ebert, "Data Transmission by Frequency-Division Multiplexing Using the Discrete Fourier Transform," in IEEE Transactions on Communication Technology, vol. 19, no. 5, pp. 628-634, October 1971.

- [20] A. Peled and A. Ruiz, "Frequency domain data transmission using reduced computational complexity algorithms," ICASSP '80. IEEE International Conference on Acoustics, Speech, and Signal Processing, 1980, pp. 964-967.
- [21] IEEE Standard for Telecommunications and Information Exchange Between Systems LAN/MAN Specific Requirements Part 11: Wireless Medium Access Control (MAC) and physical layer (PHY) specifications: High Speed Physical Layer in the 5 GHz band, in IEEE Std 802.11a-1999, pp. 1-102, December 1999.
- [22] IEEE Standard for Information Technology Telecommunications and Information Exchange Between Systems- Local and Metropolitan Area Networks Specific Requirements Part 11: Wireless LAN Medium Access Control (MAC) and Physical Layer (PHY) Specifications Amendment 4: Further Higher Data Rate Extension in the 2.4 GHz Band , in IEEE Std 802.11g-2003, pp. i-67, June 2003
- [23] IEEE Standard for Information technology Telecommunications and information exchange between systems-Local and metropolitan area networks Specific requirements Part 11: Wireless LAN Medium Access Control (MAC) and Physical Layer (PHY) Specifications Amendment 5: Enhancements for Higher Throughput, in IEEE Std 802.11n-2009, pp. 1-536, September 2009
- [24] C. Esli, B. Ozgul and H. Delic, "Space-frequency coded HIPERLAN/2," in IEEE Transactions on Consumer Electronics, vol. 50, no. 4, pp. 1162-1168, November 2004.
- [25] American National Standard for Telecommunications - Network and Customer Installation Interfaces - Asymmetric Digital Subscriber Line (ADSL) Metallic Interface, in ANSI T1.413-1998, pp. 1-264, November 11, 1998.
- [26] F. Wang, A. Ghosh, C. Sankaran, P. J. Fleming, F. Hsieh and S. J. Benes, "Mobile WiMAX systems: performance and evolution," in IEEE Communications Magazine, vol. 46, no. 10, pp. 41-49, October 2008.
- [27] IEEE Standard for Local and Metropolitan Area Networks - Part 20: Air Interface for Mobile Broadband Wireless Access Systems Supporting Vehicular Mobility -

- Physical and Media Access Control Layer Specification,” in IEEE Std 802.20-2008 , pp .1-1039, August 2008.
- [28] Y. Wang, J. Oostveen, A. Filippi and S. Wesemann, ”A Novel Preamble Scheme for Packet-Based OFDM WLAN,” 2007 IEEE Wireless Communications and Networking Conference, Kowloon, 2007, pp. 1481-1485.
 - [29] Xinrong Li, K. Pahlavan, M. Latva-Aho and M. Ylianttila, ”Indoor geolocation using OFDM signals in HIPERLAN/2 wireless LANs,” 11th IEEE International Symposium on Personal Indoor and Mobile Radio Communications. PIMRC 2000. Proceedings (Cat. No.00TH8525), London, 2000, pp. 1449-1453, vol.2.
 - [30] S. Chouhan and A. Sharma, ”Performance analysis of STBC coded MIMO-OFDM system for WIMAX (IEEE 802.16) systems,” 2015 International Conference on Innovations in Information, Embedded and Communication Systems (ICIIECS), Coimbatore, 2015, pp. 1-6.
 - [31] Y. Awad, L. H. Crockett and R. W. Stewart, ”OFDM transceiver for IEEE 802.20 standards,” 2009 17th European Signal Processing Conference, Glasgow, 2009, pp. 1-5.
 - [32] Gi Hyun Kim, Honey Durga Tiwari, Chan Mo Kim, Yong Beom Cho and Younggoo, ”Implementation of DCT based OFDM system,” 2008 International SoC Design Conference, Busan, 2008, pp. II-41-II-44.
 - [33] N. Al-Dhahir, Hlaing Minn and S. Satish, ”Optimum DCT-based multicarrier transceivers for frequency-selective channels,” in IEEE Transactions on Communications, vol. 54, no. 5, pp. 911-921, May 2006.
 - [34] F. Cruz-Roldan, M. E. Dominguez-Jimenez, G. Sansigre Vidal, P. Amo-Lopez, M. Blanco-Velasco and Á. Bravo-Santos, ”On the Use of Discrete Cosine Transforms for Multicarrier Communications,” in IEEE Transactions on Signal Processing, vol. 60, no. 11, pp. 6085-6090, November 2012.
 - [35] Shilpa Satish, ”Design and Performance of DCT-Based Multicarrier Transceiver for Broadband Communication,” Master dissertation, University of Texas at Dallas, May 2006.

- [36] N. Al-Dhahir and Hlaing Minn, "A new multicarrier transceiver based on the discrete cosine transform," *IEEE Wireless Communications and Networking Conference*, 2005, 2005, pp. 45-50, Vol. 1.
- [37] S. Satish, N. Al-Dhahir and H. Minn, "A DCT-Based Broadband Multicarrier Transceiver," *Proceedings of the IEEE SoutheastCon*, Memphis, TN, 2006, pp. 175-180.
- [38] Jun Tan and G. L. Stuber, "Constant envelope multi-carrier modulation," *MIL-COM 2002. Proceedings*, 2002, pp. 607-611 vol.1.
- [39] C. Tang and G. D. Mandyam, "Performance of OFDM modem with alternative basis functions," *IEEE Radio and Wireless Symposium*, 2006, pp. 551-554.
- [40] G. D. Mandyam, "Sinusoidal transforms in OFDM systems," in *IEEE Transactions on Broadcasting*, vol. 50, no. 2, pp. 172-184, June 2004.
- [41] R. Merched, "On OFDM and single-carrier frequency-domain systems based on trigonometric transforms," in *IEEE Signal Processing Letters*, vol. 13, no. 8, pp. 473-476, August 2006.
- [42] P. Tan and N. C. Beaulieu, "An improved DCT-based OFDM data transmission scheme," *2005 IEEE 16th International Symposium on Personal, Indoor and Mobile Radio Communications*, Berlin, 2005, pp. 745-749, Vol. 2.
- [43] Fuqin Xiong, "M-ary amplitude shift keying OFDM system," in *IEEE Transactions on Communications*, vol. 51, no. 10, pp. 1638-1642, October 2003.
- [44] P. Tan and N. C. Beaulieu, "A Comparison of DCT-Based OFDM and DFT-Based OFDM in Frequency Offset and Fading Channels," in *IEEE Transactions on Communications*, vol. 54, no. 11, pp. 2113-2125, November 2006.
- [45] G. D. Mandyam, "On the discrete cosine transform and OFDM systems," *Acoustics, Speech, and Signal Processing, 2003. Proceedings. (ICASSP '03). 2003 IEEE International Conference on*, 2003, pp. IV544-IV547, vol.4.
- [46] F. Gao, T. Cui, A. Nallanathan and C. Tellambura, "Maximum likelihood based estimation of frequency and phase offset in DCT OFDM systems under non-circular

- transmissions: algorithms, analysis and comparisons,” in IEEE Transactions on Communications, vol. 56, no. 9, pp. 1425-1429, September 2008.
- [47] A. Rushdi and J. Tuqan, ”PAPR Reduction in Trigonometric-Based OFDM Systems,” 2007 Conference Record of the Forty-First Asilomar Conference on Signals, Systems and Computers, Pacific Grove, CA, 2007, pp. 1747-1751.
 - [48]] YulinWang, Gengxin Zhang, Zhidong Xie, and Jing Hu, “Channel Estimation in DCT-Based OFDM, ” The Scientific World Journal, vol. 2014, pp. 6, March 2014
 - [49] Peng Tan and N. C. Beaulieu, ”Precise bit error probability analysis of DCT OFDM in the presence of carrier frequency offset on AWGN channels,” GLOBECOM '05. IEEE Global Telecommunications Conference, 2005, pp. 1429-1434.
 - [50] M. A. Sid-Ahmed, Image Processing: Theory, Algorithms, and Architectures. New York: McGraw-Hill, 1995.
 - [51] S. H. Oguz, A. Faibish, S. Faibish and G. Cotter, ”Objective Image Quality Metrics for DCT-Based Video Compression,” 36th SMPTE Annual Advanced Motion Imaging Conference, Dallas, TX, USA, 2002, pp. 1-13.
 - [52] H. Ochiai, ”Power efficiency comparison of OFDM and single-carrier signals,” Proceedings IEEE 56th Vehicular Technology Conference, 2002, pp. 899-903, vol.2.
 - [53] T. Svensson and T. Eriksson, ”On Power Amplifier Efficiency with Modulated Signals,” 2010 IEEE 71st Vehicular Technology Conference, Taipei, 2010, pp. 1-5.
 - [54] J. Anderson, T. Aulin, and C.-E. Sundberg, Digital Phase Modulation. New York: Plenum Press, 1986.
 - [55] T. Aulin and C. Sundberg, ”Continuous Phase Modulation - Part I: Full Response Signaling,” in IEEE Transactions on Communications, vol. 29, no. 3, pp. 196-209, March 1981.
 - [56] M. Sakai, H. Lin and K. Yamashita, ”Joint Estimation of Channel and I/Q Imbalance in OFDM/OQAM Systems,” in IEEE Communications Letters, vol. 20, no. 2, pp. 284-287, February 2016.

- [57] A. Al-Habashna, O. A. Dobre, R. Venkatesan and D. C. Popescu, "Second-Order Cyclostationarity of Mobile WiMAX and LTE OFDM Signals and Application to Spectrum Awareness in Cognitive Radio Systems," in *IEEE Journal of Selected Topics in Signal Processing*, vol. 6, no. 1, pp. 26-42, February 2012.
- [58] U. Epple and M. Schnell, "Advanced Blanking Nonlinearity for Mitigating Impulsive Interference in OFDM Systems," in *IEEE Transactions on Vehicular Technology*, vol. 66, no. 1, pp. 146-158, January 2017.
- [59] M. Kim, W. Lee and D. H. Cho, "A Novel PAPR Reduction Scheme for OFDM System Based on Deep Learning," in *IEEE Communications Letters*, vol. 22, no. 3, pp. 510-513, March 2018.
- [60] T. Hwang, C. Yang, G. Wu, S. Li and G. Y. Li, "OFDM and Its Wireless Applications: A Survey," in *IEEE Transactions on Vehicular Technology*, vol. 58, no. 4, pp. 1673-1694, May 2009.
- [61] E. Costa, M. Midrio and S. Pupolin, "Impact of amplifier nonlinearities on OFDM transmission system performance," in *IEEE Communications Letters*, vol. 3, no. 2, pp. 37-39, February 1999.
- [62] P. Banelli, G. Baruffa and S. Cacopardi, "Effects of HPA nonlinearity on frequency multiplexed OFDM signals," in *IEEE Transactions on Broadcasting*, vol. 47, no. 2, pp. 123-136, Jun 2001.
- [63] S. P. Yadav and S. C. Bera, "Nonlinearity effect of Power Amplifiers in wireless communication systems," 2014 International Conference on Electronics, Communication and Computational Engineering (ICECCE), Hosur, 2014, pp. 12-17.
- [64] K. G. Paterson and V. Tarokh, "On the existence and construction of good codes with low peak-to-average power ratios," in *IEEE Transactions on Information Theory*, vol. 46, no. 6, pp. 1974-1987, September 2000.
- [65] A. D. S. Jayalath and C. Tellambura, "Adaptive PTS approach for reduction of peak-to-average power ratio of OFDM signal," in *Electronics Letters*, vol. 36, no. 14, pp. 1226-1228, July 2000.

- [66] J. Armstrong, "Peak-to-average power reduction for OFDM by repeated clipping and frequency domain filtering," in *Electronics Letters*, vol. 38, no. 5, pp. 246-247, February 2002.
- [67] H. Breiling, S. H. Muller-Weinfurtner and J. B. Huber, "SLM peak-power reduction without explicit side information," in *IEEE Communications Letters*, vol. 5, no. 6, pp. 239-241, June 2001.
- [68] B. S. Krongold and D. L. Jones, "An active-set approach for OFDM PAR reduction via tone reservation," in *IEEE Transactions on Signal Processing*, vol. 52, no. 2, pp. 495-509, February 2004.
- [69] A. D. S. Jayalath and C. Tellambura, "Reducing the peak-to-average power ratio of orthogonal frequency division multiplexing signal through bit or symbol interleaving," in *Electronics Letters*, vol. 36, no. 13, pp. 1161-1163, June 2000.
- [70] S. C. Thompson, A. U. Ahmed, J. G. Proakis, J. R. Zeidler and M. J. Geile, "Constant Envelope OFDM," in *IEEE Transactions on Communications*, vol. 56, no. 8, pp. 1300-1312, August 2008.
- [71] H. F. Harmuth, "On the transmission of information by orthogonal time functions," in *Transactions of the American Institute of Electrical Engineers, Part I: Communication and Electronics*, vol. 79, no. 3, pp. 248-255, July 1960.
- [72] Char-Dir Chung and Shih-Ming Cho, "Constant-envelope orthogonal frequency division multiplexing modulation," *Fifth Asia-Pacific Conference on Communications and Fourth Optoelectronics and Communications Conference on Communications*, Beijing, China, 1999, pp. 629-632 vol.1.
- [73] R. A. Pacheco and D. Hatzinakos, "Error Rate Analysis of Phase-Modulated OFDM (OFDM-PM) in Awgn Channels," *2006 IEEE International Conference on Acoustics Speech and Signal Processing Proceedings*, Toulouse, 2006, pp. IV337-340IV.
- [74] M. Kiviranta, A. Mammela, D. Cabric, D. A. Sobel and R. W. Brodersen, "Constant envelope multicarrier modulation: performance evaluation AWGN and fading

- channels,” MILCOM 2005 - 2005 IEEE Military Communications Conference, Atlantic City, NJ, 2005, pp. 807-813, Vol. 2.
- [75] S. C. Thompson, J. G. Proakis and J. R. Zeidler, ”Constant envelope binary OFDM phase modulation,” IEEE Military Communications Conference (MILCOM), 2003, pp. 621-626, Vol.1.
 - [76] S. C. Thompson, A. U. Ahmed, J. G. Proakis and J. R. Zeidler, ”Constant envelope OFDM phase modulation: spectral containment, signal space properties and performance,” IEEE MILCOM 2004. Military Communications Conference, 2004, pp. 1129-1135, Vol. 2.
 - [77] S. C. Thompson, J. G. Proakis and J. R. Zeidler, ”Noncoherent Reception of Constant Envelope OFDM in Flat Fading Channels,” 2005 IEEE 16th International Symposium on Personal, Indoor and Mobile Radio Communications, Berlin, 2005, pp. 517-521.
 - [78] S. C. Thompson, J. G. Proakis, J. R. Zeidler and M. Geile, ”Constant Envelope OFDM in Multipath Rayleigh Fading Channels,” MILCOM 2006 - 2006 IEEE Military Communications conference, Washington, DC, 2006, pp. 1-7.
 - [79] Z. Liu, J. Wang, H. Tian and K. Yi, ”Reducing specific inter-symbol interference of constant envelope OFDM system through optimizing zero-padding pattern,” 2011 IEEE International Conference on Signal Processing, Communications and Computing (ICSPCC), Xi’an, 2011, pp. 1-4.
 - [80] A. U. Ahmed and J. R. Zeidler, ”Novel Low-Complexity Receivers for Constant Envelope OFDM,” in IEEE Transactions on Signal Processing, vol. 63, no. 17, pp. 4572-4582, September 2015.
 - [81] C. D. Chung, ”Spectral precoding for constant-envelope OFDM,” in IEEE Transactions on Communications, vol. 58, no. 2, pp. 555-567, February 2010.
 - [82] A. U. Ahmed, S. C. Thompson and J. R. Zeidler, ”Channel estimation and equalization for CE-OFDM in multipath fading channels,” MILCOM 2008 - 2008 IEEE Military Communications Conference, San Diego, CA, 2008, pp. 1-7.

- [83] A. U. Ahmed, S. C. Thompson and J. R. Zeidler, "Constant Envelope OFDM with Channel Coding," MILCOM 2006 - 2006 IEEE Military Communications conference, Washington, DC, 2006, pp. 1-7.
- [84] A. U. Ahmed, S. C. Thompson and J. R. Zeidler, "Threshold Extending Receiver Structures for CE-OFDM," MILCOM 2007 - IEEE Military Communications Conference, Orlando, FL, USA, 2007, pp. 1-7.
- [85] E. F. Casas and C. Leung, "OFDM for data communication over mobile radio FM channels. I. Analysis and experimental results," in IEEE Transactions on Communications, vol. 39, no. 5, pp. 783-793, May 1991.
- [86] E. F. Casas and C. Leung, "OFDM for data communication over mobile radio FM channels. II. Performance improvement," in IEEE Transactions on Communications, vol. 40, no. 4, pp. 680-683, April 1992.
- [87] Y. Tsai, G. Zhang and J. L. Pan, "Orthogonal frequency division multiplexing with phase modulation and constant envelope design," MILCOM 2005 - 2005 IEEE Military Communications Conference, Atlantic City, NJ, 2005, pp. 2658-2664, Vol. 4.
- [88] C. Sacchi, T. F. Rahman, N. Bartolomei, S. Morosi, A. Mazzinghi and F. Ciabini, "Design and Assessment of a CE-OFDM-Based mm-Wave 5G Communication System," 2016 IEEE Globecom Workshops (GC Wkshps), Washington, DC, 2016, pp. 1-7.
- [89] T. W. Wu, Y. C. Cheng and C. D. Chung, "Optimal training symbols for channel estimation in constant-envelope OFDM," 2013 IEEE/CIC International Conference on Communications in China (ICCC), Xi'an, 2013, pp. 385-390.
- [90] A. U. Ahmed, S. C. Thompson, D. W. Chi and J. R. Zeidler, "Subcarrier based threshold performance enhancement in Constant Envelope OFDM," MILCOM 2012 - 2012 IEEE Military Communications Conference, Orlando, FL, 2012, pp. 1-6.
- [91] E. S. Hassan, S. E. El-Khamy, M. I. Dessouky, S. A. El-Dolil and F. E. Abd El-Samie, "New interleaving scheme for CE-OFDM systems using chaotic maps," 2009

- IFIP International Conference on Wireless and Optical Communications Networks, Cairo, 2009, pp. 1-5.
- [92] R. B. Nunes, H. R. de O Rocha, D. A. A. Mello, F. D. Simões, M. E. V. Segatto and J. A. L. Silva, "Transmission of CE-OFDM Signals Over MMF Links Using Directly Modulated 850-nm VCSELs," in *IEEE Photonics Technology Letters*, vol. 27, no. 3, pp. 315-318, February 2015.
 - [93] J. A. L. Silva, A. V. T. Cartaxo and M. E. V. Segatto, "A PAPR reduction technique based on a constant envelope OFDM approach for fiber nonlinearity mitigation in optical direct-detection systems," in *IEEE/OSA Journal of Optical Communications and Networking*, vol. 4, no. 4, pp. 296-303, April 2012.
 - [94] L. Deng, X. Pang, I. T. Monroy, M. Tang, P. Shum and D. Liu, "Experimental Demonstration of Nonlinearity and Phase Noise Tolerant 16-QAM OFDM W-Band (75–110 GHz) Signal Over Fiber System," in *Journal of Lightwave Technology*, vol. 32, no. 8, pp. 1442-1448, April 2014.
 - [95] K. M. Rabie, E. Alsusa, A. D. Familua and L. Cheng, "Constant envelope OFDM transmission over impulsive noise power-line communication channels," 2015 *IEEE International Symposium on Power Line Communications and Its Applications (ISPLC)*, Austin, TX, 2015, pp. 13-18.
 - [96] El Ghzaoui Mohammed, B. Jamal, and B. Ali, "Performance Evaluation of CE-OFDM in PLC Channel," in *Signal Processing: An international journal (SPIJ)*, vol. 4, no. 2, pp. 318-328, 2011.
 - [97] C. Wang, G. Cui, W. Wang and Y. Zhang, "Joint estimation of carrier frequency and phase offset based on pilot symbols in quasi-constant envelope OFDM satellite systems," in *China Communications*, vol. 14, no. 7, pp. 1-11, July 2017.
 - [98] M. De Sanctis, E. Cianca, T. Rossi, C. Sacchi, L. Mucchi and R. Prasad, "Waveform design solutions for EHF broadband satellite communications," in *IEEE Communications Magazine*, vol. 53, no. 3, pp. 18-23, March 2015.
 - [99]] R. Mohseni, A. Sheikhi and M. A. M. Shirazi, "Constant envelope OFDM signals for radar applications," 2008 *IEEE Radar Conference*, Rome, 2008, pp. 1-5.

- [100] S. Sen and A. Nehorai, "Adaptive OFDM Radar for Target Detection in Multipath Scenarios," in *IEEE Transactions on Signal Processing*, vol. 59, no. 1, pp. 78-90, January 2011.
- [101] J. G. Proakis and D. G. Manolakis, *Digital Signal Processing: Principles, Algorithms, and Applications*, 4th ed., Upper Saddle River, Prentice Hall, New Jersey, 2006.
- [102] S. A. Martucci, "Symmetric convolution and the discrete sine and cosine transforms," in *IEEE Transactions on Signal Processing*, vol. 42, no. 5, pp. 1038-1051, May 1994.
- [103] T. M. Foltz and B. M. Welsh, "Symmetric convolution of asymmetric multidimensional sequences using discrete trigonometric transforms," in *IEEE Transactions on Image Processing*, vol. 8, no. 5, pp. 640-651, May 1999.
- [104] T. Jiang and Y. Wu, "An Overview: Peak-to-Average Power Ratio Reduction Techniques for OFDM Signals," in *IEEE Transactions on Broadcasting*, vol. 54, no. 2, pp. 257-268, June 2008.
- [105] R. van Nee and R. Prasad, *OFDM for Wireless Multimedia Communications*. Boston: Artech House Publishers, March 2000.
- [106] A. A. M. Saleh, "Frequency-Independent and Frequency-Dependent Nonlinear Models of TWT Amplifiers," in *IEEE Transactions on Communications*, vol. 29, no. 11, pp. 1715-1720, November 1981.
- [107] A. Jayalath, "OFDM for wireless broadband communications (peak power reduction, spectrum and coding)," Ph.D. dissertation, School of Computer Science and Software Engineering, Monash University, May 2002.
- [108] S. C. Thompson, J. G. Proakis and J. R. Zeidler, "The effectiveness of signal clipping for PAPR and total degradation reduction in OFDM systems," *GLOBECOM '05. IEEE Global Telecommunications Conference*, 2005., St. Louis, MO, 2005, pp. 2807-2811.

- [109] J. G. Proakis and M. Salehi, Communication Systems Engineering, 2nd edition, Prentice-Hall, 2002.
- [110] R. Zeimer and W. Tranter, Principles of Communications: Systems, Modulation, and Noise, Wiley, 6th ed., 2009.
- [111] J. J. Downing, Modulation Systems and Noise, Prentice-Hall, 1964.
- [112] M. K. Simon and M. S. Alouini, Digital Communication over Fading Channels, New York: John Wiley and Sons, Inc., 2000.
- [113] I. S. Gradshteyn and I. M. Ryzhik, Table of Integrals, Series, and Products, vol. 6, California, Academic Press, 2000.
- [114] M. Campanella, U. Lo Faso and G. Mamola, "Optimum bandwidth-distance performance in full response CPM systems," in IEEE Transactions on Communications, vol. 36, no. 10, pp. 1110-1118, October 1988.
- [115] D. Asano, H. Leib and S. Pasupathy, "Phase smoothing functions of full response CPM," Conference Proceeding IEEE Pacific Rim Conference on Communications, Computers and Signal Processing, Victoria, BC, Canada, 1989, pp. 316-319.
- [116] K. R. Raveendra, "Digital transmission using multimode phase-continuous chirp signals," in IEE Proceedings - Communications, vol. 143, no. 2, pp. 87-92, April 1996.
- [117] W. Hirt and S. Pasupathy, "Continuous Phase Chirp (CPC) Signals for Binary Data Communication-Part I: Coherent Detection," in IEEE Transactions on Communications, vol. 29, no. 6, pp. 836-847, June 1981.

Curriculum Vitae

Name: Rayan Hamza Alsisi

Education:

2013-2018 Ph.D. Engineering Science
Faculty of Engineering
The University of Western Ontario
London, Ontario, Canada

2006-2008 Master of Engineering Science
Faculty of Engineering
Griffith University
Brisbane, Queensland, Australia

1995-2000 Bachelor of Electrical and Computer Engineering
Faculty of Engineering
King Abdulaziz University
Jeddah, Saudi Arabia

Employment:

2001-2010 Faculty member, College of Electronics and Communications
Technical and Vocational Training Corporation
Jeddah, Saudi Arabia

2011-present Faculty member, Islamic University
Madinah, Saudi Arabia

Experience:

Teaching Assistant Department of Electrical and Computer Engineering
2013 - 2017 The University of Western Ontario, London, Canada
Electric Circuits I
Digital Logic Systems
Electronic Circuits
Introduction to Electronics for Mechanical Engineering
Software Engineering Design I
Introduction to Electronics

2001 - 2010 College of Electronics and Communications
 Jeddah, Saudi Arabia
 Communications Department
 Electronics
 Electrical Circuit
 Digital Design
 Introduction to Communications
 Digital Communications
 Transmission line and Fiber optics

Awards:

Fellowship Islamic University of Madinah
2013-2017 To pursue Doctoral studies at The University of Western Ontario

List of Publications:

- [1] Rayan H. Alsisi and Raveendra K. Rao, "Constant Envelope DCT-based OFDM System with M-ary PAM Mapper over Fading Channels," Advances in Science, Technology and Engineering Systems Journal, vol. 3, no. 1, pp. 252-260, January 2018.
- [2] Rayan H. Alsisi and Raveendra K. Rao, "Constant Envelope DCT-based OFDM System," IEIE Transactions on Smart Processing and Computing, vol. 6, no. 6, pp. 446-454, December 2017.
- [3] Rayan H. Alsisi and Raveendra K. Rao, "DCT- and FFT-based OFDM Systems with Continuous Phase Modulation over Flat Fading Channels," 2017 International Conference on Electrical and Computing Technologies and Applications (ICECTA), Ras Al Khaimah, UAE, November 2017, pp. 1-6.
- [4] Rayan H. Alsisi and Raveendra K. Rao, "Constant Envelope DCT- and FFT-based OFDM Systems with Continuous Phase Chirp Modulation over Fading Channels," 2017 2nd International conferences on Information Technology, Information Systems and Electrical Engineering (ICITISEE), Yogyakarta, Indonesia, November 2017, pp. 211-216.
- [5] Rayan H. Alsisi and Raveendra K. Rao, "Constant Envelope DCT- and FFT-based OFDM Systems with Frequency Modulation in Flat Fading Channels," 2017 8th IEEE Annual Information Technology, Electronics and Mobile Communication Conference (IEMCON), Vancouver, Canada, October 2017, pp. 576-581.

- [6] Rayan H. Alsisi and Raveendra K. Rao, "Performance Comparison of Constant Envelope DCT- and FFT-based OFDM Systems with Phase Modulation over Frequency-Nonselective Fading Channels," 2017 IEEE 28th Annual International Symposium on Personal, Indoor, and Mobile Radio Communications (PIMRC), Montreal, Canada, October 2017, pp. 1-6.
- [7] Alsisi R.H., Rao R.K. (2018) BER Comparison of Constant Envelope DCT and FFT Based OFDM with Phase Modulation. In: Barolli L., Enokido T., Takizawa M. (eds) *Advances in Network-Based Information Systems. NBiS 2017. Lecture Notes on Data Engineering and Communications Technologies*, vol 7. Springer, Cham.
- [8] Rayan H. Alsisi and Raveendra K. Rao, "Performance Comparison of Constant Envelope DCT and FFT Based OFDM Frequency Modulation "2017 IEEE International Conference on Signal Processing, Informatics, Communication and Energy Systems (SPICES), Kollam, India, August 2017.
- [9] Rayan H. Alsisi and Raveendra K. Rao, "Performance of constant envelope DCT based OFDM system with M-ary PAM mapper in AWGN channel," 2017 Annual IEEE International Systems Conference (SysCon 2017), Montreal, Canada, April 2017, pp. 1-7.
- [10] Rayan H. Alsisi and Raveendra K. Rao, " Discrete Cosine Transform Based Orthogonal Frequency Division Multiplexing with Phase Modulation and Constant Envelope," International Conference on Electronics, Information, and Communication (ICEIC 2017), Phuket, Thailand, January 2017, pp. 35-40.
- [11] Rayan H. Alsisi and Raveendra K. Rao, " Performance of Constant Envelope DCT Based OFDM System in AWGN Channel," International Conference on Computer Networks Systems and Communication Engineering (ICCNSCE 2016), Montreal, Canada, December 2016.